SAFETY ANALYSIS REPORT

FOR THE

LOW-ENRICHED URANIUM FUELED

UNIVERSITY OF VIRGINIA REACTOR

("LEU-SAR")

NOVEMBER 1989

SAFETY ANALYSIS REPORT

FOR THE

LOW-ENRICHED URANIUM FUELED

UNIVERSITY OF VIRGINIA REACTOR

("LEU-SAR")

Contributors, past and present:

J.R. Ball	T.G. Foster	J.S. Brenizer	M. Fehr
M.G. Bickel	W.R. Johnson	R.U. Mulder	S. Wasserman
J.A. Dahlheimer	J.L. Kelly	R.A. Rydin	P. Benneche
R.D. Derry	A.B. Reynolds	D.W. Freeman	
J.P. Farrar	J.H. Rust	B. Hosticka	

This report is issued in support of a license amendment to License R-66 for the conversion of the University of Virginia's 2 MW reactor (UVAR) from high enriched uranium (HEU) to low enriched uranium (LEU) fuel. The report supersedes the original SAR for HEU cores and all its revisions and amendments as well as the so-called "UVAR Design and Analysis Handbook", which was the heretofore updated SAR. The present SAR may be referred to as the "LEU-SAR" to distinguish it from the previous SAR.

Table of Contents

Table of Contents (cont.)

Table of Contents (cont.)

List of Figures

List of Figures (cont.)

List of Tables

1.0 Introduction

The University of Virginia Reactor (UVAR) first went into operation in 1960 at a maximum licensed power level of one megawatt under facility license No. R-66. The reactor core consisted of MTR plate type high enriched uranium (HEU) fuel elements. In 1971 the authorized power limit of the UVAR was increased to two megawatts. The operating license for the UVAR was extended for 20 years in September of 1982.

In 1989, high-enriched to low-enriched uranium fuel (LEU) conversion studies were concluded by the University of Virginia reactor staff. The NRC mandated conversion resulted in adoption of a higher fuel loading, with the number of plates per standard element increasing from 18 to 22, to maintain the operating characteristics of the reactor. The present safety analysis report is an updated version of the original HEU Safety Analysis Report, and for differentiation is called the Low Enriched Uranium (LEU) Safety Analysis Report (SAR). This report was reviewed and approved by the Reactor Safety Committee at the end of the summer of 1989

The UVAR is operated by the Department of Nuclear Engineering and Engineering Physics, which is part of the School of Engineering and Applied Science of the University of Virginia. The reactor is primarily utilized as a research and training facility of nuclear engineering students and for the generation of radioisotopes, neutron activation analysis, neutron radiography, radiation damage

studies and other research. The reactor and experimental facilities are made available to the entire university as well as to outside agencies under suitable contract arrangements. The facility is also made available to students from other colleges and universities in the state under a reactor sharing program sponsored by the Department of Energy.

1.1 Summary of Previous Documentation

Documentation relevant to the UVAR and Facility License No. R-66 is summarized chronologically below. Most of these documents are on file under Docket No. 50-62, License No. R-66 in the Division of Reactor Licensing, Nuclear Regulatory Commission.

1) March 14, 1957, application to AEC for Class 104 license and construction permit by Colgate W. Darden, Jr., President, University of Virginia, and Lawrence R. Quarles, Dean, School of Engineering.

2) March 14, 1957, enclosed with the above application was UVAR-3, "A Hazards Summary of the Proposed Research and Training Reactor," by Lawrence R. Quarles and Walter P. Walker.

3) June 7, 1957, Amendment to Hazards Summary submitted by Quarles and Walker.

4) Fall of 1957, Construction Permit No. CPPR-15 issued, signed by H.L. Price.

5) September 23, 1958, Application to AEC to convert Construction Permit CPPR-15 to a class 104 license, signed by Darden and Quarles.

6) September 23, 1958, enclosed with the above application was UVAR-8, "The University of Virginia Reactor, Description and Operation," by J.L. Meem.

7) May 25, 1959, Amendment No. 1 to UVAR-8 submitted by Meem and Quarles.

8) December 4, 1959, Amendment No. 2 to UVAR-8 submitted by Meem and Quarles.

9) February 5, 1960, Amendment No. 3 to UVAR-8 by Meem and Quarles.

10) June 24, 1960, Facility License No. R-66 issued and signed by R.L. Kirk.

11) January 27, 1961, Amendment requested to License R-66 for the use of boron stainless steel control rods signed by Meem and Quarles.

12) April 13, 1961, Amendment requested to License R-66 to permit irradiation of rare earths and uranium isotopes, signed by Meem and Quarles.

13) May 17, 1961, Submission of supplementary information on the use of boron stainless steel control rods, signed by Meem and Quarles.

14) September 1, 1961, Amendment No. 1 to Facility License R-66 granted, authorizing the use of boron stainless steel control rods and authorizing the irradiation of rare earths and uranium isotopes, signed by Edson G. Case.

15) November 21, 1961, Amendment requested to License R-66 to utilize a concentration reduction factor of 500 for argon and noble gases, signed by Quarles and Meem.

16) February 22, 1962, (UVAR-14), Amendment requested to License R-66 for the conduct of a broad irradiation program, signed by Meem and Quarles.

17) April 26, 1962, Amendment No. 2 to Facility License R-66 granted, authorizing the use of a concentration factor of 500 for argon and noble gases, signed by Robert H. Byran.

18) August 23, 1962, Amendment No. 3 to Facility License R-66 granted, authorizing the conduct of a broad irradiation program, signed by Robert H. Bryan.

19) December 17, 1962, Amendment requested to License R-66 to reduce the frequency of inspection of the control rods, signed by Meem and Kuhlthau.

20) January 15, 1963, Amendment requested to License R-66, for the use of 250 grams of U-235 in a fission plate, signed by J.L. Meem.

21) February 18, 1963, Supplementary information provided for January 15, amendment for use of a fission plate, signed by J.L. Meem.

22) March 19, 1963, Amendment No. 4 to License R-66 granted to reduce the frequency of inspection of the control rods, signed by Robert H. Bryan.

23) March 19, 1963, Amendment No. 5 of Facility License R-66 granted, authorizing use of 275 grams of U-235 in a fission plate, signed by Robert H. Bryan.

24) February 27, 1964, Amendment requested to License R-66 for the use of 135 grams of U-235 in a second fission plate, signed by Williamson and Meem.

25) May 18, 1964, Amendment No. 6 to License R-66 granted authorizing the use of 135 grams of U-235 in a second fission plate, signed by Roger S. Boyd.

26) Submitted August 22, 1967, UVAR-17, Safety Analysis in support of amendment of License R-66 for two megawatt operation.

27) November 18, 1968, Change No. 1 to License R-66 granted authorizing round grooves vs. square grooves in the safety shim rods.

28) January 29, 1969, Change No. 2 to License R-66 granted authorizing the replacement of the weather recording instruments with a wind vane and an anemometer, signed by Donald J. Skovholt.

29) June 4, 1969, Amendment No. 7 to License R-66 which authorized the increase of U-235 inventory limit from 6.9 kilograms to 12.0 kilograms and increase in allocation of special nuclear material from 6.9 kilograms to 12.0 kilograms U-235, signed by Donald J. Skovholt.

30) August 4, 1971, Amendment No. 8 to License R-66 to allow storage of 70,000 curies of Cobalt-60 in reactor pool, signed by Donald J. Skovholt.

31) November 4, 1971, Amendment No. 9 to License R-66 to allow operation at 2 MW and incorporate Technical Specifications into the license and to receive, possess, and use up to 7.9 kilograms of contained uranium-235 for use in connection with the operation of the reactor and receive, possess, and store up to 6.1 kilograms of contained uranium-235 not for use in connection with operation of the reactor, signed by Donald J. Skovholt.

32) February 6, 1975, Amendment No. 10 to License R-66 to receive, possess and use up to 14.0 kilograms of contained uranium-235 and 16 grams of plutonium in a Pu-Be source for use in connection with operation of the reactor. Also change No. 1 to the Technical Specification 5.1 describing the fuel elements used in the reactor, signed by Karl R. Goller.

33) May 17, 1976, Amendment No. 11 to License R-66, Change in Technical Specification 3.7 to clarify the use of fueled experiments in the reactor facility, signed by George Lear.

34) December 19, 1978, Amendment No. 12 to License R-66 to change the requirement of visual inspection of control rods as stated in Technical Specification 4.1.C, signed by Morton B. Fairtile for Robert W. Reid.

35) December 22, 1978. Amendment No. 13 to License R-66 to allow the receipt, possession, and use of 1.0 grams of Neptunium-237 in connection with the operation of the reactor. Also a change in Technical Specification 3.5 regarding the exit manhole hatch cover, signed by Morton B. Fairtile for Robert W. Reid.

36) August 25, 1981, Amendment No. 14 to License R-66 adding the Physical Security Plan to the License, signed by James P. Miller.

37) September 30, 1982, Amendment No. 15 to License R-66 renewing the operating license for 20 years, signed by Cecil O. Thomas.

38) February 25, 1986, Final Rule on Conversion to LEU fuel given in 10CFR50.64, effective March 27, 1986.

39) April 25, 1988, Amendment No.16 to License R-66 to clarify the possession, storage and use in the UVAR pool of up to 70,000 Curies of Cobalt-60 in the form of doubly encapsuled rod sources, signed by Lester S. Rubenstein.

40) December 16, 1988, Amendment No. 17 to License R-66 to change the Technical Specifications for minimum shutdown margin so that it is provided by shim rods only instead of control rods, signed by Charles L. Miller.

41) July 20, 1989, Amendment No. 18 to License R-66 to change the Technical Specifications changing the organizational structure to allow the Health Physicist to report to the Department of Nuclear Engineering.

2.0 GENERAL DESCRIPTION OF THE FACILITY

2.1 Reactor Site

The UVA reactor (UVAR) is located approximately 2000 feet west of the of Charlottesville, in Albemarle County, Virginia, [latitude 38° 2'30" N, longitude 78°, 31' W] and at an elevation of 700 feet. The Reactor Facility housing the reactor is next to an abandoned reservoir (pond), 200 feet up the ridge that runs between Mt. Jefferson and Lewis Mountain. The pond has a watershed area of 10^5 square feet. The reactor building is approximately 50 feet above the water level of the pond.

North, east, and south of the site, no closer than 2000 feet, are city residential districts, and 3/4 mile west over the ridge are suburban developments. The downtown business district of Charlottesville is two miles away.

Figures 2-1 (1967) and 2-2 (1964) are aerial photographs of the reactor site. Additional construction near the Reactor Facility occurred between 1964 to 1967, as seen in Fig. 2-1, taken in March 1967. Comparison should be made with Fig. 2-2 taken in 1964, on which newer construction is marked with an asterisk (*). The nearby buildings are: Radio Astronomy Laboratory (RAL*), a group of dormitories (Dorm#), and the 5.5 MeV Van de Graaf (VdG#). The Buildings and Grounds divisions complex (B-G) (now called Physical Plant), the City Water Filtration Plant (Filt), the Observatory (Obs), and the buildings of the former Research Laboratory for Engineering Sciences (RLES), now Aerospace Research Laboratory (ARL), were all in existence prior to construction of the reactor. An addition to the reactor building was completed in 1970.

FIGURE 2-1. AERIAL VIEW OF REACTOR SITE AND IMMEDIATE VICINITY (1967)

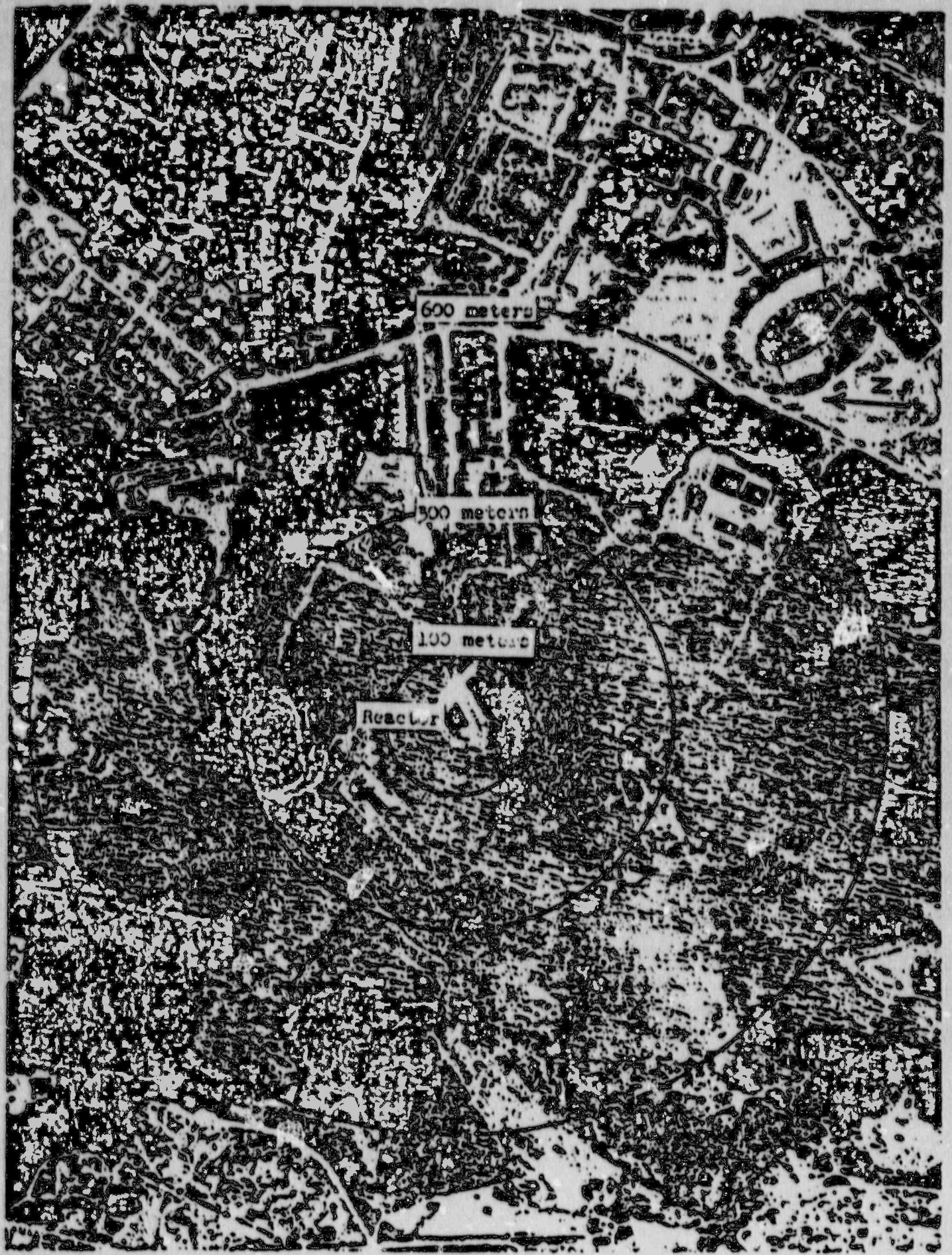

FIGURE 2-2. AERIAL VIEW OF REACTOR SITE AND IMMEDIATE VICINITY (1964)

The Van de Graaf building is approximately 125 meters to the southeast of the reactor facility and the Radio Astronomy Laboratory is about 250 meters to the northeast of the reactor. These buildings are occupied by technical people able to understand and respond to a reactor emergency. Farther away to the east, the student dormitories are at a nearest distance of about 325 meters. A copy of the Reactor Emergency Actions List is posted at the nearby Office of Environmental Health and Safety (EH&S). The University police force is prepared to evacuate any of these areas if necessary.

By virtue of its position in the draw, the reactor has a natural terrain shield for approximately 270 degrees of its circumference, with the elevation of the heavily wooded slopes ranging from 215 meters at the lowest points to 265 meters at the point of highest elevation. Therefore, the UVAR is exposed for only a 90 degree sector from the northeast clockwise to the southeast, as shown in Fig. 2-3. In the easterly direction, the elevation drops rapidly, so that approximately 1200 meters from the reactor, the elevation if 150 meters.

As shown in Fig. 2-4, residential areas are found to the north, east and south, with major business districts to the northeast and east at approximately 2500 meters and 3500 meters respectively. The population of the city of Charlottesville is estimated at about 50,000.

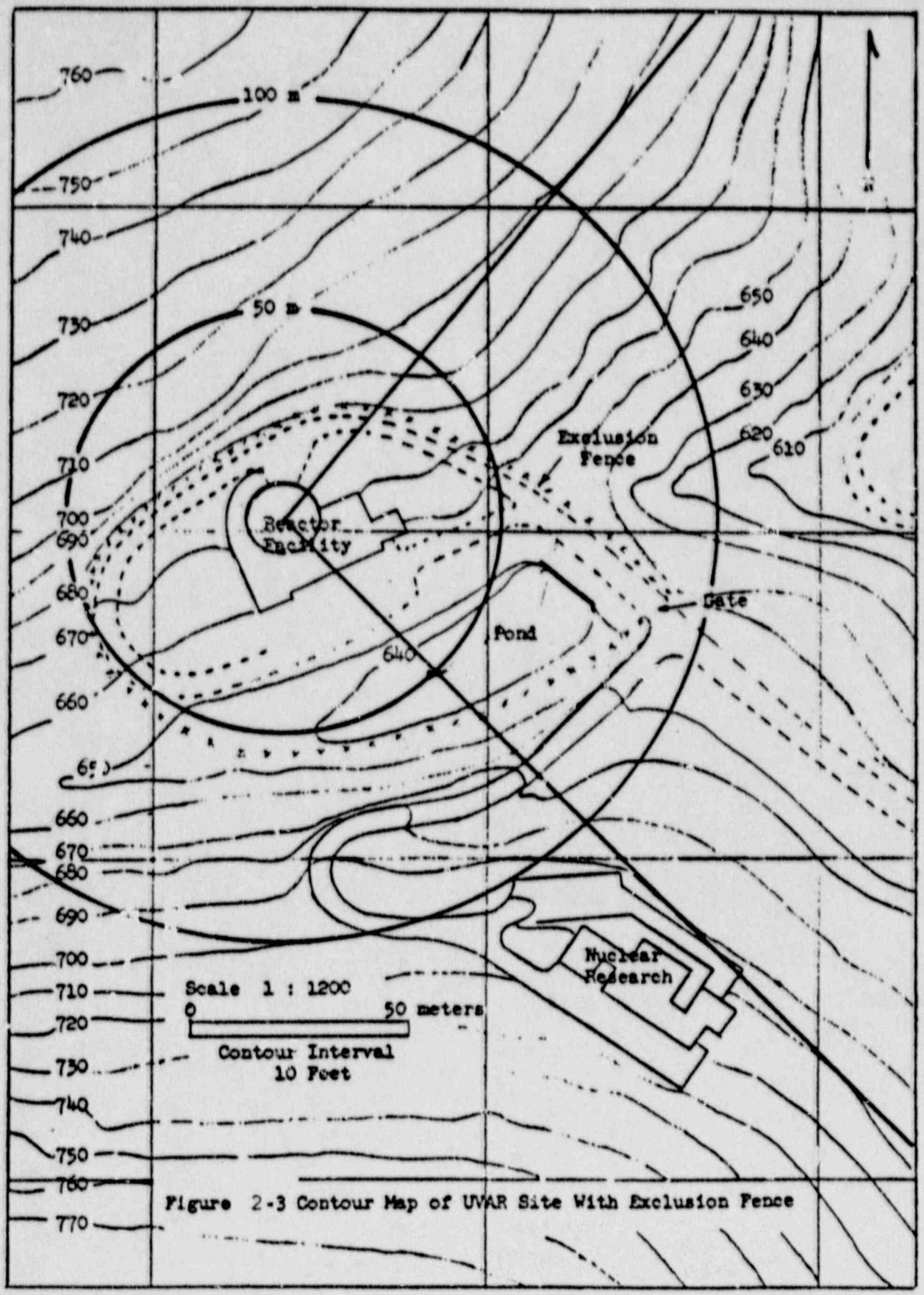

Figure 2-3 Contour Map of UVAR Site With Exclusion Fence

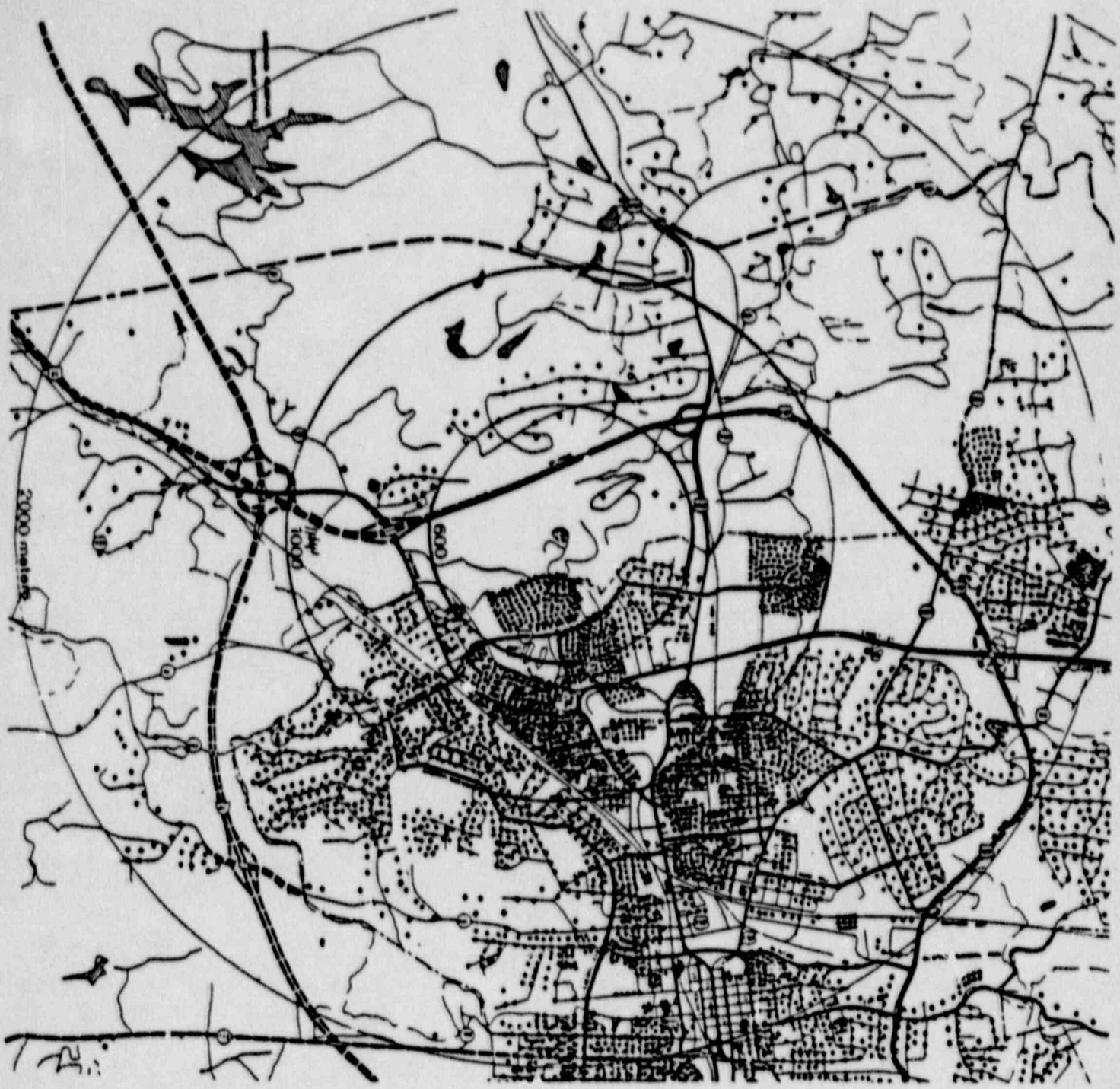

FIGURE 2-4 POPULATION DENSITY DISTRIBUTION (1968)
(Each Dot = 10 Persons)

The Reactor Facility has an exclusion fence as shown in Fig. 2-3. This fence is approximately 70 meters from the reactor building in the terrain "unshielded" direction. Within a 600 meter radius of the UVAR there are very few buildings and all of these, with the exception of approximately a dozen privately owned homes just inside this radius, are operated either by the University, City of Charlottesville or State of Virginia.

2.2 Reactor Building

The Reactor Facility building, shown in Fig. 2-5, consists of the main reactor room, radiation laboratory, supporting laboratories, hot cell and office space. Figures 2-6, 2-7, and 2-8 show floor plans for the three levels. The construction is of conventional masonry, with the exception of the main reactor room. This portion of the building is cylindrical in shape to increase its ability to withstand internal pressure. The walls are of reinforced masonry, plastered on the inside for gas tightness, while the roof is a concrete slab. This portion of the structure is windowless and the doors are gasketed. The reactor bay ventilation is described in Section 4.9.

2.3 New Construction

Construction of an addition to the Reactor Facility was completed in 1970. The new addition provides more office space, classroom, machine shop, electronics shop, low background counting room, health physics and student laboratories.

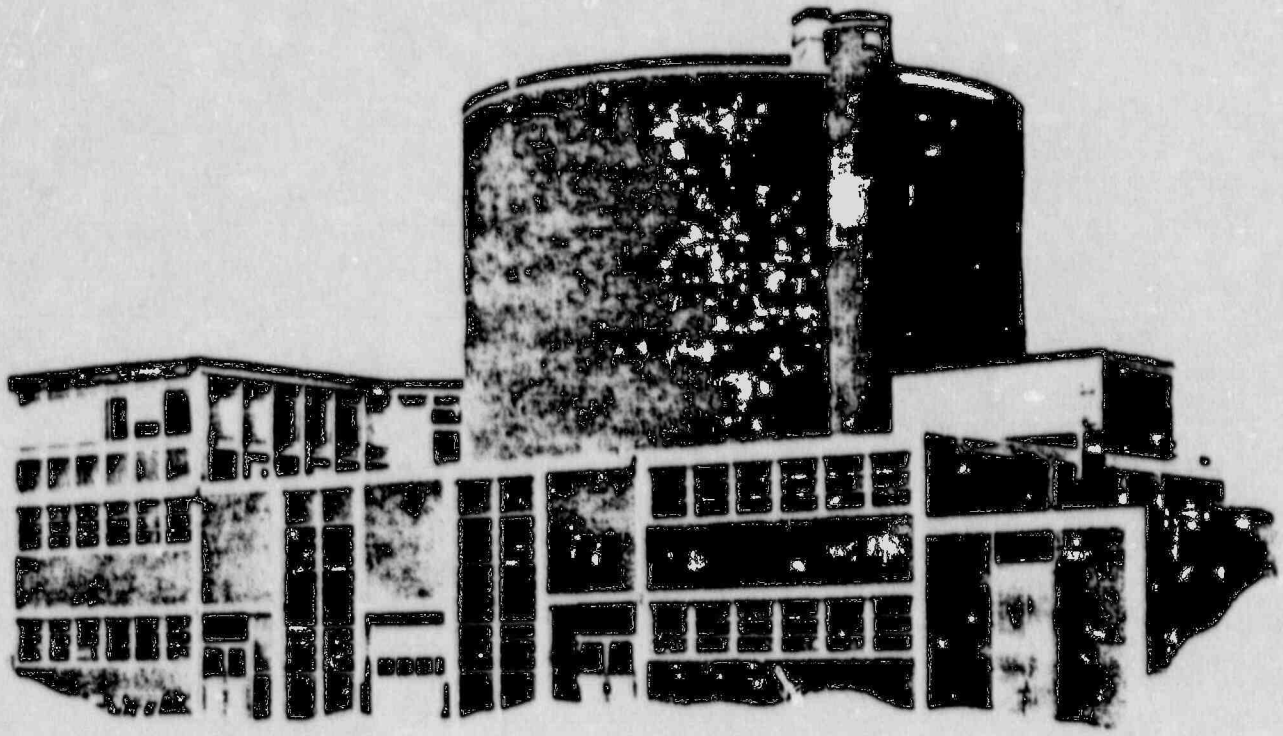

Figure 2-5 University of Virginia Research and Training Reactor Facility.

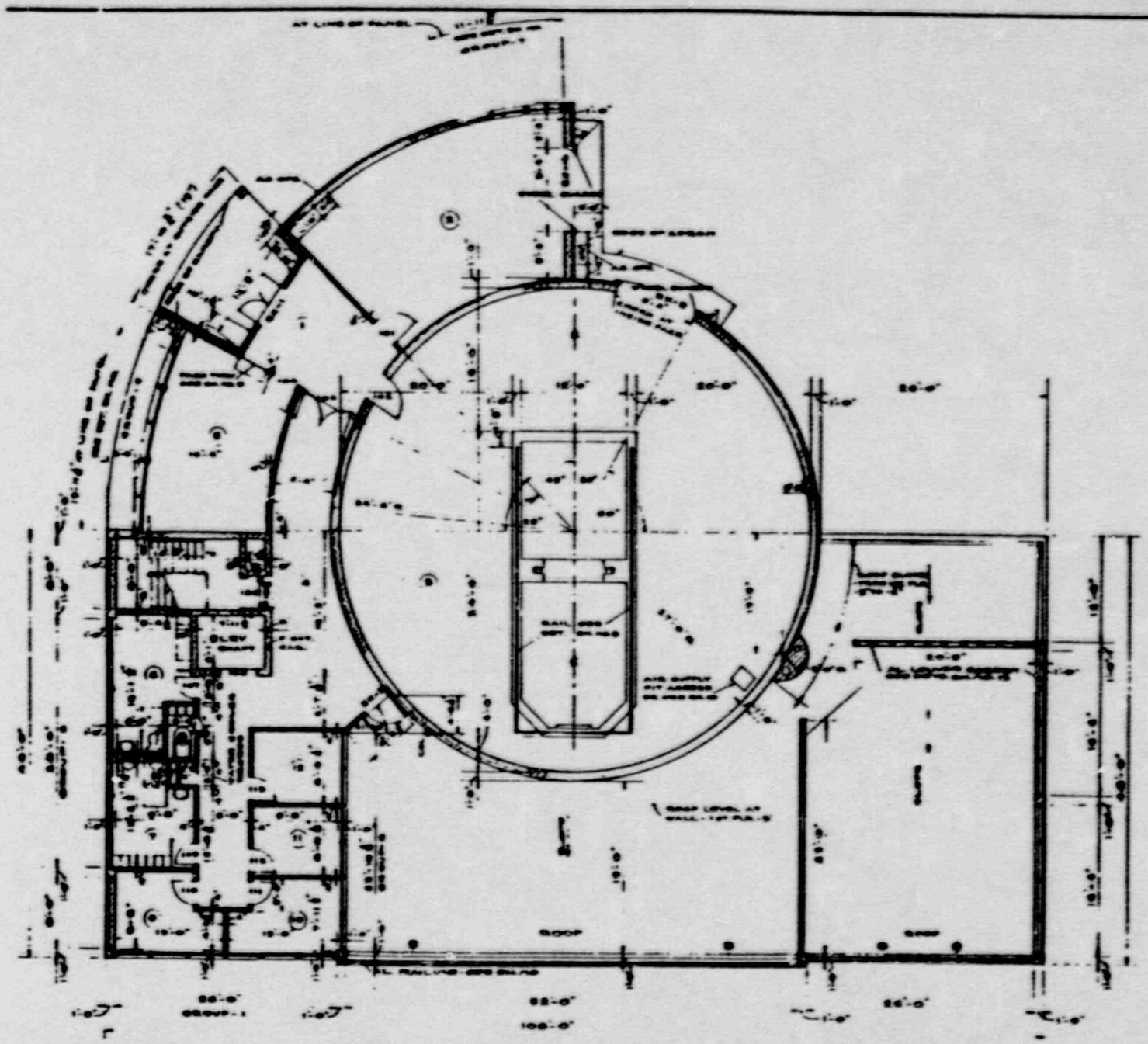

FIG. 2-6 FIRST FLOOR PLAN

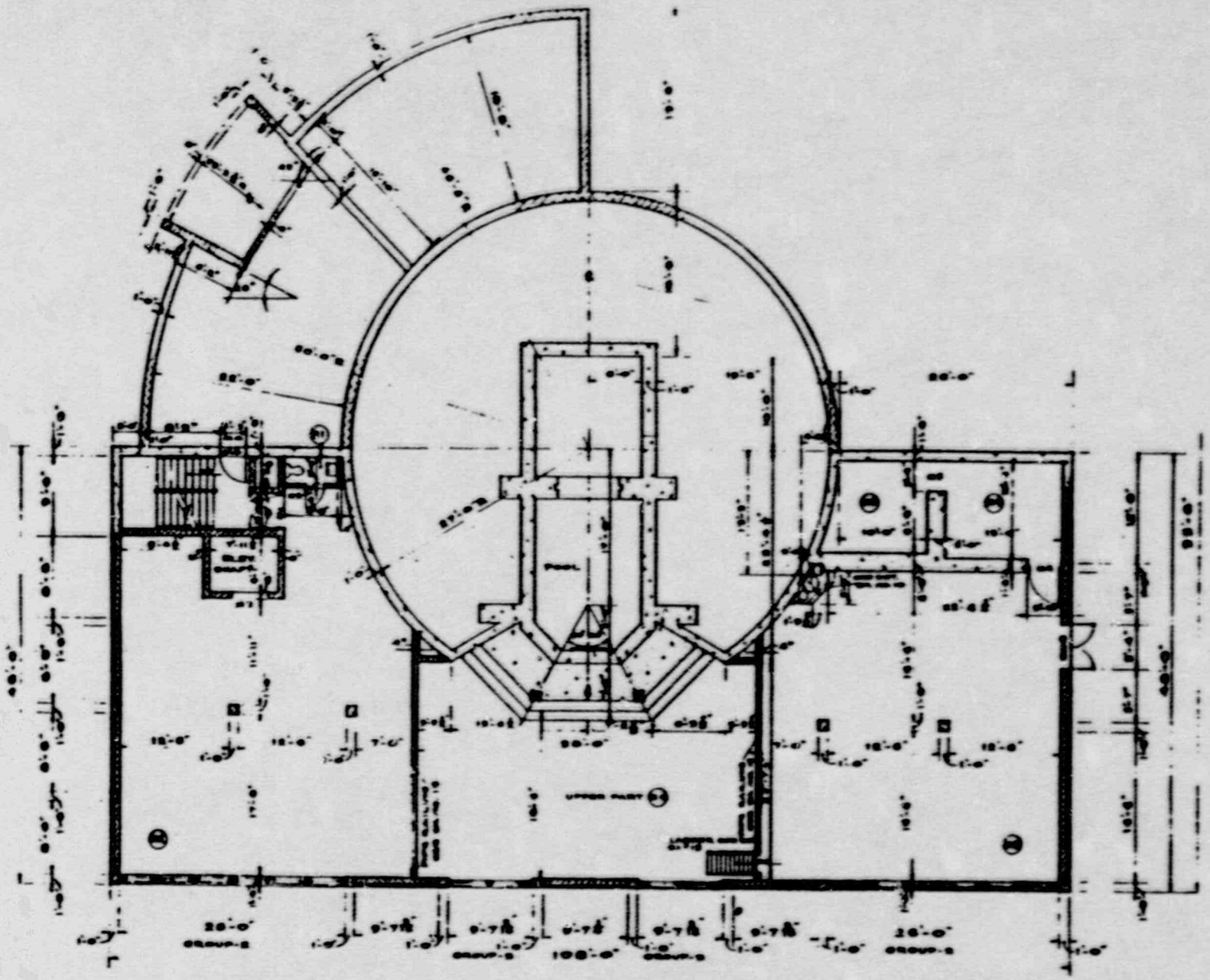

FIG. 2-7 MEZZANINE LEVEL

SCALE: 1/8" = 1'-0"

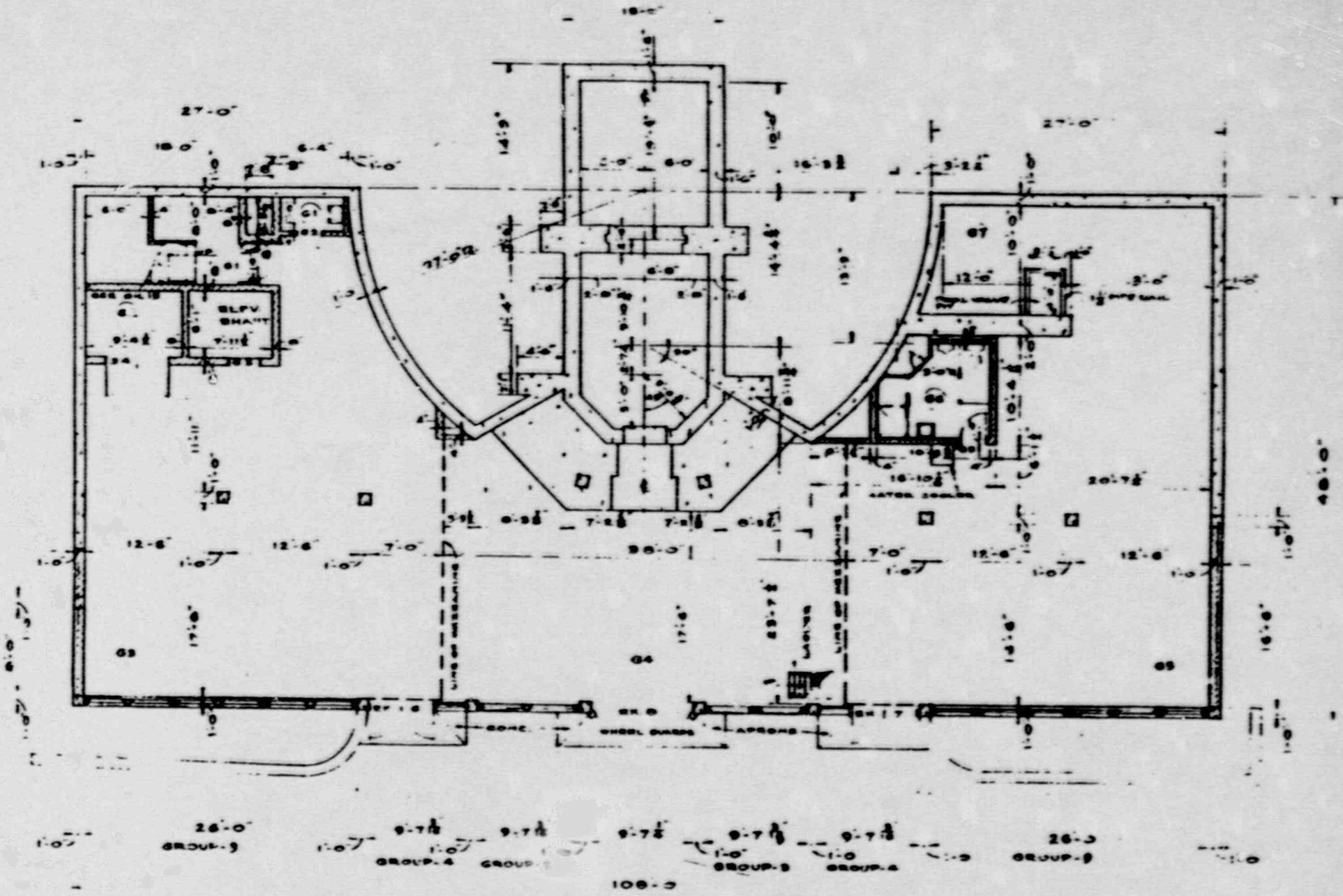

FIG. 2-8 GROUND FLOOR

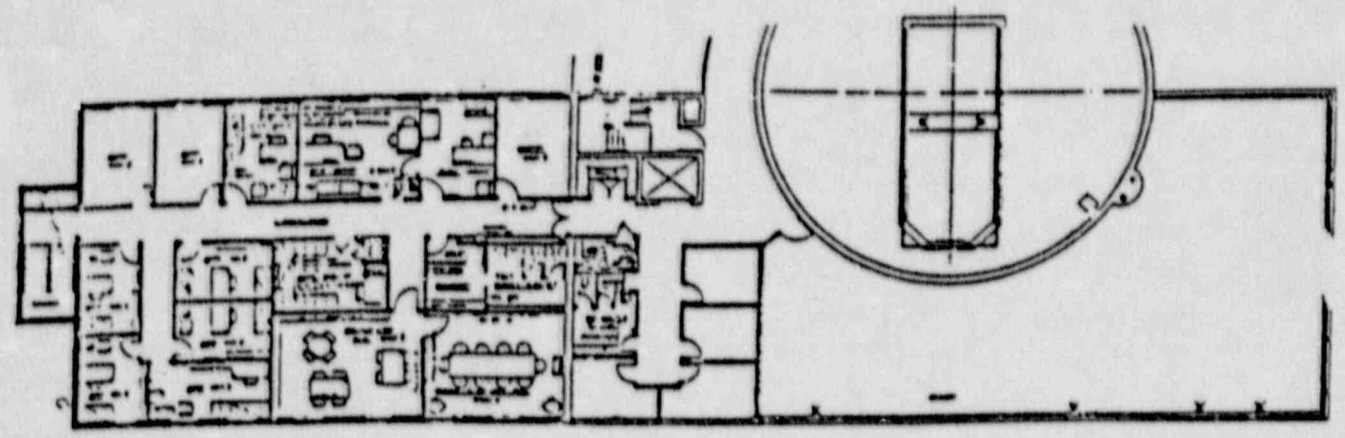

FIRST FLOOR PLAN

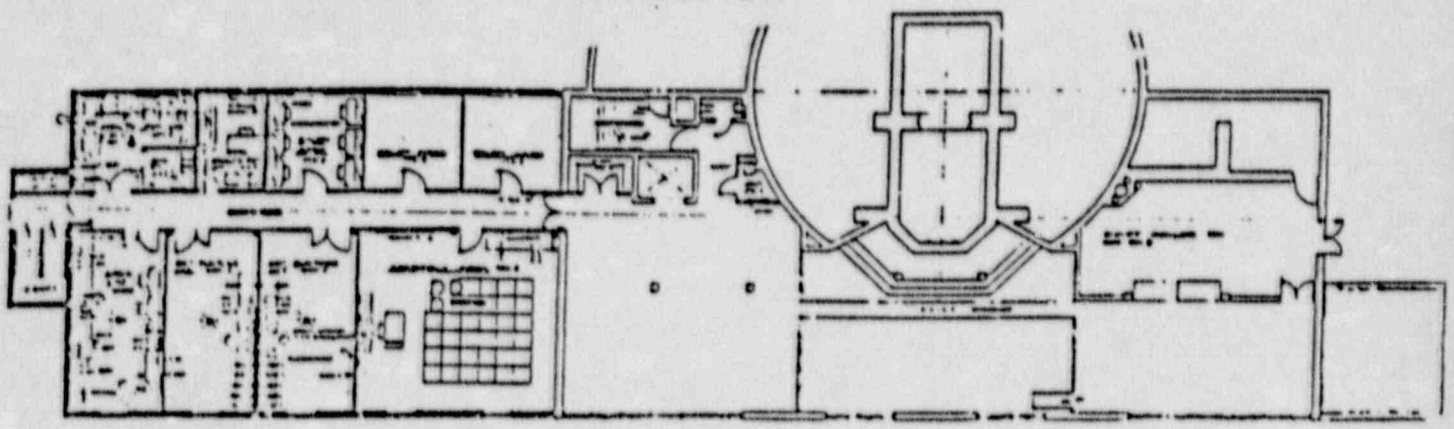

MEZZANINE LEVEL

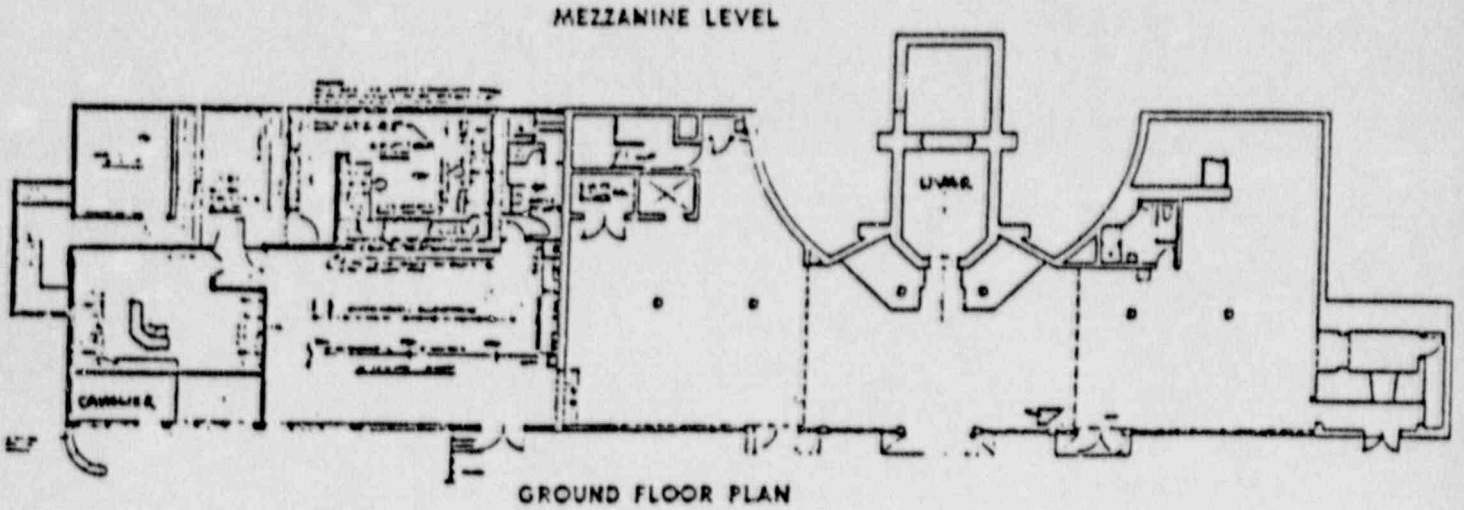

GROUND FLOOR PLAN

FIGURE 2-9 PLANS OF THE NUCLEAR REACTOR FACILITY

2.4 Wind Direction and Velocity

During the first few years of University of Virginia Reactor operation, records of wind velocity and direction at the reactor site were maintained. Tables 2.1 and 2.2 represent the equivalent of one year's data, from 21 June 1961 to 21 June 1962. For that year, winds from the Northeast to Northwest quadrant are dominant with a strong contribution from the West. The summer season has a high percentage of calms with principal winds from the Southeast to the Southwest quadrants. Therefore, gaseous effluent discharged or fission products released into the atmosphere would, with greatest probability, be transported in the direction of highest population density, except in the summer season where the reverse would be true.

2.5 Hydrology

As mentioned elsewhere (Sections 2.1 and 4.8) of this report, liquid effluents from the reactor building may discharged, upon dilution with water from the adjacent pond to concentrations below MPC, to Meadowbrook Creek which flows into the Rivanna River. Releases are made in accordance with the restrictions set forth in 10 CFR Part 20.

Due to its location on the side of a draw between Mt. Jefferson and Lewis Mountain, the reactor is not subject to flood conditions.

TABLE 2.1

RELATIVE FREQUENCY OF HOURLY WIND SPEEDS
IN PER CENT BY SEASON

Wind Speed Type - mph		Summer	Fall	Winter	Spring	Year
Calm	0-1	43.5	9.0	3.5	20.7	18.7
Light	1-3	15.3	2.0	1.4	8.1	6.4
Gentle	4-10	28.0	10.7	14.3	31.7	20.0
Moderate	11-21	11.6	33.3	61.8	37.9	36.3
Strong	21-up	1.6	45.0	19.0	1.6	18.6
Total		100.0	100.0	100.0	100.0	100.0
Avg. Speed (mph)		4.26	15.0	13.1	7.71	10.36*

*The average wind speed of 10.36 mph is equivalent to 4.63 m/sec.

TABLE 2.2

RELATIVE FREQUENCY OF HOURLY WIND DIRECTIONS
IN PER CENT BY SEASON

Direction	Summer	Fall	Winter	Spring	Year
North	5.6	27.4	30.3	8.4	1[illegible].9
Northeast	7.4	10.2	28.3	24.5	16.9
East	5.7	0.0	2.6	0.0	2.6
Southeast	7.8	12.4	8.0	2.6	8.1
South	10.6	3.8	3.0	10.2	7.8
Southwest	8.5	10.3	4.6	5.0	7.7
West	3.8	15.9	12.5	9.2	10.0
Northwest	7.1	10.9	7.5	10.4	11.4
Calms	43.5	9.1	3.5	20.7	18.7
Total	100.0	100.0	100.0	100.0	100.0

2.6 Seismology

The Central Appalachian region is characterized by a moderate amount of low level earthquake activity. Because of the low seismic energy release, this region has received very little attention from earthquake seismologists. A study by Dr. G.A. Bollinger of Virginia Polytechnic Institute covering the period of 1758 through 1968, indicates a history of 9 earth tremors in the city of Charlottesville and Albemarle County during that period.

The tremors felt in this area and their intensity on the modified Mercalli Scale, when of sufficient magnitude for assignment, are listed below:

Date	Intensity at Epicenter
August 27, 1933	VI
April 29, 1852	VI
September 1, 1886	V-VI
December 26, 1929	VI
April, 1936	Not Available
February 2, 1937	III-IV
May 24, 1946	Not Available
March 26, 1948	Not Available
September 10, 1952	IV
May 31, 1966	Not Available
November 19, 1969	Not Determined

Considering the low level of earthquake activity and intensity in this area and the reinforced construction of the pool, earthquake activity is not considered to present a danger to the facility.

3.0 REACTOR COMPONENTS AND CONTROL

3.1 Reactor Assembly

The reactor assembly is comprised of fuel elements, control rod fuel elements, control rods and graphite reflector elements; all of which sit in the reactor gridplate near the bottom of the reactor pool. The reactor gridplate is supported by an aluminum framework from a movable bridge. The bridge can be rolled back and forth across the pool in the north-south direction and is designed such that the minimum distance between the core and the pool wall is about 4 feet. This distance is sufficient to prevent significant activation of the concrete walls. The bottom of the core is about 4.5 feet above the pool floor and the top of the active core is about 2 feet below the pool surface (see Figure 3-1). The heat capacity of the pool is sufficient for steady-state operation at 200 kW with natural convection cooling; but for higher power operation, a forced convection system is required. The forced convection cooling system, described in Section 4.3, uses downflow in order to minimize nitrogen-16 activity in the reactor room.

The reactor gridplate, shown in Figure 3-2, is made of aluminum and contains an eight by eight array of holes used for positioning reactor components. Each positioning hole is approximately 2 1/2 inch in diameter. The center-to-center spacings are 3.2 inch in the East-West direction, and 3.0 inch in the North-South direction. Small holes (not shown in Figure 3-2) are interspaced between the positioning holes to provide cooling flow between reactor components.

Reactor components include: 1) fuel elements, 2) graphite elements, 3) gridplate plugs and 4) in-core experiments.

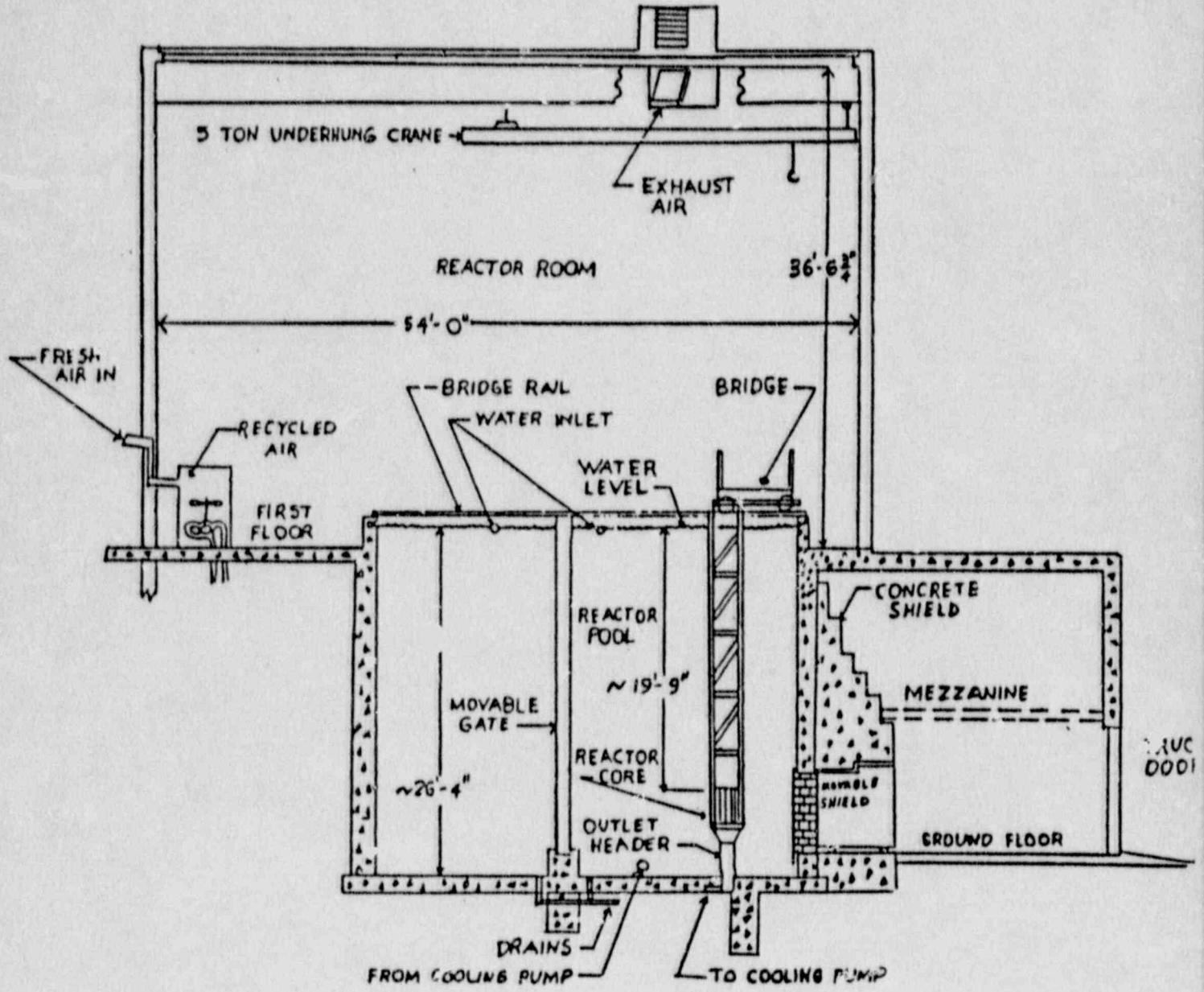

Figure 3-1. Cross-Section View of Reactor Pool and Reactor Room

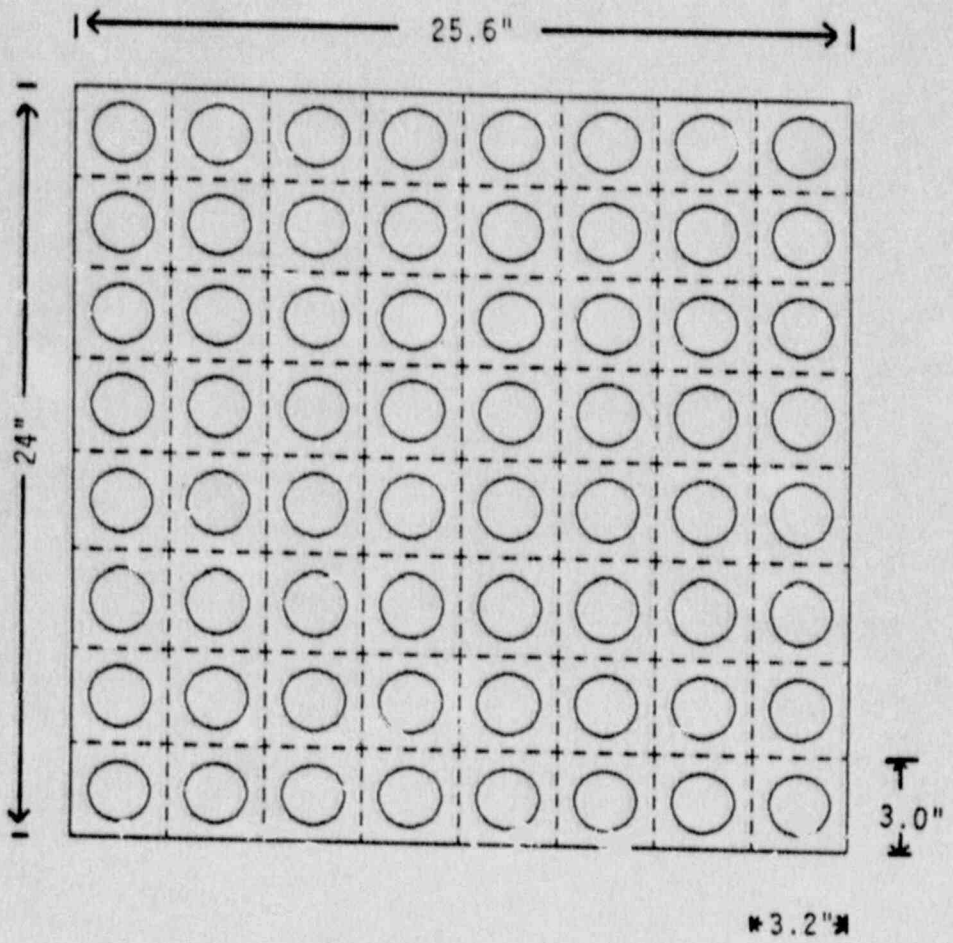

Figure 3-2. UVAR Gridplate

3.2 Fuel Elements

Three types of fuel elements are used in the UVAR: 1) standard fuel elements, 2) partial fuel elements and 3) control rod fuel elements. Each type of fuel element uses generic fuel plates (described in Section 3.3) and has similar outer cross sectional dimensions of about 3 inch by 3 inch. The standard and partial elements are about 34 inches in height and the control rod element is about 38 inches in height. The bottom of each element consists of a cylindrical tapered nozzle which fits snugly into the gridplate positioning holes.

The standard low-enriched uranium fuel element, shown in Figures 3-3 and 3-4, contains 22 fuel plates. The initial loading of a standard fuel element is 275 grams of uranium-235. The water gap between fuel plates is 0.092 inch. The metal to water ratio of the active standard fuel element is 0.76.

Partial fuel elements have the same dimensions as standard fuel elements but contain only half the amount of fuel. Partial elements are loaded into the core when relatively small changes in reactivity are desired. The partial element has 22 plates, of which 11 are fuel plates and 11 are aluminum "dummy" plates, with fuel and dummy plates alternating. Dummy plates have the same outer dimensions as fuel plates. The partial fuel element initially contains 138 grams of uranium-235.

Control rod elements, shown in Figures 3-5 and 3-6, have dimensions similar to standard fuel elements and use the same water gap between fuel plates. The control rod element contains 11 fuel plates (138 grams of uranium-235) and has an open center (referred to as the water hole) where the control rod travels. Two guide plates on either side of the water

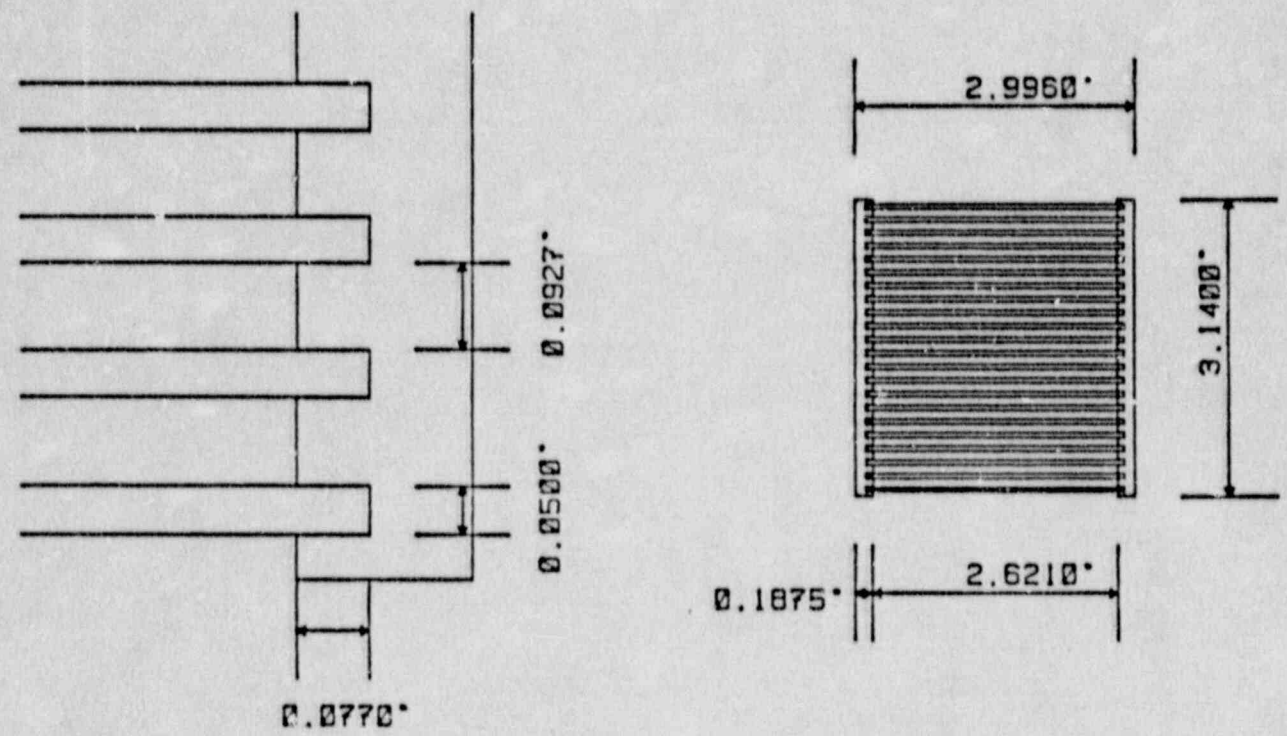

Figure 3-3. Top View Of Standard and Partial LEU Fuel Element

Figure 3-4. Side View Of Standard and Partial LEU Fuel Element

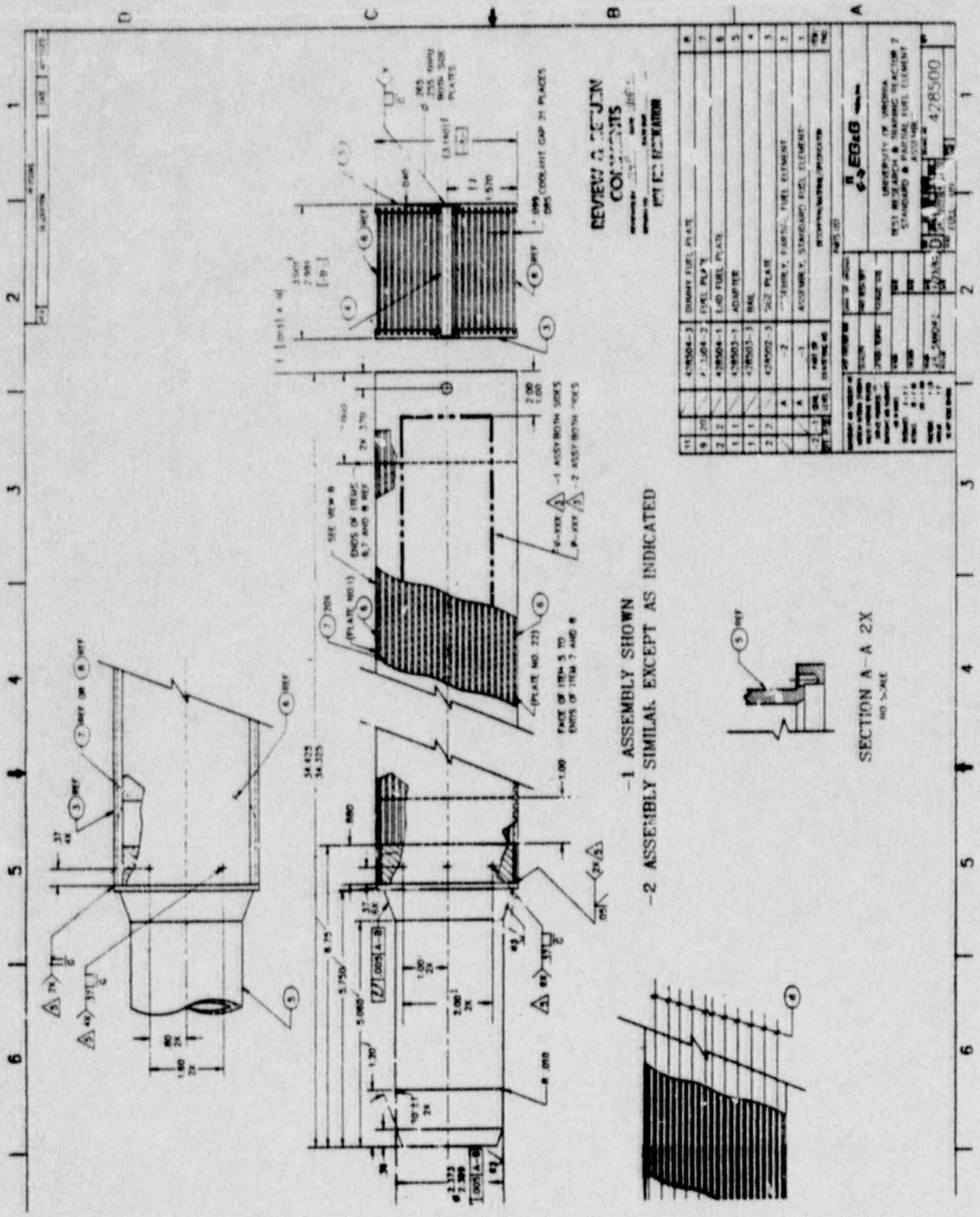

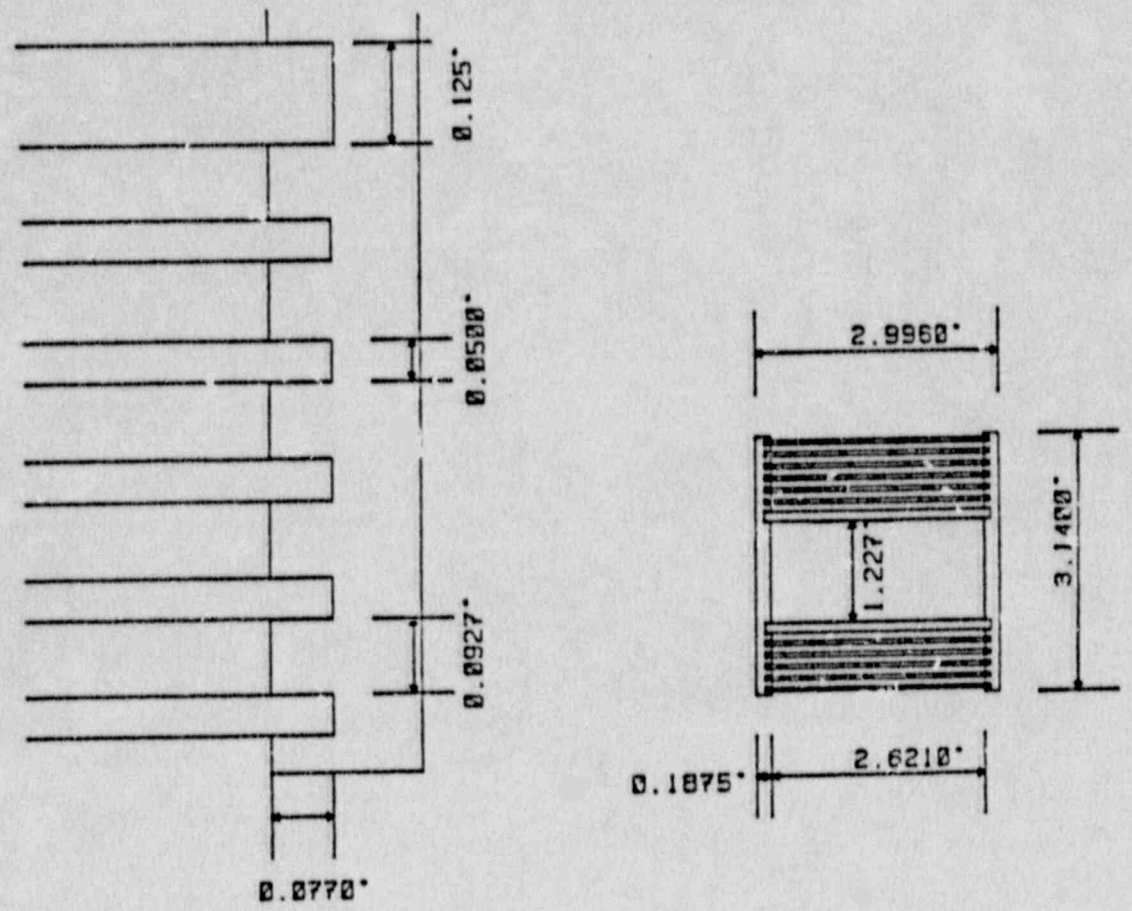

Figure 3-5. Top View Of Control Rod LEU Element

Figure 3-6. Side View Of Control Rod LEU Element

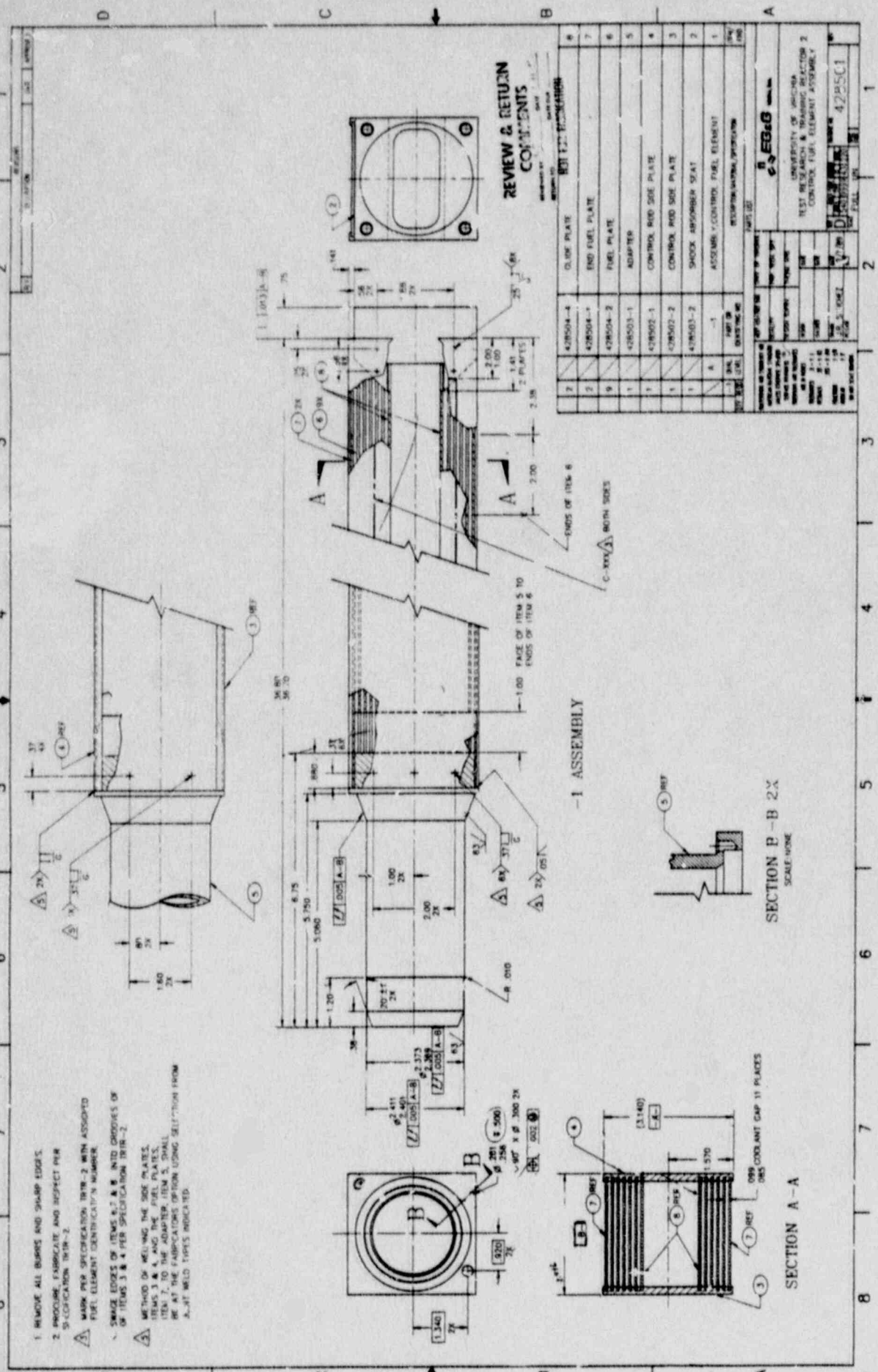

hole assure that the control rod will not contact or damage the fuel plates. The metal-to-water ratio of the control rod element is 0.52.

Detailed dimensions of UVAR LEU fuel elements are available in References [1] through [4].

3.3 Fuel Plates

The fuel plates are flat and each initially contains 12.5 grams of uranium-235. The plates contain low-enriched uranium (LEU) fuel meat clad in aluminum. The fuel plate is 0.05 inch thick, 2.80 inch wide, and 24.6 inch long. Detailed fuel plate dimensions are provided in Reference [5].

The fuel meat is composed of uranium-silicide (U_3Si_2) dispersed in an aluminum matrix. The uranium is 19.75 percent enriched in uranium-235. The fuel meat is 0.02 inch thick, 2.40 inch wide, and 23.3 inch long.

The aluminum clad is 0.015 inch thick and surrounds the fuel meat.

3.4 Control Rods and Drives

The reactor has four control rods. Three of these, designated as Shim rods (or Safety rods) are designed for gross control and safety. Shim rods are magnetically coupled to their drive mechanisms and drop into the core by gravity on a scram signal. The fourth rod is a regulating rod which is fixed to its drive mechanism and is therefore non-scramable. The regulating rod is primarily used to compensate for small changes in reactivity associated with normal operations. LEU cores use the same control rods and drive mechanisms used previously in the HEU

cores. Detailed control rod and drive specifications are presented in References [6] through [8].

The reactivity worth of the shim rods in HEU cores have typically varied between about $3 and $5, depending on factors such as core/reflector configuration, rod position in the core, core burn-up, etc. Analyses presented in Reference [9] show that the shim rod worths for the LEU core are not significantly different from shim rod worths in HEU core. Therefore, the shim rods should provide adequate control for safe operation.

The reactivity worth of the regulating rod in HEU cores has typically varied between $0.3 and $0.5. The analysis provided in Reference [9] shows that the reactivity worth of the regulating rod in the LEU cores is similar to its worth in HEU cores. Therefore, the regulating rod is expected to adequately perform its function of compensating for small reactivity changes in LEU cores.

All of the rods are of the bayonet type, fitting into the control rod fuel element water hole. The control rod, rod drive, and extension assembly is bolted to the top of the control rod fuel element, thus creating a single rod unit. A rod unit may be located in any core position by locating the control element nozzle into the desired gridplate position.

The absorbing section of the shim rods is boron-stainless steel, clad in aluminum. The stainless steel is alloyed with about 1.5% boron by volume. Each absorbing section is 24-13/16-inches long and has an oval cross section of 2-1/4 x 7/8-inches with semi-circular ends. Four

groves are cut in each side of an absorbing section to increase the surface area.

The shim rods are suspended magnetically from the drive mechanism. The drive is provided by a 115 volt, 60 cycle, split phase synchronous motor. The motor, lead screw-drive, and position indicating equipment are contained in a cylindrical tube extending from the top of the core to above the water level where it is supported from the bridge. A scram signal will de-energize the magnet holding the absorber section, allowing it to drop freely until it is hydraulically damped and stopped, fully in the core. The supporting magnet must be driven down to contact the bottom absorber section before the control rod can be raised after a scram. The shim rods are driven at about 3.7 inches per minute in both directions.

The regulating rod has the same overall dimensions as the safety rod, except there are no grooves in the regulating rod. The regulating rod is made of stainless steel and is clad in aluminum. The regulating rod is permanently fixed to its drive mechanism and does not drop on a scram signal. It is driven by a 115 volt, 60 cycle two phase control motor which, along with the lead screw and position indicating equipment, is contained in a cylindrical tube similar to that employed for the safety shim rods. The regulating rod is connected to the automatic control system of the reactor described in Section 3.12. The regulating rod travels at a speed of approximately 24 in/min in both directions.

Each shim rod is removed from the reactor and visually inspected on an annual basis. The inspection includes checking for cracks and swelling.

Rod drop times are measured semi-annually and whenever a safety rod is maintained or repositioned in the core. The maximum allowable time from scram initiation to full insertion is less than one second.

3.5 Reactor Reflectors

The primary reflectors used in the UVAR are graphite elements and pool water. Experiments located near the core may also behave as reflectors.

Graphite elements have the same approximate outer dimensions as the fuel elements and consist of a solid graphite core surrounded by aluminum. Graphite elements are significantly better reflectors than pool water.

Gridplugs are used to prevent water flow through empty gridplate locations. A gridplug is a short metal cylinder, approximately 3 inches in diameter, mounted on a tapered nozzle. When inserted in the gridplate, the plug extends no more than a few inches above the gridplate effectively providing pool water reflector at that gridplate location.

Other types of reflectors include items such as experiments or experimental facilities, located in close proximity to the core.

3.6 Core Loadings

A wide variety of critical loadings are possible with the UVAR reactor. Core loadings are limited by Technical Specification restrictions on shutdown margin (0.50$) and excess reactivity (7.00$). The minimum critical loading is a graphite reflected four-by-four array of elements, including 12 standard fuel elements and 4 control rod elements. This loading has a mass of 3850 grams of uranium-235.

Excess reactivity and shutdown margin are functions of items such as the amount of fuel in the core, fuel and reflector configuration, control rod locations, fuel burn-up, etc. The core configuration of the UVAR is frequently changed to enhance characteristics of experimental facilities, perform new experiments, or compensate for fuel burn-up. Shutdown margin and excess reactivity are experimentally determined after each core configuration change. Additionally, shutdown-margin and excess reactivity are periodically reevaluated to account reactivity changes associated with fuel burn-up.

Initial loading of a new core is performed carefully. Sub-critical multiplication data is collected with the addition of each fuel element. Analysis of this data allows a fairly accurate prediction of when initial criticality will be achieved. Final fuel additions are made in half-element increments until a desired core is achieved. Operation of the new core is limited to 1 kilowatt for the purpose of obtaining experimental data to calibrate the control rods. The shutdown margin and excess reactivity are determined from the rod calibration data and a determination of acceptability of these parameters must be made prior to operating the new core in excess of 1 kilowatt.

Analyses presented in Reference [9] show that the reactivity of unburned LEU and HEU fueled cores are similar. The loading of LEU cores is expected to result in core reactivity parameters similar to those verified through past experience with the HEU cores.

It should be noted that LEU 22 plate/element fuel is expected to have a somewhat longer core life than 18 plate/element HEU fuel. This

should result in fewer core modifications to accomodate fuel burn-up, which is beneficial with regards to experiments and fuel costs.

3.7 Fuel Storage Facilities

UVAR Technical Specifications require all fuel elements not in the reactor core to be stored in a geometric array such that the k-effective is less than 0.9. Existing fuel storage facilities at the UVAR Reactor Facility have been evaluated for compliance with the Technical Specification reactivity requirement, with regard to LEU 22 plate/element fuel.

The current fuel storage facilities are described below:

1) **Fuel Storage Room** - The Fuel Storage Room is located in the CAVALIER Room and consists of an aluminum rack with a rectangular array of square holes in which fuel elements may be stored. The center-to-center distance of the holes is 12 inches in both directions. The Fuel Storage Room is dry and is located above ground. The Fuel Storage Room is primarily used for the storage of unburned fuel elements. Elements in the Fuel Storage Room are secured with chains bolted across the rack openings.

2) **Auxiliary Fuel Storage Rack** - The Auxiliary Fuel Storage Rack (AFSR) is normally stored at the pool bottom. The AFSR contains two linear arrays of fuel storage positions. The two linear arrays are separated by a distance of two feet. Each linear array consist of twelve fuel storage locations, separated by a center-to-center distance of 6 inches. Elements

in the AFSR are mechanically held in place by the rack lids which may be bolted shut.

3) **Four Element Racks"Lunar Landers"** - There are currently 3 Lunar Landers. Lunar Landers loaded with burned fuel are stored at the pool bottom. The Lunar Landers each hold up to 4 elements in a square configuration with the elements being located at the corners of the square. The center-to-center distance between elements in the x-y direction varies from 7 to 8 inches. Elements are secured by bolting an aluminum top onto the lander.

4) **Wall Rack** - The Wall Rack is used for temporary underwater storage of fuel elements. It consists of a linear array of 12 fuel storage locations. Each fuel storage location is separated by a center-to-center distance of 3.5 inches.

An analysis applicable to the Fuel Storage Room, Auxiliary Fuel Storage Rack, and Lunar Landers has been performed using two dimensional diffusion theory computer modeling. A unit LEU fuel cell surrounded by water was modeled in x-y geometry. Flat flux boundary conditions were used to simulate an infinite array. The k-effective of a water moderated infinite array of fuel was determined to be 0.8 for a center-to-center distance of 5.5 inches. This analysis is conservative in that 1) it neglects leakage from the boundaries of a storage facility and 2) the value of k-effective = 0.8 associated with the 5.5 inch spacing is significantly lower than the required value of 0.9. Based on this information, LEU-22 fuel storage facilities with an x-y storage array with center-to-center spacings in excess of 5.5 inches meet the Technical Specification reactivity requirement.

An analysis applicable to the Wall Rack (and to the Auxiliary Fuel Storage Rack) was performed for an infinite linear array of water moderated (and reflected) LEU fuel elements positioned side-by-side, (i.e. no separation between elements). The k-effective for this array is 0.74, which also meets the Technical Specification criteria.

In summary, modeling results show that all of the existing fuel storage facilities meet the Technical Specification reactivity criteria when loaded with LEU-22 plate/element fuel.

3.8 Reactor Data

For ease in reference, pertinent data for the UVAR reactor are presented in Table 3.1. Information detailing the UVAR LEU-22 fuel elements, fuel plates, and fuel meat is provided in Reference [10].

Table 3.1 Reactor Data for LEU Cores

I. Typical 4 by-4 and 4-by-5 Core Parameters

Parameter	4-by-4 Core Configuration	4-by-5 Core Configuration
1. Core Dimensions		
a) Active height	23.3 inch	23.3 inch
b) Width	12.6 inch	12.6 inch
c) Length	12.0 inch	15.0 inch
d) Volume	3,520 inch^3	4,400 inch^3
2 Number of Elements		
a) Standard	12	16
b) Control	4	4
3. Mass U-235	3.85 kg	4.95 kg
4. Metal-to-Water Ratio (by volume)	0.70	0.74

II. Fuel Element Parameters

Parameter	Value
1. Outer Dimensions	
a) Height	34.4 inch
b) Width	3.14
c) Length	3.00
2. Water Gap	0.092 inch
3. Standard Element	
- Number of Fuel Plates	2
- Number of Side Plates	2
- U-235 Content	12.5 gram
- Metal-to-Water Ratio (by volume)	0.76
4. Control Element	
- Number of Fuel Plates	11
- Number of Side Plates	2
- Number of Guide Plates	2
- U-235 Content	6.25 gram
- Metal-to-Water Ratio	0.52
5. Partial Element	
- Number of Fuel Plates	11
- Number of Side Plates	2
- Number of "Dummy" Plates	11
- U-235 Content	6.25 gram
- Metal-to-Water Ratio	0.76

III. Fuel Plate Parameters

1.	Overall Dimensions	
	a) Length	24.6 inch
	b) Width	2.80 inch
	c) Thickness	0.050 inch
2.	Fuel Meat	
	a) Type	U_3Si_2 in Al matrix
	b) Uranium Enrichment	19.8% U-235
	c) U-235 Content	12.5 gram
	d) Length	23.3 inch
	e) Width	2.40 inch
	f) Thickness	0.020 inch
3.	Clad Thickness	0.015 inch

IV. Side Plate Parameters

Length	
a) Standard	28.5 inch
b) Control	30.9 inch
Width	3.14 inch
Thickness	0.188 inch
Composition	Aluminum

V. Guide Plate Parameters

Length	27.6 inch
Width	2.80 inch
Thickness	0.125 inch
Composition	Aluminum

VI. Control Rod Parameters

1. **Safety (Shim) Rods**

Absorber Material	Boron-Stainless Steel 1.5% Boron
Clad	Aluminum
a) Dimensions, Overall	
Width (Approx.)	1 inch
Depth (Approx.)	2.38 inch
Length (Approx.)	27.5 inch
Travel (Approx.)	24 inch
Weight (Dropping Section)	5.5 inch
b) Drive - Electric motor, 115 V 60 cycle, split phase. 3600 rpm at 60 cps. From top by lead screw.	
c) Drive Speed	3.74 in/min
d) Release - Magnetic; after release, mechanism must be driven down to re-engage absorber	
e) Typical reactivity, fully inserted	$ 3 to $ 5
f) Typical reactivity per inch	$ 0.1 to $ 0.3
g) Typical rate reactivity increase in up travel (per second)	$ 0.01 to $ 0.02
h) Excess reactivity controllable with all rods, typically	$ 9 to $15

2. Regulating Rod

a)	Absorber Material	Stainless Steel
b)	Dimensions	Same as Shim Safety (No grooves)
c)	Travel	24 in.
d)	Release	None - does not drop on scram
e)	Typical Reactivity Fully inserted	$ 0.3 to $ 0.5
f)	Typical Reactivity per in.	$ 0.02
g)	Typical rate of Reactivity increase in up travel (per second)	$ 0.01

VII. Feedback Coefficients (Reference [9])

1.	Doppler Coeff ($/°C)	1.5×10^{-3}
2.	Void Coeff ($/% void)	
	a) Uniform void (1 to 10% void)	0.3
	b) Local void (1 to 14% void)	0.8
3.	Moderator Coeff ($/°C)	0.02

VIII. Kinetics Parameters (Reference [9])

1.	Prompt Neutron Lifetime	53 to 67 microsecs
2.	Effective Delayed Neutron Fractions	0.0074

3.9 Reactor Kinetics

An analysis determining important kinetics parameters (i.e. prompt neutron lifetimes and delayed neutron fractions) for the LEU fueled UVAR core is presented in Reference [9]. This analysis provided a comparison of kinetics parameters associated with LEU and HEU fueled UVAR cores. Results of that analysis are discussed below.

Prompt neutron lifetimes determined for both LEU and HEU fueled UVAR cores are presented in Table 3.2. Both graphite and water reflected cores were evaluated.

Table 3.2. Prompt Neutron Lifetimes For LEU and HEU Fueled UVAR Cores (Reference [9])

Core Description	Prompt Neutron Lifetime (μsecs) LEU	HEU-18
1. Graphite Reflector	67	79
2. Water Reflector	53	64

Information presented in Table 3.2 shows that the prompt neutron lifetime of the LEU core is about 15 % lower than that of the HEU core. This is as expected because of the significantly higher uranium-238 loading associated with the LEU fuel. Because the prompt effect is relatively small in the normal operations of the UVAR reactor, this difference is not expected to produce a noticeable change in the UVAR response to reactivity changes.

The effective delayed neutron fractions determined for both the LEU and HEU fueled cores were found to be essentially the same, at a value of about 0.0074.

Based on the information provided above, UVAR LEU cores one expected to behave essentially the same as past HEU cores, with regard to reactor kinetics.

3.10 Fission Product Inventory

Reference [11] states that the total inventory of fission products for LEU cores will not be significantly different from that associated with HEU cores. Additionally, because there are 22 plates in each LEU element as opposed to 18 plates in the HEU elements, the inventory per plate will be less in the LEU cores for the same operating histories.

3.11 Nuclear Instrumentation

3.11.1 General Description

The UVAR nuclear instrumentation consists of those components necessary to monitor and display the operating parameters over all ranges of operation, from start-up to full power, and to automatically terminate operation before any limiting safety system setting is reached. The overall system is shown in Figure 3-7.

The Source Range contains the circuitry necessary to monitor reactor power level and period from shutdown through six decades of power level increase. The circuit utilizes a fission chamber as a neutron detecting device. The fission chamber is movable by use of a switch on the console. It is moved out of the core after start-up in order to minimize the burn-up of U-235 and buildup of fission products in the chamber while operating at high power levels. Both power level and period measurement are displayed on reactor console meters and the power level is repeated on a chart. The Source Range instrumentation also prevents rod withdrawal unless minimum source counts are present.

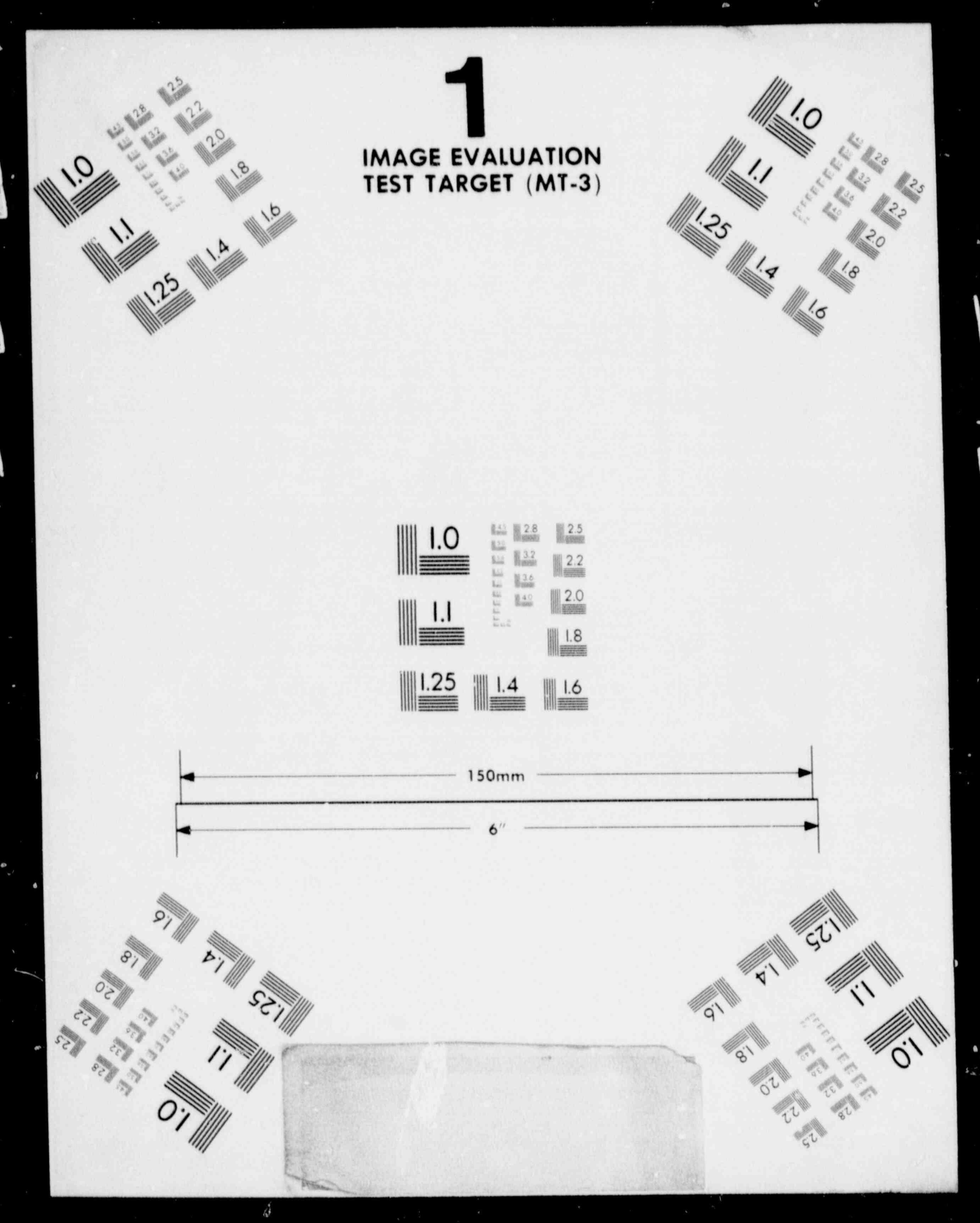
1
IMAGE EVALUATION
TEST TARGET (MT-3)
1.0
1.1
1.25
1.4
1.6
1.8
2.0
2.2
2.5
2.8
3.2
3.6
4.0
150mm
6"

1

IMAGE EVALUATION TEST TARGET (MT-3)

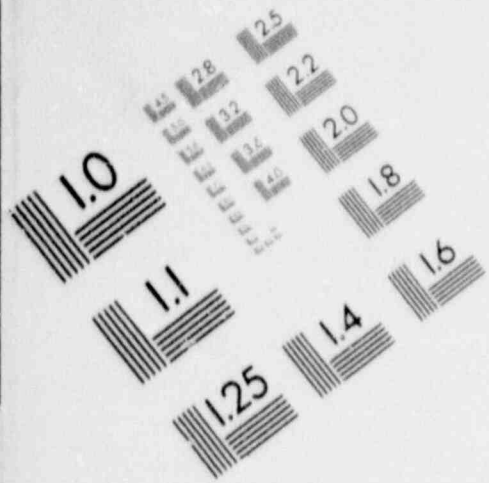

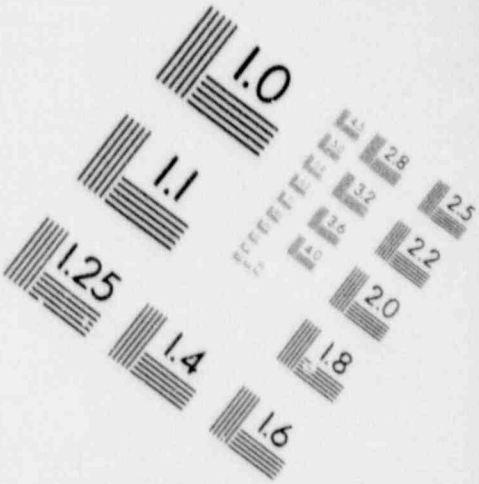

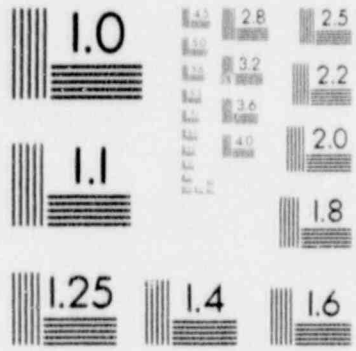

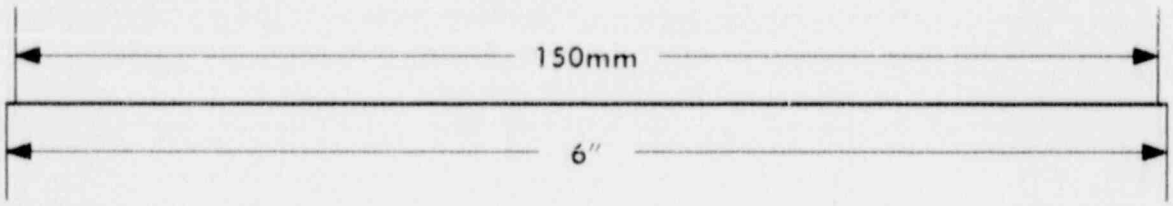

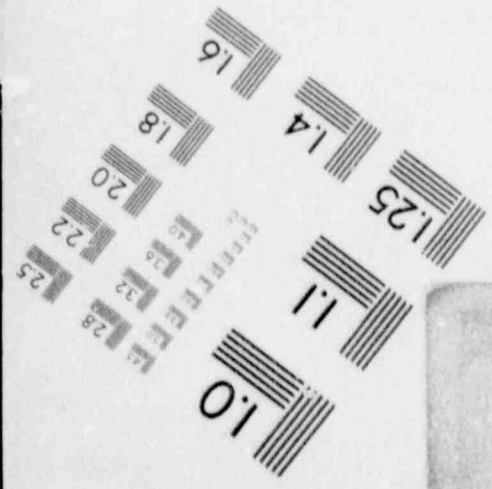

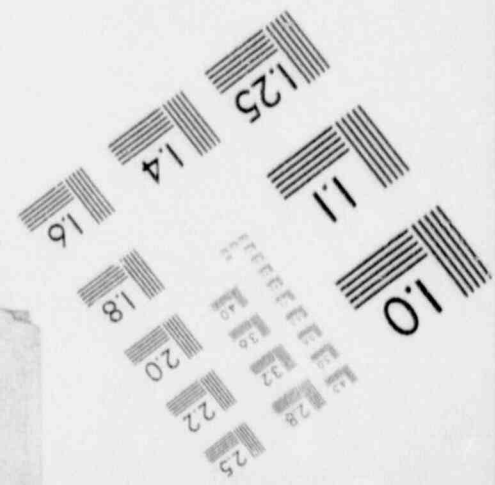

1

IMAGE EVALUATION TEST TARGET (MT-3)

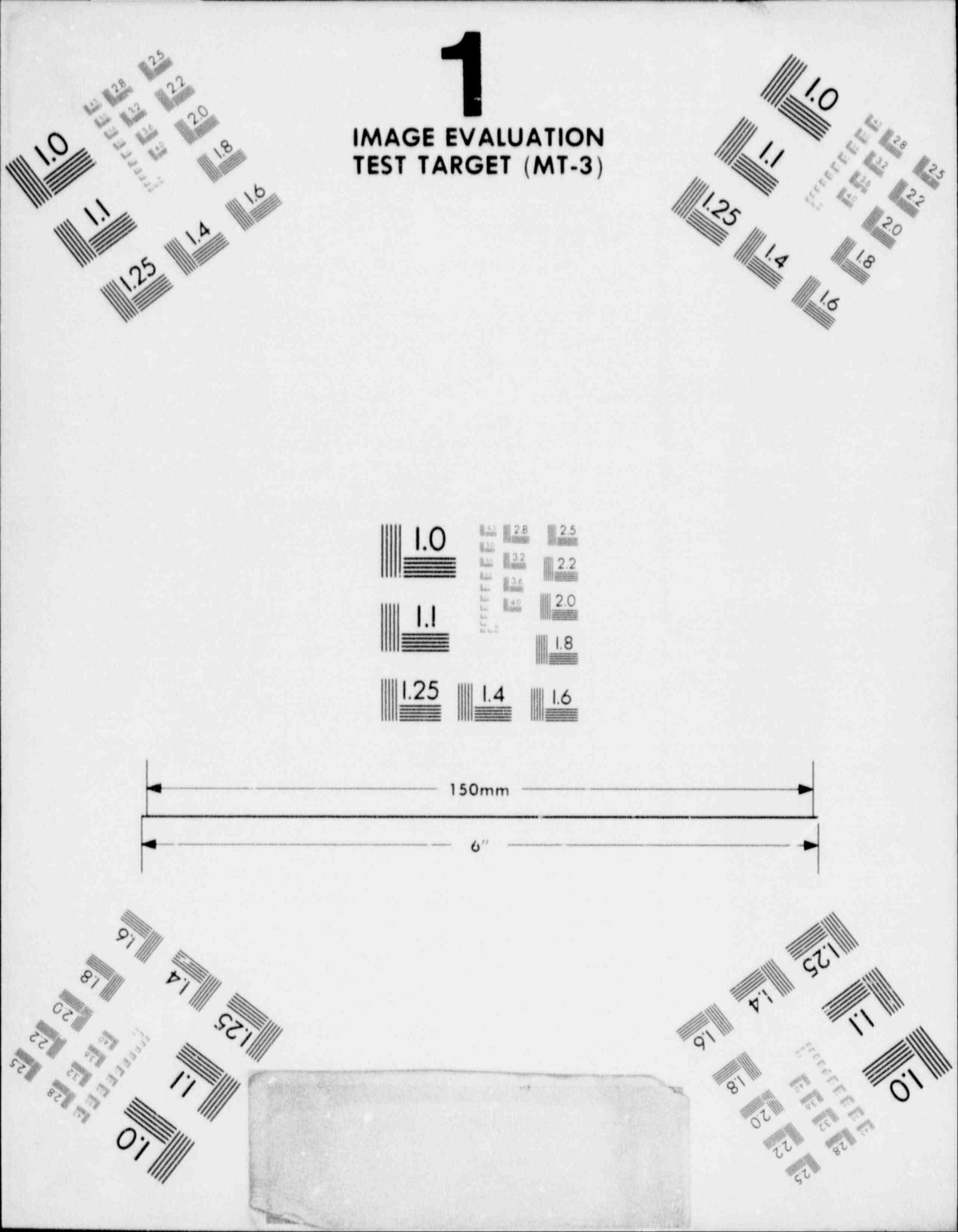

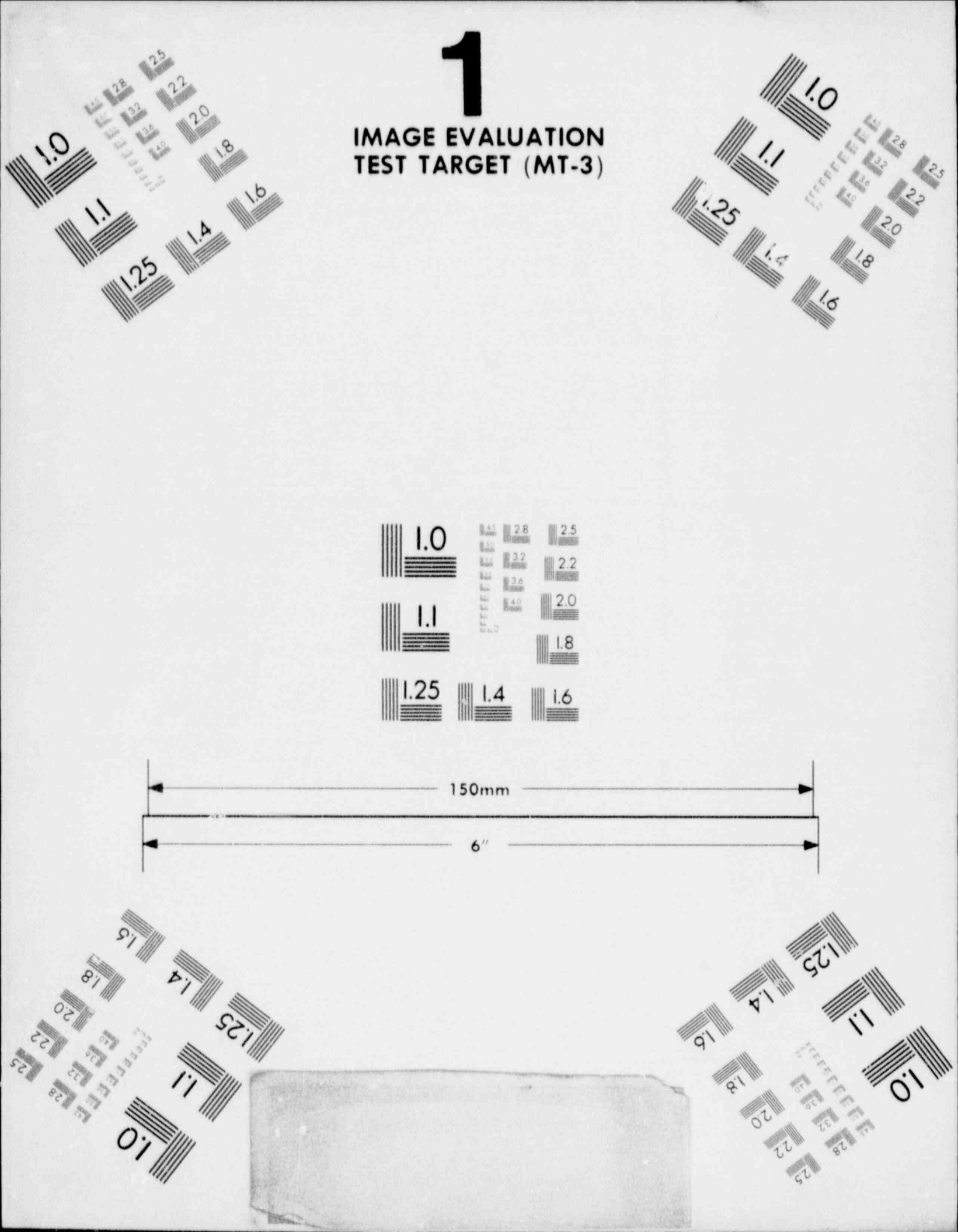
1
IMAGE EVALUATION
TEST TARGET (MT-3)
1.0
1.1
1.25
1.4
1.6
1.8
2.0
2.2
2.5
2.8
3.2
3.6
4.0
150mm
6"

FIGURE 3-7 NUCLEAR INSTRUMENTATION SYSTEM

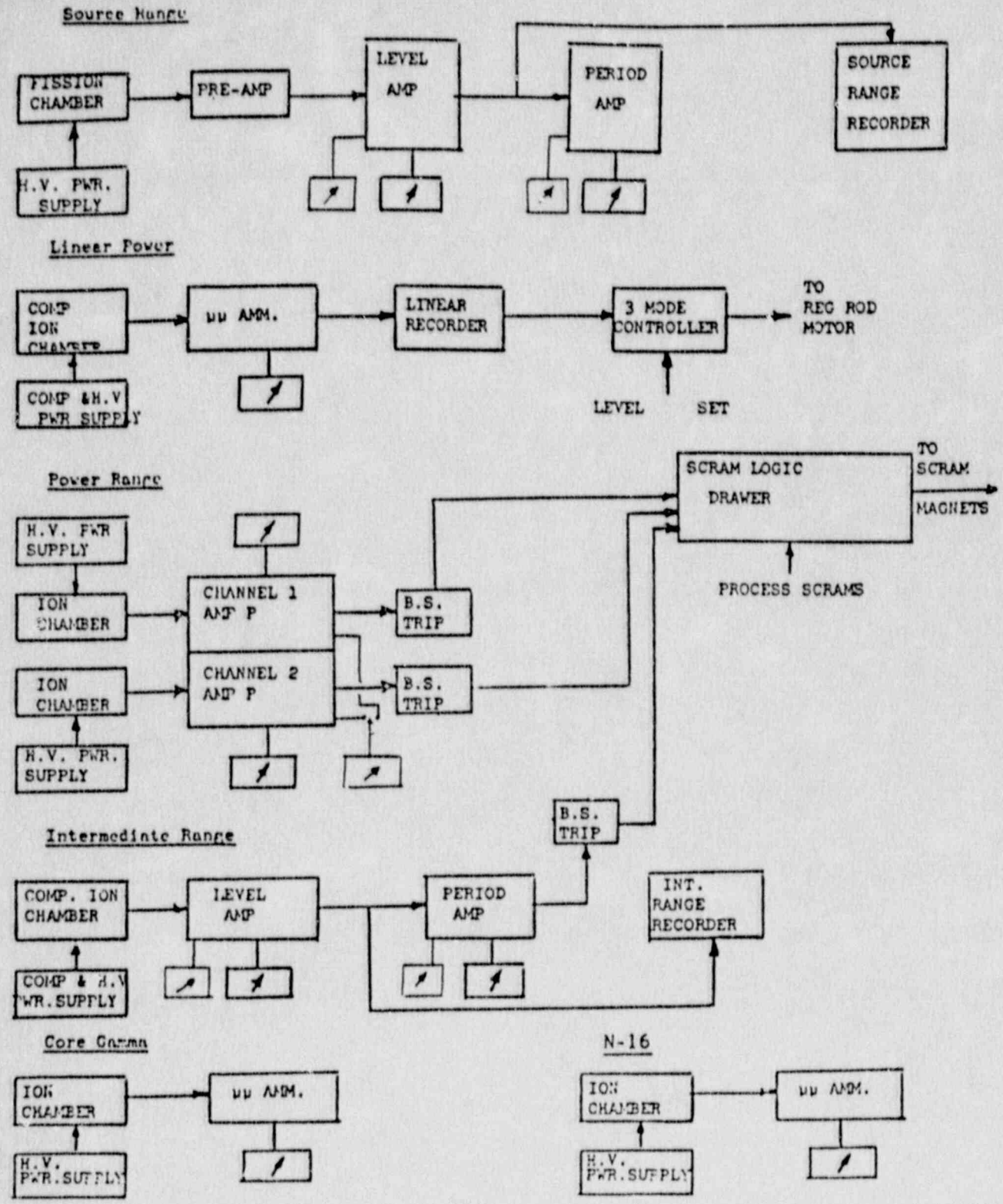

The Intermediate Range instrumentation receives its input from a compensated ion chamber and provides indication of power level and period over seven decades. Both power level and period measurement are displayed on the reactor console and power level indication is repeated on a chart. This instrument provides protection against a too rapid Figure 3.7. Nuclear Instrumentation period by scramming the reactor if the period is too short.

The Power Range instrumentation contains two completely independent power range channels, each of which indicate reactor power over a range of 0 to 150 percent. Each channel is supplied with an input signal from an independent uncompensated ion chamber. The output from these channels are displayed by separate meters on the reactor console. Each of these channels provides independent scram protection from high reactor power. There is a range switch to select full power indication of 2MW when in forced cooling or 200 kW when in natural convection.

Indication of reactor power is also provided by a linear power instrument over 9 decades of reactor power through a range selector switch. This instrument receives its input from a compensated ion chamber and its output is displayed by a meter and a chart on the reactor console. The linear power channel recorder indication also serves as the sensing element for the automatic control system (see Section 3.12) which operates the regulating rod to maintain a set power level.

In addition to the above instrumentation, the following indications are provided for comparative observations of reactor power.

An ionization chamber, located on the ground floor in the heat exchanger room (adjacent to the primary piping), is used to detect gamma

radiation from the decay of nitrogen-16. The signal from this detector is a function of reactor power and is displayed on a meter and a chart at the reactor console.

An ionization chamber, referred to as the core gamma monitor, is suspended at a fixed position typically about 7.0 feet above the reactor core. The signal from this detector is displayed on a picoammeter on the secondary console and is a measure of core gamma flux. The core gamma monitor is provided for comparative observation of power and has a floating point alarm that sounds on the common alarm panel.

3.11.2 Source Range Circuit

The Source Range Circuit (see Figure 3-8) contains circuitry required to monitor reactor power level and period from shutdown through six decades of power level increase. The circuit utilizes a fission chamber to detect neutrons.

A combination high voltage filter and pre-amp, mounted on the detector support pole, provides final high voltage filtering and a two stage pre-amplifier in one module. On entering the drawer, the input signal passes through a pulse amplifier, a discriminator, and a scale of two counter. The discriminator has a fixed discrimination level of 2.2 volts. Actual discrimination can be changed by varying the gain of the preamplifier or the pulse amplifier that precedes the discriminator. The scale of two counter divides the input frequency by two so the output is a square wave whose frequency is one-half of the input signal frequency. Log integrators A and B provide a DC voltage proportional to the log of the input frequency.

FIGURE 3-8 SOURCE RANGE DRAWER

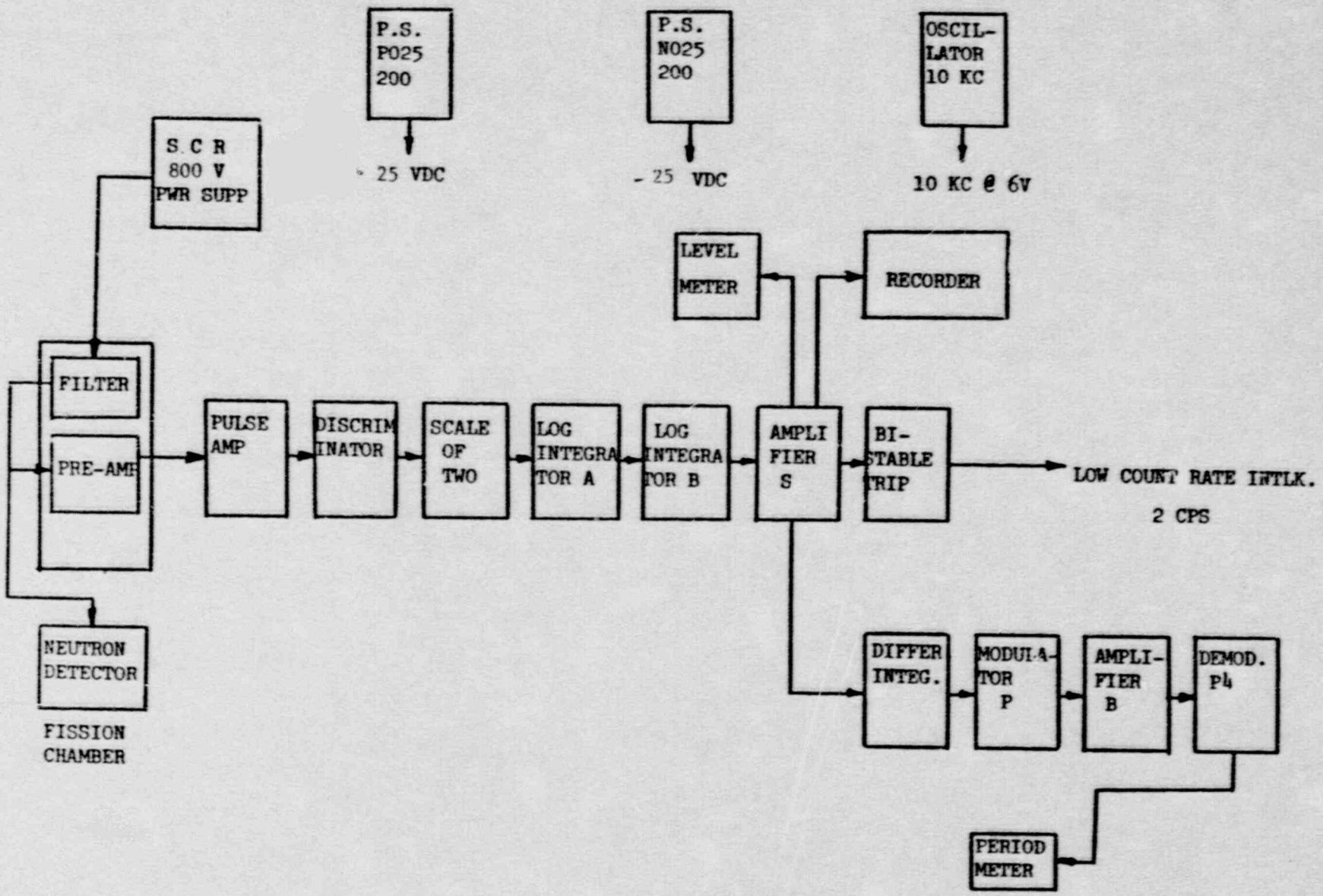

Amplifier S is a DC Amplifier whose output provides source range log level indication, level bistable trip logic, input to the source range period second, and remote recorder output.

The period section of the Source Range Drawer consists of a differentiator integrator (D-I) which converts the level input from Amplifier S to signal proportional to the rate of change of reactor power level. Modulator P combines the DC input from the D-I with a 10 KC input from the Oscillator module. The resultant, a 10 KC signal proportional in amplitude to the DC input signal, is applied to amplifier B.

Amplifier B is an AC amplifier which amplifies the signal from Figure 3-8. Source Range Drawer Moderator P and feeds it to demodulator P4 where the AC signal is converted back to a DC signal proportional to the exponential rate of change of reactor power. The Demodulator P4 feeds a front panel period meter.

The bistable module installed in the Source Range Drawer is a solid state multivibrator circuit which prevents rod withdrawal in the absence of a sufficient count rate. The output is a logic signal of 0 volts (tripped) if the count rate is less than 2 counts per second, or 10 volts (untripped) if the count rate is greater than 2 counts per second. The Source Range Drawer contains a test module that performs alignment and operational checks of both the level and period sections without the use of additional test equipment.

3.11.3 Intermediate Range Circuit

The Intermediate Range circuit (see Figure 3-9) receives its input from a compensated ion chamber (CIC) and provides log level indication

over several decades, period indication and scram and control logic outputs.

The power supply provides 200-800 volts DC high voltage to the CIC with regulation as close at ± 0.1%. A variable DC power supply provides variable compensating voltage to the CIC.

The DC current proportional to neutron level from the CIC is fed first to Modulator L where it is dropped across a string of forward biased diodes to a voltage proportional to the Log of the current and is combined with a 10 KC sine wave. The resultant is a 10 KC signal proportional in amplitude to the Log of the DC input current. The Demodulator, as the name implies, converts the AC output from Amplifier B back to a DC signal which is proportional to the Logarithm of reactor

FIGURE 3-9 INTERMEDIATE RANGE DWR.

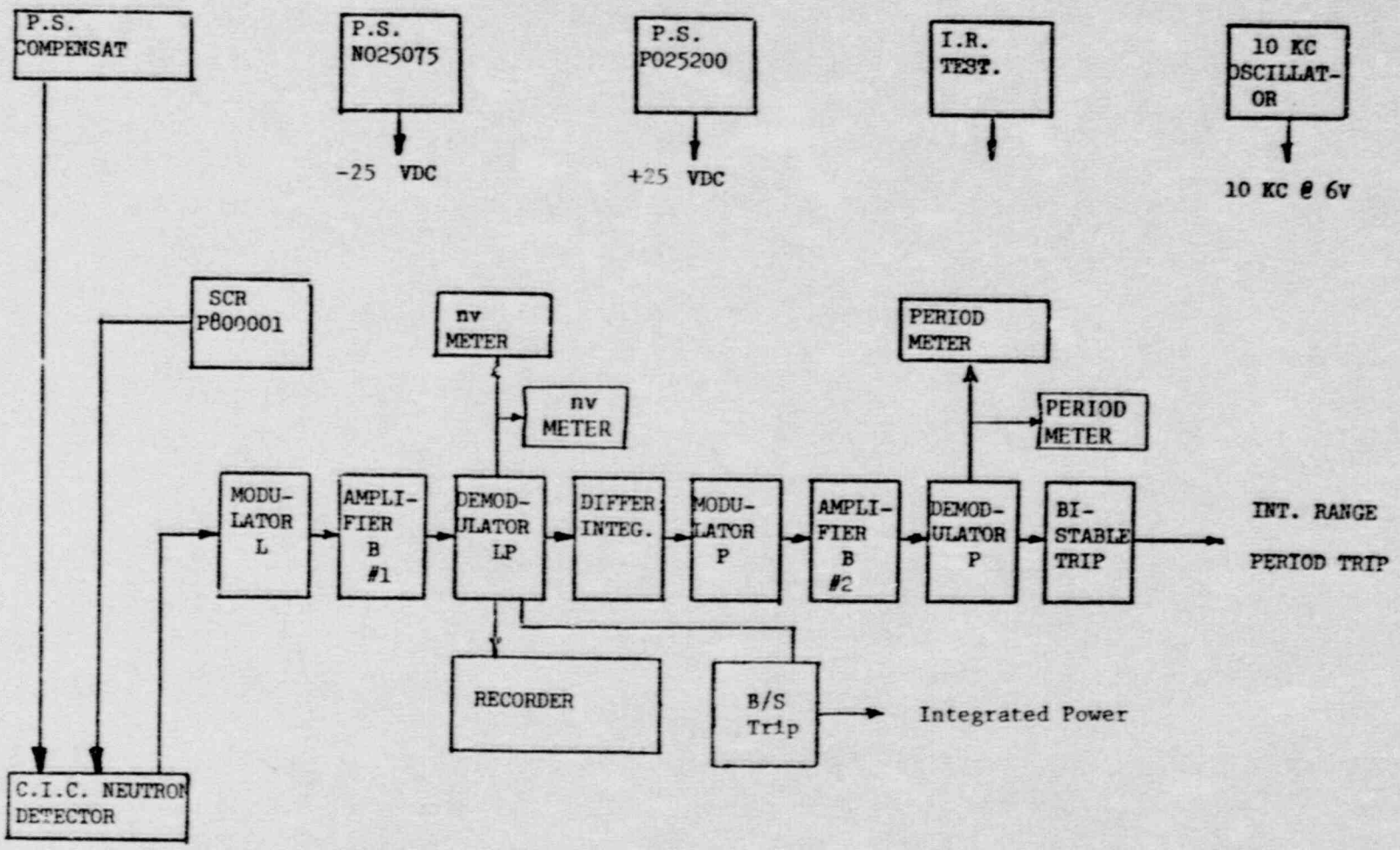

flux level. The log level output of the demodulator feeds five devices:

1) Local log level meter

2) Remote log level meter

3) Remote recorder

4) Differentiator-Integrator for the period circuit

5) A bistable that activates the power integrator

The Differentiator-Integrator accepts an input from the Demodulator and converts it to a signal proportional to the exponential rate of change of the neutron flux. Modulation of this DC period takes place in Modulator LP where the signal is combined with a 10 KC sine wave and the output feed to Amplifier B No. 2 for amplification. Demodulator P receives an amplified AC signal from Amplifier B No. 2 and converts it to a DC signal which is proportional to the exponential rate of change of neutron flux (period). The outputs of the Demodulator P are:

1. A front panel period meter

2. A remote period meter

3. A bistable period trip set at a less than 3 seconds

The bistable modules of the intermediate range circuit are identical to those in the source range circuit

The Intermediate Range drawer contains a test module that performs alignment and operational checks of both the level and period sections without the use of additional test equipment.

3.11.4 Power Range Drawer

The Power Range drawer (see Fig. 3-10) contains two completely independent power range channels which will indicate reactor power over the range of 0 to 150 percent. Each power range channel has its own detector power supply, and its own ± 25 volt power supply. The

FIGURE 3-10 POWER RANGE DRAWER

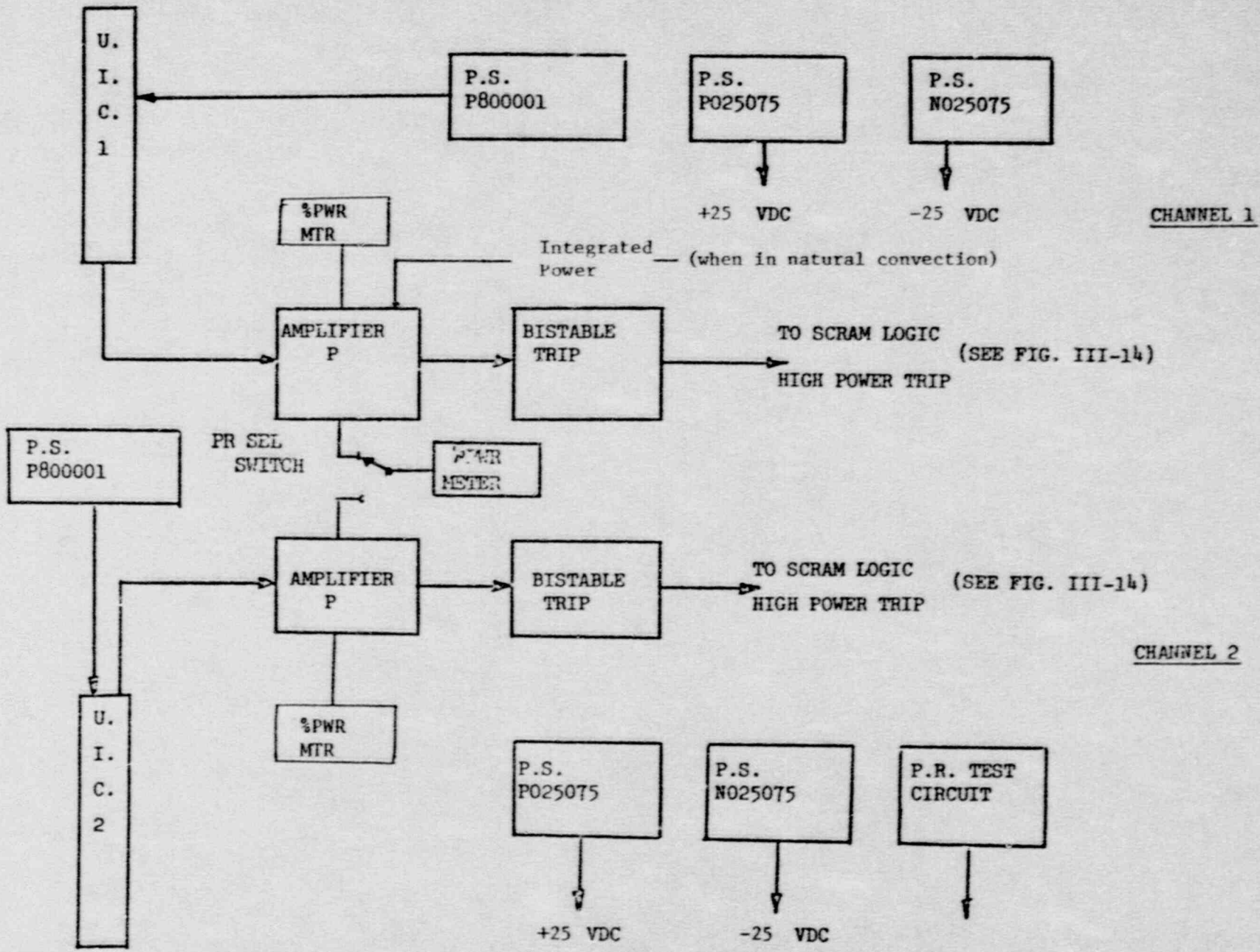

the power range drawer. Each power range channel is supplied an input from an uncompensated ionization chamber (UIC). Outputs from each channel include a common local power level meter, separate remote power level meter, and a high power bistable trip logic signal. In addition, Power Range #1 supplies a signal to the power integrator when in natural convection.

A high voltage power supply provides 200-800 volts DC to the detector. The output of the UIC is a DC current proportional to reactor power. The signal is fed to Amplifier P, which is a DC amplifier, where the signal is amplified to a level suitable for use. When in the "200 kW" range the full signal is amplified. When in the "2MW" range only one tenth of the signal is amplified. The outputs of Amplifier P are:

1. Local common percent power meter
2. Separate remote power meter
3. High Power Bistables
4. Power signal to the power integrator when in natural convection

It should be noted that the amplifier is designed so that a short or open circuit, in any of the outputs, will not cause the other outputs to vary more than a fraction of a percent.

The bistable modules of the power range circuits are identical to those described previously for the Source Range Circuit.

The Power Range drawer contains a test module that performs alignment and operational checks of each power range channel without the use of additional test equipment.

3.11.5 Scram Logic Drawer

The Scram Logic drawer (see Figure 3-11) contains the logic circuitry necessary to process the scram function inputs and to shutdown

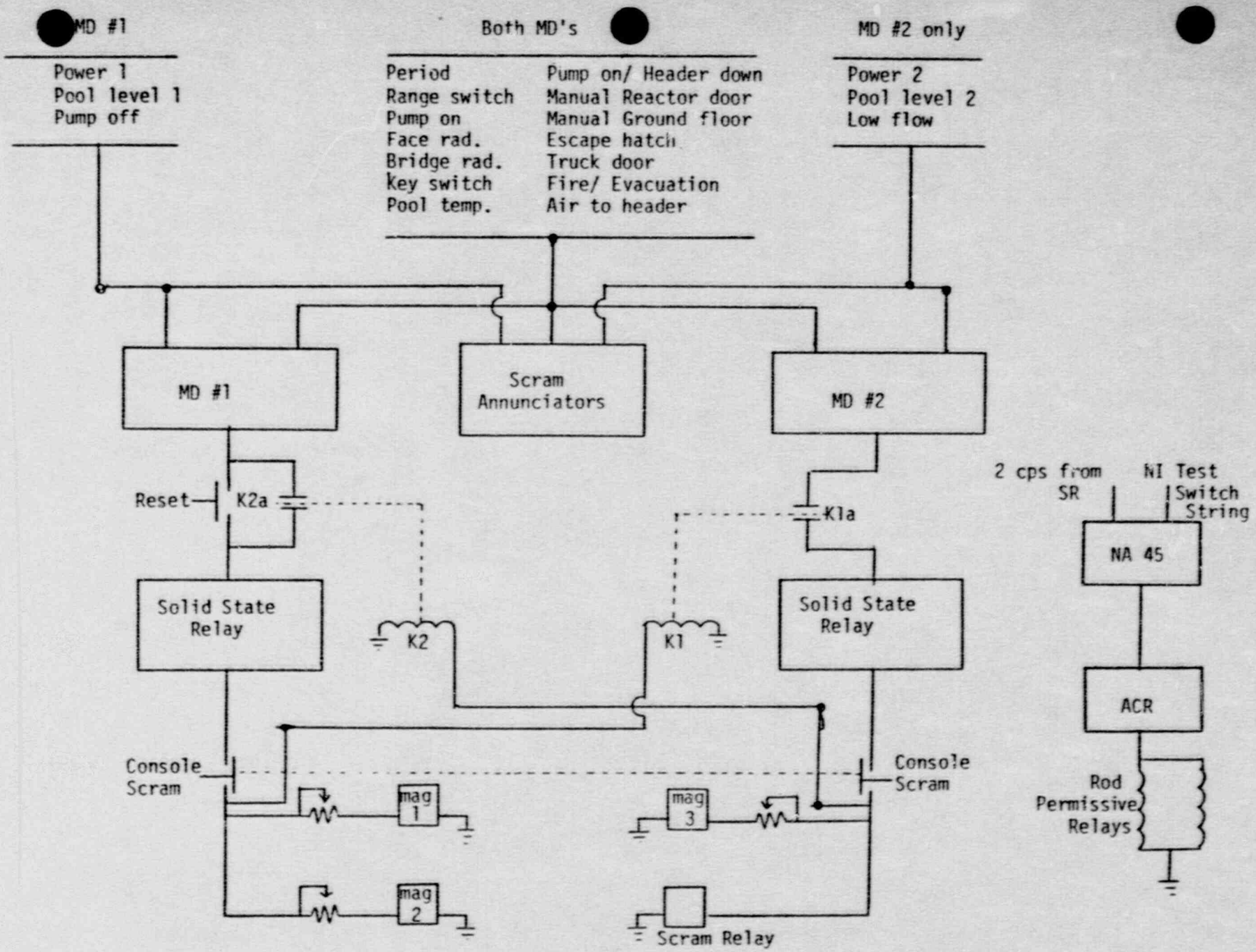

Figure 3-11 Scram Logic Drawer

the reactor automatically should conditions warrant. The drawer also contains the interlock circuitry to prohibit safety rod withdrawal if certain minimum conditions are not met.

To understand the operation of the Scram Logic circuit, it is only necessary to understand the operation of four basic modules. Negative logic is used throughout the system, in that the normal, safe, input signal ±10 volts and the abnormal, unsafe, signal is 0 volts. All available inputs to these modules may or may not be used.

1. Transistor Gate NA-45 consists of five separate, four-input, negative logic AND gates, hence the designation NA-45. For each separate AND gate, all four inputs must fall to zero volts to obtain a 0-volt output signal. Any input at +10 volts will hold the output of that gate at +10 volts. The inputs (up to 20) are logic 0 or +10 volt signals and the outputs (up to 5) are also logic 0 to +10 volt signals. As explained later, the rod withdrawal interlock is derived from two logic inputs to NA-45.
2. The Auxiliary Control Module takes logic inputs in the form of 0 or +10 volt signals and provides a relay output capable of handling 110 VAC and 2 amps. The input stage consists of a four input OR gate where all inputs must be at +10 volts to have the relay energized. The relay is de-energized if any input is at zero volts.
3. There are two Mixer Driver B's. A Mixer Driver B is essentially a 28 input OR gate. Any one of the 28 logic inputs falling to 0 volts is sufficient to cause the output to fall to

0 volts. Only when all inputs are at +10 volts is the output at +10 volts. The input is 28 logic signals, while the outputis one logic signal.

4. There are two Solid State Relay modules. A Solid State Relay Module takes one logic signal (0 to +10 volts) as its input and provides up to 5 amps DC of output current to the scram magnets if a safe input condition exists. The Solid State Relays are subject to one type of failure that could render the model inoperable as a device for cutting off magnet current. This type of malfunction of the entire module would necessitate the simultaneous failure of two components within the module, in the form of a short circuit in two series silicon controlled rectifiers (SCR). Built-in circuitry within the drawer has been provided that will annunciate a short circuit in one SCR as a warning light. If a short circuit occurs subsequently in the other SCR, the solid state relay will continue to provide current to the scram magnets even if a unsafe input is applied. As will be explained in the overall operation of the Scram Drawer, even the existence of the above mentioned conditions will not render the entire system inoperable as a parallel network exists which could de-energize at least one safety rod and thereby shut the reactor down.

The Scram Logic Drawer, as a safety system, can be divided into two sections. Namely, a scram logic process section and an activation section. The process section takes logic signals from the various

bistables, power supplies and relays; processes these signals with respect to preconditions and emits output signals that exercise either scram control or rod interlock control. The modules included in this section are the NA-45 gate circuits and the Auxiliary Control Relay. The actuation section, consisting of the Mixer-Drivers and the Solid State Relays, take only safe or unsafe logic inputs, and, depending on the nature of the inputs, control current to the safety rod scram magnets.

The rod withdrawal interlock is derived from two logic inputs to NA-45 (1). A +10 volt signal is emitted from the source range level bistable if the source count rate exceeds 2 counts per second. A second +10 volt signal comes from a series circuit that is closed when source range, intermediate range, pool temperature, and power range instruments are not in test. These two signals are fed to one gate. If these inputs are at +10 volts the appropriate output is at +10 volts on an Auxiliary Control Relay (ACR) which energizes its output relay permitting safety rod withdrawal. If either input to the ACR drops to zero, this zero volt input signal will cause the output relay to de-energize, preventing the withdrawal of any shim rod.

The reactor can be operated at 2 megawatts with forced convection cooling or at 200 kilowatts with natural convection cooling. The High Power Trips are initiated from the power range drawer (see Figure 3-10) and provide overpower protection in both the natural convection cooling mode and the forced convection cooling mode of operation as shown in Figure 3-12. A range switch is used to determine the scram point for each mode.

In the natural convection mode (see Figure 3-12), the flow header is down and header position relay CE is de-energized. A safe +10 volt logic

FIGURE 3-12 HIGH POWER TRIP

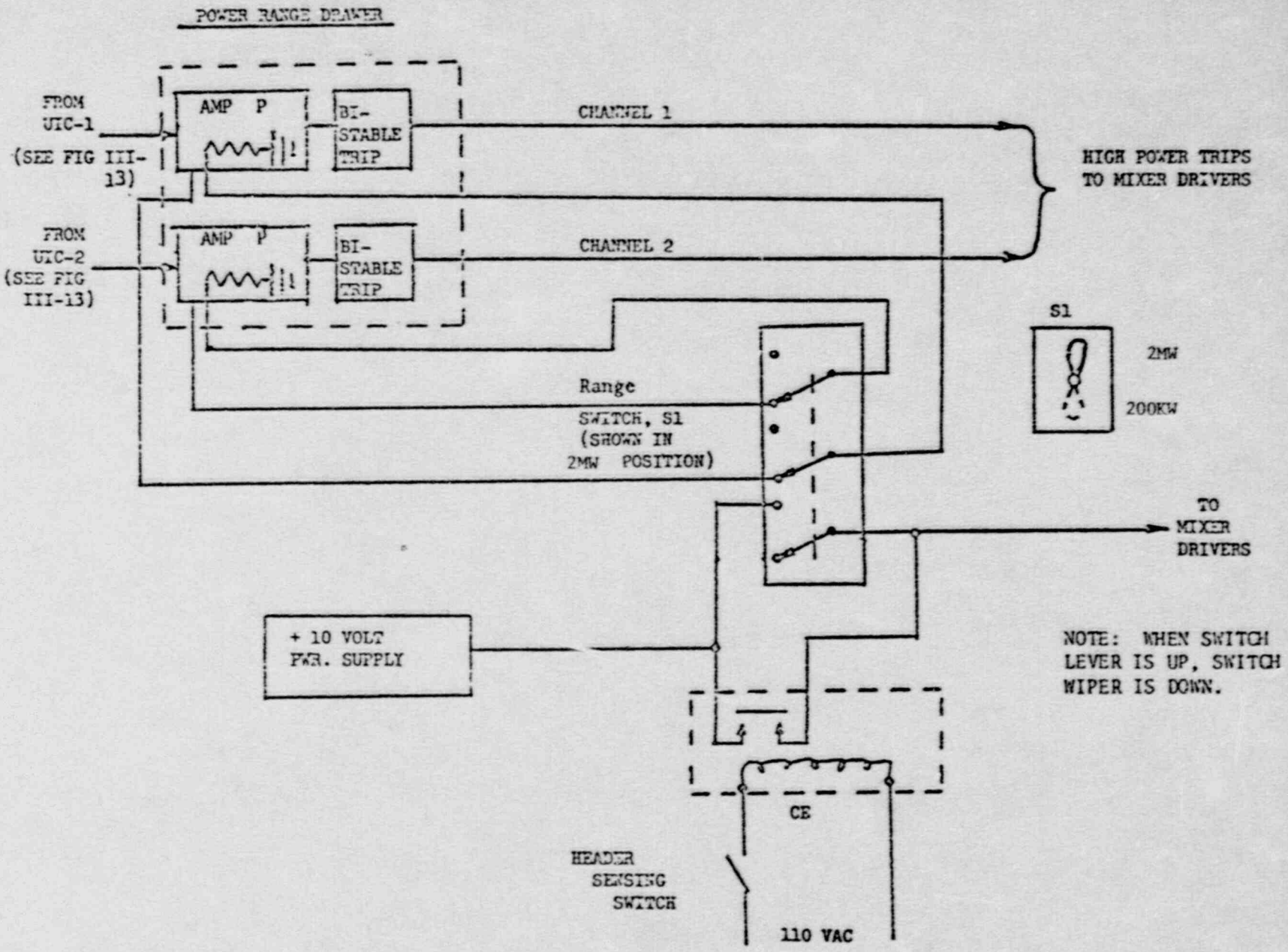

signal is passed through the range switch only if the switch is in the 200 kW position. Under this condition, the power range channels are sensitive over a range of 0-300 kW for an amplifier output of 0-150% of normal range, i.e., 100% of output from the amplifier corresponds to 200 kW. If the reactor power level reaches 250 kW, the power range channel will indicate a power level of 125% and will send an unsafe (0 volt) Figure 3-12 High Power Trip signal to the mixer drivers scramming the reactor.

When the reactor is operating in the forced convection mode, the flow header is in the UP position. Therefore, relay CE is energized, which allows the range switch to be placed in the 2MW position without losing the 10 volt safe signal. In the 2MW position, the range switch also reduces the output sensitivity of the two power range amplifiers by a factor of ten. Each channel indicates over a range of 0-150%, which corresponds to a maximum reactor power of 3MW. The scram trip point is also increased by a factor of ten by placing the range switch in the 2MW position and will scram the reactor when reactor power reaches 2.5 MW. When operating in the natural convection mode, any attempt to change the position of the range switch to the 2MW position will immediately initiate the scram, through loss of the 10 volt signal through the switch.

Referring again to Figure 3-11, the intermediate range period trip function originates at the period trip bistable, (see Figure 3-9). This logic signal is sent directly to the Mixer Drivers.

The scram actuating portion of the Scram Logic Drawer consists of two independent channels cross connected in such a way as to afford

maximum scram protection against component malfunction. The two Mixer Drivers receive several logic inputs in parallel. If one of these inputs is an unsafe signal (0 volt), the output of both MD's will be at zero volts. The input to each Solid State Relay going to zero causes the outputs to stop conducting, cutting off current flow to the scram magnets. To nullify the effects of a complete failure of one MD, the two scram channels are cross connected through relays R1 and R2. If a failure occurred in one of the MD's, say MDB1, which would prevent it from tripping off when an unsafe input signal is received, MDB2 would be tripped off by the same unsafe input signal, SSR2 would stop conducting, dropping magnet 3 and de-energizing relay R2. The contacts on R2 which feed an input to SSR1 would be opened, causing SSR1 to also stop conducting the dropping magnets 1 and 2.

Both mixer drivers receive separate inputs from redundant channels (i.e. high power, low pool level, and low flow). An unsafe (0 volt) signal from one of these inputs causes the affected mixer driver to give a 0 volt output causing a reactor scram.

The simultaneous failure of both MD's in the safe mode or a failure of four diodes in two separate modules, the SSR's, could result in the scram logic system being rendered as "can't scram."

3.12 Scrams, Interlocks, and Alarms

3.12.1 Scrams

The following scrams are required by the UVAR Technical Specifications:

Scram	Operating Mode Required
1. 2 Safety Channels for high power scram	
a) range switch in high power position	Forced convection
b) range switch in low power position	Natural convection
2. Bridge radiation monitor scram	All modes
3. Pool water high temperature scram	All modes
4. Loss of power to primary pump scram	Forced convection
5. Application of power to the primary pump scram	Natural convection
6. Low primary coolant flow rate scram	Forced convection
7. Manual scram button	All modes
8. Fast reactor period scram	All modes
9. Air pressure to header scram	All modes
10. Low pool level scram	Forced convection

The above listed scrams must be operational as required during reactor operation. Other scrams, not listed, may be added as appropriate to provide for added protection of personnel, experiments and equipment.

3.12.2 Interlocks

The UVAR Technical Specifications requires an interlock on the Source range instrument which prevents shim rod withdrawal unless a minimum of 2 cps are detected.

3.12.3 Alarms

Both audible and visual alarms are used at the reactor console to alert the operator of alarm conditions. A continuous tone audible alarm and a red light visual alarm accompanies a reactor scram signal. This audible alarm may be silenced by either resetting the scram logic drawer

or pressing the "silence" button on the common alarm panel. The visual alarm is cleared only by resetting the scram.

An intermittent tone sounds and a visual indicator is actuated for each of the following conditions:

a) Regulating rod control shifting from automatic to manual

b) High radiation on any area monitor or on either argon monitor

c) High radiation on core gamma monitor

d) High radiation on criticality monitor

e) High radiation on constant air monitor

f) Entry into the demineralizer room

g) Entry into the heat exchanger room

h) High differential temperature across reactor core

i) High demineralizer conductivity

j) Secondary pump de-energized

The audible alarm will automatically reset after about two minutes or may be reset manually by pressing the "silence" button.

Local alarm bells are supplied at the heat exchanger room and demineralizer room when the key switch is on which warns personnel entering the area of a possible high radiation area.

Other audible and visual alarms may be used, as necessary, to provide extra personnel safety or equipment protection.

3.13 Automatic Control For Maintaining Constant Power

A voltage signal proportional to reactor power is developed by a slide wire potentiometer in the linear power recorder. This signal is compared to the voltage developed by the "Power Set" potentiometer on the control console. Any difference in these signals is displayed on a

deviation meter and supplied to the controller as an error signal. The controller converts this small error signal into 60 cycle power either in phase or 180° out of phase with line voltage. This power supplied to the servo motor for the regulating rod will drive the rod in if the linear signal is higher than the power set voltage or out if the linear signal is below the power set voltage.

Several conditions will automatically cause control to shift into the manual mode and sound an alarm to alert the operator that power is no longer being controlled automatically. These are:

1) Any attempt to move the regulating rod with the normal control switch; this insures that manual control is always instantly available to the operator.

2) The regulating rod either at its top limit or bottom limit; this insures that regulating rod has free movement to control reactor power.

3) The error signal, as displayed on the deviation meter, exceeds 7.5% (arbitrary units); this insures control is shifted if the regulating rod is unable to control power for any reason, such as the reg rod being stuck.

4) The linear power recorder is turned off. This ensures the feedback loop is complete.

5) A switch is provided that allows the operator to select either the manual or automatic mode of operation.

References For Chapter 3

1. EG&G Idaho, Inc.,"University of Virginia Test Research And Training Reactor 2, Standard And Partial Fuel Element Assembly", Drawing Number 428500, Revised August, 1989.

2. EG&G Idaho, Inc., "University of Virginia Test Research And Training Reactor 2, Control Fuel Element Assembly", Drawing Number 428501, revised August, 1989.

4. EG&G Idaho, Inc.,"University of Virginia Test Research And Training Reactor 2, Sideplates", Drawing Number 428502, Revised August, 1989.

3. EG&G Idaho, Inc.,"University of Virginia Test Research And Training Reactor 2, Shock Absorber Seat, Adapter, & Bail", Drawing Number 428503, Revised, August 1989.

4. EG&G Idaho, Inc.,"University of Virginia Test Research And Training Reactor 2, Fuel & Guide Plates", Drawing Number 428504, Revised August, 1989.

5. EG&G Idaho, Inc.,"Test Research And Training Reactor LEU Fuel Plate", Drawing Number 422264, Revised August 1989.

6. Diamond Power Speciality Corporation, "Shim Safety Rod Assembly Top Magnet Control", Drawing #EX-7935-0, April 21, 1958.

7. Diamond Power Speciality Corporation, "27 Feet Regulating Rod Assembly", Drawing #EX-7769-0, April 21, 1958.

8. Diamond Power Speciality Corporation, "Element-Shim Safety", Drawing #7006181122, October 26,1960.

9. Freeman, D., Neutronic Analysis For The UVAR Reactor HEU To LEU Conversion Project, Master's Thesis For The Nuclear Engineering and Engineering Physics Department, University Of Virginia, July, 1989.

10. EG&G Idaho, Inc.,"TRTR-2 For University of Virginia Standard, Partial And Control Fuel Element Assemblies For The University Of Virginia Reactor", Revision 1, June, 1989.

11. U.S. Nuclear Regulatory Commission, Safety Evaluation By The Office Of Nuclear Reactor Regulation Supporting Conversion Order To Convert From High Enriched To Low Enriched Uranium Fuel, Facility Operating License NO. R-61, Worchester Polytechnic Institute, Docket No. 50-134, September 12, 1988.

4.0 REACTOR SYSTEMS

4.1 Reactor Pool

The pool in which the reactor operates is 32 feet long, 12 feet wide, 26 feet 4 inches deep, and holds about 75,000 gallons of water. An aluminum gate is provided approximately mid-way of the pool so that either side may be drained independently of the other while the reactor itself is adequately shielded by the water in the undrained side. With the reactor in position at a far end of the pool, the radiation level in the emptied section will be low enough to permit personnel to alter or set up experimental equipment and perform maintenance.

The south end of the pool is above ground level and faces the main radiation laboratory experimental area. The shielding provided by the water and the pool wall is augmented by the addition of sufficient concrete to reduce the radiation well below tolerance levels at maximum operating power. The south wall of the pool is penetrated by experimental facilities which will be further explained in Section 6.0.

The level of the water is about 20 feet above the active core when the pool is full. An alarm and scram is actuated by two pool level devices if the pool level drops 19 feet 2 inches above the top of the active core.

Figure 3-1 shows a vertical section of the pool and related building spaces.

4.2 Filling and Draining the Pool

Two systems may be used for filling the UVAR pool; 1) a

dedicated fresh water make-up system, and 2) the main demineralizer system.

The dedicated fresh water make-up system is located in the UVAR room and consists of a small filter and H-OH mixed bed ion exchangers to which city water is supplied. The system discharges deionized water into the UVAR pool through a stand-pipe to preclude the possibility of pool water backflow into the city water system. The system has a flow rate of about 5 gallons per minute.

The pool can also be filled using the main demineralizer system as shown in Figure 4-1. City water enters a catch tank through a hand valve and a float valve. The water entering the pool through the demineralizer system is drawn from this tank. The float valve discharge is higher than the tank overflow, thus precluding the possibility of any backflow of radioactive water into the city water system. The pool can be filled at a rate up to about 20 gallons per minute through a mixed bed demineralizer. With the pool gate in place, either side of the pool may be filled independently.

The pool is drained through two manually operated valves located in a sump pit in the heat exchanger room. These valves are normally locked shut. Either side of the pool may be drained when the gate is in place. The discharge from the drainage system empties into the waste pond and is described in Section 4.8.

4.3 Primary Cooling Systems

With the reactor in position at the south end of the pool, an air operated header may be raised into place. This header is actuated by the emission of compressed air at about 50 psi into a header skirt which floats the header up to the reactor grid plate. Once positioned the header is held in place by a differential pressure of 0.30 psi created by the downward flow in excess of 1000 gallons per minute through the reactor to the primary piping system. After the pump has started and sufficient flow is established to hold the header in place, the air pressure is vented to allow the header to drop automatically for natural convection cooling in case of pump failure. Such pump failure initiates a scram as does the existence of 2 psi air pressure in the header. This precludes the possibility of raising the header while the reactor is operating in the natural convection mode with the pump secured. The reactor is in a scram condition if the pump is operating with the header down.

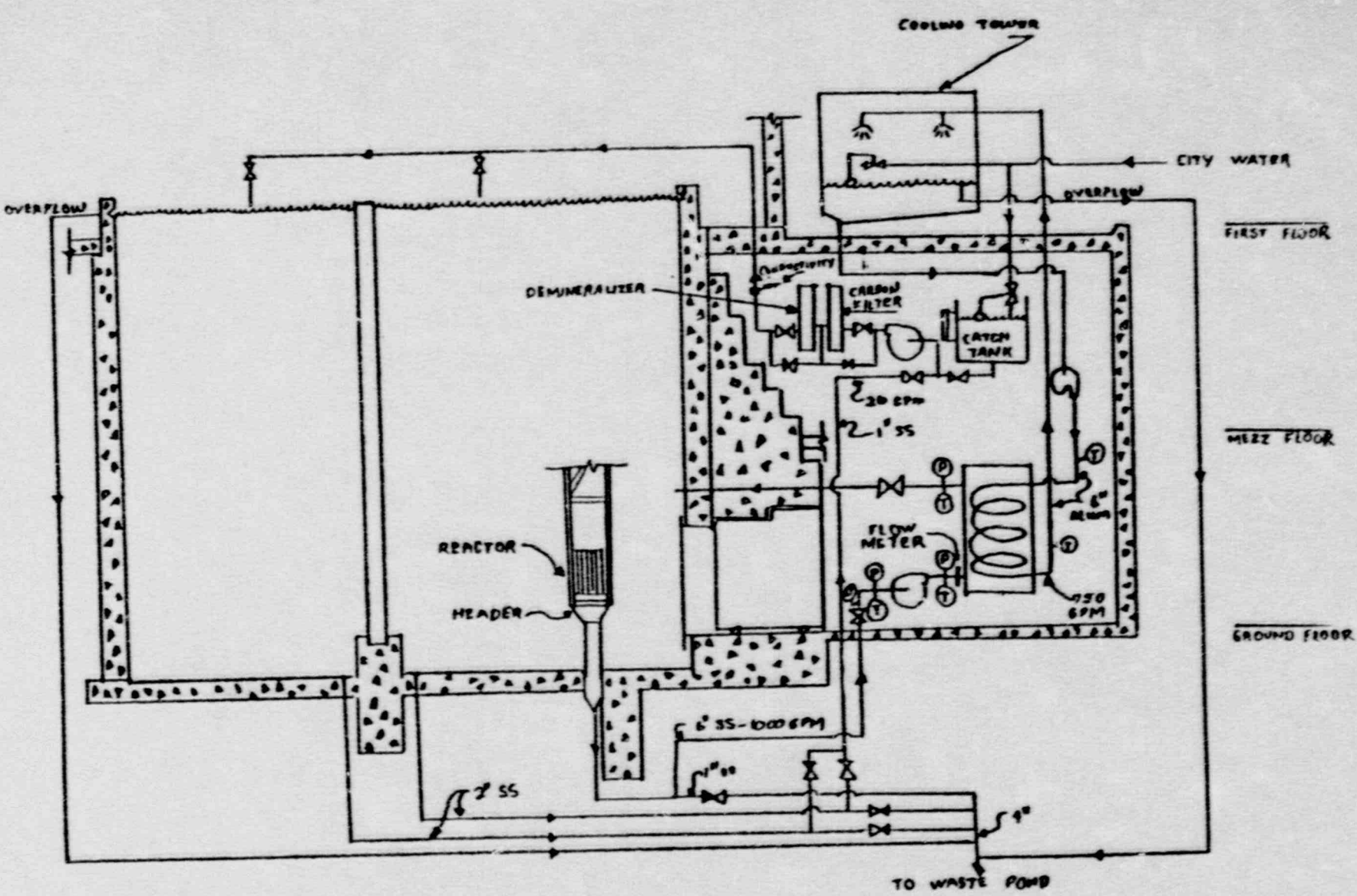

Figure 4.1 Cooling System Flow Diameter

The water flows from the header through a six inch line to a strainer and the primary pump. The primary pump is of the centrifugal type with a stainless steel casing, impeller, and shaft. A self-adjusting mechanical seal is used to seal the shaft. The pump is driven by a 30 horsepower 1700 RPM induction motor and is rated at ~ 1100 gallons per minute flow against a 50 foot head of water. The actual flow rate is ~1055 gal/min. The flow rate is measured by the differential pressure across an orifice in the primary piping and displayed on the secondary console.

The water proceeds through the six inch line, through an orifice, used to measure the flow rate, into the shell side of an aluminum tube and shell heat exchanger. The primary water makes one pass through the heat exchanger and is returned to the pool. The water enters the pool through a flow diverter which directs it toward the wall at the greatest distance from the reactor, thus gaining the greatest mixing and minimizing nitrogen-16 gamma activity at the pool surface.

Water temperature and pressure are measured on the inlet and outlet sides of the heat exchanger. The temperatures are displayed on the secondary console in the reactor room. A separate continuous monitor is located above the core which will initiate a scram if the pool water temperature exceeds 105°F.

4.4 Measurement of Temperature Differential

A system has been installed to continuously monitor the temperature differential across the reactor core when it is operated with forced convection cooling. The ΔT value, measured directly by this system, can be related to the reactor thermal power level. Separate coolant inlet and outlet temperatures are read periodically and subtracted manually to obtain this information in addition to the constant monitor.

The sensing elements used in the system are platinum resistance bulbs. One is located in the reactor pool, about three feet above and to the side of the top of the core, to indicate core inlet temperature. Core outlet temperature is sensed in the primary coolant line, just upstream of the primary coolant pump. The sensing elements are placed in a resistance bridge network where the differential temperature values are measured, then amplified and displayed on a digital meter. An alarm with an adjustable setpoint is provided to give alarm signals for ΔT values in excess of pre set levels. The range of the instrument is 0-20°F, while the normal ΔT across the reactor (at two megawatts) is about 13°F.

4.5 Secondary Cooling System

Water on the secondary side of the heat exchanger is pumped at about 1200 gallons per minute from the basin of a conventional cooling tower rated at a cooling capacity of 2 MW with a 95°F entering water

temperature and 73°F wet bulb atmospheric temperature. The system utilizes a conventional centrifugal pump driven by an induction motor. Water for evaporative cooling in the cooling tower comes directly from the city water supply and overflows to the waste pond. Water temperature is measured on the inlet and outlet of the heat exchanger and is displayed on the secondary console in the reactor room.

4.6 Design Specifications

The design specifications for the Heat Exchanger, Cooling Tower, Secondary Pump and Primary Pump are given in Tables 4.1 through 4.4.

4.7 Water Purification

The pool water purity is maintained by circulating it at a rate of 20 gallons per minute through a carbon filter and a mixed bed ion exchange demineralizer. The water is normally maintained at a pH of 6.0 to 7.0 with a conductivity of less than 5 micro mohs.

4.8 Liquid Waste Disposal System

The reactor facility can collect radioactive liquid waste in two underground retention tanks of 5000 gallons each located outside of the Reactor Facility building, but within the site area. The waste is recirculated and filtered, as well as given decay time before it is either discharged into the pond or discharged along with the pond as normal procedure. Other storage tanks within the Reactor Facility may also be used to temporarily store liquid waste. The option for sanitary sewer release has not been exercised but is not precluded. All radioactive releases are made in conformance with applicable regulations.

Two additional tanks of 250 gallons receive all waste from the Hot cell. These tanks were installed as underground retention tanks in the

TABLE 4.1 Heat Exchanger Specifications

Heat Transferred -- 6.83×10^6 Btu/h

Materials -- Aluminum. All materials must be compatible with aluminum. For this reason no copper containing alloys can be used.

Maximum Length -- 18 feet

	Shell Side	Tube Side
Fluid Circulated	High purity water	Cooling tower water
Liquid Flow	1100 gallons/minute	1200 gallons/minute
T inlet	110.2°F	82°F
T outlet	95°F	93.4°F
Pressure Drop Allowed	8 psi	8 psi
Design Pressure	50 psi	50 psi
Test Pressure	75 psi	75 psi
Design Temperature	150°F	150°F
Inlet and Outlet Pipe	8 inch	8 inch

To be fabricated in accordance with ASME Code, Section VIII, Division 1. Shall be inspected, certified, and stamped with the Code U - Symbol.

TABLE 4.2 Cooling Tower Specifications

Water Flow Rate	1200 gallons/minute
Heat Transferred	6.03×10^6 Btu/h
Wet Bulb Temperature	73°F
Water On	93.4°F
Water Off	82°F

Fill and construction materials -- Redwood

All materials must be compatible with aluminum. For this reason no copper-containing alloys can be used.

TABLE 4.3 Secondary Pump Specification

Centrifugal end suction pump

To pump 85°F chromated water from cooling tower

Flow Rate: 1200 gallons/minute

Dynamic Head: 70 feet

All wettable parts to be stainless steel

To include Teflon packing

Flooded suction

Mounted on base plate with coupling

Motor: 1750 rpm, 3-phase, 60-cycle, 220-volts

Open drip proof enclosure

TABLE 4.4 Primary Pump Specification

Centrifugal end suction pump

To pump 70° - 100°F Demineralizer water from pool through heat exchanger

Flow Rate: ~1100 gallons/minute

Dynamic Head: 50 feet

All wettable parts to be stainless steel\

Size of Impeller: 10 Inches

Mounted on Base Plate with Coupling

Motor: 30 H.P., 3 phase, 60-cycle, 220 volts

event of waste discharge from the hot cell. These tanks empty into the pond.

The water released from the pond is sampled prior to, at the beginning, during and at the end of each release. The results of these sample analyses are maintained by the reactor health physicist. No waste is released off-site with an active concentration in excess of $1x10^{-7}$ microcuries per milliliter, annual average. This limit is based on 10 CFR Part 20 limits for facilities producing waste where no iodine 129 or radium are present.

4.9 Building Ventilation System and Airborne Effluents

The reactor building ventilation system consists of the following major items.

1. An axial vane exhaust fan on the reactor room roof, the primary function of which is to provide circulation for the reactor room.

2. A short, duct-work stack on the reactor room roof.

3. A centrifugal blower on the mezzanine which exhausts the ground floor experimental facilities, hot cell, and fume hoods, through duct-work, to the suction of the roof top fan.

A schematic diagram of the system is shown in Figure 4-2 showing the fan, blower, nominal flow rates, and the general layout of the various connecting duct work. Ducts leading from the reactor experimental facilities (beamports, large access and thermal column access), the hot cell, and fume hoods are all provided with in-line filters and either have, or have provision for, in-line radiation monitoring.

As a result of normal reactor operations, and in the event of certain types of experimental failures that may be expected to occur,

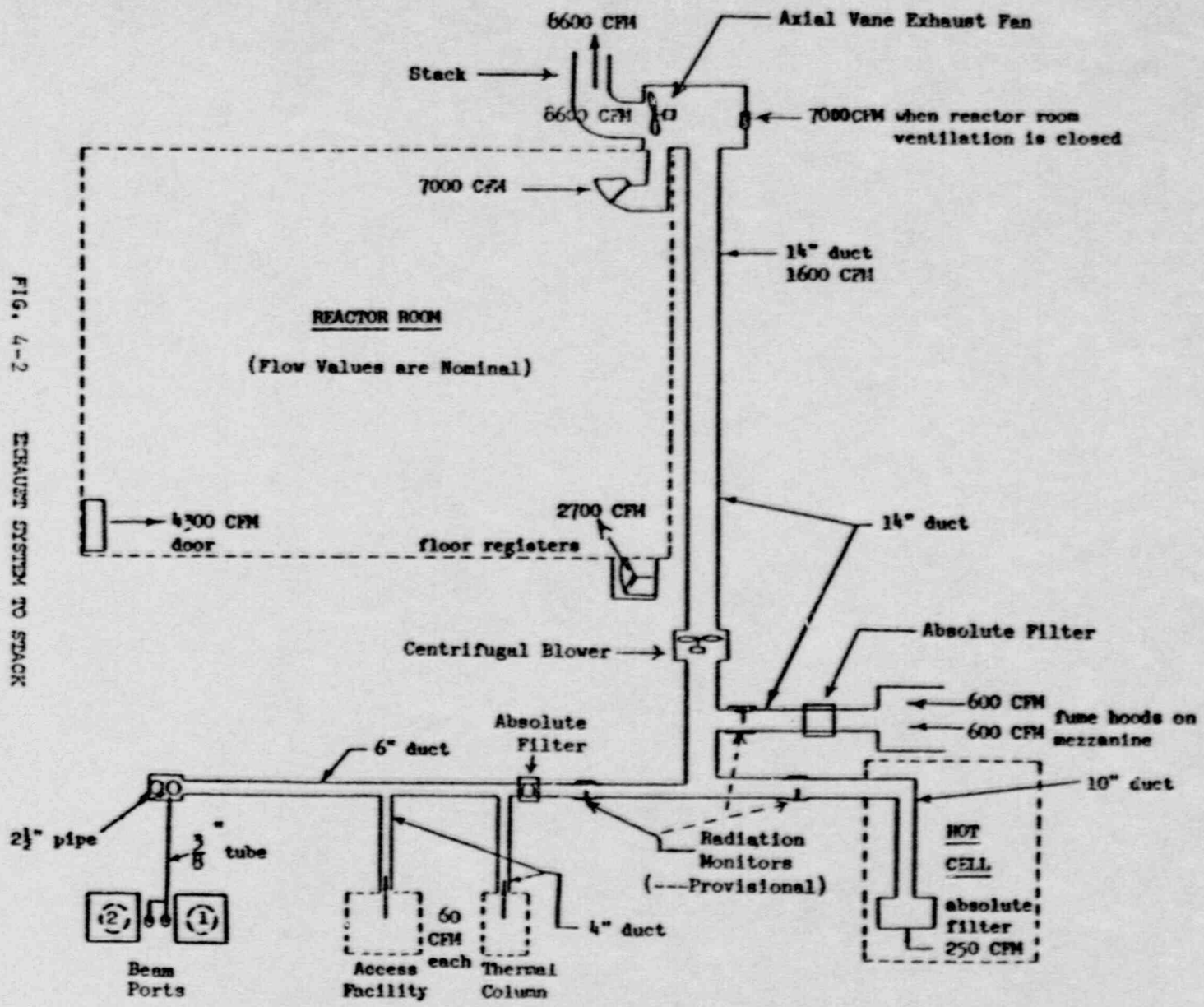

FIG. 4-2 EXHAUST SYSTEM TO STACK

there may be some release of gaseous, or airborne particulate, radioactive material from the facility. In general, such effluents would be released from the stack. The purpose of this section is to identify normally occurring and potential sources of such effluents, and to evaluate the consequences of both.

4.9.1 Sources

The gaseous radioactive isotope produced during normal operations which is of potential concern is Argon-41, produced by thermal neutron capture in the stable Ar-40 isotope present in air to about 1.3% weight. A small amount of Ar-41 is produced and released, as a result of air dissolved in the reactor pool water, being irradiated in passing through the reactor, and then coming out of solution into the reactor room atmosphere. This isotope is subsequently released as the reactor room is normally ventilated. While Ar-41 is continuously produced while the reactor is operating, its release is somewhat variable and to a large extent uncontrollable. However, the Ar-41 releases from the UVAR are small and of negligible consequence, as shown below.

Ar-41 may also be produced if air is irradiated in the various facilities on the ground floor experimental area. This source can be controlled by limiting the volume of air exposed and is thus very small. Brief releases of Ar-41 would be a normal consequence of reflooding a beamport, in which air had been irradiated. However, when in operation the beamports are usually filled with a low activatable gas, such as helium or carbon dioxide.

Accidental gaseous releases may occur as a result of experiment failure, either in an experimental neutron irradiation facility, in a

fume hood or hot cell. A severe case of such a failure, the complete melting of a 1-watt U-235 fueled experiment, is analyzed in Section 5.4 of this document.

4.9.2 Consequences of Gaseous Effluent Release - General

Figure 2-1 is an aerial photograph which indicates the position of buildings nearest to the reactor, including those constructed since the photograph shown in Figure 2-2 was taken. There follows an analysis of the atmospheric dilution of the reactor stack effluent at 2 points on the site boundary (fence) and at the seven buildings nearest to the reactor, identified in Figure 2-1. This analysis is performed on a yearly average or long-term basis and is thus pertinent to the calculation of the consequence of materials continuously released during operations.

The following assumptions are made in the calculations:

1. Wind frequency and velocity data taken at the site, Table II-1 and II-2, are representative of average conditions.

2. Pasquill-D type of dispersion conditions exist on the average over a year's time, with a wind speed of 2/3 of the annual average measured (Reference 1 at end of this Chapter).

3. No elevation differences are accounted for (i.e., "0" stack height).

4. Effluent materials are uniformly distributed over each 45° sector (Reference 2 at end of this Chapter).

5. No credit is taken for the rise or mixing of materials leaving the stack, although the stack effluent velocity is ~ 15 ft/sec.

The dispersion equation recommended in Reference 2 for releases is:

$$\frac{X(x_i)}{Q} = \left(\frac{2}{\pi}\right)^{1/2} \frac{f_i}{\sigma_z(x_i)\bar{\mu}(2\pi x_i/N)}$$

where

$X(x_i)$ = the concentration of material at x_i, Ci/M^3

Q = the average release rate of materials at the stack, Ci/sec.

f_i = the fraction of time during a year that the wind blows into compass section i.

x_i = distance to site, in sector i, M.

$\sigma_z(x_i)$ = standard deviation of plume in vertical direction at distance x_i, for Type-D conditions M.

$\bar{\mu}$ = average wind velocity, M/sec ($\bar{\mu}$ = 4.63x2/3 = M/sec)

N = number of compass sectors for which there is data (N=8)

The results of the application of this equation to the 9 sites are presented in Table 4.5. Column 8 shows the percent of the 10 CFR Part 20 limit of Ar-41 that would result from a continuous release of 10^{-5} Ci/sec. (10 μ Ci/sec).

For long term releases, dilution factors, X/Q, of about 2.5×10^{-4} exist even very close to the release point, resulting in an average Ar-41 concentration of about 6.5% of the Part 20 limit for Unrestricted Areas assuming a 10 μ Ci/sec release rate. This rate will be shown to be higher by at least a factor of 20, than that which may be expected for this isotope.

For accidental releases and other short term releases, Pasquill-F type conditions, a 1 meter/sec wind speed, and 0 stack height will be

conservatively assumed as described in TID-14844. A dilution factor at 70 meters of 0.039 for these conditions will be used to determine downwind isotopic concentrations. the consequence of noble gas release under stable meteorological (Type F) conditions will be evaluated by determining whole body dose from the cloud, as an undiluted line source.

4.9.3 Specific Cases

In this section, several specific cases of gaseous release will be considered and the consequences thereof evaluated.

4.9.3.1 Argon-41 from Reactor Room, Long Term

The production and release to the reactor room of Ar-41 was discussed in Section 4.9.1. The specific activity of this isotope in the reactor room has been monitored for several years. With the reactor room ventilated, the concentration normally does not exceed 1/30 of the MPC for Ar-41 in Restricted Areas (2×10^{-6} μ Ci/cm^3. The normal exhaust rate for this room is 7,000 CFM (3.3×10^6 cm^3/sec). If one assumes that an Ar-41 concentration of 6.7×10^{-8} μCi/cm^3 exists continuously in the reactor room, the resulting effluent source is:

$$(3.3 \times 10^6 \text{ cm}^3/\text{sec})(6.7 \times 10^{-8} \mu\text{Ci/cm}^3) = 2.2 \times 10^{-1} \mu\text{Ci/sec}$$

or about a factor of 45 lower than that assumed for the calculations of Column 8, Table 4.5.

Even considering the factor of 2 increase for 2 MW operation, the release associated with Ar-41 production in the reactor pool appears to be of insignificant consequence.

4.9.3.2 Reactor Room Ar-41, Persistent, Stable Conditions

The most extreme case for this type of release would be that of a long persistence of Type F dispersion conditions. As is standard

TABLE 4.5

PERCENT OF 10 CFR PART 20 LIMIT OF A-41 RESULTING FROM CONTINUOUS RELEASE OF 10^{-5} Ci/SEC

Site No.	Site Identification	Distance (x_i) Meters	$\sigma_z(x_i)$ Pasquill-D (Ref. 3)	Bearing from Reactor	f_i	$\frac{X}{Q} \times 10^4$	% of MPC for A-41 with $Q=10^{-5}$ Ci/sec
1	North Fence[a]	50	2.6	N	0.10[a]	2.6	6.5
2	South Fence[a]	70	3.4	S	0.17[a]	2.5	6.3
3	Van de Graaf Bldg.	115	5.1	SE	0.12	0.72	1.8
4	RLES Laboratory	160	6.5	NW	0.09	0.30	0.75
5	Radioastronomy Lab.	265	11.0	NE	0.08	0.095	0.24
6	Observatory	300	13.0	SSW	0.17	0.15	0.40
7	Building & Grounds	300	13.0	E	0.10	0.089	0.23
8	Dormitory	375	15.0	ESE	0.12	0.072	0.18
9	Filter Plant	430	17.0	SE	0.12	0.058	0.15

a) The North and South Fence sites represent average distances to the facility fence in these two directions, and the corresponding wind frequencies are averaged over all northerly and southerly directions. The University of Virginia also owns the land out to at least 300 meters in all directions from the reactor, and controls its use. Other than the sites listed above, there are no areas normally occupied within the 300 meter distance.

practice for noble gas exposure (Reference 3 at end of this Chapter), this situation has been analyzed on the basis of the direct, whole-body gamma-ray dose to an individual standing at the center of the narrow plume that would result. For these calculations, the plume is considered to be an infinitely long, line source passing the receptor at a distance of 6-inches. Since no dispersion in the atmosphere is accounted for, this model is independent of source-to-receptor distance. Assuming that the Ar-41 release rate at 2 MW is twice that calculated in 4.9.3.1 for 1 MW, the whole-body dose rate in the plume is about 0.006 mR/hr. For 24-hour persistence of this condition, the total calculated dose would be 0.15 mR.

4.9.3.3 Exhaust from Reactor Room after Ar-41 Buildup

If the reactor room exhaust is stopped temporarily, the Ar-41 concentration within the reactor room could eventually build up to Restricted Area Limits (2×10^{-6} μ Ci/cm^3). If the room is then exhausted, a short-term source of 6.7 μ Ci/sec exists, but will quickly die away as the reactor room inventory is depleted (exhaust half-period of about 10 min.) The calculated dose rate in the stable plume under these conditions is only 0.1 mR/hr, and the total dose to someone in the plume of 0.02 mR.

4.9.3.4 Exhaust from Beamport

The standard UVAR beamports have a section near the core which is filled with water when the port is not in use, and is drained prior to use. During port operations this section may be filled with air (although He or CO_2 is preferred), under neutron irradiation. If the port is refilled with water after operation, the Ar-41 produced when air

is used is exhausted into the experimental area exhaust system, and hence to the stack and atmosphere. A pump unassisted beamport drain takes several hours, and the refill (and thus the Ar-41 exhaust portion) 20-30 minutes.

Flooding a beamport immediately after a long period of operation at full power with air in the beamport results in the most severe Ar-41 dose that can be reasonably postulated. This situation is evaluated using stable meterological conditions and the line source approximation. Constants and assumptions used in the calculation are listed below.

1. Activation cross section of Ar-41 in normal air

   $\Sigma_a = 1.59 \times 10^{-7}$ cm^{-1}

2. Volume of 8-inch beamport, for 4.7 foot length,

   $V = 4.7 \times 10^4$ cm^3

3. Thermal neutron flux, $\phi = 2 \times 10^{12}$ n/cm^2-sec

4. Flooding time 1000 sec (16.7 min)

5. Saturation Ar-41 inventory, 0.4 Ci (product of $\Sigma_a \phi V / 3.7 \times 10^{10}$)

Using the line source approximation, the calculated dose rate in the plume during the 1000 seconds of discharge is 5.8 mR/hr. The calculated total dose to an individual in the plume as a result of the Ar-41 discharge is 1.6 mR.

During the spring of 1983 the North Neutron Beamport was modified into a closed loop system to eliminate the buildup of Ar-41 activity. The system incorporates demineralized water and a helium cover gas and a reversible peristaltic pump. When the front tube (pool side) is drained it is replaced with Helium gas, thereby eliminating Ar-41 activity

production in the tube. This beamport is being used extensively for neutron radiography experiments. The drain-fill operating mechanism is remotely located to reduce personnel exposure while the reactor is at power.

4.9.3.5 Experimental Failures

In Section 5.4 the offsite consequences of gaseous release as a result of an experimental failure are evaluated for the case of a fission gas release from a U-235 plate operated at 1 watt for a long time. Such an incident represents an upper bound on the type of major experimental failures which may be postulated, in view of the past and currently projected experimental programs.

4.9.4 Effluent Monitoring

Each of the ducts leading from the experimental facilities may be fitted with an internal G-M tube radiation monitor. Such a monitor has been used on the duct leading from the beamports and access facilities for many years. (See Figure 4.2).

A thin-walled G-M tube inside a duct has a count rate signal proportional to the specific beta activity of radioactive materials in the duct. In addition, the count-rate depends on the beta energies, the diameter and length of the duct. The exact relationships defining these dependencies are complicated but in general the count rate, for a given specific activity in the duct, will vary directly as the duct volume, and will be rather insensitive to beta energy unless the average beta particle range is less than the wall thickness of the G-M tube.

The best means for calibrating such a monitor for a particular isotope is by filling the duct with the beta emitting material in known

concentration and measuring the count rate. This has been done with Ar-41 in a section of duct similar to that in which the monitor is located in the exhaust line for the beamport and access facilities. The calibration of this monitor, thus obtained, was about 200 cpm, for an Ar-41 concentration of 10^{-6} μ Ci/cm^3 in the duct. Once a monitor has been calibrated, it can be checked for proper operation by noting the G-M tube's response to a gamma-ray source located outside of the duct.

4.9.4.1 Monitoring Performance for Ar-41

The function of the exhaust duct radiation monitor is to notify the reactor operator of abnormal levels of airborne radioactive effluent in the duct. The monitor in the beamport and access facility exhaust duct is normally set to alarm in the reactor room for a count-rate in excess of 800 cpm. For a normal background of 100 cpm, this count-rate would indicate an Ar-41 concentration in the duct of

$(700/200)\times10^{-6} = 3.5 \times 10^{-6}$ μ Ci/cm^3.

The nominal flow in this duct is 150 cfm, or 7.1×10^4 cm^3/sec. Thus a monitor alarm corresponds to an Ar-41 release at the stack of about 0.25 μ Ci/sec. This amount, on the basis of the conservative analysis of Section 4.9.3.2, would lead to a maximum offsite dose rate of 0.004 mR/hr. The expected Ar-41 production rate for any experimental facility can be determined analytically, if the thermal neutron flux and volume of air irradiated are known. One cubic foot of air, exposed to a flux of 10^9 n/cm^2-sec will yield about 0.013 μ Ci/sec of Ar-41.

4.9.4.2 Monitor Performance for Other Isotopes

The G-M tube duct monitors will respond to other radioactive gases or airborne particulates in a manner similar to its response for Ar-41,

as long as their beta particle ranges are well above the wall thickness of the G-M tube. The latter dimension for the current tube is 30 mg/cm^2 (0.0044" Al), equivalent to the range of an electron of ~ 0.16 MeV. Table 4.6 gives beta particle decay for various activation and fission product gases, and the rate at which the latter would be produced in a fueled experiment operating at 1 watt. Inspection of the Table shows that the isotopes of Chlorine and Bromine, and the more intense fission product isotopes I-132, I-134, and Kr-87 have beta energies similar to that of Ar-41, and would thus be expected to produce a similar monitor response. Thus, a fission product gas release of 0.25 μ Ci/sec would be sufficient to cause a monitor alarm. This value amounts to 1% of the fission products being produced by a 1-watt, fueled experiment.

4.9.4.3 Consequence Evaluation, Fission Gas Release

The consequences of a fission gas release that would produce a count rate just below the duct monitor alarm setting have been determined and are presented in Table 4.7 for the iodine isotopes. Two types of release are considered -- long term in which the dispersion factors at the site fence (Table 4.5) are used, and a short term release under stable, Pasquill-F type conditions.

The results of Table 4.7 show that for long term operation at the alarm point, the release of fission product gases produces site boundary concentrations of less than 2% of Part 20 limits for Unrestricted Areas. The short term release at this level, using extremely conservative dispersion conditions yields concentrations which are only 2.5 times these limits. Thus, the duct monitor appears to provide adequate protection in the case of accidental fission product gas releases.

TABLE 4.6

DATA FOR RADIOACTIVE GASES

Isotope	Major Beta Particle: Maximum Beta Energy	Major Beta Particle: Fraction of Emission	Production Rate for a 1 Watt Fueled Experiment μ Ci/sec	MPC, μ Ci/cm³ Part 20 Appendix B, Table 2
Ar-41	1.2 MeV	0.99		4×10^{-8}
Cl-38	>1.1 MeV	1.0		7×10^{-8}
Br-80	2.0 MeV	0.92		
Br-82	0.44 MeV	1.0		6×10^{-9}
Fission Products				
I-131	0.61	0.90	0.027	1×10^{-10}
I-132	>1.0	0.79	3.2	3×10^{-9}
I-133	1.3	0.93	0.53	4×10^{-10}
I-134	>1.2	1.00	14.90	6×10^{-9}
I-135	>1.0	0.65	1.53	1×10^{-9}
Xe-133	0.34	0.99	0.086	3×10^{-7}
Xe-135	0.93	0.97	1.15	1×10^{-7}
Kr-85m	0.82	0.77	0.049	1×10^{-7}
Kr-87	>1.3	1.00	3.30	2×10^{-8}
Kr-88	0.85	0.23	2.10	2×10^{-8}
		Total *Fission Products*	26.9	

TABLE 4.7

IODINE ISOTOPE CONCENTRATIONS FOR A 0.25 μ Ci/SEC FISSION PRODUCT RELEASE

Isotope	Release Rate μ Ci/sec	Long Term Conc. at Fence μ Ci/cm³	Long Term Fraction of 10 CFR 20	Short Term Conc. at Fence μ Ci/cm³	Short Term Fraction of 10 CFR-20
I-131	2.7×10^{-4}	6.8×10^{-14}	0.00068	1.04×10^{-11}	0.01
I-132	3.2×10^{-2}	8×10^{-12}	0.0027	1.2×10^{-9}	0.40
I-133	5.3×10^{-3}	1.3×10^{-12}	0.0033	2.0×10^{-10}	0.50
I-134	1.5×10^{-1}	3.8×10^{-11}	0.0064	5.8×10^{-9}	1.00
I-135	1.5×10^{-2}	3.8×10^{-12}	0.0038	5.8×10^{-10}	0.60
Totals			0.017		2.5

4.10 Core Spray System

The UVAR reactor is equipped with two independent core spray systems. Their function is to provide protection against a postulated core damage in the event of a very sudden and severe loss of coolant accident (LOCA). Each system consists of a pair of spray headers and an emergency water storage tank. The two water storage tanks are mounted on the inner side of two of the pool walls and each holds approximately 200-foot^3 (1500 gallons). Either system is designed to deliver an average spray flow of 10 gpm to the core for at least 1 1/2 hours, considered to be an adequate flowrate and time to prevent core damage. The two core spray systems are illustrated (elevation and plan view) in Figures 4-4 and 4-5.

Recirculating water from the demineralizer continuously flows into each of the emergency water storage tanks. The tank overflows are located about 2-inches above the highest operating level of the pool water. Accordingly, there is a slight head (2") of water on the tanks and a continuous flow of water through the headers into the pool. This assures that the tanks are always full and that stagnant water and resultant corrosion does not occur in the spray headers. The material used in the construction, aluminum, and the flexible stainless steel couplers, serve to enhibit corrosion.

The two sets of spray headers are mounted on either side of the core support structure, approximately 5-feet above the top of the core. A spray header consists of an approximately 1-inch diameter aluminum pipe, 2-feet long, with approximately 80 small holes drilled at a proper angle and spacing to provide a uniform spray over the top of the core. A mockup of one pair of core spray headers is shown in Fig. 4-3. (The flow rate was 10 gpm when this picture was taken.)

Technical Specifications require a core spray flowrate of at least 10 gpm at 30 minutes after LOCA onset. Actually, the calculated spray flowrate is 10.8 gpm after 30 minutes, reaching 10 gpm only after 47 minutes.

When the reactor bridge is returned to the full power position, the piping connecting the storage tank to its pair of spray headers is engaged with a remote coupler. After the coupling is made, a pressure test is conducted using an insert tube screwed into the pipe leading from the bottom of the storage tank, as shown on the right hand tank in Fig. 4-4. Air pressure is applied and a visual observation made to ensure that air bubbles are not leaking from the remote coupling. Air bubbles will emerge from the spray headers at approximately 7 1/2 psig air pressure. At 1/2 psig the coupler will be filled with air but the spray headers will not. The absence of air bubbles from the coupler will be a positive verification that the coupler is securely engaged and is not leaking.

The pressure test insert tube is removed after it has been verified that there is no leak from the coupler. A coupler leakage test is made every time the reactor bridge is moved and returned to the high power position, after the coupler has been re-engaged. A flowrate test, using a small water tank to provide a known head, is repeated at least once each year for each of the two spray systems, to demonstrate that at least 10 gpm are available for emergency core cooling for the first 30 minutes after a loss of coolant accident.

In summary, the emergency core spray system is expected to provide an immediate supply of water to the core in case coolant is suddendly lost. The system has no moving parts that can fail and no automatic electronic or mechanical devices are required to function. SAR Section 9 discusses the loss of coolant accidents.

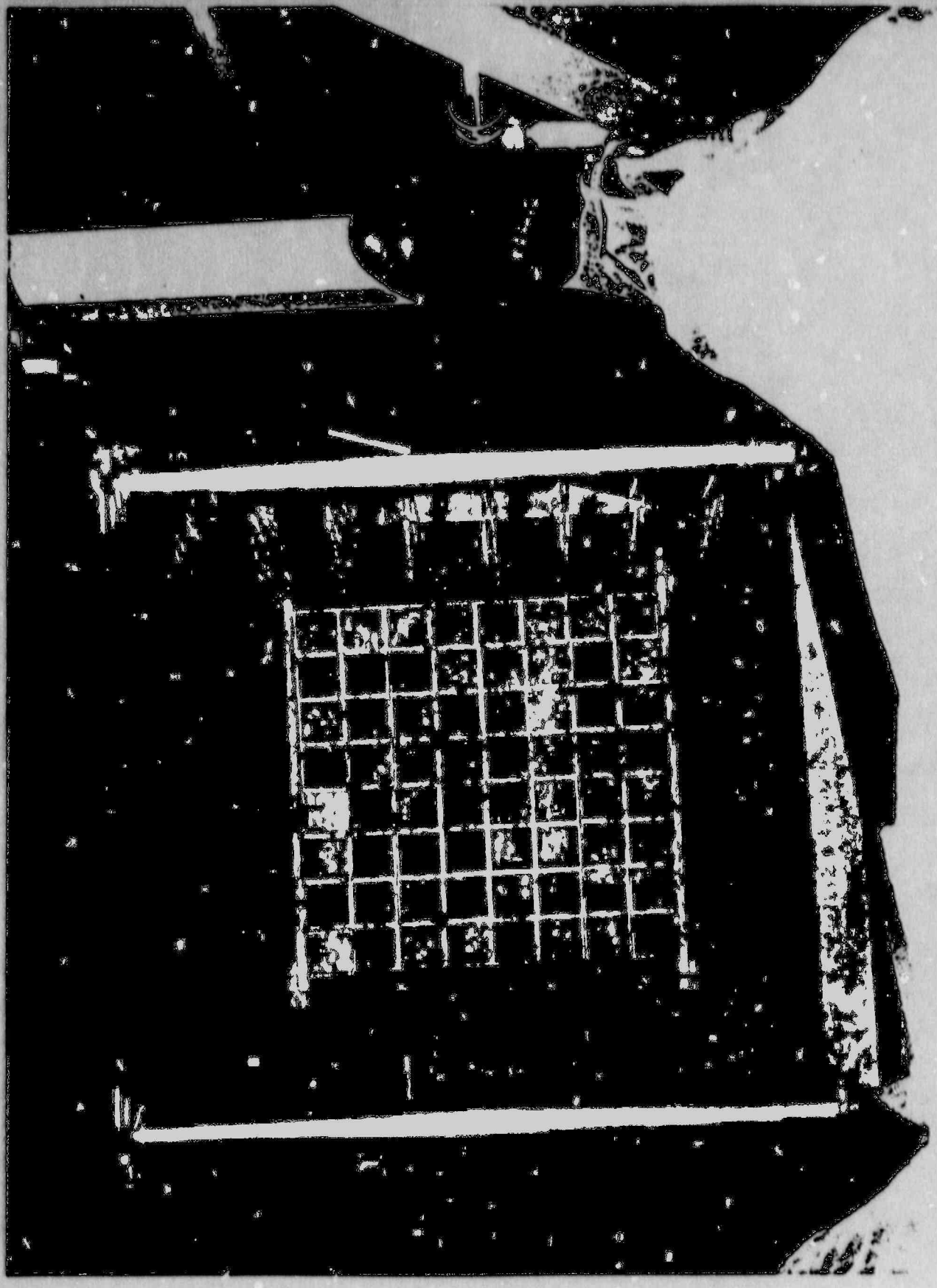

TOP VIEW

FIGURE 4-3 MOCKUP OF CORE SPRAY HEADERS

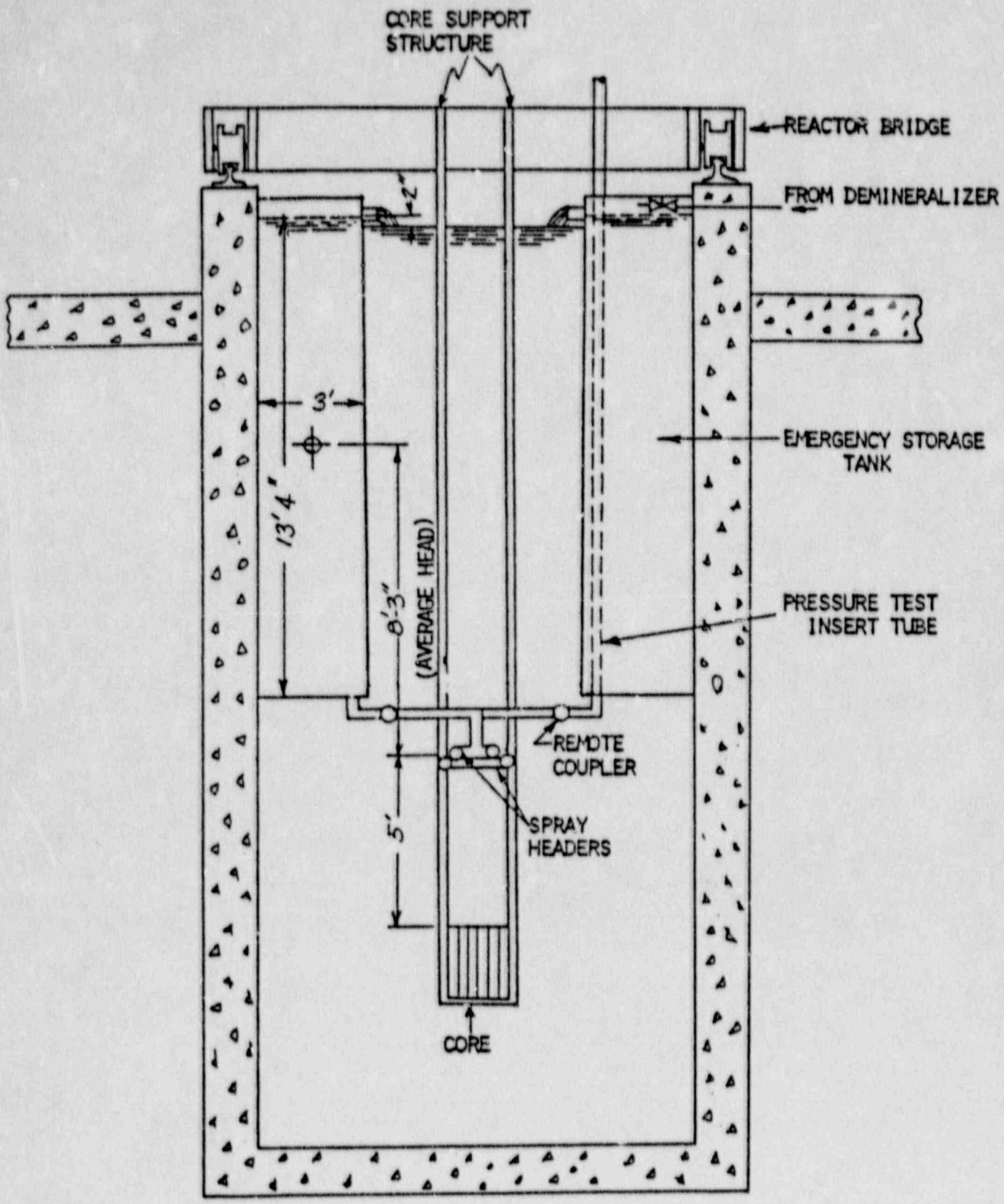

FIGURE 4-4 , CORE SPRAY SYSTEM ELEVATION VIEW

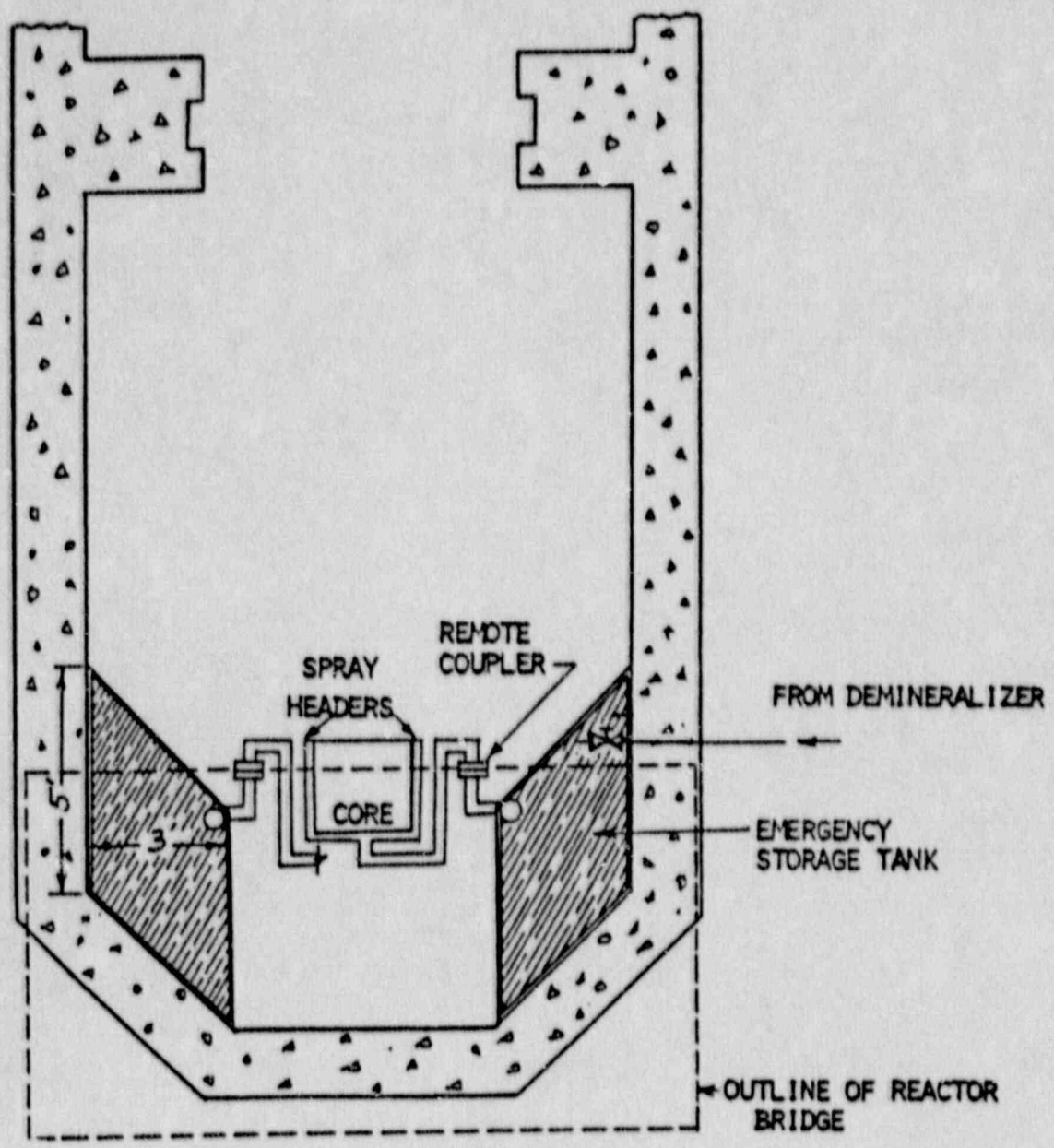

FIGURE 4-5 , CORE SPRAY SYSTEM PLAN VIEW

References for Chapter 4.0

1. "Radiation Dose Evaluation Model for Maximum Credible Accidents," p. 23, Proposed DRL Safety guide -- Private Communication.

2. Slade, David H., Edt. "Meteorology and Atomic Energy, 1968," Section 3-3.5.4, p.113, USAEC, July 1968.

3. Rogers, Lester, and C.C. Gamertsfelder, "U.S. Regulations for the Control of Releases of Radioactivity to the Environment in Effluents from Nuclear Facilities," I.A.E.A. SM-146/8, p. 8, paper presented at I.A.E.A. Symposium on Environmental Aspects of Nuclear Power Stations, U.N. Headquarters, New York City, N.Y., August, 1970.

5.0 Experimental Facilities

5.1 Beamports

Two 8-inch neutron beamports penetrate the concrete shield in the southwest side of the pool. The ports extend through the wall and up to the side of the reactor. The ports on the pool side are normally filled with water when not in use. A blank flange aluminum plate separates the aluminum port extension from the concrete shield penetrations. Beam hole design is shown in Figure 5-1.

The South Beam Port Extension (see Figure 5-1a) is vented to the duct exhaust system. The North Beam Port is used for Neutron Radiography experiments and its extension is a closed system. The system uses demineralized water with a helium cover gas and a reversible peristaltic pump as shown in Figure 5-1b. When the front tube is filled with water, the tank holds an amount of excess water and a large volume of helium gas. When the front tube is drained the tank is almost filled with water causing the front tube to be filled with helium gas. This eliminates the production and release of argon-41 to the atmosphere. The drain/fill pump circuitry requires switch actuation by both the experimenter and the reactor operator.

There is a concrete shielding block wall around the beam ports on the ground floor (see Figure 5-1a). The wall is roofed with steel and wood beams and plywood decking which holds graphite, paraffin and borax shielding. The back wall thickness is three blocks. The beam stop is constructed of cadmium sheets, lead sheets, concrete and paraffin. Access to this structure is limited by a lockable door. Entrance to the inside of the blockhouse is procedurally controlled at all times. When

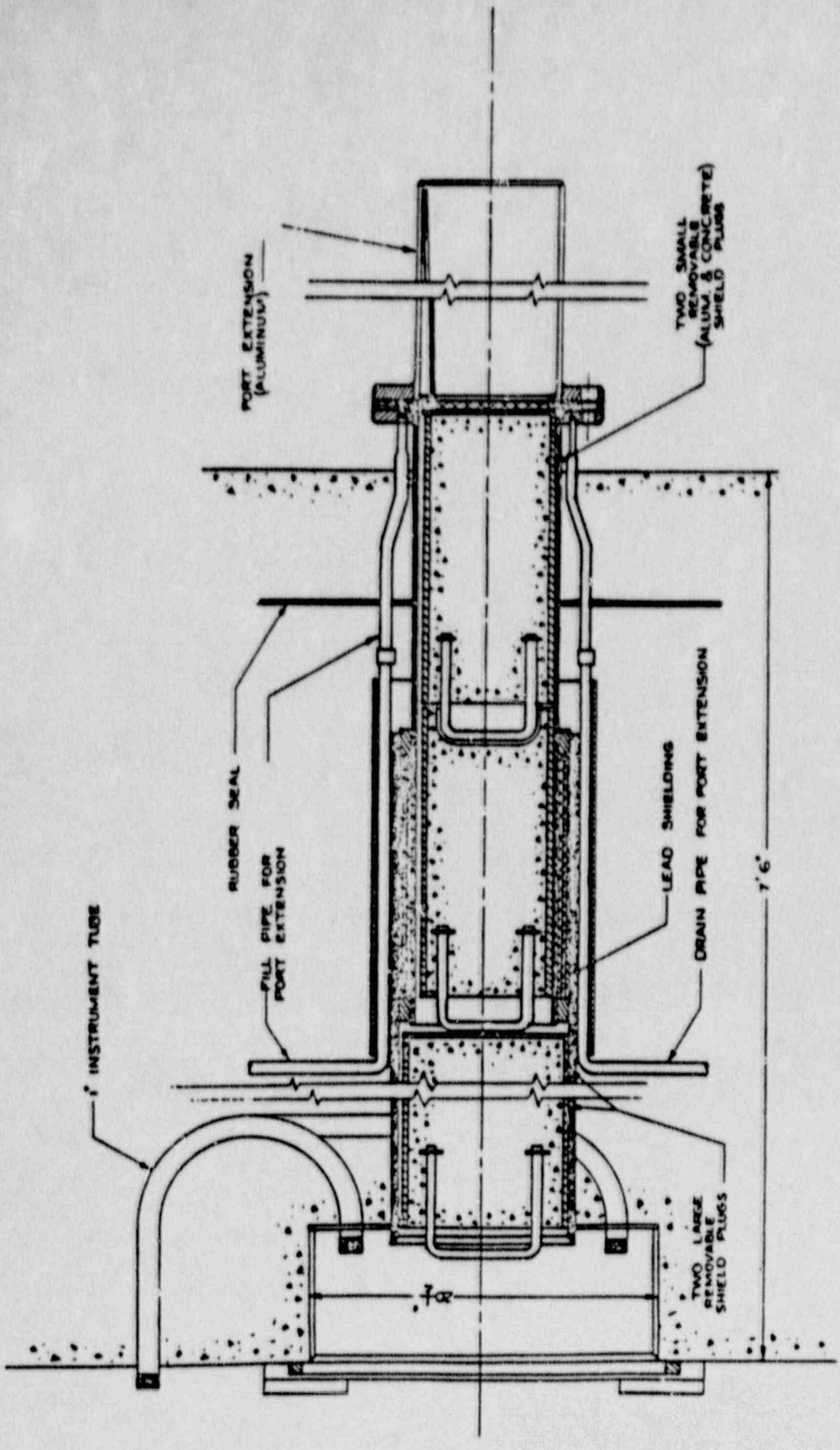

FIG 5-1 BEAM HOLE DETAIL

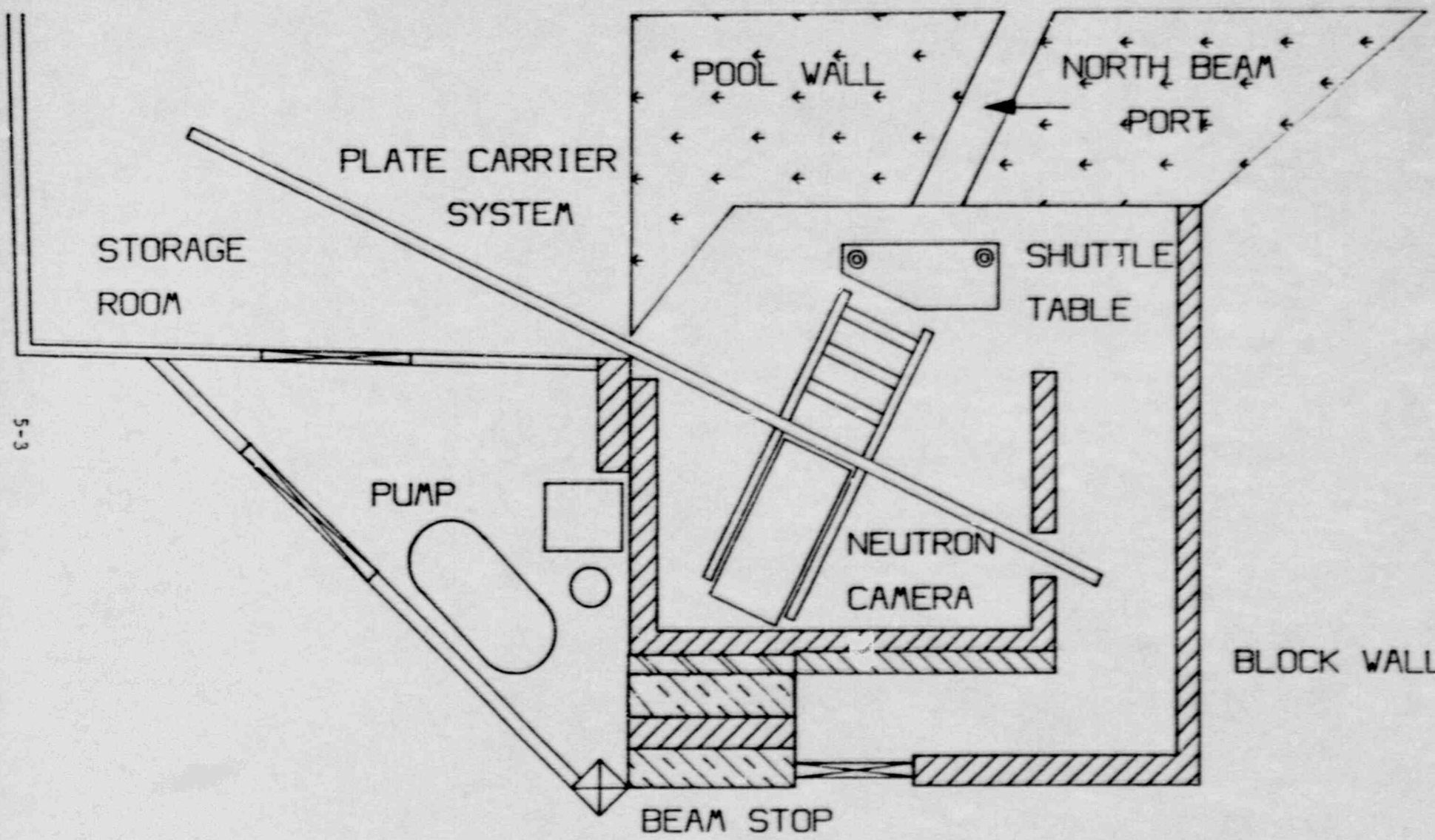

Figure 5-1a Top View of North Beam Port Shielding and Access Control Walls

Revised 4/89

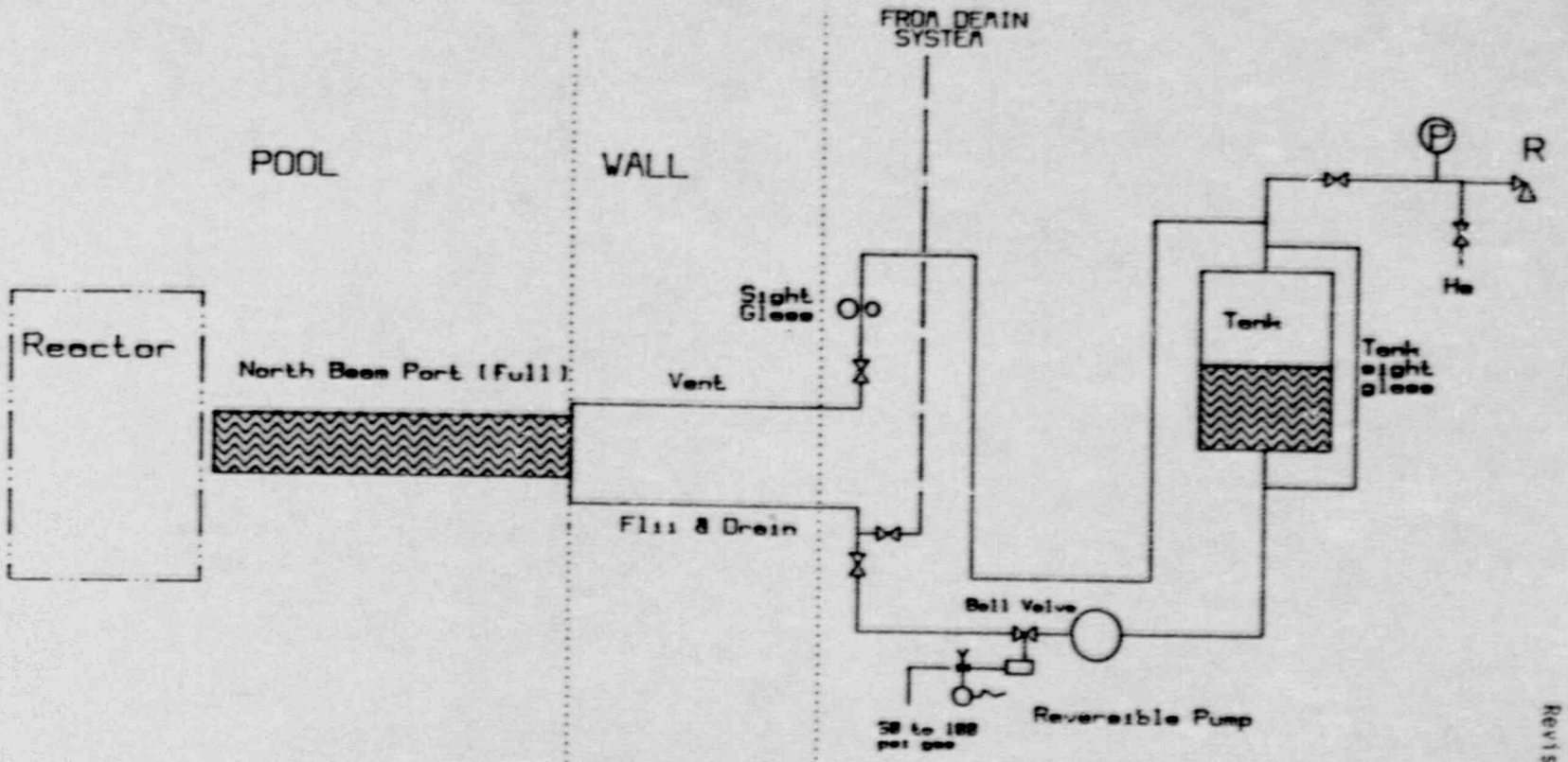

Figure 5-1b North Beam Port Drain/Fill System Schematic

Revised 4/88

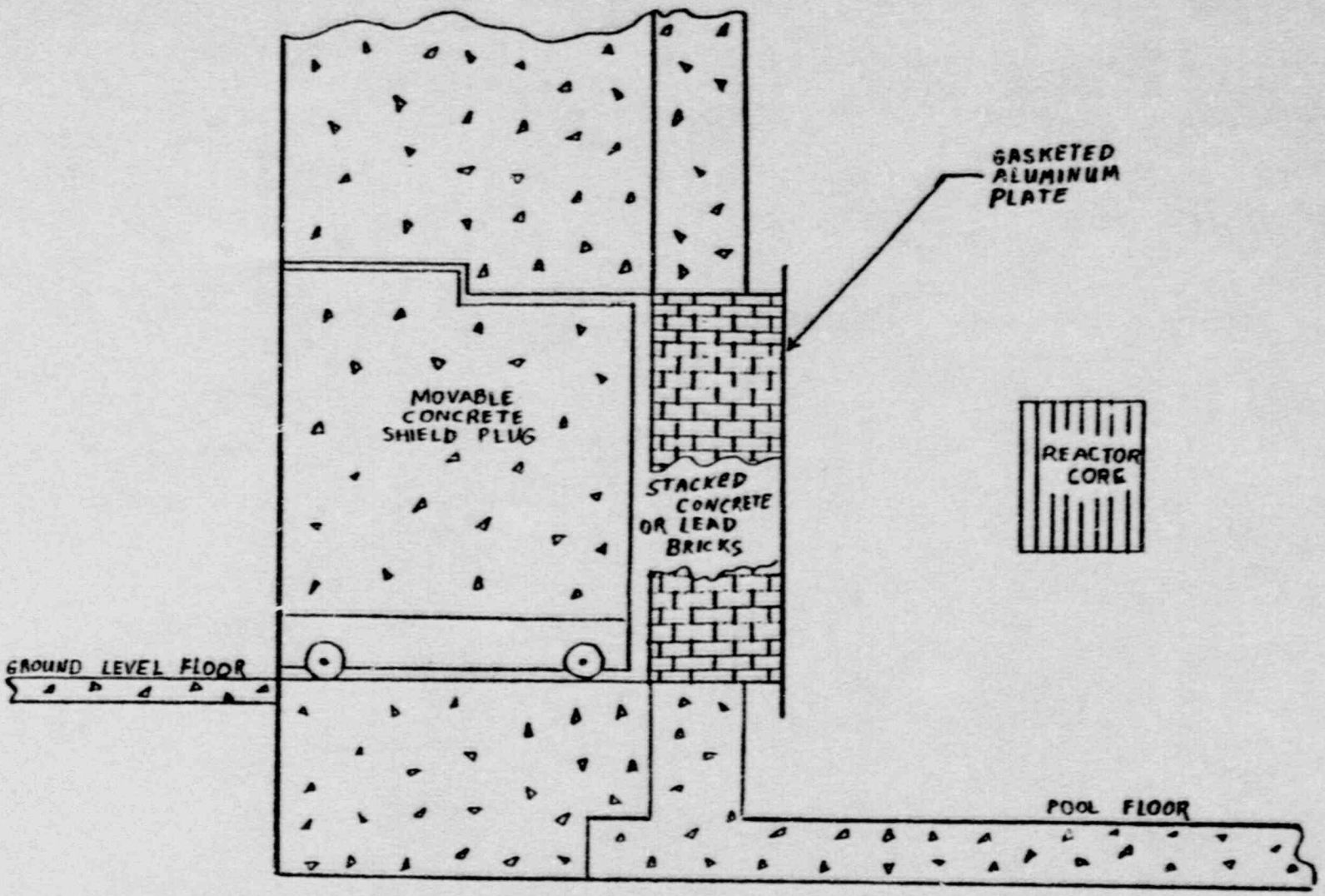

Figure 5-2 LARGE ACCESS FACILITY

the front tube of the beamport is partially or fully drained, several alarm systems are activated. These include:

1. An audible alarm on the opening of the blockhouse door based on signals from either the LED water detector on the vent tube, or the LED water detector on the top sight glass tube, or a BF_3 neutron detector within the beam tube. This is a one of three logic system.
2. An LED sensor on the top sightglass tubes of both neutron beamports which gives a drained/filled indication at the reactor console. The north beamport LED detector enables an alarm and reactor scram upon breaking a light beam actuator placed inside the blockhouse corridor prior to entering the north beamport beam path.
3. A neutron detector located on the reactor side of any movable shielding or experimental apparatus enables a scram and a local alarm associated with the light beam actuator whenever neutrons are detected in the beam. The Radiation Area lights and the door alarm and beam open light are also controlled by this detector. The setpoint of the detector is chosen based upon neutron and gamma ray sensitive portable survey instrument readings in the beam.

5.2 Large Access Facilities

The south wall also accommodates two large access solid concrete facilities measuring 5-feet wide by 6-feet high, rolled in the wall recess on dollies. Each facility is closed off from the pool by a

plate. A large access facility is shown in Figure 5-2. A thermal column may be incorporated in a large access facility. Small diameter beamports are available for use in conjunction with the access facilities.

5.3 Rabbit Facilities

a) Two pneumatic rabbit facilities are located on the reactor grid plate to accommodate thermal and epithermal irradiations, and they are used primarily for activation analysis experiments. The pneumatic transfer system may be connected to either the thermal or epithermal irradiation facility by manually changing the tubing at the top of the reactor bridge. Samples may be loaded in a room next to the counting room on the lower level of the building and pneumatically sent to the top of the reactor pool. The reactor operator then takes control of the sample and can by computer control insert it in the rabbit facility for a preset amount of time. When the sample is removed it can be stopped approximately 5 feet under water and measured for radiation exposure. An administrative limit of 240 mR/hr(Gamma) at one foot is placed on samples transported through this system. If the radiation is less than this the reactor operator can activate the system to transport the sample to the counting room for analysis. This system is very useful for investigating short-lived isotopes.

b) A hydraulic rabbit facility is also located in the reactor grid plate. Samples run in this facility must be loaded and unloaded from the top of the reactor pool. The overall configuration of possible experimental facilities is shown in Figure 5-3. All facilities shown are not necessarily in place at one time.

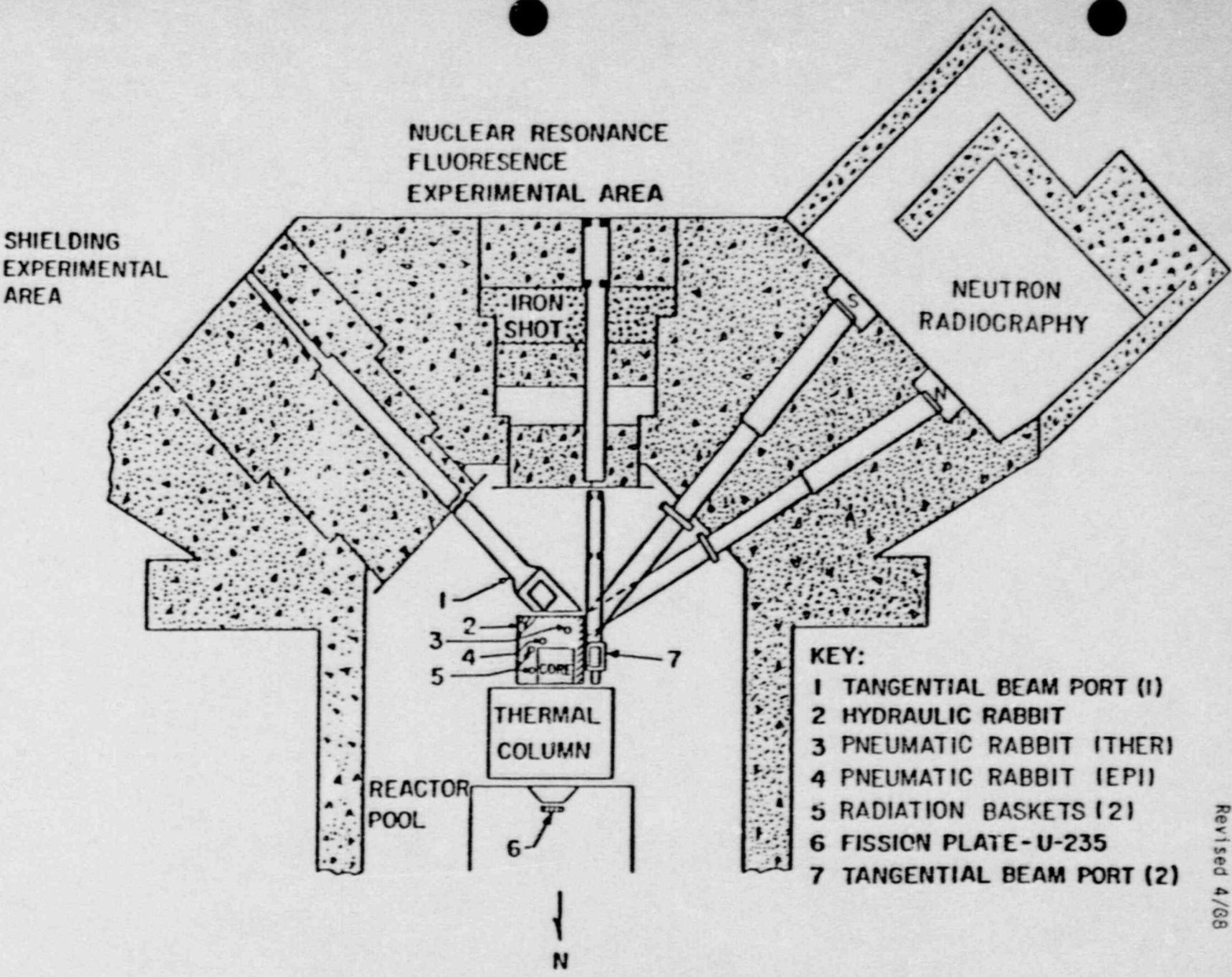

FIGURE 5-3 UNIVERSITY OF VIRGINIA REACTOR OPTIMUM CONFIGURATION
CORE IN FORCED CONVECTION COOLED POSITION.

Revised 4/88

5.4 Fueled Experiments

5.4.1 Introduction

The purpose of this analysis is to assess the hazard associated with the failure of a fueled experiment and subsequent release of its fission product inventory. The Maximum Permissible Concentrations of 10CFR-Part 20, averaged over a 1-year period, will be used as a measure of the consequence of a fission product release. Exposure to an isotope, in the concentration shown in Table II, Appendix B of 10 CFR-20, for a year (3.15×10^7 sec) is considered to be the Part 20 limit. Accident exposures to concentrations of the same isotope, for specific time periods, are evaluated according to the following equation.

$$\text{Fraction Exposure(FE)} = \frac{(\text{Accident Concentration}, \frac{\mu c}{cc} \times (\text{Time of Exposure})(\text{BRR})}{\text{MPC (Table II)}(3.15 \times 10^7 \text{ sec})} \qquad (5.4.1)$$

where BRR = breathing rate ratio, the ratio of the breathing rate assumed during an accident to an average breathing rate.

Only the isotopes of Iodine and Strontium-90 are considered in this analysis. The reason for this is that these are isotopes having relatively high fission yield and very low permissible concentrations. If the concentrations of these isotopes are within permissible levels, the concentration of others will also be tolerable.

5.4.2 Isotope Release

The amount of radioisotope released from a fueled experiment and becoming airborne is assumed to be that specified by TID-14844: 100% Noble Gas; 50% Halogen; 1% Solid Fission Products. These values provide

a very conservative upper limit for fission product release from a fueled experiment over a broad spectrum of accidental conditions (e.g., fission plate clad failure).

Isotopes initially released to the reactor building in general (other than to the reactor room), are assumed to be released subsequently to the atmosphere at a uniform rate, over a 2-hour period. This assumption maximizes the inhalation dose (or isotope concentration) for a 2-hour exposure time, by making the entire isotope inventory available for inhalation. For material released to the reactor room, which is automatically closed upon receipt of a high radiation level signal, the isotopes are assumed to be released at a uniform rate over a period of 20-hours.* The retention properties of the reactor room, a windowless structure designed to provide confinement, have been measured, and the 50%-in-20 hours exfiltration value verified (see Section 6.1).

In case of fueled experiments which are operated in the reactor pool, a reduction of a factor of 10 will be assumed for iodine isotopes released to the atmosphere. This "partition factor" accounts for the

---

*A gamma-ray sensitive chamber at the top of the reactor pool provides automatic closure of the reactor room (and a reactor trip) for radiation levels above the set point, normally 30 mR/hr. In addition there are 2 independent air monitoring instruments in the reactor room which would sense a fission produce release and alarm. The operator would have ample time to close the reactor room to prevent an excessive amount of exfiltration by the building exhaust system--normal rate ~11% per minute. Note that forced exfiltration by the building exhaust would give an elevated, puff-type release, resulting in lower site boundary doses.

solubility of iodine gas in water, and the fact that any fueled experiment operating in the pool, at a significant power level, must be located near the reactor core--under approximately 20 feet of water. In a fission gas release from a fission plate at the UVAR on May 3, 1968, isotopic concentrations of noble gases were measured in the reactor room, amounting to ~0.1% of the total fission plate inventory. Iodine isotope concentrations were too low to be detected. However, by inference from the instrument sensitivity, they were released form the pool in amounts smaller by at least a factor of 10 than the noble gases.

5.4.3 Offsite Exposures

For isotope releases from the facility, the following information is used to determine fractional exposure to an isotope. Accident concentrations are computed using the conservative meteorological model of TID-14844, and a 70 meter exclusion radius. The time of exposure is taken to be 2 hours (7200 sec). An accident breathing rate of 3.47×10^{-4} M^3/sec is assumed, and a yearly average breathing rate of 2.32×10^{-4} M^3/sec (i.e., BRR = 1.56). MPC values used are taken from 10 CFR Part 20, Appendix B, Table II.

5.4.4 In-Facility Exposures

Fractional exposures due to inhalation of isotopes by personnel within the building are computed by assuming mixing of the isotope in question with the air in the space in which the release occurs. For calculational purposes, the exposure times are set at 5 minutes, a period considered long enough a detect a release and evacuate the affected areas. No correction is made for exfiltration from the building during exposure time.

5.4.5 Calculations

5.4.5.1 Offsite Exposures

Fractional exposures (FE_i) for each isotope, and the doses due to each may be calculated. The atmospheric diffusion expression of TID-14844 (Section B) may be used to determine the downwind, site boundary, concentration of any isotope.

Concentration:

$$X_i(d) = \frac{2Q_i}{\pi \bar{\mu} C_y C_z d^2 n} \qquad (5.4.2)$$

where $X_i(d)$ = concentration of isotope "i" at a distance of d, Ci/M^3

Q_i = isotope "i" source, Ci/sec, = inventory/exfiltration time

$\bar{\mu}_i$ = wind speed, 1 meter/sec

C_y = horizontal diffusion coefficient, 0.40 $meters^{n/2}$

C_z = vertical diffusion coefficient, 0.07 $meters^{n/2}$

d = distance downwind, 70 meters for exclusion radius

n = 0.5

$$\frac{X_i\ (70\ M)}{Q_i} = \frac{1}{\pi \cdot 1 \cdot (0.4)(0.07)(590)} = 0.039$$

Fraction exposures are determined using Eq. (5.4.1), in which the accident concentration, $X_i(70)$ found by calculating a value of Q_i for each isotope:

$$Q_i = \frac{\text{(Inventory of Isotope "i") x (Release Fraction)}}{\text{Exfiltration Time (2 or 20 hrs.)}}$$

Table 5.4.1 presents fractional exposures calculated for the iodine isotopes and Strontium-90. The iodine inventories refer to infinite-time experiment operation at 1 watt, and the Strontium-90 concentration to 6 years of continuous operation at 100 watts. The period of isotope release (exfiltration time) and of inhalation exposure are both two hours.

For the case release from the pool to the reactor room, the iodine inventories specified are 100 times greater, corresponding to infinite operation at 100 watts. Here a water-to-air iodine partition of 10 and a 20-hour exfiltration time are assumed. These factors combine to reduce the iodine isotopic release to exactly that of a 1-watt building release (2-hour), and the Fractional Exposures are the same as in Table 5.4.1 for the iodine isotopes. Sr-90 Fractional Exposure for a reactor room release would be lower than for a building release by a factor of 10, due to the increased exfiltration time.

5.4.5.2 Building Exposures

To calculate building exposures, the isotope concentrations are found by dividing the fraction of the isotope inventory released by the volume of the space into which the exposure takes place. Fractional exposure is then calculated in the same manner as for offsite releases. The results of such computations are shown in Tables 5.4.2a and 5.4.2b below, for the reactor room ($2.3 \times 10^3 M^3$) and first floor experimental area ($1.7 \times 10^3 M^3$).

TABLE 5.4.1

EXCLUSION RADIUS FRACTIONAL EXPOSURES

Isotope	Isotope Inventory, Curies	Accident Release, 50% or 1%	2-Hour Release Rate Q_1, Ci/sec^1	70 Meter Concentration, X_1, Ci/M^3	10 CFR-20 Appendix B, TABLE II MPC_1 Values	Fractional Exposures $\frac{(X_1)(7.2\times10^3 sec)(BRR=1.56)}{(MPC_1)(3.15\times10^7 sec)}$
I-131	0.0251	0.013	1.93×10^{-6}	7.5×10^{-8}	1×10^{-10}	0.27
I-132	0.0381	0.019	2.64×10^{-6}	1.03×10^{-7}	3×10^{-9}	0.012
I-133	0.0563	0.028	3.9×10^{-6}	1.52×10^{-7}	4×10^{-10}	0.136
I-134	0.0658	0.033	4.6×10^{-6}	1.8×10^{-7}	6×10^{-9}	0.010
I-135	0.0510	0.026	3.6×10^{-6}	1.4×10^{-7}	1×10^{-9}	0.051
Total Iodine	0.2363					0.49
Sr-90	0.75	0.0075	1.04×10^{-6}	4.1×10^{-8}	3×10^{-11}	0.49*

*Sr-90 Fractional Exposure = 0.05 for a reactor room release.

TABLE 5.4.2a

REACTOR ROOM - 5 MIN. EXPOSURE

Isotope	Isotope Inventory, Ci	Accident Release, (0.05 or 0.01) Ci	X_i in Room Ci/M^3	Fractional Exposures $\frac{(X_i)(300\ sec)(BRR)}{MPC(3.15x10^7 sec)}$
I-131	2.51	.13	$5.7x10^{-5}$	8.5
I-132	3.81	.19	$8.3x10^{-5}$	.41
I-133	5.63	.28	$1.2x10^{-4}$	4.4
I-132	6.58	.33	$1.44x10^{-4}$	.36
I-135	5.1	.26	$1.14x10^{-4}$	1.7
Total Iodine				15.4*
Sr-90	.75	.0075	$3.3x10^{-6}$	1.63

*The reactor room is a Restricted Area, thus the MPC values of Table II, Appendix B, 10 CFR-20 do not apply strictly. Since yearly dose limits on such areas are ~10 times greater than for unrestricted areas, the total iodine FE value of column 5 is the order of 1.5 times allowable.

TABLE 5.4.2b

EXPERIMENTAL AREA - 5 MIN. EXPOSURE

Isotope	Isotope Inventory, Ci	Accident Release, (0.5 or 0.01) Ci	X_i in Area Ci/M^3	Fractional Exposures $\frac{(X_i)(300\ sec)(BRR)}{MPC(3.15 \times 10^7 sec)}$
I-131	0.0251	0.013	7.7×10^{-6}	1.15
I-132	0.0381	0.019	1.12×10^{-5}	.05
I-133	0.0563	0.028	1.62×10^{-5}	.60
I-134	0.0658	0.033	1.95×10^{-5}	.05
I-135	0.051	0.026	1.55×10^{-5}	.23
Total Iodine				2.0
Sr-90	0.75	0.0075	4.5×10^{-6}	2.2

5.4.6 Conclusion

The offsite Fractional Exposures for Iodines and Strontium-90 (Table 5.4.1) are within the limits of 10-CFR-20, for very conservative isotope release assumptions (TID-14844). The Fractional Exposures for spaces within the reactor building, considering the same conservative release fractions, and a 5-minute exposure, are only slightly greater than the 10 CFR-20 limits for these isotopes.

It is concluded that fueled experiments can be operated within power limits set by the Technical Specifications without undue hazard to the general public, the reactor staff or visitors. It is noted that the isotope inventories are related to fueled experiment thermal power or fission rates. These values can be ascertained by fission product radiation intensity measurements, or from fission neutron yield measurements (G.I. Coulbourn and T.G. Williamson, NSE, 35, 367 (1969)).

6.0 RADIATION HAZARDS

6.1 Confinement

The reactor room above the pool level is of cylindrical construction 54 feet in diameter and 36 1/2 feet high. It is designed to withstand a differential pressure of 1/2 psi. The walls are of reinforced masonry, plastered on the inside for gas tightness while the roof is a concrete slab. The openings into the room are the truck door, the personnel door, the escape manhole, and the air intake and exhaust ducts.

The truck door is of steel construction and is opened and closed by use of a manually operated chain fall and gear arrangement. It initiates a scram condition to the reactor when moved from the fully closed position, thereby precluding reactor operations when confinement is broken at this point.

The personnel door swings closed against a rubber gasket by gravity. It is held open during operations by a magnet which releases automatically in the event of a high radiation level in the reactor room as detected by the monitor located on the reactor bridge. Should an incident occur and pressure build up in the reactor room, the pressure will seal the door tightly. The personnel door is illustrated in Fig. 6-1.

In the event of an accident which seals the personnel door, the operator would be trapped in the room. A simple underwater escape hatch is provided as an emergency exit. The emergency escape hatch is normally closed and secured with a slide bolt which will allow easy opening from the inside in the event of an emergency. The escape system is shown in Fig. 6-2.

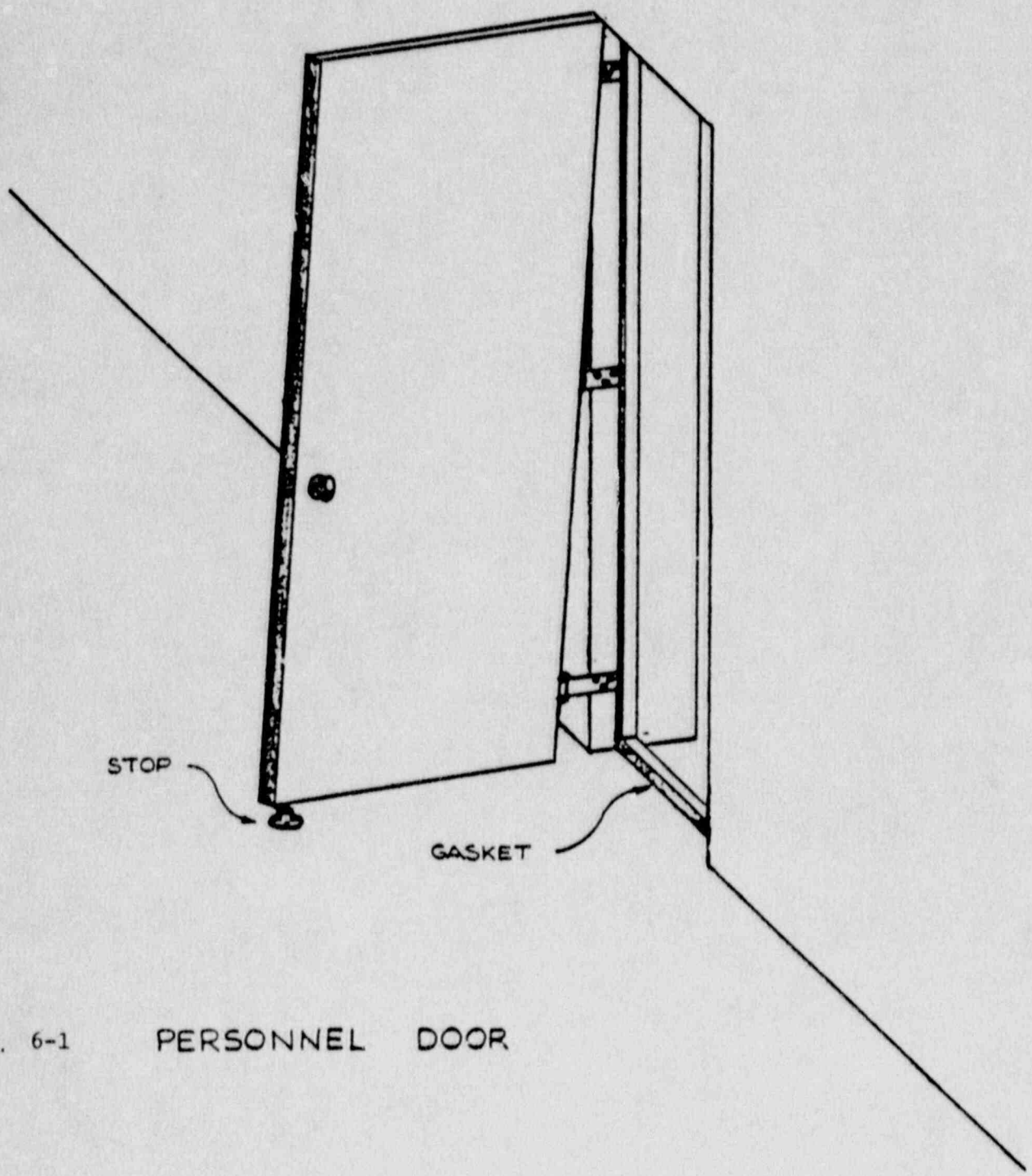

FIG. 6-1 PERSONNEL DOOR

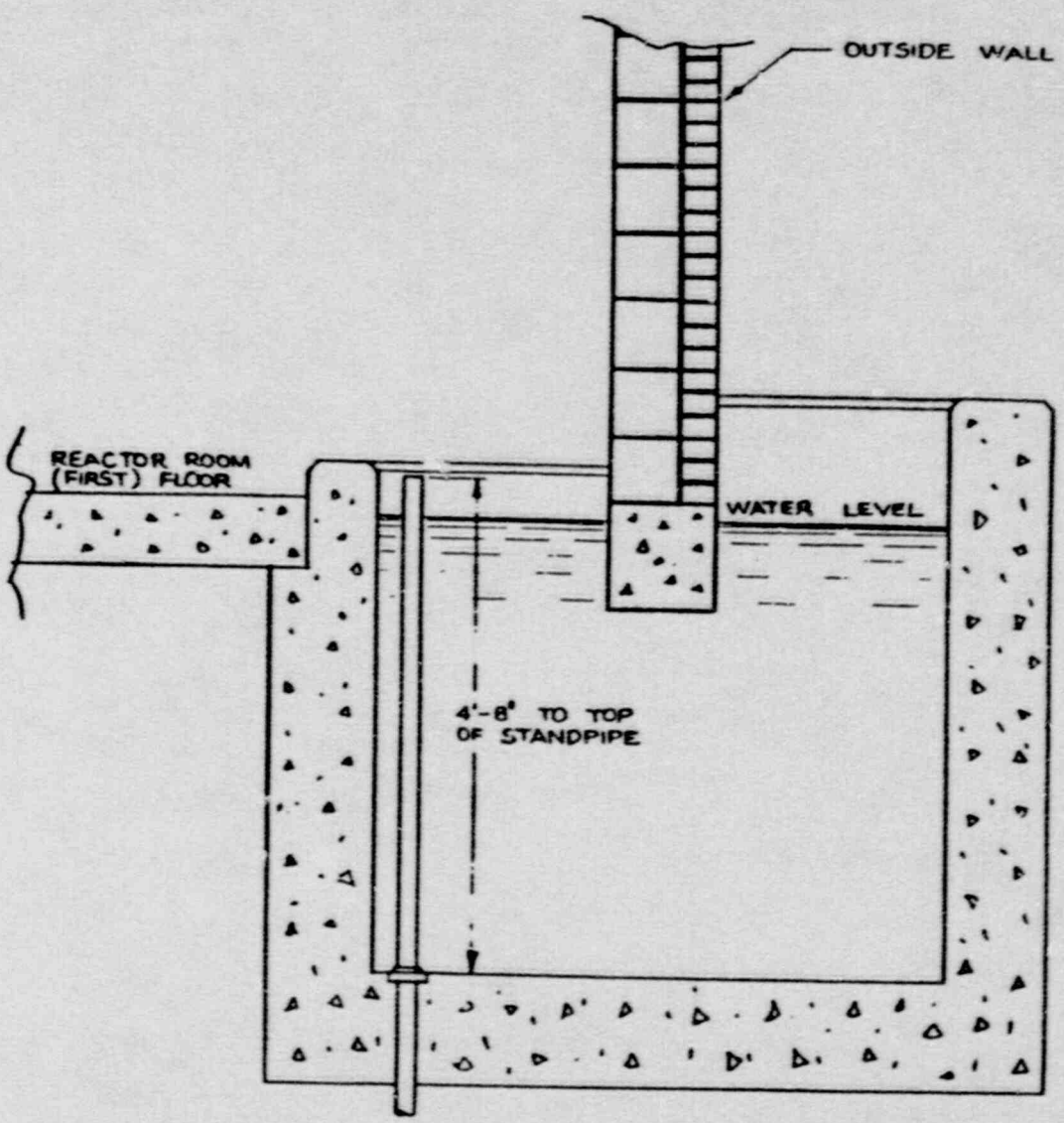

Fig. 6-2 EXIT MANHOLE

The reactor room ventilation exhaust ducts are operated in a manner similar to the personnel door. Each duct has a gasketed, solid, inside door which is opened manually and held open by a magnet. As in the case of the personnel door, these magnets release automatically upon a high radiation level at the reactor bridge. The pressure tight air duct is shown in Fig. 6-3.

Past measurements of the leak rate from the reactor room verified that the exfiltration rate is less than 100% in 20 hours. The leak rate of the reactor room was measured using ^{85}Kr as a tracer. The measurement involves releasing a small amount of the tracer isotope into the containment volume, and subsequently monitoring changes in the relative specific activity of the air in the room. Such changes can be related to the rate of air leakage.

Krypton itself is one of the principal fission product gasses, so its use allows the measurement to be made with an actual isotope of interest. ^{85}Kr has a half-life of 10.7 years, and decays with the emission of a 0.67 MeV beta particle (99+%), and a gamma ray of energy 0.52 MeV (0.7%). The two decay products allow two independent measurements to be made.

To make the measurements, detectors are arranged so that they view the air space within the containment. The beta counting channel need only consist of relatively thin-walled G-M tubes. The range of ^{85}Kr beta particles in air is about two meters, thus the count rate in this channel reflects the local specific activity and is indicative of average specific activity only if there is good air mixing. The gamma-ray counting channel must be able to detect selectively the 0.52

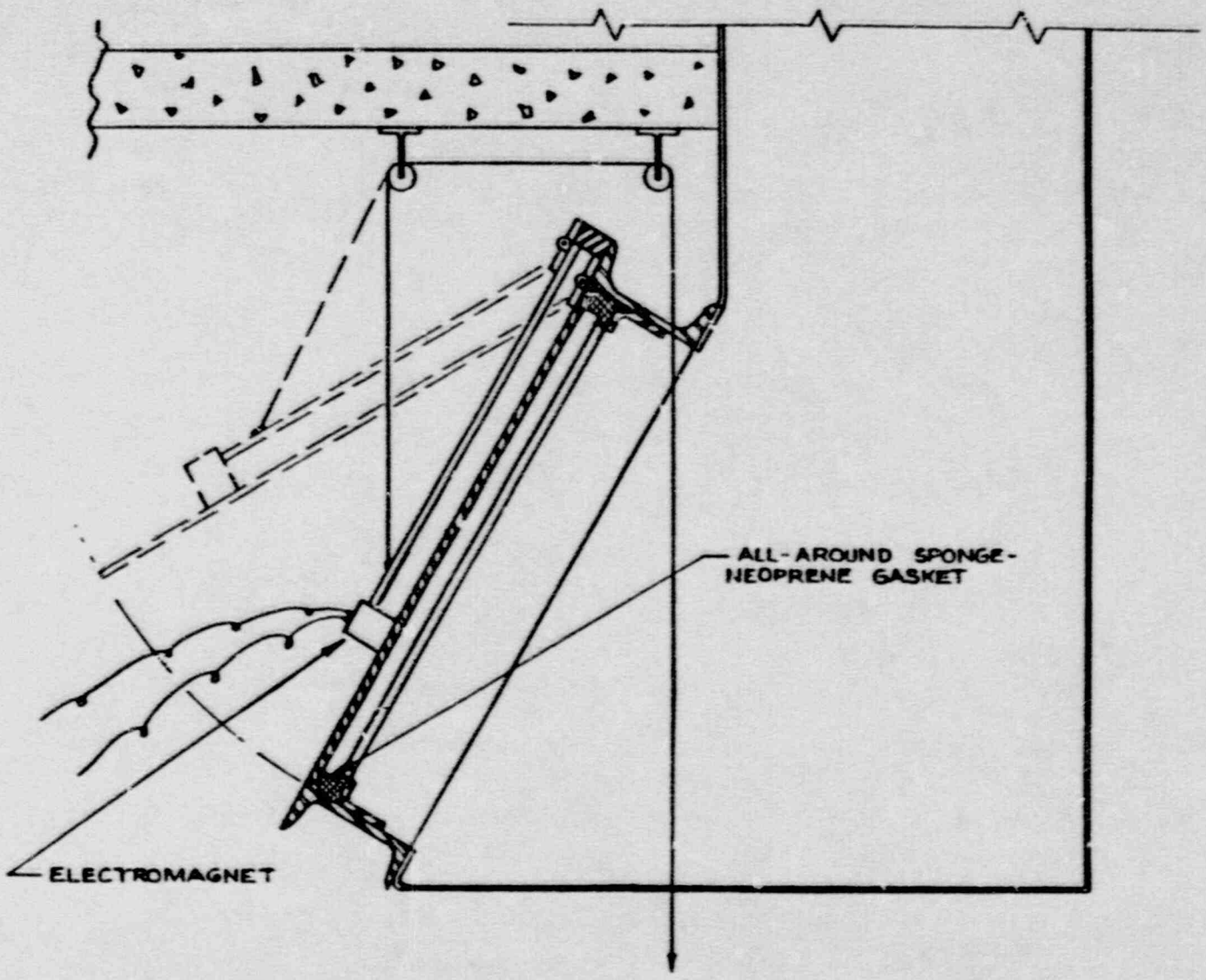

FIG. 6-3 PRESSURE-TIGHT AIR DUCT

MeV photon from ^{85}Kr. The gamma ray count rate provides a direct measurement of the average specific activity, because of the long range of these photons in air (relaxation length about 90 meters).

The release of a concentration of ^{85}Kr of 8×10^{-6} $\mu Ci/cm^3$ provided an initial count rate of 3000 cpm above background from a bank of 3 aluminum-walled G-M tubes, 3-inches long, and 3/4-inch in diameter. The 0.5 MeV photopeak count was 50 cpm, for a 3-inch x 3-inch NaI(Tℓ) crystal.

Figure 6-4 shows the count rate as a function of time for both beta and gamma rays. The leak rate of 26% per 20 hours was well within the Technical Specification 3.7 exfiltration rate of 50% in 20 hours.

6.2 Shielding

The pool is shielded by earth on three sides, but the fourth side consists of a massive concrete shield with thicknesses ranging from a maximum of 90-inches at the bottom, near the core region, to a minimum of 30-inches at the extreme top. This shield is penetrated by two 8-inch beam holes, a large access facility and a thermal column. These penetrations are filled with concrete plugs when not in service. Further descriptions of these facilities are provided in Section 5.0.

A complete survey of the University of Virginia Reactor Shielding was made by the Neutron Physics Division of the Oak Ridge National Laboratory. The results from that survey with the reactor at a power of one megawatt are described in the next paragraphs.

The thermal-neutron dose rates observed over the surface of the shield are plotted in Fig. 6-5, in which the three accessible surfaces have been developed, or "unfolded" to lie flat on the page.

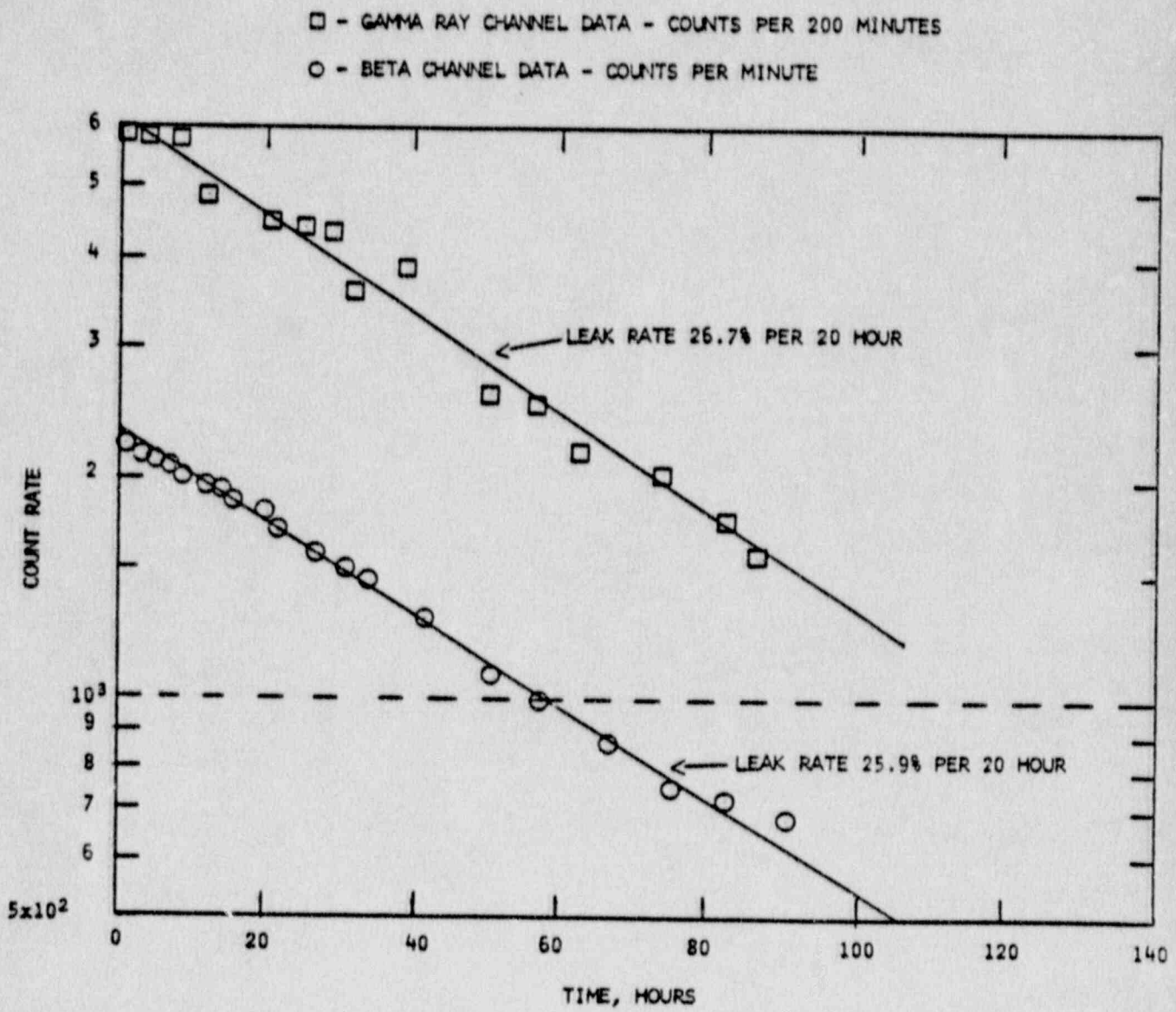

FIGURE 6-4 UVAR CONFINEMENT ROOM COUNT RATE DATA

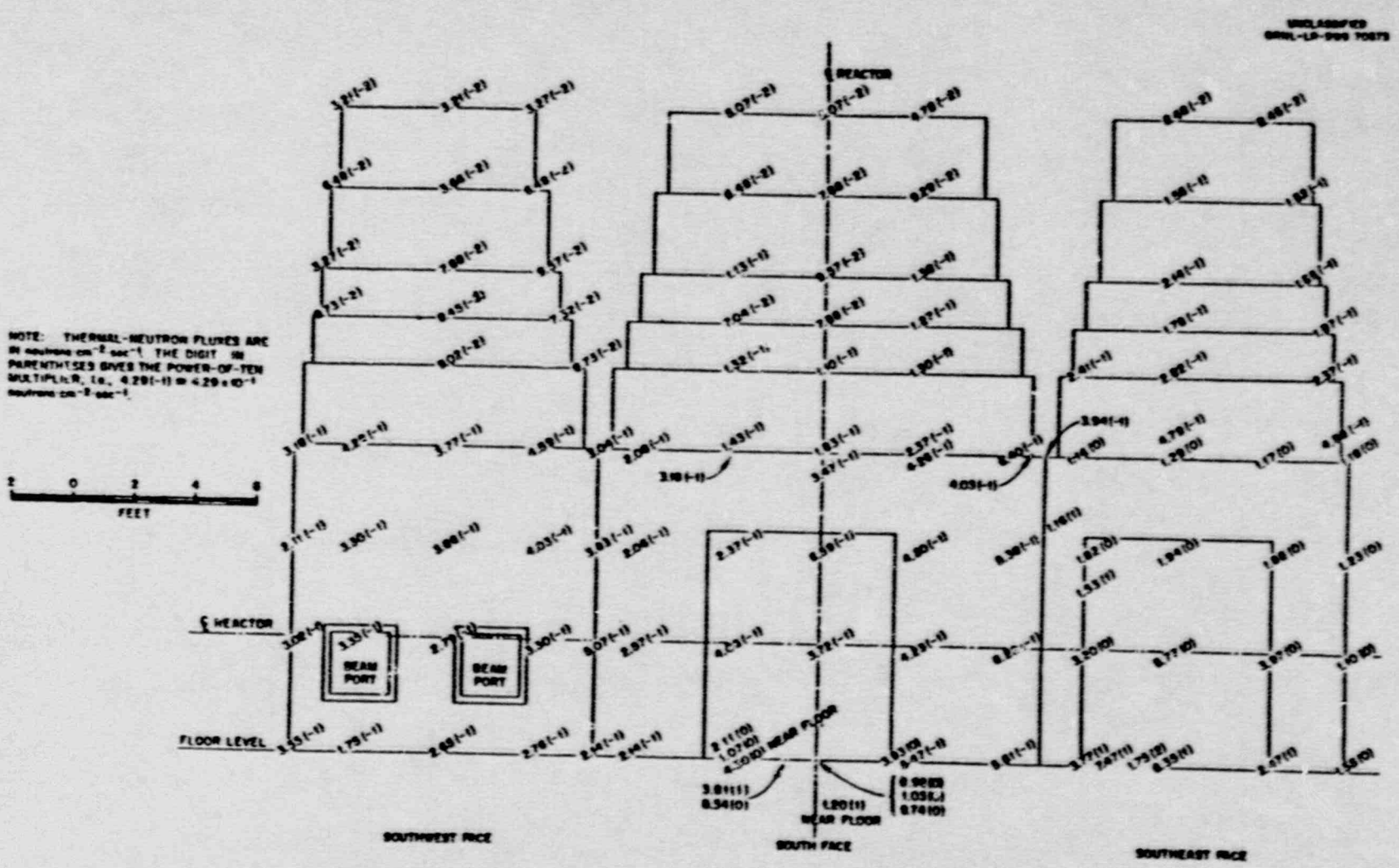

Figure 6-5 Thermal-Neutron Fluxes at the Surface of the University of Virginia Reactor Shield.

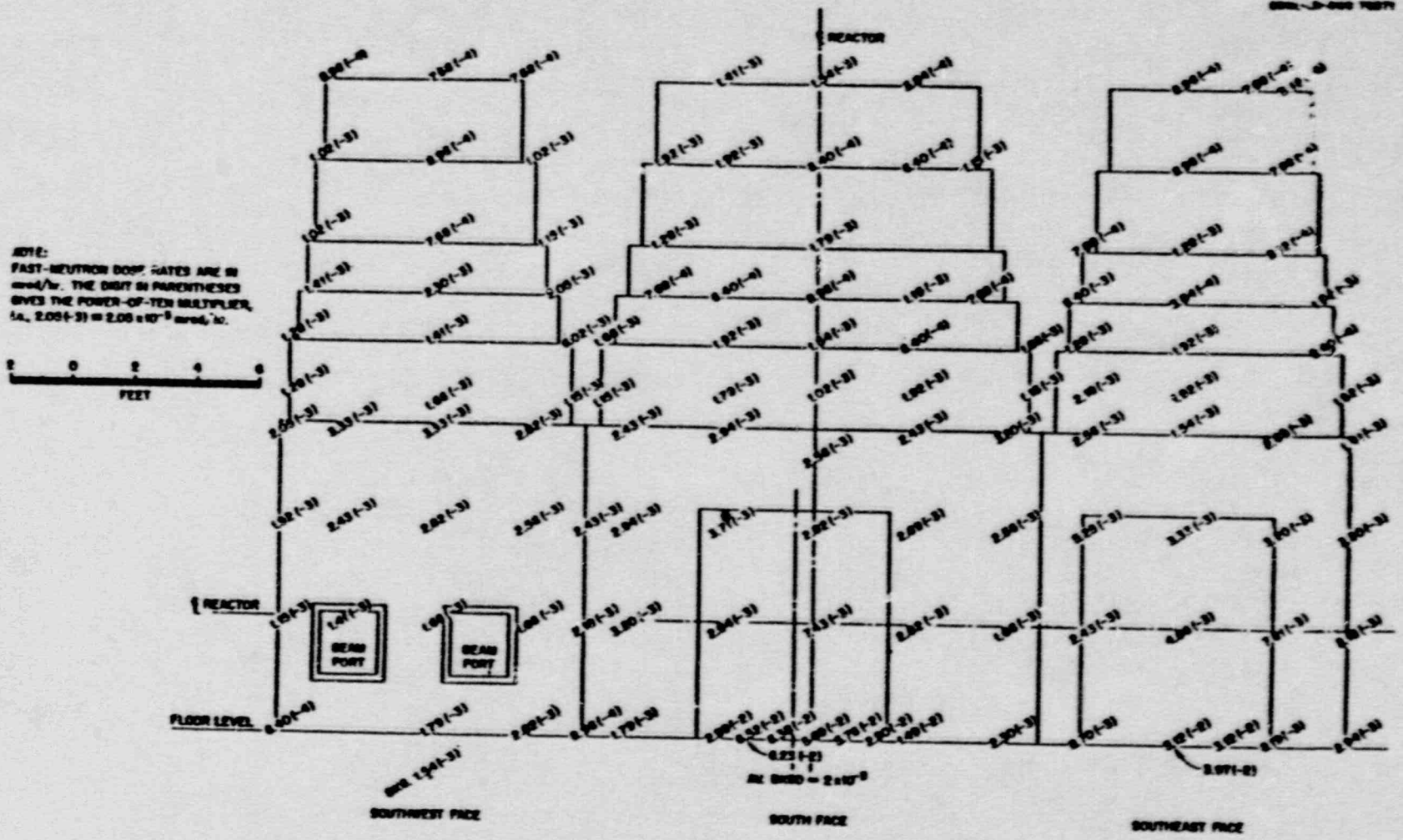

Fig. 6-6 Fast-Neutron Dose Rates at the Surface of the University of Virginia Reactor Shield.

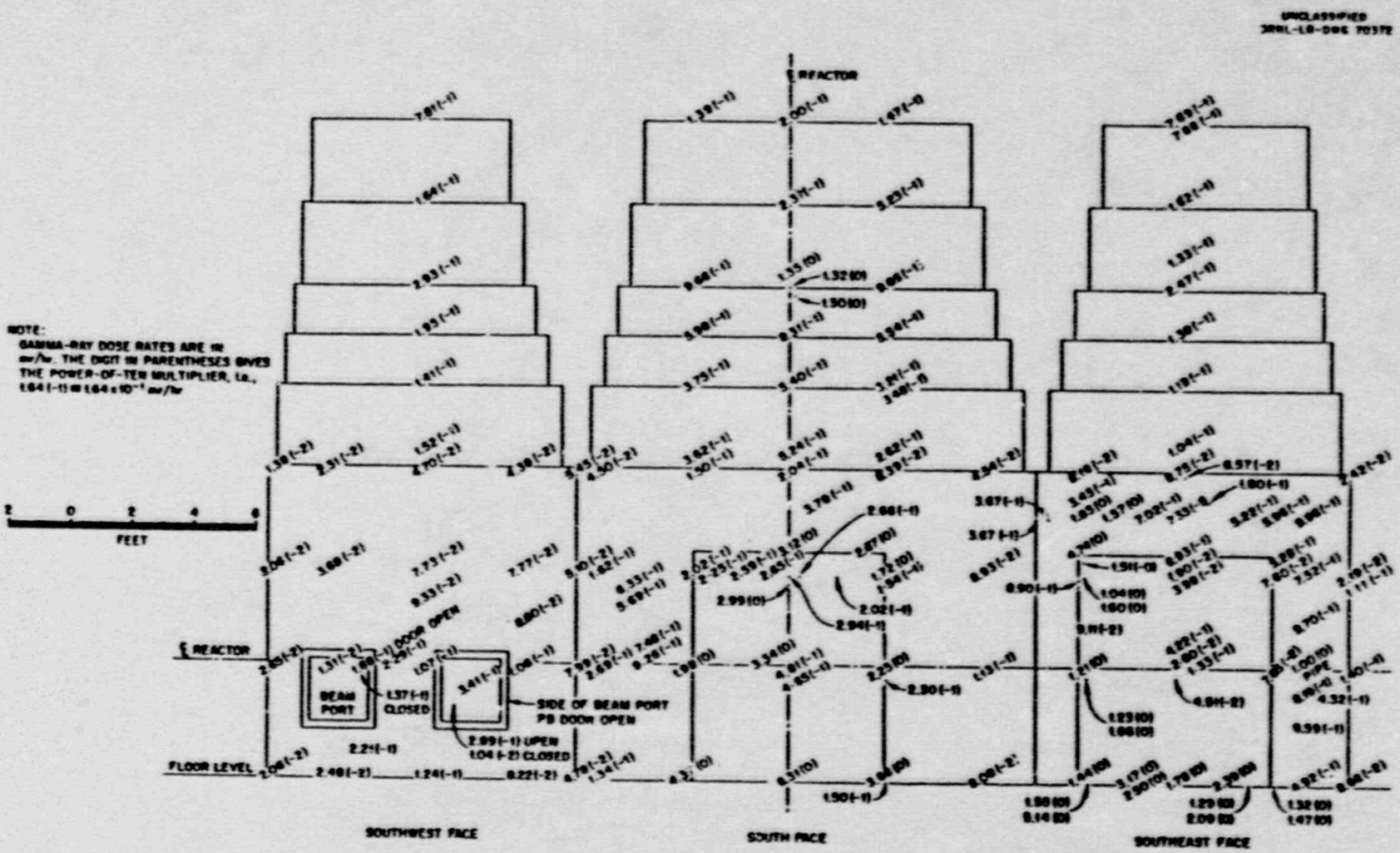

Figure 6-7 Gamma-Ray Dose Rates at the Surface of the University of Virginia Reactor Shield.

Fast-neutron dose rates are plotted in similar fashion in Fig. 6-6, and gamma-ray dose rates in Fig. 6-7.

In connection with the fast-neutron dose rates reported in the present work, some comments are required. The modified long counter with which the fast-neutron data were obtained is strongly directional, responding in terms of correct dose only when the neutrons are incident upon its front face. This factor is inherent in its design. Its response to neutrons impinging upon its sides is considerably higher. Thus, the dose rates measured by the modified long counter must be considered to be an upper limit to the true fast-neutron dose at the point of the measurement. Against a shield face, or in measuring neutron streaming through a crack or hole in a shield, the dose rate measured is probably very close to the true value. As the neutron field surrounding the counter approaches isotropicity, the dose measured is expected to be an overestimate, possibly a considerable overestimate. This latter condition would apply to measurements made in the vicinity of the heat exchanger.

Fluxes and dose rates were in general very low. Streaming around the thermal column and access facility closures was somewhat evident, amounting to a maximum fast-neutron dose rate of 0.0652 mrad/hr, a thermal-neutron flux of 10 to 12 neutrons cm^{-2} sec^{-1}, and gamma-ray dose rates of roughly 6 mr/hr.

Data was also obtained at distances from 4 to 6-inches above the pool water surface. These values are plotted in Fig. 6-8. Gamma-ray dose rates as high as 7 mrad/hr were measured.

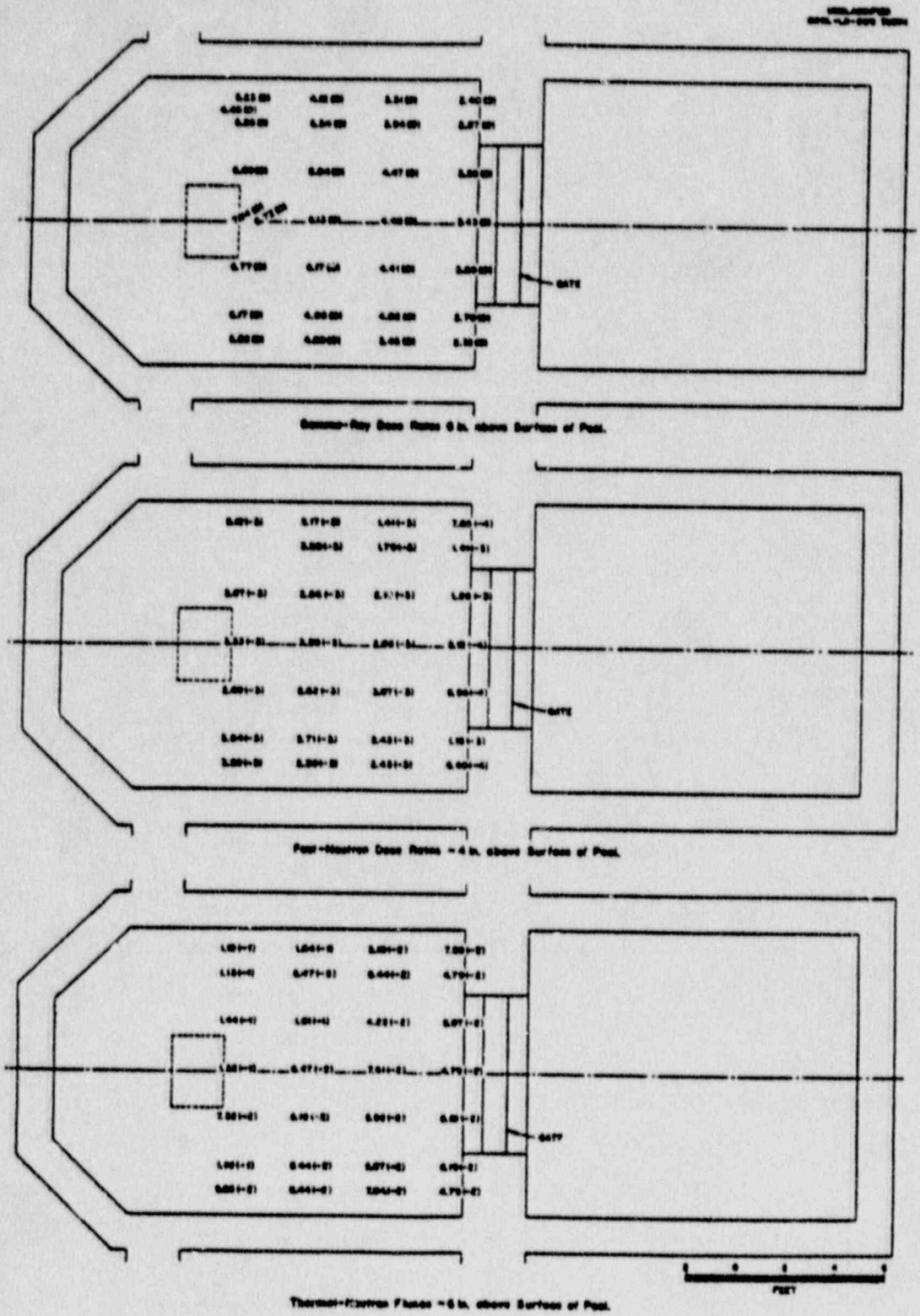

Figure 6-8 Gamma-Ray and Fast-Neutron Dose Rates and Thermal-Neutron Fluxes Near Surface of University of Virginia Reactor Pool.

6.3 Hazards During Normal Operation

Calculation of the concentration of Argon-41 in the beamport extension after prolonged operation at 2 MW predict a discharge to the atmosphere that was approximately a factor of two below the maximum permissible concentration. Comparison of experimental measurements by the ORNL team and calculated values of Argon-41 concentrations demonstrated that the assumptions made in the calculation were conservative by an additional factor of three. These factors, combined with the ease with which the concentration of radioactive Argon-41 can be reduced by delaying release after operation to permit decay, indicate that this hazard presents no problem at a reactor power level of 2 MW.

The measurements of radiation intensity by the ORNL team at 2 MW indicate high gamma-ray dose rates at four locations: (1) at the surface of the pool immediately above the reactor core, (2) around the shield plug of the large access facilities, (3) in the heat exchanger room, (4) in the main demineralizer room and (5) in the source storage room. Current policies limit access to the heat exchanger room during operation and the safeguards are adequate to control this hazard. When the limited amount of time spent at the other three locations is considered, these do not appear to be a serious hazard. However, marking these locations will serve to remind personnel of the existing dose rate at 2 MW.

7.0 HEALTH PHYSICS

7.1 General Information

The Reactor Facility is a research tool of the University and as such, subject to use by all of its schools. It is the responsibility of the operations staff and the Health Physicist to provide and maintain full use of this tool, yet prevent undue risks and hazards to the individual workers, the University and the Community at large.

The Health Physicist is responsible for assuring that those measures and regulations pertaining to the Health Physics aspects of the reactor and its operation are carried out and mantained. The Director of the Reactor Facility is advised by the Health Physicist in all pertinent matters. The close association but independence of the Health Physics and Reactor Facility operations has worked well at other reactor installations, and the University has patterned its organization accordingly.

7.2 Education in Health Physics

It shall be the duty of the Health Physicists, or his designee, to periodically instruct Reactor Facility personnel about the risks and hazards of radiation and the means of lessening this danger to themselves and others. This shall be done as follows:

(A) Each individual with unescorted access to the Reactor Facility will be given an initial indoctrination lecture about Health Physics, followed by a question and answer period, so that the biologic aspects and the genetic aspects of radiation change are understood.

(B) On-the-spot lectures may be given by the Health Physicist, during a particular phase of operations, to emphasize the protection aspects of Health Physics.

(C) Pre-experiment evaluation of hazards associated with a particular experiment will be performed first by the individual proposing a new experiment and then by the Health Physicist.

(D) A radiation log will be prepared for each "permanent" worker at the facility. In this log the monthly dose data will be recorded.

7.3 Personnel Monitoring and Protection

The Health Physicist is charged with the procurement and maintenance of the detection equipment and the dose badges for personnel exposure monitoring.

Badges: These will be used for monthly checking of personnel neutron and/or gammma dose, with the dose evaluations performed by a commercial supplier.

Pocket chambers: Direct reading - will be worn by personnel working in suspected high radiation areas.

Finger badges - will be worn by personnel handling highly radioactive material.

Protective clothing - street clothes are worn by the majority of workers at the facility; however if there is a possibility of personal or area contamination, protective and/or disposable clothing is provided and will be worn.

7.4 Permanent Monitoring and Surveys

Fixed Radiation monitors are mounted in the following areas:

1) On the reactor bridge,

2) Ground floor wall (reactor face area),

3) Outside the hot cell,

4) In the demineralizer room.

The readings of these monitors are displayed individually on the

secondary console in the reactor room. The existence of excessive radiation in any of these areas causes an audible alarm to sound at the console. The initiation of the reactor bridge monitor alarm and the ground floor monitor alarm isolates the containment, as described earlier, and scrams the reactor. In addition, numerous portable instruments are available for surveying all areas in the facility.

Calibration of these instruments on a regular basis will be assured by the Health Physicist. Calibration records will be mantained.

The initial run of a new experiment or the use of radioactive materials will be extensively monitored and a record maintained of the results, if the work is such that the Health Physicist determines a possible radiological hazard to personnel exists.

Facility radiation surveys, air sampling, and contamination smears will be performed in work areas on a regular basis by the Health Physicist or his designee. Such official will be recorded. Informal surveys made by the experimenters of their work areas to confirm typical (safe) radiation levels may be made unofficially and need not be recorded. However, if excessive levels not previously identified are found, the experimenter will notify the Health Physicist, who will then make an official survey.

7.5 Prohibitions and Sanctions

The Reactor Safety Committee and the Reactor Facility Director are responsible for enforcing all applicable Federal, State and University regulations necessary to run the facility. The Health Physicist will report irregularities and recommend necessary steps for

their correction to the Director and the Safety Committee. The Director will determine corrective actions to be taken in such cases. However, the Health Physicist may issue emergency orders if necessary, on his own responsibility.

Safe areas for eating and drinking will be designated by the Health Physicist. Smoking is permitted in private offices and specially designated common areas where unsealed radioactive materials are not used.

The University of Virginia has established a whole body personnel dose limit of 0.5 rem/year which is 10% of the limits in 10CFR, Part 20. If an individual receives a radiation dose in excess of these limits as determined by ionization chambers, dosimetry badges or other methods, the Health Physicist will notify the Facility Director. The Health Physicist will provide information concerning the amount and type of exposure and recommend actions to be taken by the individual to avoid further, similar exposures.

7.6 Waste Disposal

The Health Physicist will check radioactive waste and refuse from the Reacator Facility, monitoring it prior to legal disposal. The public water system will be separate from water drainage systems used to collect and discard radioactive material. The disposal of liquid radioactive wastes is discussed in Section 4.8 of this document. Dry litter and waste will be stored until it has decayed to safe levels or can be shipped to a licensed burial site. Radioactive materials may be released only with the approval of the Health Physicist.

7.7 Shipping and Transport

Radioactive material produced or purchased by the Reactor Facility will generally be used on-site. However, in instances where material must be shipped from the reactor to one of the schools on the University grounds, or to national or international recipients, applicable DOT regulations governing shipments of radioactive material, as outlined in 10 CFR Part 71, will be followed. Radioactive material will not be allowed to leave the reactor site unless the recipient is qualified to receive the materials under NRC or international regulations, as applicable.

8.0 ADMINISTRATION

8.1 General Organization

The reactor is operated under NRC License R-66 granted in 1960. The Reactor Facility organization responsible for assuring safe reactor operations and use of radioactive materials at the University of Virginia is shown in Fig. 8-1. This organization includes two major committees: the University Radiation Safety Committee and the Reactor Safety Committee.

8.2 Radiation Safety Committee

The Radiation Safety Committee is appointed by the President of the University and must approve the possession and use of radioactive materials at the University of Virginia with the exception of those associated with the Reactor Facility. Production, possession and usage of radioactive materials at the reactor comes under the reactor license and is reviewed by the Reactor Safety Committee.

8.3 Reactor Safety Committee

As required by the license, a Reactor Safety Committee is active. As a minimum, the Reactor Safety Committee is composed of at least five members and includes the University's Radiation Safety Officer, the Reactor Director and a professor from a department other than Nuclear Engineering. Senior members of the Reactor staff attend committee meetings in an advisory capacity, but there is only one vote by the Reactor Staff which is cast by the Reactor Director. This is to prevent domination of the Committee by members of the operating organization of the reactor. The Reactor Health Physicist is also welcome to attend Reactor Safety Committee meetings.

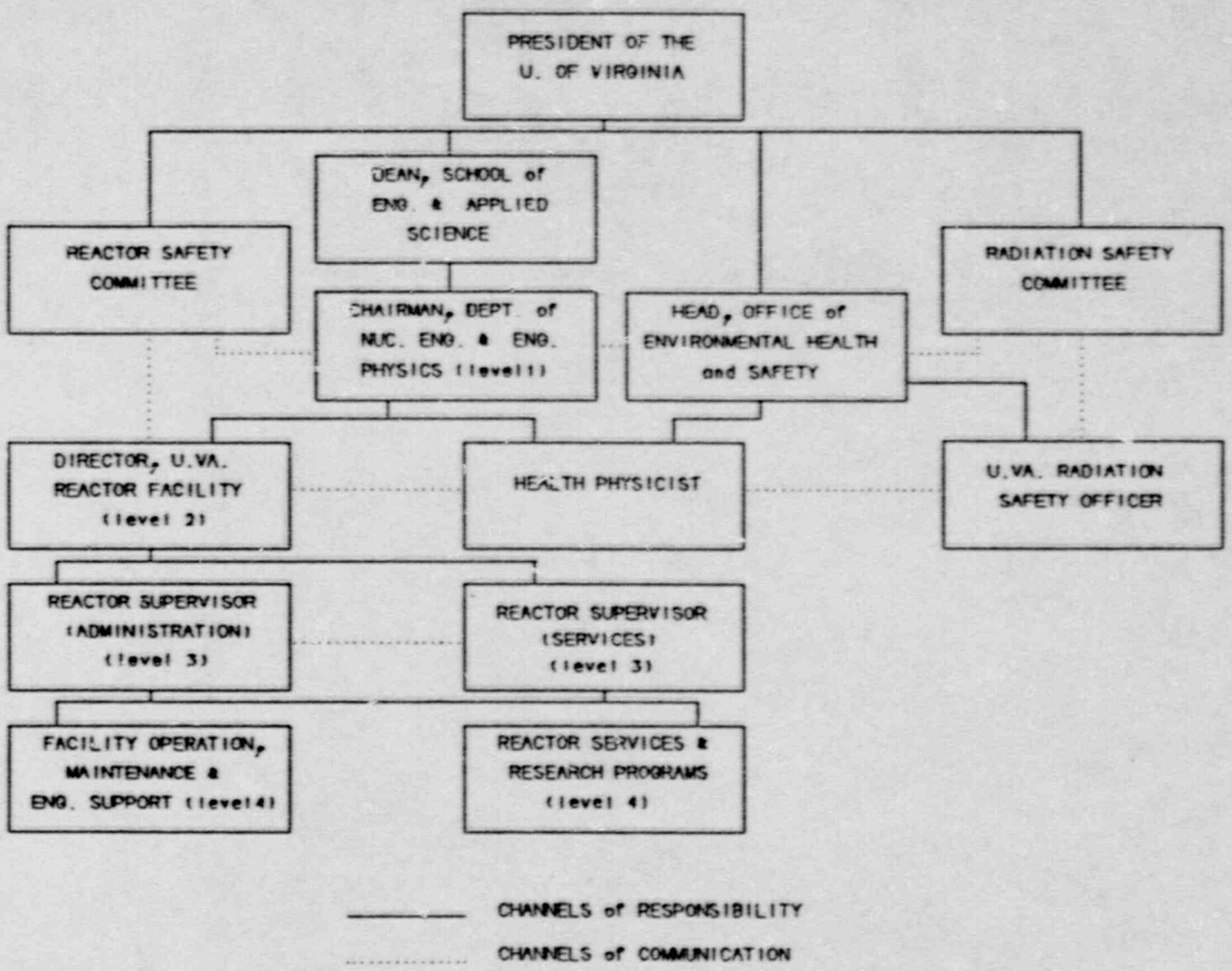

Figure 8.1 Organizational Structure of U.Va. Reactor Facility

The Committee reviews and passes on new experiments that could affect the safety of the reactor. These include critical experiments, as well as experiments in which the reactor is used as a radiation source. Written standard operating procedures (SOP's) and emergency plan and implementing procedures (EPIP's) approved by the Committee are in effect for reactor operations. Experiments involving the reactor are run under written and Reactor Safety Committee approved procedures. While the Reactor Safety Committee approves the procedures to be followed for safe operations and experiments, the detailed routine enforcement of reactor safety is the responsibility of the operating staff. Also, while the Reactor Safety Committee has the authority to require and approve specific procedures to prevent unacceptable exposure of personnel to radiation, the immediate responsibility for compliance with Title 10, Code of Federal Regulations, Part 20, rests with the Reactor Staff and, in particular, with the Health Physicist.

8.4 Procedures

The reactor is operated in accordance with written standard operating procedures (SOP's) approved by the Reactor Safety Committee. These procedures include normal startup, operation and shutdown of the reactor. Emergency plan implementing procedures (EPIP's) exist to implement a Reactor Safety Committee and NRC approved Emergency Plan (EP). General procedures for the handling of radiation experiments are promulgated by the University but these are supplemented by special procedures which apply only to the experiment under consideration.

Procedures dealing with the operation of the reactor and associated experiments must have the approval of the Reactor Safety Committee.

Changes to these procedures require the approval of this committee, however, minor deviations not changing their intent may be made by the Reactor Director, and is permitted by the SOP's. When deviations to SOP's occur, the RSC is informed by memo from the Reactor Director. It is to be recognized that procedures notwithstanding, the safe operation of the reactor is dependent upon the Reactor Staff and their exercise of good judgement.

All personnel, including students who work routinely at the Reactor Facility, wear dosimetry badges. Occasional visitors are issued self-reading pocket dosimeters. For large groups of visitors, two pocket dosimeters are worn by the staff member acting as a guide. This permits tours to be conducted without issuing large number of individual pocket dosimeters.

8.4 Records

The reactor log book and all other records are open for inspection by the Reactor Safety Committee. These records, plus all the records of the activities of the Safety Committee, are also available for review by NRC compliance inspectors. An annual report is submitted to the NRC listing changes made to the facility under 10CFR50.59 and describing minor accidents pertinent to safety. Major incidents are reported to the NRC as required by the Technical Specifications.

9.0. Safety Analysis

The UVAR's MTR type LEU fuel elements contain plates with low enriched uranium fuel clad with aluminum. Standard elements contain 22 flat fuel plates, control rod elements contain 11 fuel plates, and partial elements contain 11 fueled and 11 non-fueled plates in an alternating array. The overall external dimensions of these three element types are essentially the same, so that they may fit anywhere on the 8 by 8 reactor core grid plate. Details of the physical arrangement are contained in Section 3.0.

The limiting conditions of reactor power, coolant water flow rate and inlet pool water temperature are given in the UVAR Technical Specifications. The bases for the Safety Limit and Limiting Safety System Settings and the thermal-hydraulic analysis are presented in this chapter. References used in the analysis are listed at the end of this chapter.

9.1. Thermal Hydraulic Analysis of the UVAR

To establish the safety limit, limiting safety system settings, limiting condition of operation, and normal operating conditions for pool reactors it is necessary to examine factors such as burnout, or an excursive hydraulic instability resulting in subsequent burnout, which may lead to the disruption of fuel plate integrity. In addition, it is necessary to determine by calculation the operating conditions at which the onset of nucleate (incipient) boiling will occur in a coolant channel, so that reactor operating conditions may be set at levels which prevent these phenomena.

An analytical procedure was developed to predict: 1) burnout, 2) hydraulic instability, and 3) incident boiling, in the hot channel of a UVAR LEU 22 plate fuel element. The effects of the following parameters were studied: (1) channel inlet (pool) temperature, (2) heat flux distributions, i.e. uniform, chopped cosine and exit peak, and (3) coolant flow rate.

The Gambill[1] correlation was used for estimating burnup heat fluxes for subcooled boiling. Only downflow was considered for forced cooling in the analysis. An equation proposed by Rohsenow and Bergles[2] was used for predicting the onset of nucleate boiling and a comparison was made with experimental data obtained from the Oak Ridge Research Reactor.[3]

Three vertical power profiles were considered in the analysis: 1) uniform power profile, 2) chopped cosine power profile, and 3) exit peak power profile. The exit peak power profile illustrated in Figure 9-1 was found to be the most limiting and was used throughout this analysis. The exit peak power profile is based upon neutron flux measurements in the hot channel of the UVAR HEU core which is located in a control rod element and is next to the water filled gap left by the withdrawn control rod.

Numerous empirical correlations were used in the thermal-hydraulic analysis of the LEU UVAR. Because of the importance of justifying the use of these correlations, the following sections provide a brief discussion of the correlations and the ways in which they were employed in the calculations. Where possible, comparisons of analytical calculations with experimental data are made.

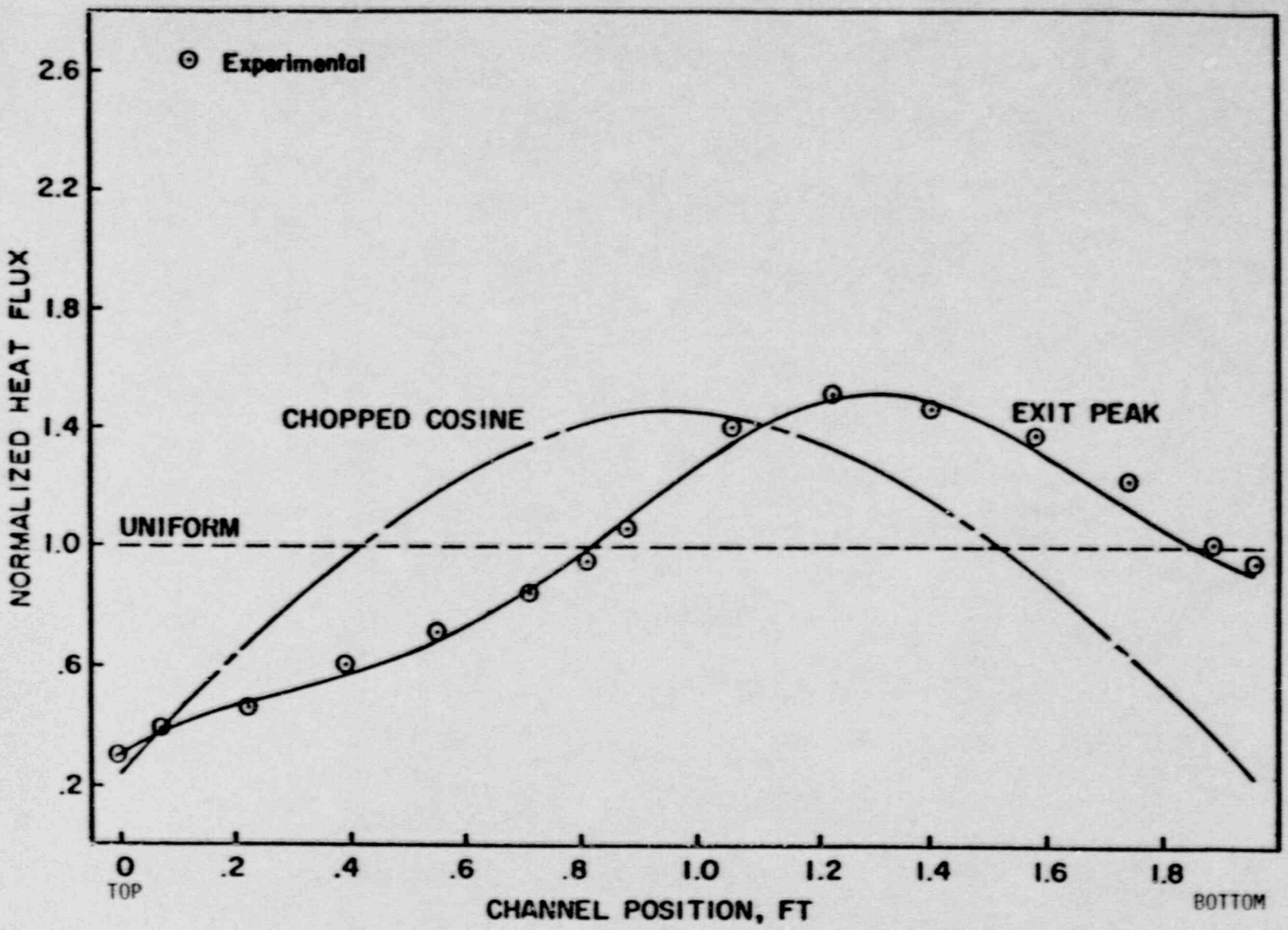

FIG. 9-1 HEAT FLUX DISTRIBUTIONS

9.2. Forced Convection Heat Transfer

In the thermal-hydraulic analysis of the LEU UVAR, the flow velocities are small and the channel length-to-equivalent diameter ratio is 130. As a consequence, part of the analysis involves flows in the transition Reynolds number range and entrance effects exist over a substantial portion of the channel length. The Hausen[4] equation accounts for these factors and was therefore used. The expression for the local heat-transfer coefficient is given by

$$h(z) = 0.116 \left(\frac{k}{D_e}\right) \left[N_{Re}^{2/3} - 125\right] N_{Pr}^{1/3} \left[1 + \frac{1}{3}\left(\frac{D_e}{z}\right)^{2/3}\right] (\mu_b/\mu_w)^{0.14} \quad (9.1)$$

where: $h(z)$ = local heat-transfer coefficient, BTU/hr-ft^2-^{o}F

k = fluid thermal conductivity, Btu/hr-ft-^{o}F

D_e = channel equivalent diameter, ft

N_{Re} = Reynolds number

N_{Pr} = Prandtl number

z = axial location in channel, ft.

μ_b = fluid viscosity at local bulk temperature, lb_m/sec-ft

μ_w = fluid viscosity at local wall temperature, lb_m/sec-ft

Except for μ_w, the fluid physical properties in Eq. (9.1) are evaluated at the local bulk temperature. Since the wall temperature is needed to use Eq. (9.1), an iterative technique is required in its application.

9.3. Prediction of Incipient Boiling

Based upon a semi-empirical approach, Bergles and Rohsenow obtained a correlation for predicting incipient boiling that is dependent only on pressure and wall temperature. Although some of their experimental data indicated that bulk fluid subcooling had an effect upon incipient boiling, this factor was not incorporated in the correlation. For water, over a pressure range from 15 to 2000 psia, the heat flux at incipient boiling is given by[2]

$$q''_{IB} = 15.6\, p^{1.156}\, (T_w - T_{Sat})^{2.30}/p^{0.0234} \qquad (9.2)$$

where q''_{IB} = incipient boiling heat flux, Btu/hr-ft^2

p = pressure, psia

T_w = local wall temperature, ^oF

T_{sat} = fluid saturation temperature, ^oF

For pool reactors with low velocity flows, Eq. (9.2) generally predicts incipient boiling at lower wall superheat temperatures than is actually the case. This is attributed to an absence of very large cavities which would support nucleation at the lower heat fluxes in such a system[2].

The wall temperature must be determined in order to use Eq. (9.2). This quantity is calculated using the heat-transfer coefficient given by Eq. (9.1). The solution q_{IB}'' requires an iterative procedure since h is dependent upon wall temperature, which is related to the local heat flux.

In order to test the validity of the use of Eqs. (9.1) and (9.2) for pool reactor thermal analysis, a comparison was made between calculated incipient boiling and experimental results obtained from the Oak Ridge Research Reactor (ORR). Figure 9-2 shows the results of the comparison, and as seen, a very good agreement exists. For the experimental curve, the anomalous behavior shown by the dashed line has not been explained. However, the Oak Ridge investigators thought that gas bubbles other than steam may have been produced in the core during this part of the experiments.

9.4. Burnout Heat Flux

Numerous correlations have been proposed for the prediction of subcooled and quality burnout. Unfortunately, most of these correlations are not applicable to the UVAR parameter range. Selection of burnout correlations should be made on the basis of burnout data that fall within the pertinent parameter range. Data collected by Gambill were at conditions representative of the UVAR parameter range.

Gambill's correlation for subcooled burnout was used for the UVAR analysis because it is quoted as being applicable for the UVAR parameter range and its predictions are reasonably accurate when applied to the available data that is closest to the UVAR parameter range.

Gambill proposes a superposition approach for treating burnout which is given by[1]

$$q_c'' = q_{PB}''(\text{pool boiling}) + q_{FC}'' \text{ (forced convection)} \qquad (9.3)$$

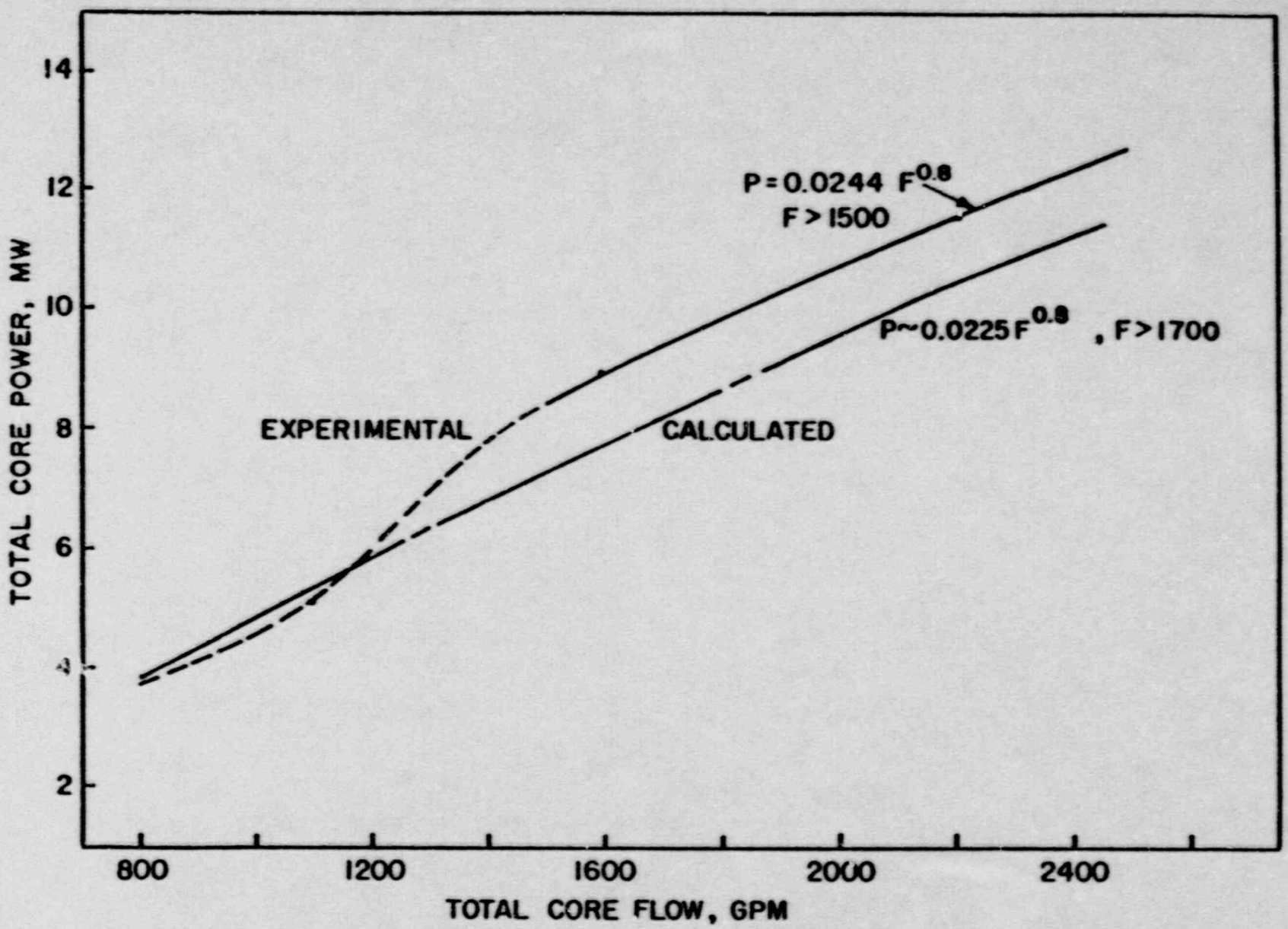

FIG. 9-2 -CALCULATED vs. EXPERIMENTAL INCIPIENT BOILING IN THE ORR

The pool boiling term for conditions representative of pool reactors is[5]

$$q''_{IB} = 0.15\, h_{fg}\sqrt{\rho_g}\left[\sigma g g_c\ (\rho_f - \rho_g)\right]^{1/4} \times \left[1 + \left(\frac{p_f}{p_g}\right)^{3/4} \frac{c_p(T_{Sat} - T_b)}{9.8\, h_{fg}}\right] \tag{9.4}$$

where h_{fg} = latent heat of vaporization, Btu/lb_m

σ = liquid-vapor interface surface tension, lb_f/ft

g = acceleration of gravity, ft/sec^2

$$g_c = 32.2 \frac{lb_m}{lb_f} \frac{ft}{sec^2}$$

ρ_f = saturated liquid density, lb_m/ft^3

ρ_g = saturated vapor density, lb_m/ft^3

c_p = liquid specific heat, btu/lb_m - ^oF

T_{Sat} = saturation temperature, ^oF

T_b = local bulk fluid temperature, ^oF

The forced convection term is

$$q''_{FC} = h(T_{WB} - T_b) \tag{9.5}$$

where h is the Hausen local heat-transfer coefficient given by Eq. (9.1) and T_{WB} is the Bernath critical wall temperature given by[6]

$$T_{WB} = 102.5 \ln p - 97.2 \left(\frac{p}{p + 15}\right) - 0.45u + 32,\ ^oF \tag{9.6}$$

where p is the fluid pressure in psia and u is the mean fluid velocity in ft/sec.

Because radiation exposure to personnel from N-16 activity in the pool water is a concern, the UVAR uses coolant downflow which has an adverse effect upon burnout. Buoyancy effects reduce bubble velocities and as a result burnout heat fluxes are reduced. Gambill has studied the effects of downflow at low velocities and pressures and recommends the following corrections be applied to his burnout correlation.[5]

$$\frac{q_c''(\text{downflow})}{q_c''} = \frac{1}{6.58\ (N_{Gr}/N_{Ka})^{0.39}} \tag{9.7}$$

The ratio of Grashof to Karman numbers if given by

$$N_{Gr}/N_{Ka} = \frac{p_f^2\ g\ \beta(T_b - T_l)D_e}{f_w G^2} \tag{9.8}$$

where β = liquid volumetric coefficient of expansion, $^{o}F^{-1}$

T_b = local channel bulk temperature, ^{o}F

T_l = channel inlet temperature, ^{o}F

f_w = Darcy-Weisbach friction factor

G = mass velocity, lb_m/ft^2

The evaluation of f_w is addressed later in the discussion of flow stability. All fluid properties in Eq. (9.8) are evaluated at the average channel temperature up to the point of consideration. The range of applicability of Eq. (9.8) is for $0.008 \leq (N_{Gr}/N_{Ka}) \leq 1.0$, for $N_{Gr}/N_{Ka} > 1.0$, and it is recommended that the value 1.0 be used for the ratio in Eq. (9.8).[5]

Some of the downflow burnout data collected by Gambill were at conditions representative of the UVAR parameter range. These data were taken in a 0.9 cm diameter tube of 25 and 30 cm lengths. The pressure was 16.2 psia, the fluid inlet velocities ranged from 0.29 to 7.7 ft/sec and the fluid bulk inlet temperatures ranged from 51°F to 71°F. Figure 9-3 shows Gambill's ratios of calculated burnout heat fluxes (from Eqs. (9.3) through (9.8)) to experimental burnout heat fluxes. As shown, the agreement is quite good with 90 percent of the predictions falling within ± 30 percent of the experimental values. This agreement causes a considerable amount of confidence to be attached to the analytical procedures.

Two further uncertainties exist in using Gambill's burnout correlation for the UVAR burnout analysis. These uncertainties are: (1) the effects of non-uniform heat generation in the UVAR and (2) the validity of applying a burnout correlation based upon circular tube burnout data to rectangular channels. As regards the first uncertainty, experiments by Todreas[7] indicate that for subcooled burnout the effects of non-uniform heat generation are not substantial. A review of the Non-Uniform Heat Generation Experimental Program of the Babcock and Wilcox Company indicates that the total channel power at burnout is essentially independent of heat flux distribution. As concerns the second uncertainty, it appears the effects of geometry are small or advantageous for rectangular channels[8,9], when burnout data with tubes and rectangular channels having the same equivalent diameter are compared. Some researchers have observed up to 40 percent[8,10] increases in burnout heat fluxes for rectangular channels. For the UVAR thermal analysis,

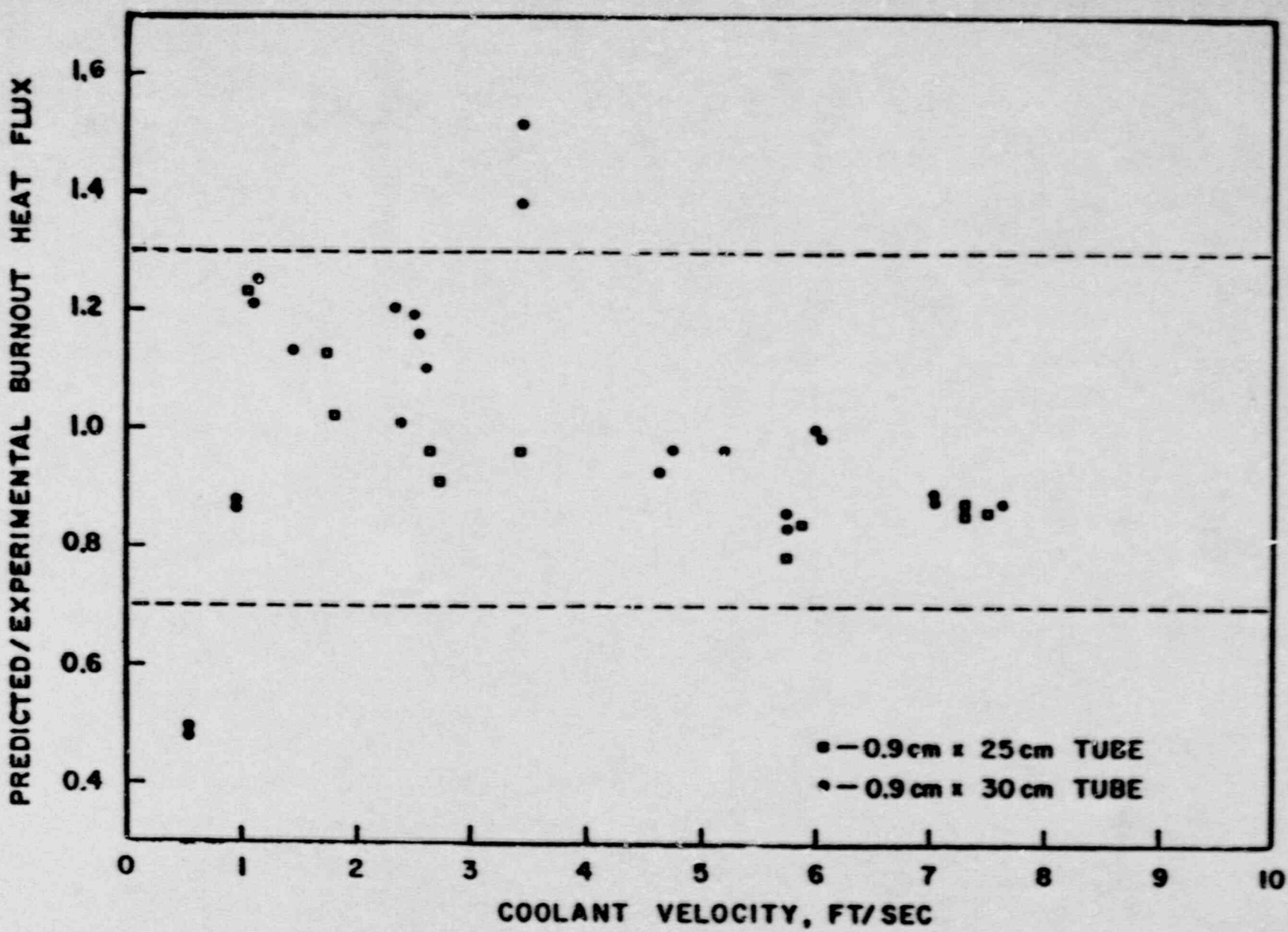

FIG 9-3 -COMPARISON OF CALCULATED WITH EXPERIMENTAL BURNOUT HEAT FLUXES

burnout or a flow instability usually occurs before the water reaches its saturation temperature and burnout is assumed to occur when it reaches its saturation temperature at the channel exit.

9.5. Flow Instability

Due to the effects of increased pressure loss with subcooled nucleate boiling and adverse buoyancy from coolant downflow, an excursive hydraulic instability can occur in pool reactor hot channels. Such an instability occurs with flow in parallel channels when the pressure loss in one or more channels increases with decreasing flow rates. The end result of this effect is a drastic flow reduction or a flow reversal in the unstable channels.

A flow instability is determined by calculating channel pressure losses for successively decreasing flow rates. A minimum on the channel pressure loss-flow rate characteristic curve locates the minimum stable flow rate.

Pressure loss across pool-reactor element coolant-channels is due to the following: (1) inlet and exit losses, (2) channel friction loss, (3) loss due to changes in fluid momentum, and (4) loss due to change in elevation. Since burnout was assumed to occur when the fluid reaches its saturation temperature at the channel exit, only single-phase pressure losses were considered.

Pressure losses were calculated incrementally down the channel in order to account for fluid property changes and transition from regimes of forced-convection heat transfer to subcooled nucleate boiling.

The total pressure loss of the channel inlet was calculated using[11]

$$\Delta p(\text{inlet}) = \frac{K \rho_i u_i^2}{2 g_c} \tag{9.9}$$

where Δp (inlet) = total pressure loss at channel inlet, lb_f/ft^2

K = loss coefficient, dimensionless

ρ_i = fluid density at channel inlet, lb_m/ft^3

u_i = fluid velocity inside channel inlet, ft/sec

The loss coefficient K depends upon the shape of the channel inlet and the ratio of the downstream-to-upstream channel cross section areas, A_2/A_1. For shape-edged entrances K is given by[11]

$$K = 1.5 - 0.4 (A_2/A_1) - (A_2/A_1)^2 \tag{9.10}$$

for

$A_2/A_1 < 0.715$, and

$$K = 1.75 - 0.75 (A_2/A_1) - (A_2/A_1)^2 \tag{9.11}$$

for

$A_2/A_1 \geq 0.715$.

For a sudden expansion in flow area, the pressure rise due to decreased fluid momentum is larger than the pressure loss due to friction. Consequently, there is a pressure rise outside the channel exit. The total pressure change at the channel exit was calculated using[11]:

$$\Delta p \text{ (exit)} = - \frac{\rho_e u_e^2}{g_c} \left[\frac{A_1}{A_2} - \left(\frac{A_1}{A_2}\right)^2 \right] \tag{9.12}$$

where Δp(exit) = total pressure loss at channel exit, lb_f/ft^2

ρ_e = fluid density at channel exit, lb_m/ft^3

u_e = fluid velocity at channel exit, ft/sec

A_1/A_2 = ratio of upstream-to-downstream channel cross section areas at exit.

Friction pressure losses across channel increments were calculated with the following equation[11]

$$\Delta p \text{ (friction)} = f_W \frac{\rho u^2 \Delta L}{2 g_c D_e} \tag{9.13}$$

where f_W = Darcy-Weisbach friction factor

ρ = fluid density, lb_m/ft^3

u = mean fluid velocity, ft/sec

ΔL = axial length of channel increment, ft

D_e = channel equivalent diameter, ft

Experiments have shown that, for isothermal flow, rectangular channel friction factors are close to the Moody curve for smooth tubes.[12] The isothermal friction factors on the Moody curve are well approximated by the von Karman equation[13]

$$f_{W_{ISO}} = \left[\frac{1}{2 \log \left(N_{Re} f_{W_{ISO}}^{1/2}\right) - 0.8} \right]^2 \tag{9.14}$$

Friction factors are reduced with heating because of the decreased fluid viscosity near the wall. Therefore, to account for the decreased friction factors with heating[14], the isothermal friction factors are multiplied by $(\mu_W/\mu_b)^{0.14}$, or

$$f_W = f_{W_{ISO}} (\mu_W/\mu_b)^{0.14} \tag{9.15}$$

Equation (9.14) is only applicable for fully developed turbulent flow, which implies its range of applicability is for entrance L/D_e ratios greater than 50. Since the L/D_e ratio for the UVAR is 130, the flow is developing over a large portion of the channel length. The friction factors in developing flows are larger than those predicted by Eq. (9.14). Since friction pressure losses add to the stability of parallel channel systems, the use of Eq. (9.14) over the non-boiling channel length is a conservative approach in a stability analysis.

With the occurrence of subcooled nucleate boiling in channels, friction pressure losses increase. A correlation proposed by Reynolds[15] was used to calculate subcooled nucleate boiling pressure loss in the UVAR hydraulic analysis. The correlation is given by

$$\frac{(dp/dL)_{NB}}{(dp/dL)_{ISO}} = \cosh \left[(4.6 \times 10^{-6}\, q'' + 1.2) \left(\frac{T_b - T_{b_{IB}}}{T_{Sat} - T_{b_{IB}}} \right) \right] \tag{9.16}$$

where $(dp/dL)_{NB}$ = local friction pressure gradient with subcooled nucleate boiling, lb_f/ft^3

$(dp/dL)_{ISO}$ = isothermal pressure gradient, lb_f/ft^3

q'' = wall heat flux, $Btu/hr\text{-}ft^2$

$T_{b_{IB}}$ = fluid bulk temperature at incipient boiling, °F

T_b = local bulk temperature, °F

T_{Sat} = fluid saturation temperature, °F

The isothermal pressure gradient is calculated using Eqs. (9.13) and (9.14) with all fluid properties evaluated at the average channel temperature.

The approach used in the analysis was to let q" be the average heat flux in the channel from the position of incipient boiling to the position under consideration. However, because of the low heat fluxes involved with pool reactors, the contribution of the term 4.6×10^{-6} q" in Eq. (9.16) is small compared to 1.2. Consequently, the approach used in evaluating q" is not too important. It should be noted that at conditions in which flow instabilities occur in pool reactors, the heat fluxes are smaller than the heat fluxes used in developing Eq. (9.16).

In heated channels, the fluid undergoes a slight density decrease which in turn causes an acceleration. The increased fluid momentum produces a pressure loss which is quite small compared to the other losses in the channel. However, this loss was incorporated in the hydraulic analysis and the pressure loss across a channel increment is given by

$$\Delta p \text{ (momentum)} = \frac{\rho u^2 \alpha \beta \Delta T}{2 g_c} \qquad (9.17)$$

where α = correlation factor to account for non-uniform velocity in the channel

β = fluid volumetric coefficient of expansion,

ΔT = temperature rise across the channel increment, ^{o}F

Since the flow is turbulent "a" is close to 1.0, which is the value used in the analysis.

With downflow the elevation pressure loss is given by

$$\Delta p \text{ (elevation)} = - \frac{g}{g_c} \int_{\text{Inlet}}^{\text{Exit}} \rho dz \qquad (9.18)$$

where g is the acceleration of gravity. For single-phase flow in a channel increment, Eq. (9.18) is well-approximated by

$$\Delta p \text{ (elevation)} = - \frac{g}{g_c} \rho_1 \Delta L (1 - \beta \Delta T_2) \qquad (9.19)$$

where ρ_1 = liquid density at inlet to channel increment, lb_m/ft

ΔL = length of channel increment, ft

β = liquid volumetric coefficient of expansion, $^{o}F^{-1}$

ΔT = temperature rise of fluid in channel increment, ^{o}F

The adverse buoyancy effect due to a decreasing fluid density downstream in a heated channel is the major contribution to flow instabilities in single-phase downflow.

9.6. Burnout Ratio

Because of non-uniform heat generation in the channel, it is possible to calculate two types of burnout ratios defined by the following equations:

$$\text{Local Burnout Ratio} = \frac{q''_c \text{ (predicted)}}{q''\text{(local)}} \tag{9.20}$$

$$\text{Average Burnout Ratio} = \frac{q''_c \text{ (predicted)}}{q'' \text{ (average up to position considered)}} \tag{9.21}$$

In the UVAR safety analysis both burnout ratios were calculated along the channel length. The smaller of these ratios was used in determining the burnout limit.

Equation (9.20) implies that local conditions determine burnout. However, experimental data comparing uniform and non-uniform heat generation burnout indicates that burnout depends on upstream heat flux conditions[16,17,18]. The results of experiments performed by Babcock and Wilcox for uniform, chopped-cosine, inlet peak, and exit peak heat flux distributions, indicate that the total channel power at burnout or the average channel burnout heat flux is essentially independent of axial heat flux distribution[17,18]. Since burnout correlations are developed from uniform heating burnout data, it appears that the non-uniform heat flux burnout data indicates that the use of Eq. (9.21) for calculating burnout ratios is probably a better criterion for determining the burnout safety margin. Equation (9.21) usually predicts smaller burnout ratios than Eq. (9.20) for positions far downstream from the peak heat flux in a

channel. The results of calculations on the UVAR showed that Eq. (9.21) was the limiting criteria for determining the UVAR safety limit.

For relatively high power levels and flow rates, the burnout ratio is the limiting criteria for establishing the safety limit. At lower power levels and flow rates, an excursive flow instability is the limiting criteria. The flow instability in the UVAR hot channel is predominately caused by the adverse buoyancy effect due to downflow.

9.7. Nomenclature Used in Thermal Hydraulic Analysis

A_2/A_1	Ratio of downstream-to-upstream channel cross section areas at channel inlet
c_p	Specific heat, $Btu/lb_m \cdot {}^oF$
D_e	Equivalent diameter, ft
f_W	Darcy-Weisbach friction factor
$F_{W_{ISO}}$	Isothermal Darcy-Weisbach friction factor
g	Local acceleration, ft/sec^2
g_c	Conversion factor, $32.18 \frac{lb_m}{lb_f} \frac{ft}{sec^2}$
G	Mass velocity, $lb_m/ft^2 \cdot sec$
h	Heat-transfer coefficient, $Btu/hr\text{-}ft^2 \cdot {}^oF$
h_f	Saturated liquid enthalpy, Btu/lb_m
h_g	Saturated vapor enthalpy, Btu/lb_m
h_{fg}	Heat of vaporization, Btu/lb_m
k	Thermal conductivity, $Btu/hr\text{-}ft\cdot {}^oF$
K	Inlet pressure loss coefficient
L	Channel length, ft

ΔL	Incremental channel length, ft
N_{Gr}	Grashof number, dimensionless
N_{Ka}	Von Karman number, dimensionless
N_{Pr}	Prandlt number, dimensionless
N_{Re}	Reynolds number, dimensionless
p	Pressure, Psia
q''	Local wall heat flux, Btu/hr-ft^2
q''_c	Burnout heat flux, Btu/hr-ft^2
q''_{FC}	Forced convection heat flux, Btu/hr-ft^2
q''_{IB}	Incipient boiling heat flux, Btu/hr-ft^2
q''_{PB}	Pool boiling burnout heat flux, Btu/hr-ft^2
$(dp/dL)_{ISO}$	Isothermal pressure gradient, lb$_f$/ft^3
$(dp/dL)_{NB}$	Subcooled nucleate boiling pressure gradient, lb$_f$/ft^3
T_b	Local bulk temperature, ^oF
T_1	Channel inlet temperature, ^oF
T_w	Local wall temperature, ^oF
ΔT	Fluid temperature rise in a channel increment, ^oF
T_{Sat}	Fluid saturation temperature, ^oF
T_{WB}	Bernath's wall temperature at burnout, ^oF
$T_{b_{IB}}$	Fluid bulk temperature at incipient boiling, ^oF
u	Mean coolant velocity, ft/sec
u_1	Coolant velocity outside channel exit, ft/sec
z	Axial position in channel, ft
α	Correction factor for non-uniform flow in a channel
β	Fluid volumetric coefficient of expansion, $^oF^{-1}$

ρ	Local fluid density, lb_m/ft^3
ρ_f	Saturated liquid density, lb_m/ft^3
ρ_g	Saturated vapor density, lb_m/ft^3
ρ_1	Fluid density at inlet to channel increment, lb_m/ft^3
σ	Liquid-vapor interface surface tension, lb_f/ft
μ_b	Local fluid viscosity at bulk temperature, $lb_m/ft\text{-}sec$
μ_w	Local fluid viscosity at wall temperature, $lb_m/ft\text{-}sec$

9.8. Hot Channel and Minimum Core Loading

The hot channel is related to the nominal channel by the radial peaking factor. The hot channel considered in this analysis was calculated for a 4 x 4 core which is the minimum core loading. Larger cores were analyzed; however, their lower power densities and lower non-elemental flows more than compensate for their higher radial peaking factors, resulting in less limiting conditions.

The radial peaking factor for a 4x4 core was determined to be 1.66 using a two dimensional diffusion theory computer model of the LEU 22 plate-per-element UVAR core[27]. This radial peak was found to be in the channel adjacent to a control rod water hole as shown in Figure 9-4. Sternberg[19] performed a complete map of a UVAR 4x4 HEU 12 plate-per-element core. The location of the measured radial peak flux in Sternberg's core corresponds to the location of the computer calculated peak flux in the 4x4 LEU 22 plate-per-element core.

Sternberg's work provided an exit peak axial distribution which was fitted to a polynomial for the analysis of the 22 plate/element core. Figure 9-5 shows Sternberg's axial flux map in the hot channel. For

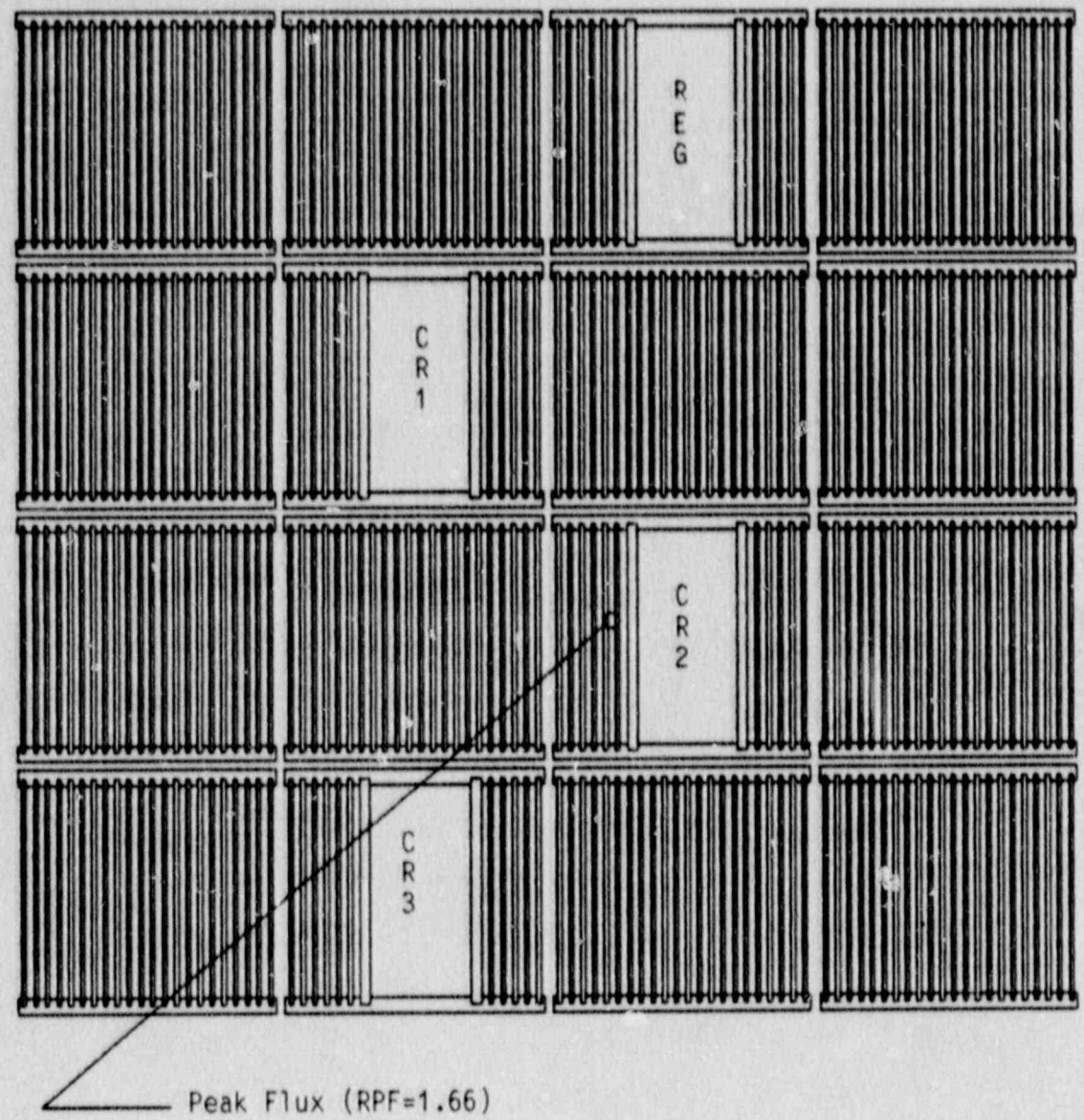

FIGURE 9-4 Core Loading Showing Peak Flux Location

FOIL LOCATION IN FUEL ELEMENT AC5

AN5	AN18	AC4	AN2
AN17	AC6	AN10	AN14
AN9	AN6	AC5	AN13
AN1	AC1	AN20	AN 8

ELEMENT LOCATION IN THE CORE

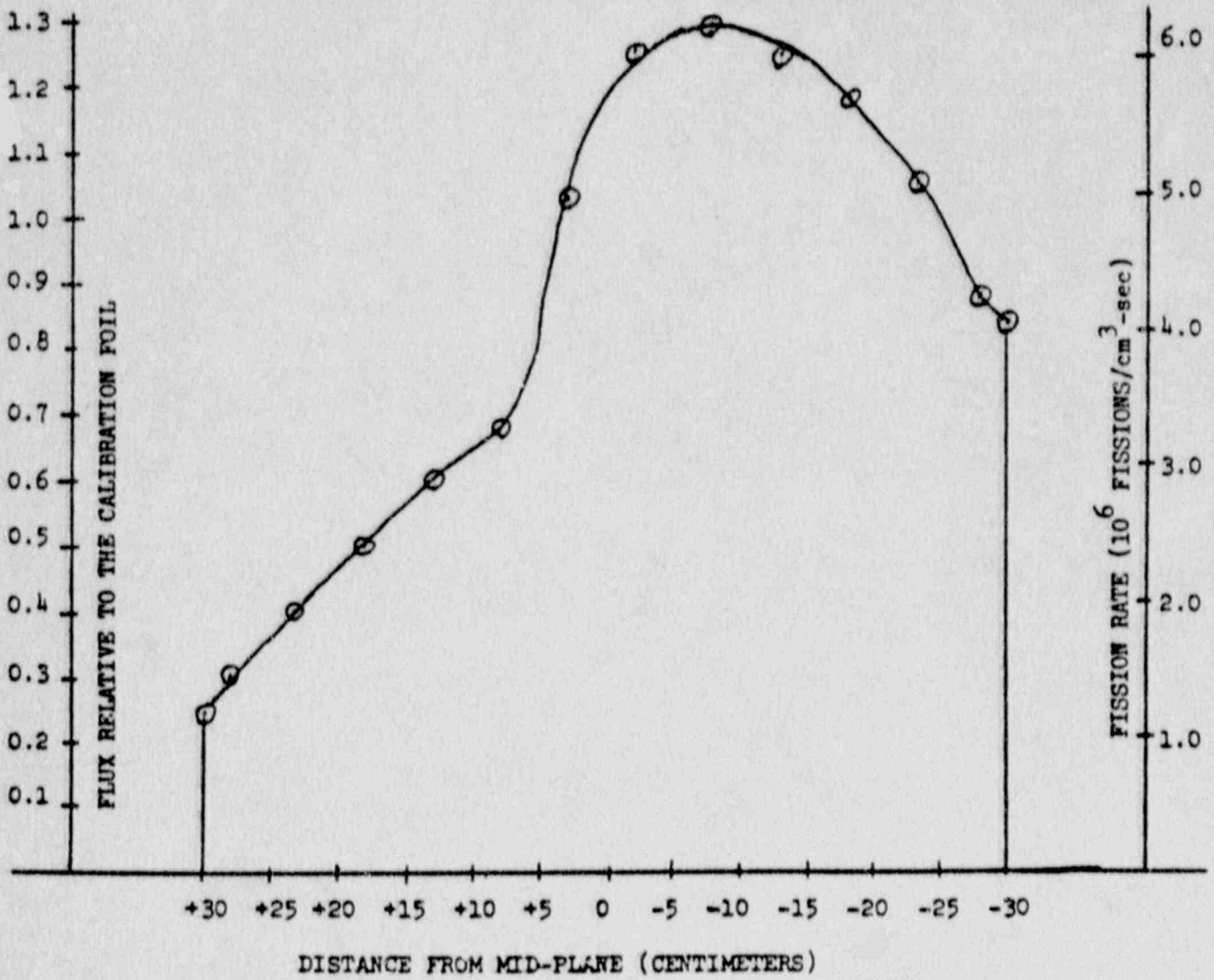

FIGURE 9-5 VERTICAL FLUX TRAVERSE IN POSITION OF AC-5

these measurements, the rods in channel rod elements AC-1 and AC-4 were completely withdrawn and the tips of the rods in control rod elements AC-5 and AC-6 were at about six centimeters above the midplane. This results in the most severe axial flux peaking possible in the reactor. The curve in Figure 9-5 is the basis for the Exit Peak Heat Flux distribution used in this analysis.

9.9. Allowance for Error in the Burnout Determination

In Figure 9-3, a comparison is given of the ratio of calculated to experimental heat fluxes. With the assumption that the points in this figure form a normal distribution (Gaussian error curve), an analysis was performed to find the standard deviation, σ, from the expression

$$\sigma^2 = \frac{1}{n-1} \sum_{1}^{n} (X_1 - \bar{X})^2 \qquad (9.27)$$

where n is the number of points, and $\bar{X}$ is the mean value of all points. A value of $\sigma = 0.21$ was obtained. For 2.32 standard deviations above and below the mean, the probability of occurrence of ratios outside this range is 2%. Half of these occurrences will be above and half will be below this range. Accordingly, for 2.32 σ or a burnout ratio (BOR) of 1.49, there is a 99% confidence factor that burnout will not occur based on Gambill's experimental data.

9.10. Safety Limit

A steady state heat transfer code for downflow in rectangular channels, THERHYD, that incorporates the correlations discussed in the preceding sections, was developed by Dahlheimer[25].

The limiting core power to system flow derived from THERHYD channel power and channel flow define the burnout limit curve for the UVAR with forced convection cooling. The UVAR Safety Limit is set so that the fuel and cladding do not melt. If power and flow conditions that can be reached during various transients are always below the burnout limit curve (lower power for a given flow) the safety limit will not be exceeded. Thus the safety limit is actually based upon the burnout criteria since if burnout (either departure from nucleate boiling or dryout) does not occur, the fuel and cladding will not melt. The Limiting Safety System Settings (LSSS) for power and flow are chosen (see section 9.11) so that the reactor will always operate below the burnout limit curve during any analyzed transient. The LSSS's also take into account uncertainties in measuring the core power, system flow, and pool temperature.

THERHYD was run using the channel and plate dimensions for the 22 plate/element LEU fuel to find the limiting channel flow for a range of channel powers. The exit peak axial flux distribution measured by Sternberg[3] and fitted to a fifth order polynomial by Dahlheimer[25] was used for all analysis. Additional THERHYD runs were performed to obtain differential pressure information for a wide range of powers and flows.

The primary output from THERHYD is the channel flow for various channel powers at a specified limiting condition. The limiting condition used throughout the calculations was a Burnout Ratio (BOR) of 1.49 which section 9.9 demonstrates allows for errors in the correlations used in THERHYD.

Radial peaking factors from 2DB-UM[26] computer models of various

proposed LEU cores were used to convert individual channel power calculated by THERHYD to full core power. Reference fuel element flow parameters experimentally determined by Brunot[4] along with calculated differential pressures from THERHYD were used to convert the individual channel flow calculated by THERHYD to system flow.

The effect of tolerances in fuel loading, fuel width, flow distribution within a fuel element and channel size (Summarized in Table 9-1) were all individually converted to a corresponding increase in channel flow needed to account for each effect. The total increase in flow for these four effects was determined by taking the root of the sum of the squares of the individual effects. The resulting core power vs. system flow is the burnout limit curve for the particular core. In the calculations, the bulk pool water temperature limit of 111° F is used as the inlet temperature and the depth of water to the center of the core is 20.36 feet.

Brunot measured the single element flow in a 4x4 core using 12 plate HEU elements to be 48 GPM when the system flow was 940 GPM. The dynamic differential pressure across the core for this flow condition was calculated using THERHYD to be 0.0776 psi. These conditions are used as a reference point to calculate non-element flow in other core configurations. Non-element flow is any flow that does not go through the fuel portion of the elements. Examples of non-elemental flow are the flow through the 49, 3/4-inch holes in the grid plate used to cool the reflector and channels between elements, and the flow through the rod channels.

TABLE 9-1.

Leu-22 Data and Parameters

Core size	4x4	4x5
Number of Plates	308	396
Number of Channels	294	378
Radial Peaking Factor	1.66	1.71

Axial Power Distribution. Exit Peak as defined by 5th order polynomial in Dahlheimer.

Inlet Temperature: 111° F

Pool Depth to Core Center: 20.36 Ft.

Flow Distribution Factor: 16.5 %

Reference Non-Element Flow Parameters:

Core:	4x4 12 Plate HEU
System Flow:	940 GPM
Element Flow:	48 GPM
Dynamic D.P.:	0.0776 psi

Element Dimensions:

		Tolerances
Channel Gap	0.0927"	(+/- 0.007")
Channel Width	2.621"	(+/- 0.013")
Fuel Width	2.395"	(+/- 0.075")
Plate Thickness	0.05"	
Plate Loading U-235	12.5 g	(+/- 0.35 g)

THERHYD was run for the nominal channel dimensions as well as for the minimum channel dimensions (both gap and width) to calculate the minimum channel flow with high resolution (0.01 GPM) for a BOR of 1.49. Additional runs were performed with the BOR limit set at 1.00 to obtain differential pressure data for a wide range of flow rates at both nominal and minimum dimensions.

In the computer runs, the resulting channel power for the nominal channel dimensions, with BOR 1.49, were converted to core power using the appropriate radial peaking factor (RPF) and number of plates in the core, according to the relationship:

$$\text{Core Power} = (\text{Channel Power} * \#\ \text{of Plates}) / \text{RPF} \qquad (9.28)$$

For each limiting channel flow rate from the above runs, the corresponding dynamic differential pressure (DP) across the core was calculated and the channel flow was converted to system flow, using:

$$\text{Sys Flow} = \text{Chan Flow} * \#\ \text{of Channels} + \text{Non-Element Flow} \qquad (9.29)$$

where Non-Element Flow is given by

$$(940\ \text{GPM/sys} - 48\ \text{GPM/elem} * 14\ \text{elem/sys}) * \text{SQRT}(\text{DP}/\text{DPref}) \qquad (9.30)$$

where DPref is the dynamic differential pressure calculated for the conditions at which 48 GPM per element at 940 GPM system flow was measured and DP is the dynamic differential pressure for the core

conditions under study. Dynamic differential pressure is the total differential pressure across the core (or channel) minus the difference in hydrostatic head between the inlet and outlet of the core.

Use of equation (9.30) assumes that the non-elemental flow area does not vary from core to core. The 49 small holes are never plugged and the number of rod channels remains fixed at four.

The resulting function of Core Power versus System Flow is the nominal burnout limit without considering any tolerances. The slope of the nominal burnout limit curve was calculated to convert the tolerances on fuel width, fuel loading and power to tolerances on flow. Separate THERHYD runs were performed to determine the limiting flow with a BOR of 1.49 in a channel with the minimum gap and width. The total differential pressure (dynamic and static) required to maintain safe flow in the smallest channel must be applied across the entire core. Therefore, the flow rate in a nominally sized channel at each power level was calculated using the differential pressure required for safe flow in the smallest channel. This results in a significant increase in nominal channel flow. Each increase in flow to account for the tolerances was normalized to the nominal channel flow and added to the nominal channel flow in quadrature.

The dynamic differential pressure for the adjusted channel flow was calculated and again using equations (9.29) and (9.30), the system flow for each core power was calculated. The resulting power to flow curve is the burnout limit for a particular core configuration and set of dimensional tolerances.

The burnout curve in Figure 9-6 is based upon the minimum core

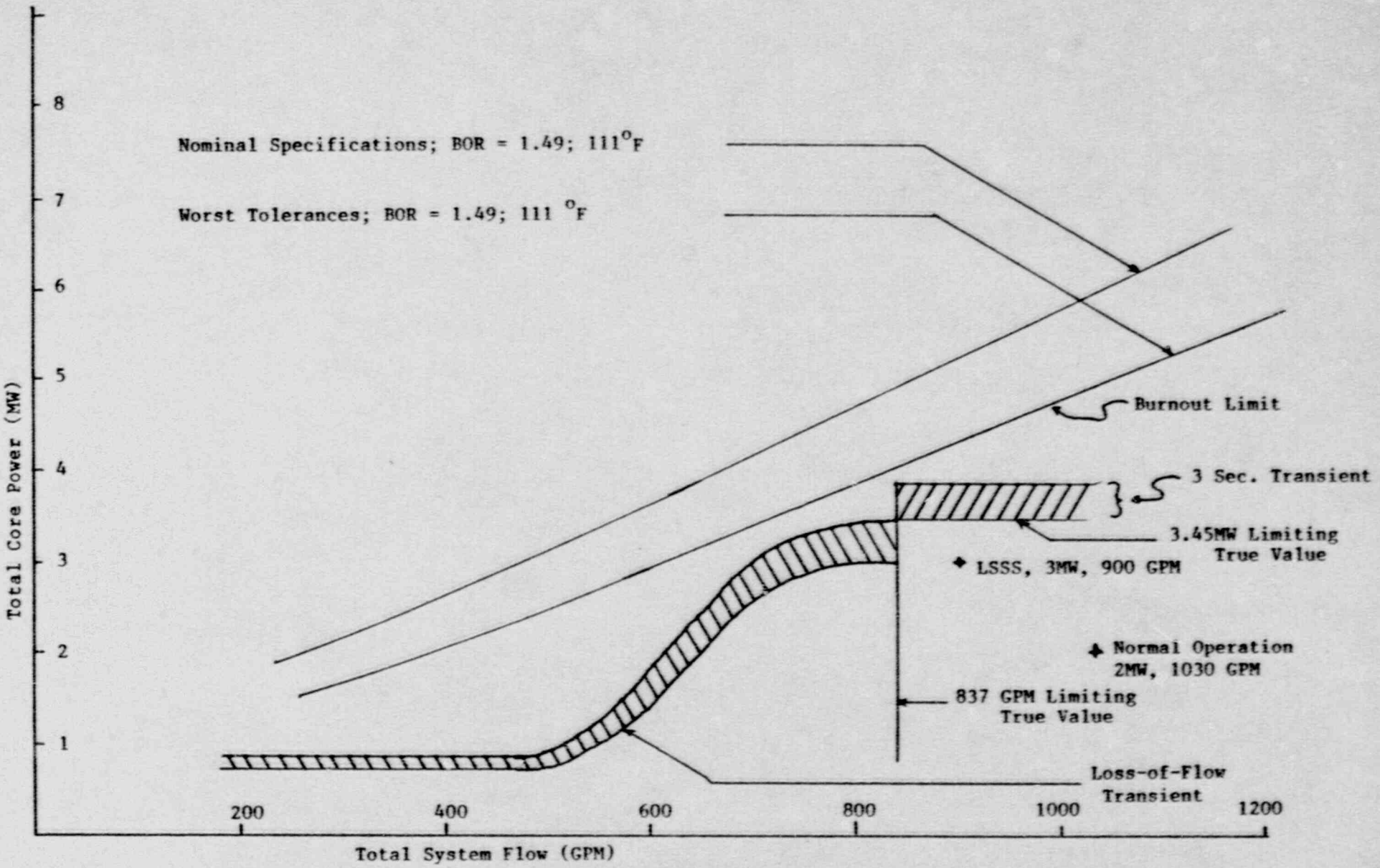

FIGURE 9-6 LEU Core Power vs System Flow, 4x4, RPF=1.66

loading of 14 normal elements and 4 control rod elements in a 4x4 array. Larger cores were analyzed; however, their lower power densities and lower non-elemental flows more than compensate for their higher radial peaking factors, resulting in less limiting conditions.

9.11. Limiting Safety System Settings and Measurement Errors

a) Coolant Inlet Temperature

The Limiting Safety System Setting (LSSS) on coolant inlet temperature (pool temperature) is 108°F. Normal operation is at 105°F or less. The manufacturer's specified probable error on the measuring instrument is ± 0.75°F. The standard deviation would then be ± 1.125°F and using 2.32 standard deviations for a 99% confidence factor, the temperature can be determined within 2.6°F. For an LSSS of 108°F, the limiting true value on the coolant inlet temperature is therefore less than 111°F. All calculations for the curves in Figure 9-6 are based on an inlet temperature of 111°F.

b) Flow Rate

The primary coolant flow is detected by measuring the differential pressure across an orifice in the primary piping. The manufacturer's specified probable error is ± 2% or a standard deviation of ±3%. For a 99% confidence factor that the flow rate will be no less than a specified amount we take 2.32 standard deviations, or 7%. The limiting safety system setting on flow rate is set at 900 gpm. Hence, the true value should then be no less than 0.93 x 900 = 837 gpm. This is the limiting true value on flow rate shown in Figure 9-6.

c) Reactor Power

The reactor power is determined from the product of flow rate x ΔT, where ΔT is the differential temperature across the core. The probable error with the ΔT measurement could be as much as $\pm 0.4^{\circ}F$. At a power of two megawatts the ΔT is about $13^{\circ}F$, for a probable error of ±3.2%. The safety level scram point is set by adjusting the neutron chambers to read the same power level as the thermal power. Here, the limiting accuracy is the readability of the indicator which can be read with a probable error of ±2%.

There are then three independent probable errors in determining the power level setting:

a) Flow rate	±2%
b) ΔT	±3.2%
c) Chamber Setting	±2%

The combined probable error is obtained from the square root of the sum of the squares and corresponds to ± 4.27%, with a standard deviation of ±6.4%. For a 99% confidence factor, 2.32 σ is 14.8%. Therefore, with a measured value of 3 MW for the LSSS on reactor power, the true value should be no greater than 3 x 1.148 or 3.45 MW. This is the limiting true value on reactor power shown in Figure 9-6.

9.12. Short Period Transient

A limiting condition for operation is that the magnet release time be less than 50 milliseconds. The minimum setting on the period scram is 3 seconds. From the rod calibration curves, the three rods must drop about 3 1/2-inches from the fully

withdrawn position of 26-inches above the bottom of the core to overcome this period. This is the least reactive position of the rods, and normally the rods are operated at a level well below this. However, to allow for variations in core loading, it is assumed that the rods must drop 5-inches from the fully withdrawn position of 26-inches, to overcome a 3-second period. This is a very conservative assumption.

A rod drop time cannot be measured unless the drop terminates on the seating switch at the fully inserted position. Accordingly, drop times were measured from 3, 4, 5, and 6-inches above the fully inserted position as well as from the fully withdrawn position (26-inches). The results obtained are presented in Table 9-2.

TABLE 9-2

TIME TO DROP FROM A PREDETERMINED POSITION

(All times in milliseconds)

	Initial Position				
	3"	4"	5"	6"	26"
Rod 1	160.0	185.0	205.0	225.0	481.2
Rod 2	170.0	195.0	210.0	227.5	506.0
Rod 3	162.5	182.5	203.0	230.0	482.5
Average	164.2	187.5	206.2	227.5	489.9
True Gravity	124.6	143.9	160.9	176.2	366.8

The times for True Gravity (last line) are calculated from:

$$S = \frac{1}{2} g t^2 \qquad (9.31)$$

The actual time for the rod to drop is greater than the True Gravity time because of the friction of the water as the rod drops through it. Of more significance is the slowing up of the rod as it enters the dash pot during the last few inches before it is seated at the bottom of its travel.

The action of the dash pot in slowing the drop time is illustrated by the times to drop from 26 inches (last column). The measured values of the drop times from 3 inches, 4 inches, 5 inches, and 6 inches include some delay from the dash pot action. The drop time for any one of these distances from the fully withdrawn position would be less. For example, a 5-inch drop from 26 inches to 21 inches should be less than 206 milliseconds. On the other hand it would be greater than the true gravity time of 161 milliseconds as there is some frictional resistance from the water as soon as the rod starts to move.

For conservatism, it is assumed that the time for the rods to drop 5 inches from the fully withdrawn position is 3/7 of the time to drop the full travel of 26 inches. Accordingly, for a measured free drop time of 490 milliseconds for full travel, the time to drop 5 inches will be no greater than 210 milliseconds. A maximum free drop time for the full travel is established at 700 milliseconds in the Technical Specifications. Therefore, the time to drop 5 inches will never be greater than 300 milliseconds. Adding the 50 millisecond release time to the 5-inch drop time, the time from the initiation of a scram until the rods are inserted 5 inches will never be greater than 350 milliseconds.

It is not easy for the reactor to go on a short period at high power due to the negative temperature coefficient, which has been determined to

be about -1×10^{4} $\Delta k/k\text{-}^{\circ}F$[27]. Neglecting the temperature coefficient, and assuming the reactor is on a period just greater than 3 seconds, and goes through the maximum true value of the LSSS at 3.45 megawatts, the power will rise to a value no greater than

$$P = 3.45 \exp [0.350/3] = 3.88 \text{ MW}. \quad (9.32)$$

The range between 3.45 MW and 3.88 MW is the allowance for a 3 second period transient in Figure 9-6. Thus, 3.88 MW is the maximum power for any transient because transients shorter than 3 seconds will scram the reactor at a lower power on period while longer transients will scram the reactor on high power with less power overshoot.

9.13. Loss-of-Flow Transient and Natural Convection

A loss-of-flow transient is illustrated by the shaded area extending to the left of the LSSS in Figure 9-6. It is assumed for this transient that the reactor is operating at the LSSS of 3.0 MW and 900 gpm, with the flow header jammed in the UP position, and there is a power failure to the pump which then results in a reactor scram signal.

The following sections 9.14 and 9.15 are the original analysis[24] for loss of flow and natural convection. NATCON[28] runs for 22 plate, 18 plate, and 12 plate fuel elements show that the margin of safety increases with the increase in heat transfer area and lower power densities associated with the increase in the number of fuel plates in the 22 plate LEU core over the 12 plate HEU core used in sections 9.14 and 9.15.

To determine the coolant flow coastdown curve, measurements were made for the HEU SAR of the decrease in flow rate versus time, starting with a flow rate of 800 gpm and followed by pump cut-off. For these measurements the output signal from the differential pressure cell across the orifice plate was used after this signal had been calibrated against various flow rates through the primary system with the flow header in the UP position. For the LEU SAR, the results were linearly shifted to a starting point of 900 gpm and are shown in Figure 9-7. The flow coastdown curve is expressed by the following equation (shifted from equation (9.34)).

$$\text{Flow (gpm)} = 900 - 636 \times t(\text{sec}) \qquad (9.33)$$

9.14. HEU Analysis for Loss-of-Flow Transient

A loss of flow transient is illustrated by the shaded area extending to the left of the LSSS in Figure 9-6A. It is assumed that the [HEU] reactor is operating at the [previous HEU] LSSS of 3.0 MW and 800 gpm with the flow header jammed in the UP position. There is a power failure to the pump and the loss of power to the pump then initiates a scram signal to the reactor.

Measurements were made of the decrease in flow rate versus time starting with a flow rate of 800 gpm, and then cutting off the pump. The measurements were made using the output signal from the differential pressure cell across the orifice plate, after calibrating this output signal versus various flow rates through the primary system with the flow header in the UP position. The results are shown in Figure 9-7 and the flow coast down curve is expressed in the following equation:

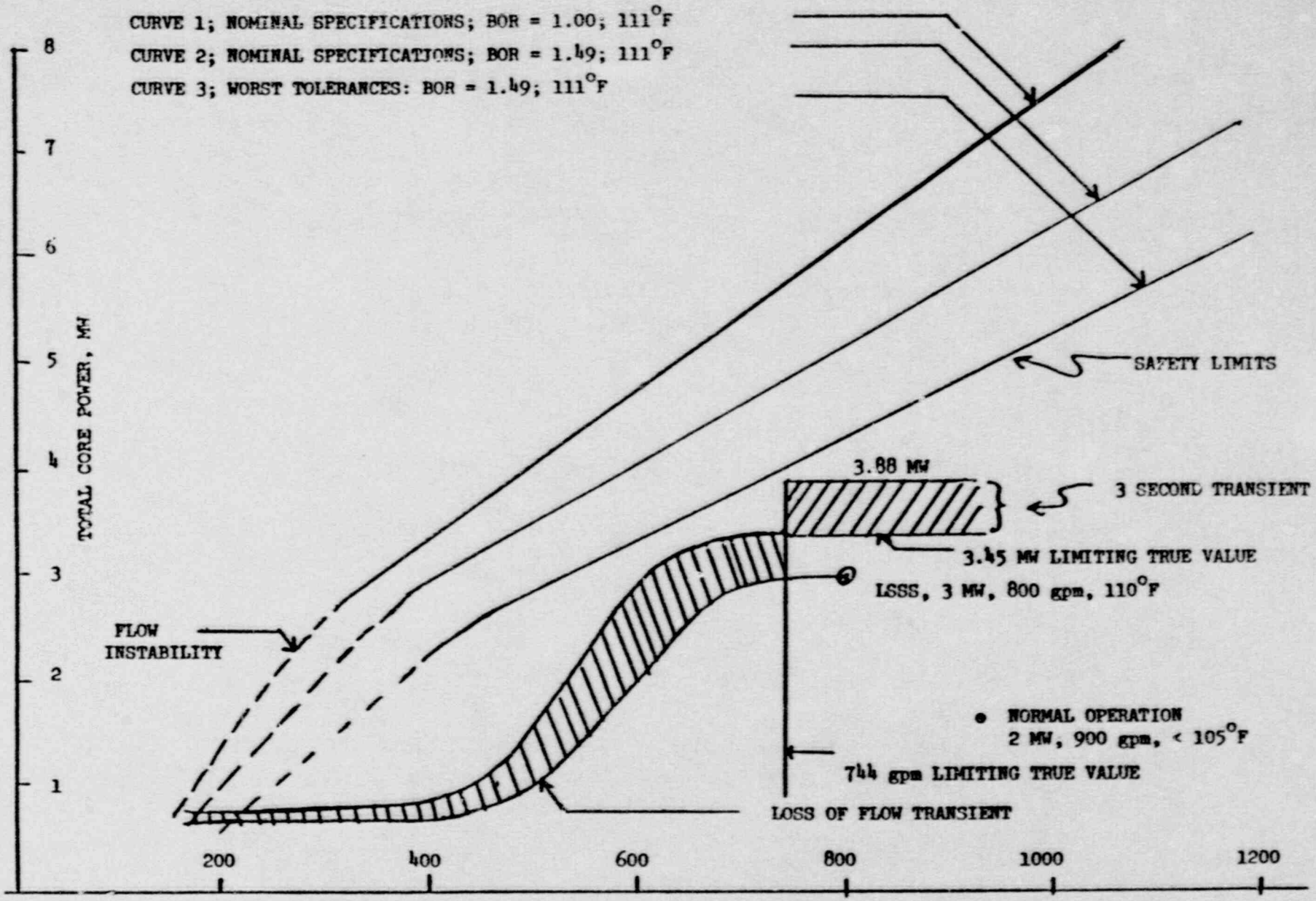

FIGURE 9-6a HEU Core Power vs System Flow, 4x4, RPF=1.37

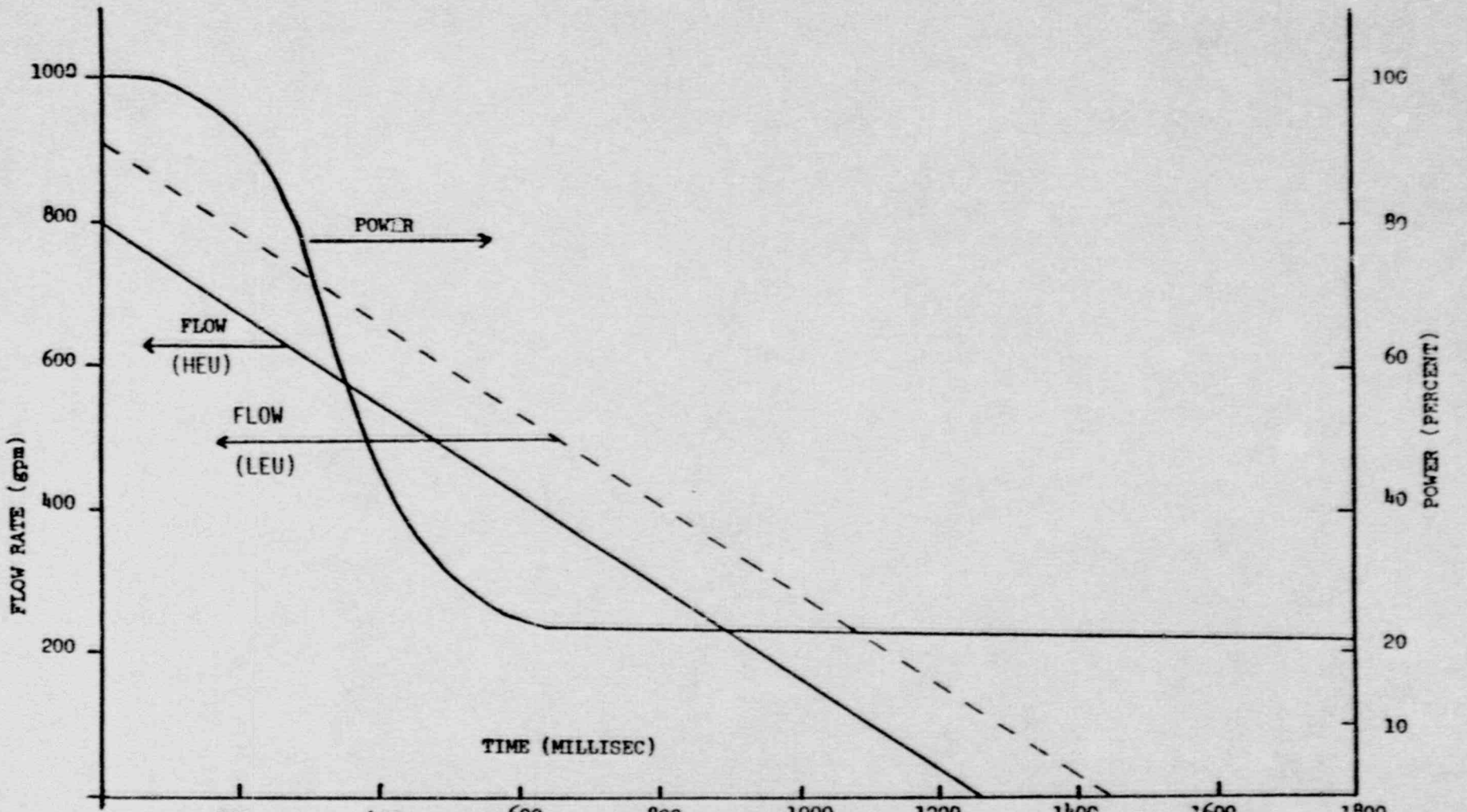

FIGURE 9-7 FLOW AND POWER COASTDOWN (HEADER UP)

$$\text{Flow (gpm)} = 800 - 636 \times t(\text{sec}) \qquad (9.34)$$

The power coast down curve was calculated by solving the kinetic equations with six groups of delayed neutrons on a digital computer using 0.01 second time increments for the first two seconds and 0.1 second time increments thereafter to 100 seconds. It was assumed that the rods did not move for 50 milliseconds until after initiation of the scram and that they moved with constant acceleration until they had traveled the full length of 26-inches in 700 milliseconds. These assumptions are most conservative but are consistent with the limitations on rod drop times given in the Technical Specifications.

The complete reactivity insertion was assumed to be only 3%Δk/k and the rods were assumed to drop from the fully withdrawn position (also very conservative assumptions). By comparing with rod calibration curves determined experimentally in the reactor, a curve of negative reactivity insertion versus time was plotted, and this data was input to the computer.

It was assumed that 6% of the power at the instant of scram was from the decay of fission products and this was held constant in time thereafter. The power coast down curve is plotted along with the flow coast down curve in Figure 9-7. Because of the same amount of negative reactivity inserted, the power does not approach the 6% in fission products until about 100 seconds. At the instant the flow rate reaches zero (1.258 seconds), the power is still at 21.7% full power. By picking

off powers and flows at equivalent times the curve of power versus flow extending to the left from the LSSS in Figure 9-6A was determined. This is the expected result of a loss-of-flow transient. However, since the true values of power and flow at the LSSS could be 744 gpm and 3.45 megawatts, the procedure was repeated starting from this point in Figure 9-6A. The shaded area between the two curves represents the range of uncertainty for a transient resulting from a loss of flow after steady state operation at the LSSS. Not included in the figure are the results as the flow rate decreases to zero and then reverses due to buoyancy effects. At a downflow rate of 225 gpm and a power of 790 kW, the loss of flow transient curve intersects Curve 3 in Figure 9-6A. The significance of the point of intersection is that if the reactor were operating in the steady state at this power, and this flow rate, a flow instability would occur in the hot channel. (See Section 9.5).

However, the reactor is not in the steady state and the flow rate is changing rapidly. Also, it is impossible for the flow header to jam in the fully UP position. The header is raised by flotation with air as described in Section 4.3. After the header is raised, the pump is started and the header is held up by the pressure drop of the flow through the core. The air pressure which raised the header is vented and the reactor cannot be started until this pressure has dropped below 2 psi. If there is a loss of coolant flow, gravity will cause the header to drop. However, it is possible for the header to jam in a cocked position. The worst possible position in which the header could jam is shown in Figure 9-8. In this case, the header would be wedged with a minimum gap of 0.956-inches between the header and grid plate on one

side.

A transient analysis was made for a loss of flow incident from 3.45 megawatts reactor power with power and flow coast down as shown in Figure 9-7 [HEU]. The header is assumed jammed in the position shown in Figure 9-8 and the transient response of the average flow, average fuel temperature, and average coolant temperature are shown in Figure 9-9. As will be shown, a safety limit can be established, using the maximum fuel plate temperature as a criterion.

The response was calculated with a computer code which treated transient heat transfer at the average power location. Heat transfer coefficients were calculated as a function of flow rate, starting in the turbulent flow regime at rated flow and switching to a laminar flow correlation for Re < 2300. Upflow resulted from buoyancy, which was set equal to the combined effect of (1) the inertia of the water in the core flow channel and the header below the core, and (2) the friction loss through the gap between the wedged header and the grid plate and friction loss in the core-coolant channel.

The pressure drop through the 0.956-inch gap relative to the pressure drop through the core after flow reversal was calculated in order to solve the transient flow equations, as follows:

$$\Delta P = f \frac{h}{D_e} \frac{\rho \bar{V}^2}{2g_c} + 1.5 \frac{V \rho_{gap}}{2g_c} \qquad (9.35)$$

where: first term = friction pressure drop through core

$\bar{V}$ = average velocity in core

second term = pressure drop through gap

V_{gap} = velocity through gap

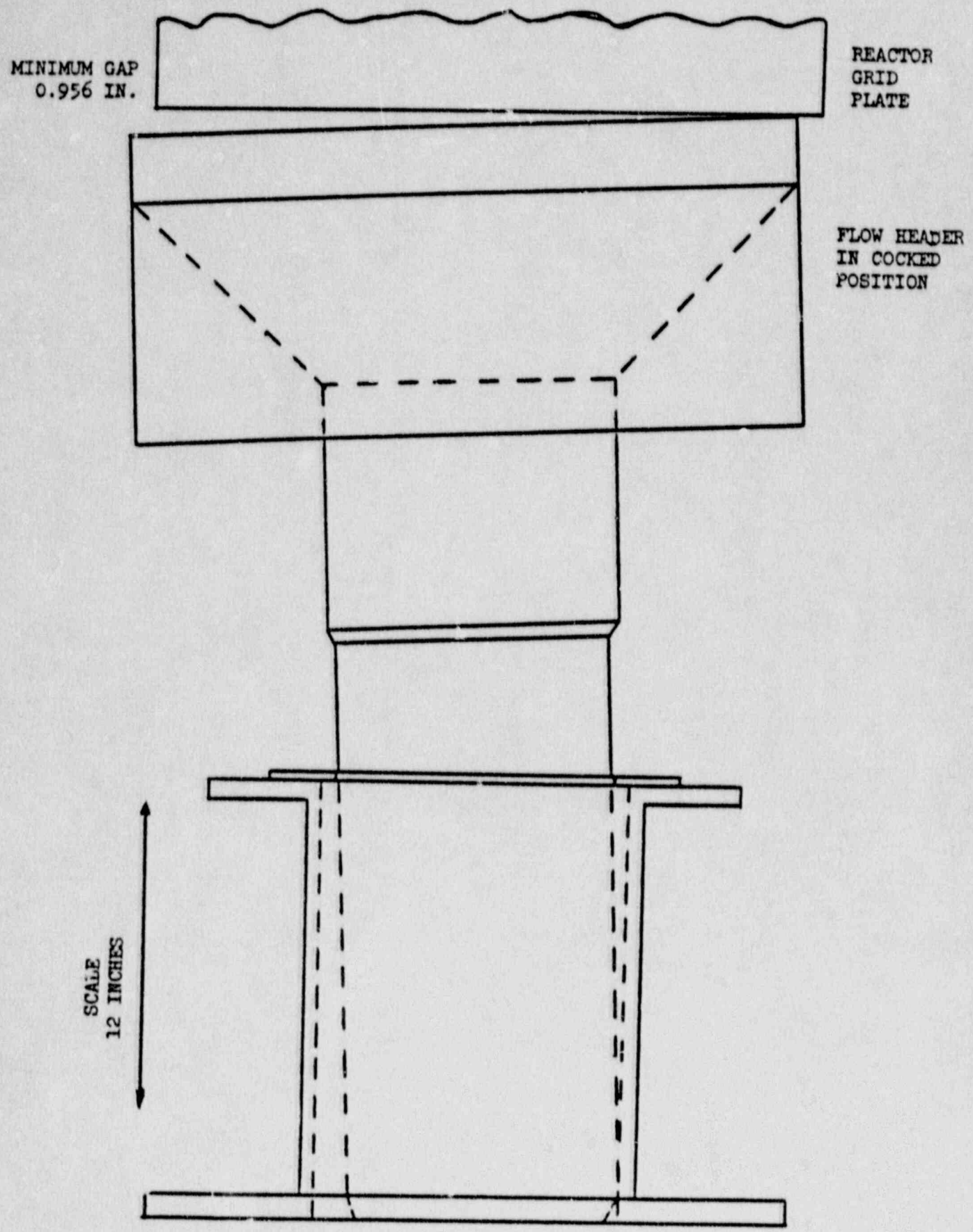

FIG. 9-8 FLOW HEADER JAMMED IN COCKED POSITION

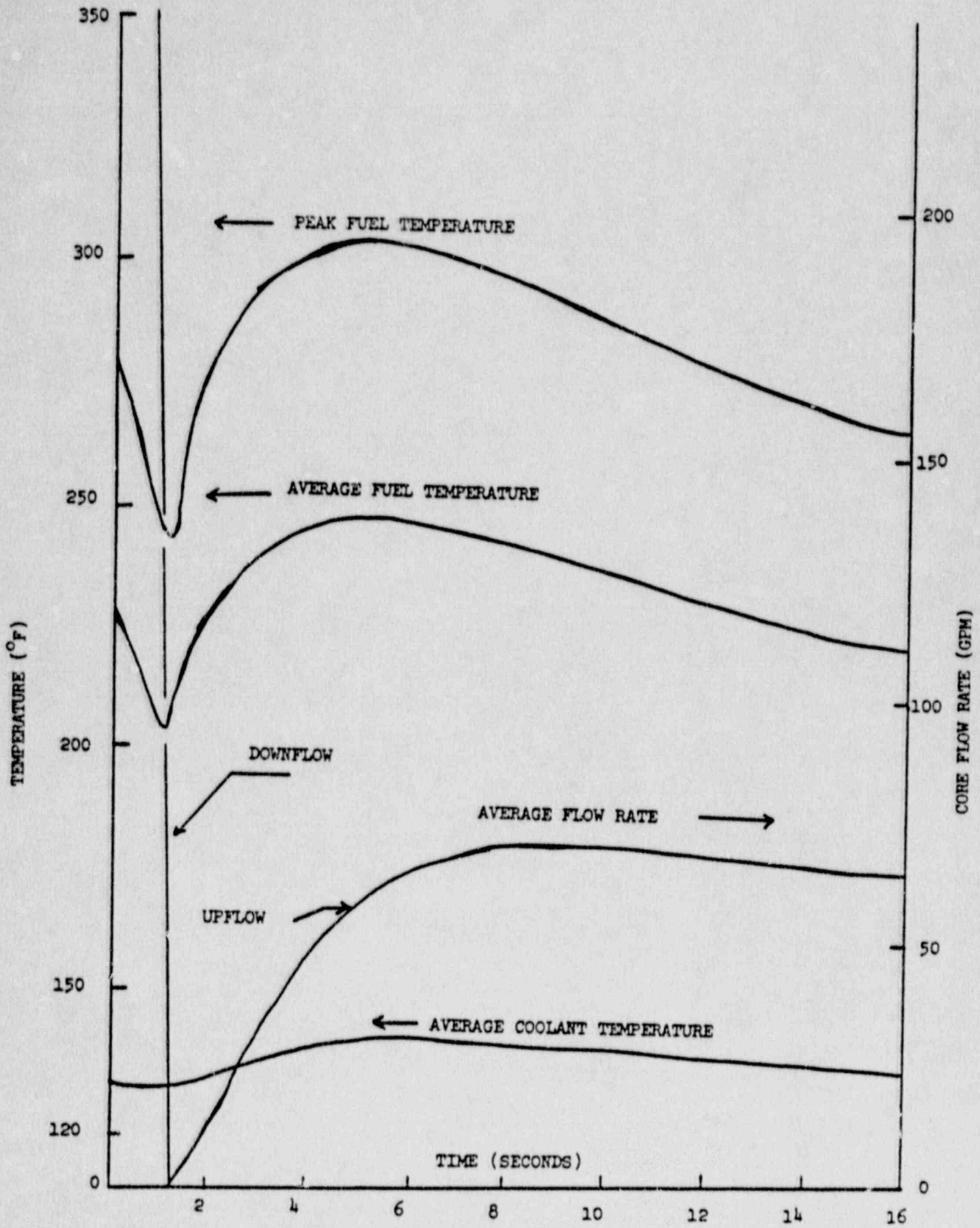

FIGURE 9-9 FLOW REVERSAL AFTER LOSS OF FLOW TRANSIENT FROM 3.45 MW

From continuity, it was found that, for the gap width of 0.956-inches, $V_{gap} = 1.86\ \bar{V}$. The transient heat transfer code has the standard point reactor kinetics and heat transfer equations. The only unusual feature is the momentum equation which controls the coolant flow rate. The time dependent momentum equation was:

$$(\bar{\rho}-\rho_o)\, h\frac{g}{g_c} = f\,\frac{h}{D_e}\,\frac{\rho_o V^2}{2g_c} + 1.5\,\frac{\rho_o V_{gap}^2}{2g_c} + \frac{\rho_o h}{g_c}\,\frac{d\bar{V}}{dt} + \frac{\rho_o L}{g_c}\,\frac{dV_{gap}}{dt} \qquad (9.36)$$

where: $\bar{\rho}$ = average density in heated channel in core

ρ_o = density of water at pool temperature

h = core height

L = equivalent length of flow path between the gap above the funnel and the core.

The flow velocity in the peak channel can be related to the flow velocity in the average channel by setting the pressure drop across both channels equal. For laminar flow and steady state, this results in a value of velocity in the peak channel 1.17 times the velocity in the average channel together with a temperature rise across the core, ΔT, of 1.17 times the ΔT for the average channel. These values assume a radial peaking factor of 1.37. The basis for the factor of 1.17 is as follows: The pressure drop, ΔP, across the hot channel and the average channel are equal, or Buoyancy ΔP = Friction ΔP in both hot channel and average channel.

Define x such that:

Buoyancy ΔP in hot channel = x times greater than Buoyancy ΔP in average channel (9.37)

Since buoyancy ΔP = Friction ΔP at steady state, then Friction ΔP in hot channel = x times friction ΔP in average channel (9.38)

$$\text{Friction } \Delta P = f \frac{L}{D_e} \frac{\rho V^2}{2g_c} \tag{9.39}$$

$$\text{In Laminar flow, } f = \frac{64}{R_e} = \frac{64}{\rho V D_e/\mu} \tag{9.40}$$

$$\therefore \text{Friction } \Delta P = \frac{64\, L\mu}{VD_e^2} \frac{V^2}{2g_c} = cV \tag{9.41}$$

where: c = constant, independent of channel.

Since Friction ΔP in hot channel = x times friction ΔP in average channel and since Friction ΔP = cV

$$\text{Then } V(\text{hot channel}) = x \cdot V(\text{average channel}) \tag{9.42}$$

Return to buoyancy ΔP to obtain a relation between ΔT (hot channel) and ΔT (average channel).

$$\text{Buoyancy } \Delta P = (\rho_o - \bar{\rho}) L \frac{g}{g_c} \tag{9.43}$$

where: ρ_o = density at inlet temperature (111°F)

$\bar{\rho}$ = average density in channel

From Eq. (9.37)

$$(\rho_o - \bar{\rho})_{\text{hot channel}} L \frac{g}{g_c} = x.(\rho_o - \rho)_{\text{avg. channel}} L \frac{g}{g_c} \tag{9.44}$$

Since the change with density is about linearly proportional to a change in temperature over a limited temperature range, $\rho_o - \bar{\rho}$ can be written as follows for the hot channel:

$$(\rho_o - \bar{\rho})_{hot} = a(\bar{T} - T_o)_{hot} = 2a(T_{exit} - T_o)_{hot} = 2a\,\Delta T_{hot} \qquad (9.45)$$

Similarly, for the average channel, using the same a,

$$(\rho_o - \bar{\rho})_{avg} = a(\bar{T} - T_o)_{avg} = 2a\,\Delta T_{avg} \qquad (9.46)$$

Substituting Eqs. (9.45) and (9.46) into (9.44) gives:

$$\Delta T_{hot} = x.\Delta T_{avg} \qquad (9.47)$$

We now have two relations, relating V_{hot} to V_{avg} Eq. (9.42) and ΔT_{hot} to ΔT_{avg} Eq. (9.47).

The energy equation allows us to evaluate x as follows:

The <u>Energy Equation</u> is:

$$(\dot{m}\, c_p\, \Delta T)_{avg.\ channel} = \bar{Q}(\text{Btu/h, heat production rate in average channel}) \qquad (9.48)$$

$$(\dot{m}\, c_p\, \Delta T)_{hot\ channel} = 1.37\,\bar{Q}\ (\text{where } 1.37 = \text{Radial peaking factor}) \qquad (9.49)$$

But $m = \rho VA$, where ρ and A are essentially the same for both the hot and average channels.

Hence, Eq. (9.48) can be rewritten as

$$\rho A c_p\, V_{avg}\, \Delta T_{avg} = \bar{Q} \qquad (9.50)$$

Substituting Eqs. (9.37) and (9.47) and V_{hot} and ΔT_{hot} into Eq. (9.49) gives:

$$Ac_p(xV_{avg})(x\Delta T_{avg}) = 1.37\ Q \tag{9.51}$$

Dividing Eq. (9.51) by Eq. (9.50) gives

$$x^2 = 1.37 \qquad \text{or} \qquad x = 1.17 \tag{9.52}$$

Hence, from EQ. (9.42) and Eq. (9.47),

$$V(\text{hot channel}) = 1.17\ V\ (\text{average channel}) \text{ and}$$
$$\Delta T(\text{hot channel}) = 1.17\ \Delta T(\text{average channel}) \tag{9.53}$$

The safety limit [HEU] during a loss-of-flow transient is established such that the maximum fuel temperature shall not exceed 350°F. The average fuel temperature does not exceed 247°F in Figure 9-9 as calculated by the transient heat transfer computer code. This occurred at 5.2 seconds where the average coolant temperature was calculated to be 140°F.

To compare with the steady state heat transfer code it was assumed that the reactor was in steady state at the conditions existing at 5.2 seconds. The steady state code gave an average fuel temperature of 214°F and an average coolant temperature of 143°F. The coolant temperatures are in good agreement, but as to be expected, the fuel temperature is considerably higher in the transient than in the steady state.

The transient code will not give the peak fuel temperature in the hot channel, but a conservative approach is to calculate this temperature for the steady state and ratio up accordingly. From the steady state

code, the peak fuel temperature in the hot channel was 252°F. This occurred near the mid point, axially along the channel where the coolant temperature was 147°F.

The heat transfer coefficients do not vary greatly, so for a given rate of coolant flow in a channel, the channel power, P, is closely proportional to the temperature difference, T, between the fuel plate and the bulk coolant. Accordingly

$$\frac{P(\text{hot channel in transient})}{P(\text{average channel in transient})} = \frac{P(\text{hot channel in steady state})}{P(\text{average channel in steady state})} \tag{9.54}$$

and to a very good approximation

$$\frac{\Delta T(\text{hot channel in transient})}{\Delta T(\text{average channel in transient})} = \frac{\Delta T(\text{hot channel in steady state})}{\Delta T(\text{average channel in steady state})} \tag{9.55}$$

or abbreviating

$$\frac{\Delta T(hc,tr)}{\Delta T(ac,tr)} = \frac{\Delta T(hc,ss)}{\Delta T(ac,ss)} \tag{9.56}$$

Using the data from the steady state code at 5.2 seconds given above

$$\frac{\Delta T\ (hc,ss)}{\Delta T\ (ac,ss)} = \frac{(252-147)}{(214-143)} = 1.48 \tag{9.57}$$

We assume this ratio is constant at time other than 5.2 seconds. At times far from 5.2 seconds the assumption is poor, but at times near 5.2 seconds where the peak temperatures are encountered, the assumption is quite valid. Accordingly,

$$\Delta T(hc,tr) = 1.48\Delta T(ac,tr). \tag{9.58}$$

$\Delta T(ac,tr)$ can be obtained at any time by subtracting the average coolant temperature from the average fuel temperature shown in Figure 9-9. At 5.2 seconds

$$\Delta T(ac,tr) = 247 - 140 = 107^{\circ}F \quad (9.59)$$

and therefore, (still at 5.2 seconds)

$$\Delta T(hc,tr) = 1.48 \times 107^{\circ}F = 158^{\circ}F \quad (9.60)$$

As mentioned before in laminar flow, to obtain equal pressure drops across both channels, the hot channel must have a flow rate 1.17 times the flow rate in the average channel. The temperature rise of the coolant along the hot channel must also be 1.17 times the temperature rise of the coolant along the average channel. (These two factors of 1.17 combine to give the radial peaking power factor of 1.37 [HEU]).

From Figure 9-9, at 5.2 seconds the average coolant temperature is 140°F, and subtracting the 111°F entrance temperature, gives a temperature rise of 29°F to the mid point of the average channel. For the hot channel the temperature rise is 1.17x29°F = 34°F giving a temperature at the mid point along the hot channel of 145°F.

Therefore, the peak flux fuel temperature in the hot channel in the transient is

$$T(pf,hc,tr) = 145^{\circ}F + 158^{\circ}F = 303^{\circ}F$$

This is at 5.2 seconds after the start of the loss-of-flow transient. In general, it is assumed that at any time during the transient, the peak fuel temperature in the transient is

$$T(pf,hc,tr) = 111^{\circ}F + 1.17\ T(aw,ac,tr) - 111^{\circ}F) + 1.48\ \Delta T(ac,tr) \quad (9.61)$$

where T(aw,ac,tr) is the average water temperature in the average channel

in the transient and 111°F is the coolant entrance temperature (pool temperature). T(pf,hc,tr) is the peak fuel temperature shown in Figure 9-9. The maximum is 303°F and is well below the [HEU] safety limit of 350°F. This method of analysis predicts a peak fuel temperature of 279°F at the start of the transient (time zero). The more accurate steady state code gave a peak fuel temperature of 252°F in the hot channel prior to the transient, indicating the conservatism of the method.

9.15. HEU Analysis for Natural Convection

[This section, as is the previous section, is the analysis performed for the HEU SAR. Refer to section 9.13 for justification for the validity of including this analysis for LEU]

According to Figures 9-6A and 9-7 and also Figure 2.1 in Technical Specification 2.1 [HEU Technical Specification Ref 29] a loss of flow transient from 3.45 megawatts will result in a flow coast-down followed by natural convection cooling at a reactor power of 750 KW. This power is due to fission product decay and dies off gradually with time. To be consistent with the Loss of Flow Transient Analysis (Section 9.14), 750 KW was chosen as the maximum power for the Safety Limit[29] in the natural convection mode of operation.

The transient heat transfer code (see Section 9.14) was used to determine the equilibrium flow rate established at 750 KW of power with natural convection flow. A flow rate of 129 GPM through 168 channels was established in about 25 seconds and remained steady in time thereafter. With 168 channels (Sec 9.4 of Ref. 24) the average power per channel is

750/168 = 4.46 KW. Multiplying by the radial peaking factor of 1.37 gives 6.12 KW as the power in the hot channel.

The flow rate in the average channel is 129/168 = 0.768 GPM. The velocity in the peak channel is 1.17 times the velocity of the average channel (see Section 9.14). Therefore, the flow rate in the hot channel is 0.768 x 1.17 = 0.90 GPM. Using the power of 6.12 KW and a flow rate of 0.90 GPM in the hot channel as input to the steady state thermal hydraulics code with natural convection upflow, the maximum fuel plate temperature was found to be 259°F with an inlet coolant temperature of 111°F. 750 KW and 111°F were conservatively chosen as the [HEU] Safety Limits in the Natural Convection Mode of Operation, Specification 2.1.2 [HEU Technical Specifications Ref. 29]. A maximum fuel plate temperature of 259°F is well below the temperature at which fuel clad damage could occur.

9.16. Maximum LEU 22 Plate Fuel Temperatures Following LOCA

9.16.A. Introduction

The maximum fuel temperature reached after loss of coolant from the limiting UVAR LEU 22-plate core was calculated using semi-empirical relationships similar to those developed for the safety analysis of the Omega West Reactor (OWR) at Los Alamos[22], which is an MTR-plate-type pool reactor. The fuel clad melting temperature for the UVAR is the melting point of aluminum alloy 6061 at 1080°F, but structural integrity may be lost if the fuel is held above the softening temperature of for a sustained period of time. For the purposes of these analysis, a softening temperature of 840°F[33] was chosen as the limiting criteria for the analysis of a LOCA.

For several potential coolant loss mechanisms, the time required to uncover the core was calculated because it is an important parameter in calculating the maximum fuel temperature following a LOCA. However, the UVAR relies upon the Emergency Core Spray System (ECSS) (analyzed in Section 9.17) to cool the reactor following any LOCA that takes less than 90 minutes to uncover the core after the reactor scrams due to low pool level. Therefore, the minimum time after a shutdown to shift from water cooling to air cooling is taken to be 90 minutes.

The fission fragment heat source used in the analysis was the "Simplified Method for Determining Decay Heat Power and Uncertainty" given in Section 3.6 of ANSI/ANS Standard 5.1[31]. This decay heat power can be 1.5 times as high as the power predicted by the Way-Wigner relation during the limiting LOCA transient. A modification to the heat transfer correlation developed by OWR was made such that, when used with the ANSI/ANS 5.1 heat source, it safely enveloped the temperatures calculated with the original OWR heat transfer correlation and the Way-Wigner heat source. For the benchmark transient based upon uncovering the OWR core 30 minutes following shutdown, the modified heat transfer correlation with the ANSI/ANS 5.1 heat source gave a peak temperature 140°F higher than the original OWR calculations and was higher throughout the transient. Figure 9-10 compares the benchmark OWR transient when calculated using the UVAR correlation and the ANSI/ANS 5.1 heat source with the same transient calculated with the OWR correlation using the Way-Wigner heat source. This comparison, along with similar comparisons in reference 22 between the OWR correlation and experimental data,

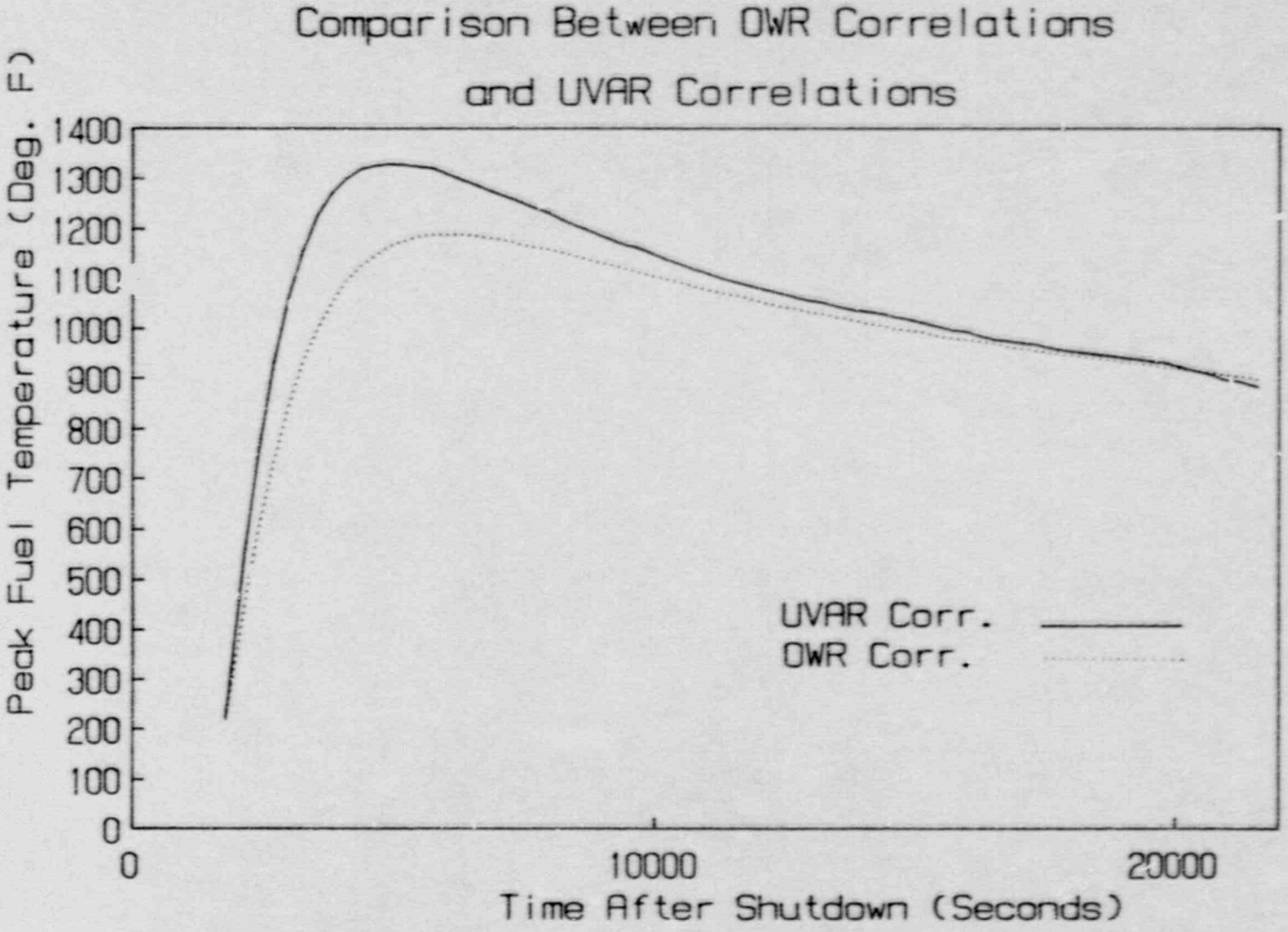

Figure 9-10 Comparison Between OWR Transient using UVAR Correlelations ans OWR Correlations

indicates that the new correlation together with the ANSI/ANS 5.1 heat source will overestimate the maximum temperature reached following a LOCA.

9.16.B Calculation of Peak Fuel Temperature Following a LOCA

After loss of water cooling, the reactor is cooled predominantly by ambient air flowing through the core by natural convection. Since heat conduction to the grid plate and to the upper part of the fuel element occurs together with natural convection and some radiation, the calculation of maximum fuel temperature from first principles is too complex to be reliable. Hence, experimental data from LITR was used by OWR[22] in their safety analysis to develop a heat transfer correlation that, together with the Way-Wigner decay heat relation, safely enveloped the maximum axial temperatures measured in the LITR experiments.

In the LITR experiments, an element was actually removed from an operating core and the maximum fuel temperature along the axial profile was measured as a function of time while the element was cooled by air convection. As described in Reference 22, the LITR experimental data was safely enveloped by the following transient equation which is solved for the difference, θ, between the peak fuel-plate temperature, T_F, and the ambient air temperature, T_a.

$$mc_p \frac{d\theta}{dt} = Q(t) - hA\theta \qquad (9.61)$$

where

$\theta = T_F - T_a$ (^oF)

$Q(t)$ = time dependent heat source (MW)

hA = product of the natural convection heat transfer correlation and the effective heat transfer area of one fuel element (MW/°F)

mc_p = heat capacity of a fuel element, with m being the mass and c_p being the specific heat of the associated fuel element material.

Mc_p for the UVAR 22-plate fuel element was calculated by determining the mass of aluminum and U_3Si_2 in the standard element from the fuel plate specification and the preliminary construction drawings for the elements and applying formulas determined by Argonne National Laboratories[30] for the c_p of these materials as a function of temperature.

$$c_p \text{ Al} = .892 + .00046T \ (J \cdot g^{-1} \cdot K^{-1}) \tag{9.62}$$

Mass Al = 5195 g per element

$$c_p \ U_3Si_2 = .199 + .00010T \ (J \cdot g^{-1} \cdot K^{-1}) \tag{9.63}$$

Mass of U_3Si_2 = 1505 g per element

Therefore, the total mc_p for a standard element is

$$mc_p \text{ Element} = 4933 + 2.54T \ (J \cdot K^{-1}) \tag{9.64}$$

For the heat source, Q(t), the method given in Section 3.6 of ANSI/ANS Standard 5.1 for heat production from fission products after shutdown was used. The one sigma uncertainty associated with the decay heat power was included as a positive bias.

$$P_d(t,T) = P'_d(t,T) * G(t) + \Delta P_d \qquad (9.65)$$

and

$$P'_d(t,T) = 1.02 \frac{Pmax}{Q}[F(t,\infty) - F(t+T,\infty)] \qquad (9.66)$$

where:

P_d = decay power

G(t) = a correction factor for the activation of fission fragments given in Table 10 of ANSI/ANS 5.1

ΔP_d = one-sigma error associated with P_d (see ANSI 5.1)

Q = 200 Mev/fission (conversion factor)

Pmax = the operating power of the hottest fuel element

$F(t,\infty)$ = the fission fragment heat source for thermal fission of U-235 given in Table 4 of ANSI/ANS 5.1

t = time since shutdown from operating at Pmax

T = the time operated at Pmax

Non-linear interpolation between time steps given in the ANSI/ANS 5.1 tables for Eq. (9.65) was done using the time dependency in the Way-Wigner expression for decay heat generation.

The value used for T was 120 hours, or 5 days. The value used for Pmax was 0.209 MW, which is the power of the highest power element in a 4x4 LEU core, at 2 MW total core power, as determined from 2DB-UM[26] flux maps. Larger cores were evaluated and found to be less limiting than the 4x4 element core.

The heat transfer parameter hA was found at OWR by fitting coefficients in the form

$$hA = C(a\theta^n + b) \qquad (9.67)$$

to get an expression for hA which was then used in Eq. (9.61) to fit the data from the LITR experiments using the Way-Wigner decay heat source and the appropriate mc_p. The coefficient C includes the heat transfer area

of the fuel plates. The expression for hA used for the present analysis was found by searching for a new constant C in Eq. (9.67) (retaining the other constants found by OWR) that when used in Eq. (9.61) with the ANSI/ANS 5.1 heat source and the case specific input data from OWR, safely enveloped the transients calculated with the original OWR correlations in their safety report. The new expression for hA which incorporates the higher h per plate and includes the number of plates per element as a variable is:

$$hA = 9\times10^{-8}(PN)(6.4\times10^{-3}\ \theta^{0.72} + 0.5)\ \frac{MW}{F^{o}} \qquad (9.68)$$

where PN is the number of fuel plates in the standard element.

Substituting Eqs. (9.64), (9.66), and (9.68) into Eq. (9.61) gives a transient expression which was solved for θ, with the initial conditions of $\theta = 112^{o}F$ at the time at which air cooling starts. The peak fuel temperature, T_f, was obtained from $\theta = T_f - T_a$ assuming that the ambient air temperature, T_a, was $100^{o}F$, or

$$T_f(peak) = \theta + 100.$$

The peak fuel-plate temperatures versus time after shutdown, with time to shift to air cooling in the core as a parameter, are plotted in Figure 9-11. Transients assuming no ECSS and a shift to air cooling 0.3 hours and 1 hour following shutdown are plotted as dotted lines whereas the transient for the minimum specified time to shift to air cooling with ECSS (1.5 hours for flow dropping below 7.5 gpm, see Table 9.4) and a later transient (2 hours) are plotted as solid lines. The maximum fuel temperatures corresponding to these transients are listed in Table 9-3. For the limiting case where the ECSS is used to provide cooling for 90 minutes following a reactor scram due to low pool level, the maximum

temperature reached during the transient is 775°F. This is well below the aluminum cladding softening temperature of 840°F assumed for this analysis.

TABLE 9-3

MAXIMUM FUEL TEMPERATURES

(Operation Time = 120 h at 2 MW)

Time to Shift to Air Cooling (min.)	Maximum Temperature ($^{\circ}F$) w/o ECCS	w/ ECCS
20	975	775
60	835	775
90		775
120		730

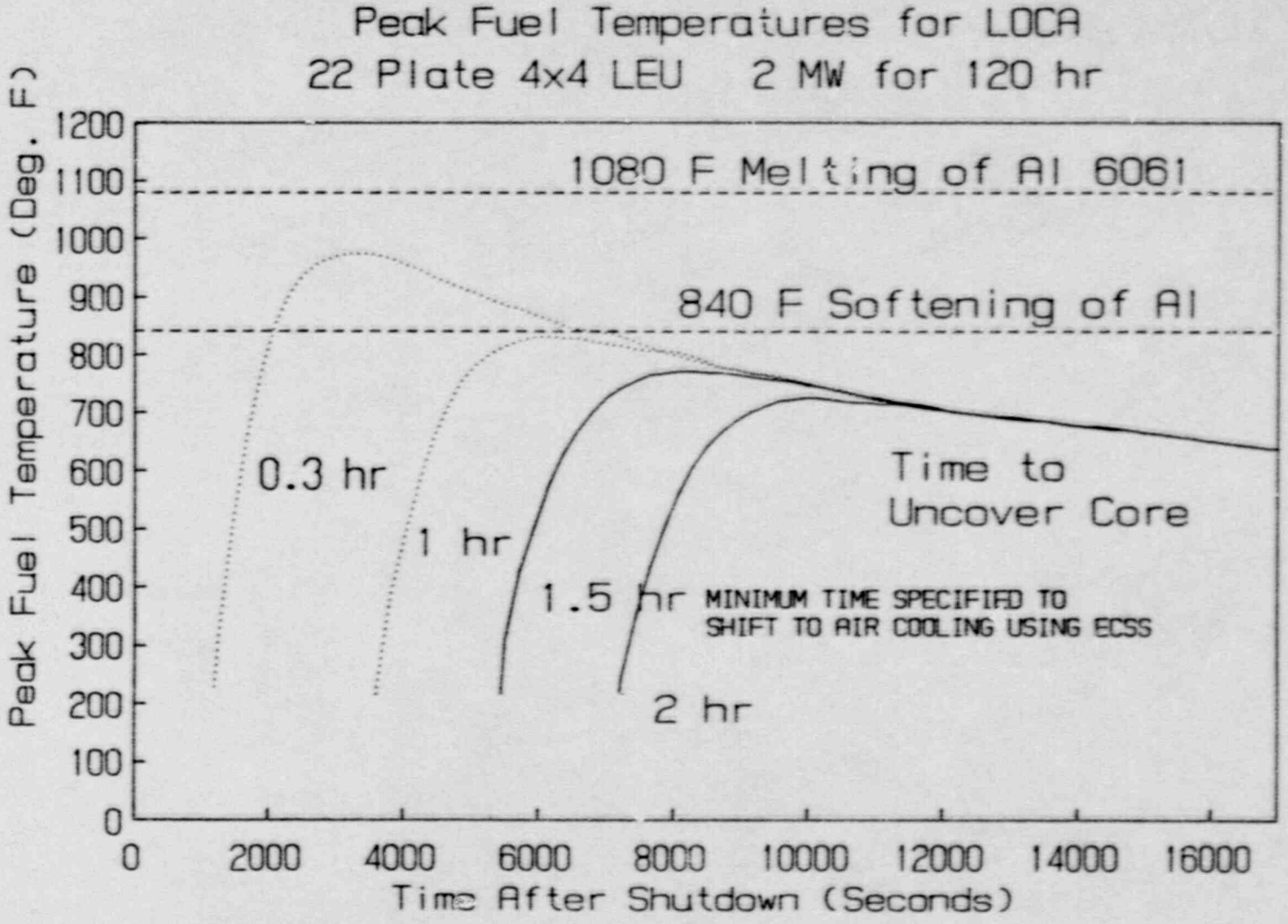

Figure 9-11 Peak Fuel Temperatures for Various LOCA Transients

9.17 Emergency Core Spray System Analysis

The emergency core spray system is described in Section 4.10. Using the decay heat source in ANSI/ANS 5.1 as described in section 9.17, the decay heat power in the hottest element 0.3 hours after shutdown (minimum credible time to uncover the core) is 3.5 kw. Assuming the cooling water is initially at 100°F, a water flow of 0.184 pounds per minute or 0.0221 gal/min is required to remove the decay heat from the hottest element (assuming complete evaporation of the water). A coolant flow of 10 gallons per minute over the entire grid plate will provide an average flow of 0.156 gallons per minute to each of the 64 fuel element positions. Using a flow maldistribution factor of $1/2^{32}$, the minimum flow to any fuel element position is 0.078 GPM. This flow is capable of removing 12.3 kw per fuel element. Thus, the rated flow of 10 gallons per minute to the core area is greater than the flow rate required to remove the decay heat of the hottest element after 0.3 hours by a factor of about 3.5. From 30 minutes to 90 minutes, the rated flow of the ECSS is 7.5 GPM which can remove 9.2 kw per fuel element. During this time the decay heat in the hottest element falls from 3.4 kw to 1.9 kw providing a minimum safety factor of 2.8 for the time the ECSS is relied upon to cool the reactor core.

At five second after shutdown, the decay heat power is 11 kw. This value is well below the 12.3 heat removal capability of the spray system. Even in the incredible situation where all water is lost from the pool in a matter of seconds, the spray system should be able to cool the reactor and prevent core damage. No operator action, automatic electronic, or automatic mechanical mechanism is required for the ECSS to function.

As the water level drops below the level of the spray headers, the

spray system begins to spray water on the core. Using the mockup of the core spray system shown in Fig. 4-3, tests were run of the flow rate versus head of water above the spray headers. Theoretically, if W is the flow rate (gpm) and Z is the head of water above the spray headers, then

$$W = KZ^{0.5} \tag{9.69}$$

Using the spray headers in the mockup it was found experimentally that

$$W(\text{gal/min}) = 0.48\ Z^{0.45} \tag{9.70}$$

where Z is in feet. From this relationship the characteristics of the spray system can be predicted as shown in Table 9-4.

LEU Technical Specifications for the spray system are based on this table, and require that each of the two systems shall be capable of delivering at least 10 gal/min for the first 30 minutes and at least 7.5 gal/min for the next 60 minutes after a LOCA onset. Ideally, this flow would be distributed equally to each of the 64 fuel element positions, but in actuallity this is not practical. It is practical to have (1/2 x 1/64) or 1/128 of the total flow delivered to each element. At the initial installation, measurements[32] were made to verify that each of the two spray systems is capable of delivering 10/128 or 0.078 gpm to each of the 64 fuel element positions at the end of 30 minutes of flow.

Figure 9-12 gives the decay power of the hottest element as a function of time for the first 2 hours after shutdown, the specified heat removal capacity of one ECSS sub system, and the actual heat removal capacity of each ECSS sub system based upon actual flow testing of the ECSS.

TABLE 9-4

CHARACTERISTICS OF SPRAY SYSTEM
(EACH TANK)

Time (min)	Head of Water (feet)	Flow Rate (gal/min)	Volume of Water Used (gal)
0	14.92	12.1	0 (Tank full)
7.8	14	11.8	103
16.6	13	11.4	215
25.7	12	11.0	328
35.2	11	10.6	440
45.1	10	10.1	552
55.6	9	9.7	664
66.7	8	9.2	776
78.4	7	8.6	889
91.0*	6	8.1	1000
105	5	7.4	1113
120	4	6.7	1225
137	3	5.9	1337
158	2	4.9	1450
168	1.58	4.4	1497(Tank empty)

* Flow beyond 90 minutes may be less than the specified 7.5 gal/min and therefore credit is not taken for this flow in the calculations.

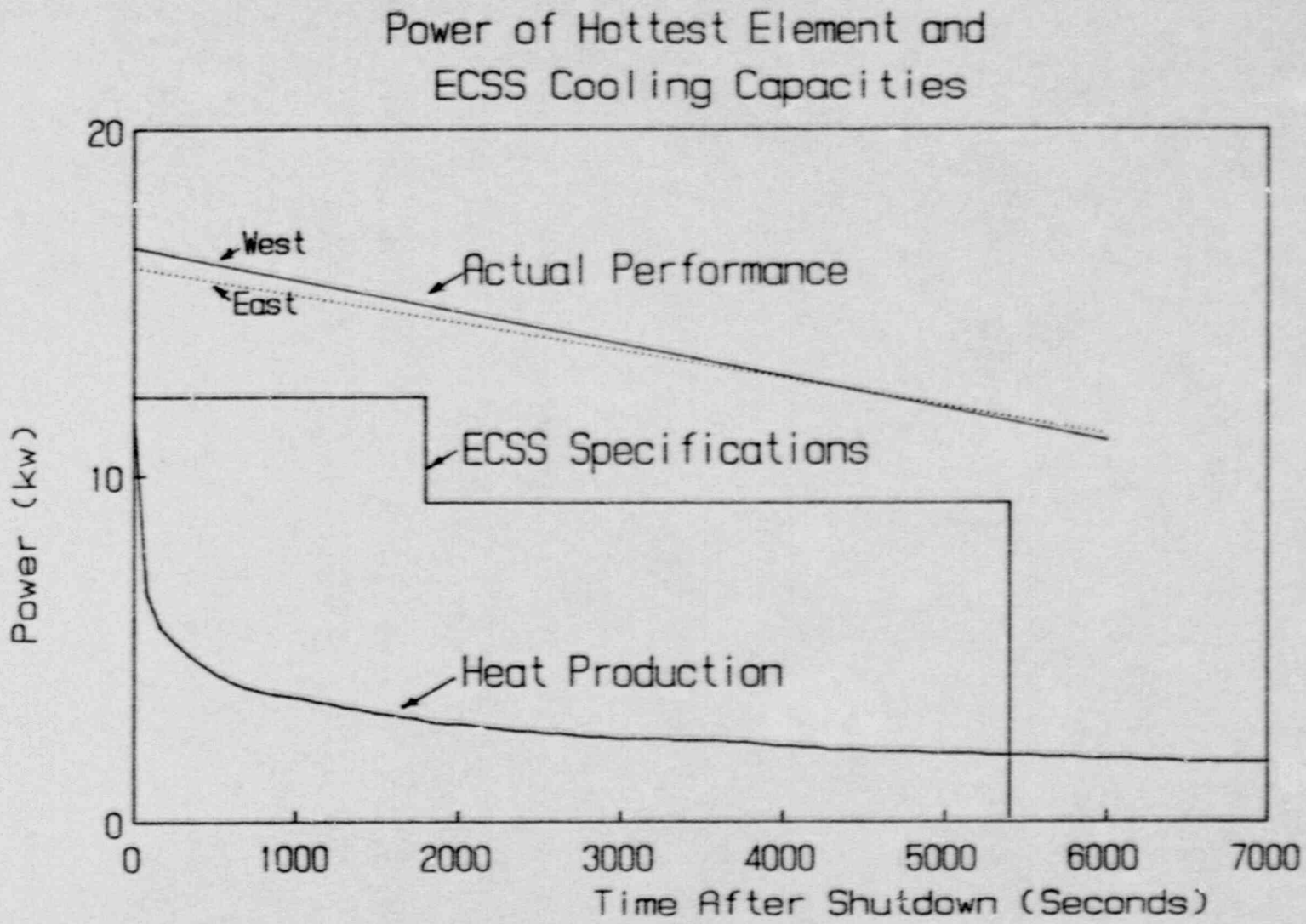

79-64

Figure 9-12 Power of the Hottest Element and ECSS Cooling Capacities

9.18. Time to Uncover the Core Following A LOCA

Table 9-5 shows the time it takes to uncover the core for the various mechanisms of pool leakage calculated in Section 9.18.

Table 9-5

Time to Uncover Core

For Various Leakage Mechanisms

Leakage Path	Time to Uncover Core
1) Double ended break at lowest point in 6-inch primary piping	19 minutes
2) Rupture of 8-inch beam port and flange	22 minutes
3) Double ended break in the 6-inch primary pipe at the level of the floor in the heat exchanger room	23 minutes
4) Quarter-inch, vertical crack extending the entire depth of pool, assuming no frictional losses	36 minutes

It is postulated that a guillotine pipe break in the six-inch diameter pipe between the reactor and the heat exchanger is the most rapid way for the UVAR core to uncover. Without subsequent closure of the isolation valves, such a double-ended pipe break would allow flow from both ends of the pipe. The geometry of the system is shown in Fig. 9-13.

Calculations were made assuming that a pipe break would occur at heat exchanger room floor level and at the lowest pipe level. It is noted that this pipe is surrounded by either concrete or earth wherever

it is below the floor level. Since a guillotine pipe break is not likely to occur at this location and water could not freely flow away if it did, the calculations are considered to be conservative. Because the break is assumed to occur close to the pool, there would be little frictional resistance to flow through one end of the break. However, flow through the other end of the break must first travel through the pipe and the heat exchanger, and consequently the resistance would significantly decrease this flow rate. This was taken into account in the calculation of the time to uncover the core.

9.18.A. Flow Rate without Frictional Loss

The flow velocity V_2 through the pipe end for which no frictional loss was assumed was calculated using Bernoulli's equation. With positions 1 and 2 defined on Fig. 9-13, Bernoulli's equation for flow between 1 and 2 is:

$$\frac{V_1^2}{2g_c} + \frac{P_1}{\rho} + z_1 \frac{g}{g_c} = \frac{V_2^2}{2g_c} + \frac{P_2}{\rho} + z_2 \frac{g}{g_c} \qquad (9.71)$$

From Fig. 9-14,

$V_1 = 0$ (i.e., V_1 is velocity before the water enters the pipe)

$z_1 = z_2$

$P_1 = P_o + \rho z \frac{g}{g_c}$ (where z is the water level above the pipe break)

$P_2 = P_o = 1$ atm

Hence, for the present case, Bernoulli's equation reduces to

$$\frac{V_2^2}{2g_c} = \frac{P_o + \rho z \frac{g}{g_c} - P_2}{\rho}$$

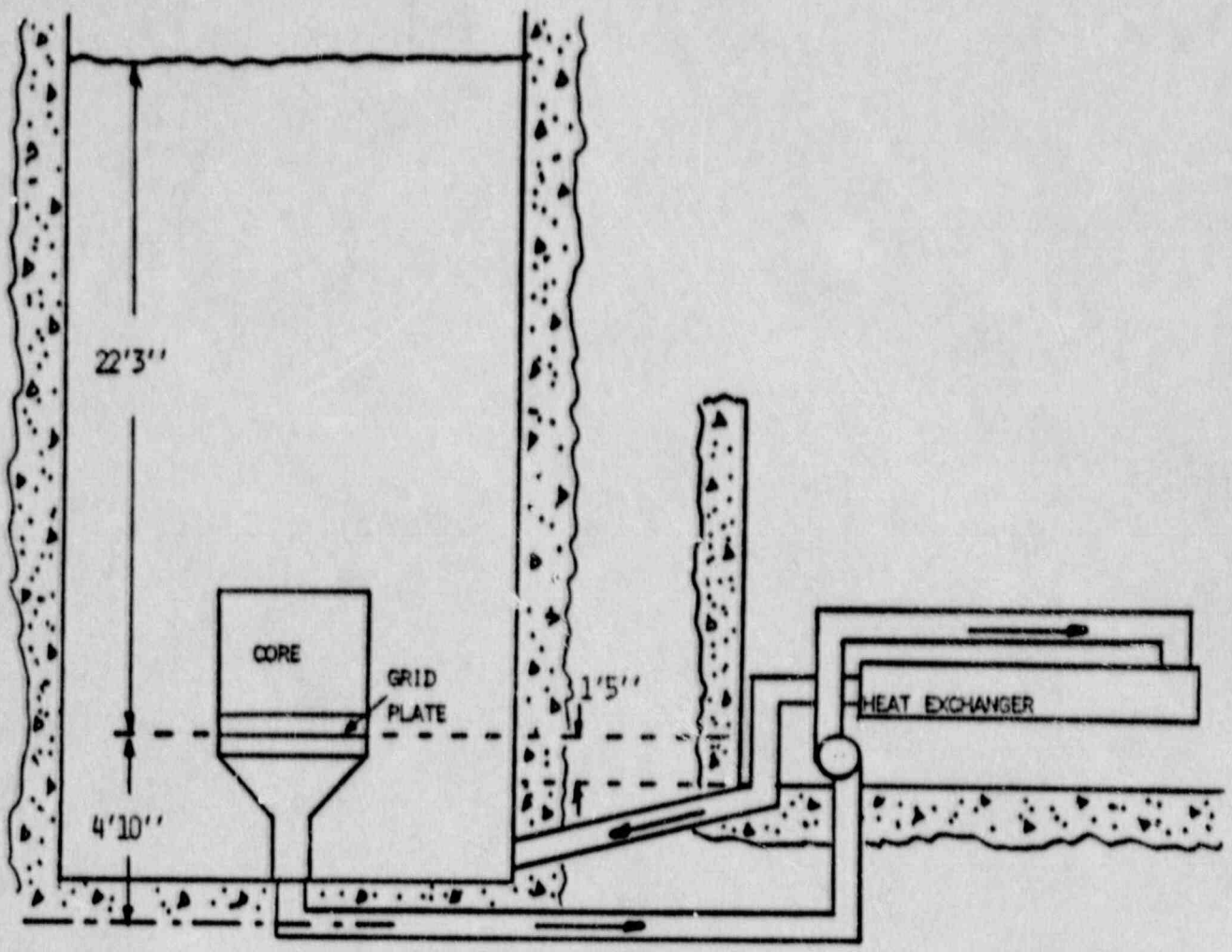

FIGURE 9-13 PRIMARY PIPING

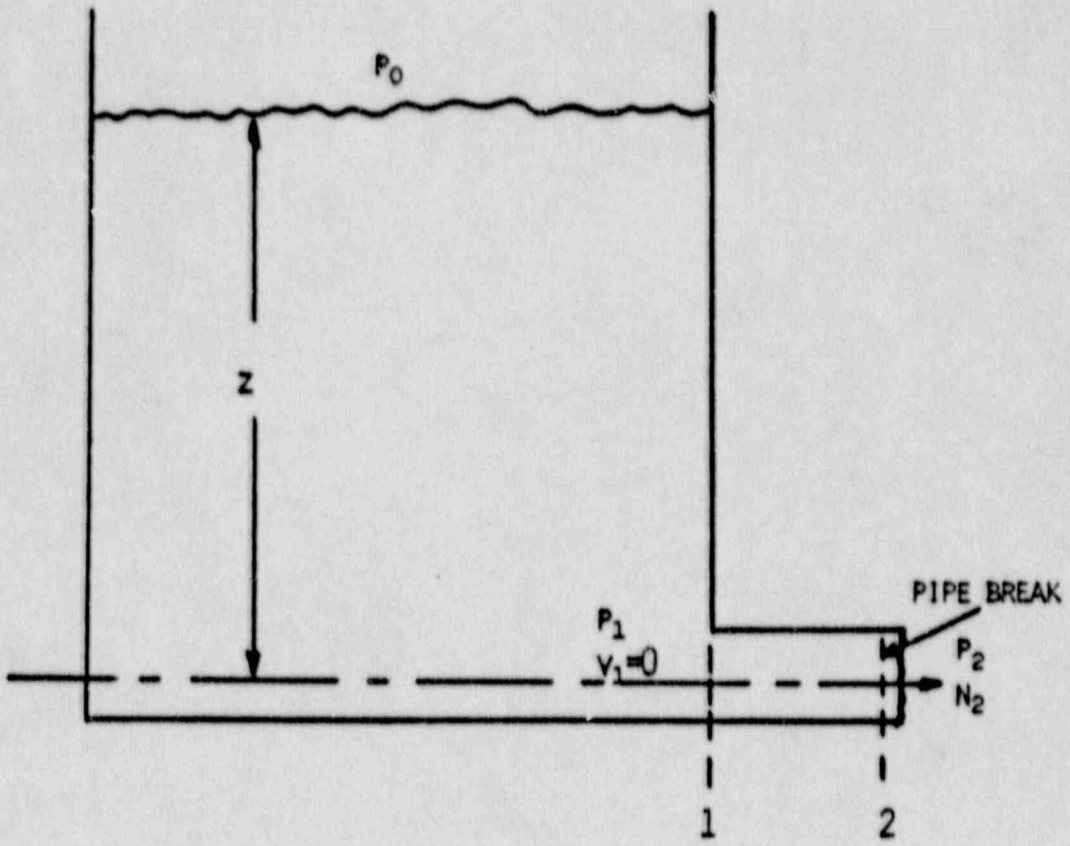

FIGURE 9-14 GEOMETRY FOR CALCULATING V_2

or

$$V_2 = \sqrt{2gz} \tag{9.72}$$

9.18.B Flow Rate with Frictional Loss

The effect of the frictional loss in the pipe and the heat exchanger is to add an energy loss term to the Bernoulli equation, as follows:

$$\frac{V_1^2}{2g_c} + \frac{P_1}{\rho} + z_1 \frac{g}{g_c} = \frac{V_{2,f}^2}{2g_c} + \frac{P_2}{\rho} + z_2 \frac{g}{g_c} + H_\ell \tag{9.73}$$

where $H_\ell = \frac{\Delta p_f}{\rho}$ (and where Δp_f is the frictional pressure drop)

The subscript f is added to V_2 to denote the velocity at position 2 with friction loss taken into account.

Equation (9.73) reduces to:

$$\frac{V_{2,f}^2}{2g_c} + \frac{\Delta p_f}{\rho} = z \frac{g}{g_c} \tag{9.74}$$

In order to solve for $V_{2,f}$, it is necessary to express Δp_f in terms of $V_{2,f}$. This can be done by recognizing that the form of the frictional pressure drop is

$$\Delta p_f = f \frac{L}{D} \frac{\rho V^2}{2g_c}$$

By neglecting the dependence of the friction factor "f" on velocity, this expression for Δp_f has the form,

$$\Delta p_f = aV^2 \tag{9.75}$$

where "a" is a constant. Neglecting the dependence of "f" on the velocity is sufficiently accurate for the present calculation, as can be

shown as follows. The velocity through the 6-inch pipe during normal operation is 11.4 ft/sec, and the associated friction factor is 0.0144. The maximum velocity in the pipe at the beginning of a pipe break, with no resistance to flow, is 41 ft/sec, and the friction factor for this velocity in a 6-inch pipe is 0.0136. The velocity remains between 11.4 and 41 ft/sec until the water level in the pool is 2.0 ft above the pipe break.

The constant "a" in Eq. (9.75) can be evaluated from a knowledge of the pressure drop and velocities for the piping and heat exchanger during rated flow conditions, as follows:

Mass flow rate during normal operation = 500,000 lbm/h (900 gal/min)

V (through 6" dia. pipe) = 4.1×10^4 ft/h

Δp_f (Heat Exchanger) = 9.5 psi = 1370 lbf/ft^2 (during normal operation, as experimentally measured)

Length of pipe in external line, exclusive of heat exchanger ≈ 70 ft.

Re (in 6" pipe) = 7.7×10^5

f = 0.014

Δp_f (pipe) = 1.7 psi = 250 lbf/ft^2

Δp_f (pipe) + Δp_f(heat exchanger) = 11.2 psi = 1620 lbf/ft^2

$g_c = 4.17 \times 10^8 \ \frac{\text{lbm ft}}{\text{lbf hr}^2}$

Using the form for Δp from Eq. (9.75), together with continuity, one can express the sum of the pipe and the heat exchanger pressure loss as a function of the velocity in the pipe as:

$$\Delta p_f = \Delta p_{pipe} + \Delta p_{heat\ exchanger} = a V^2_{pipe}$$

or

$$a = \frac{1620 \text{ lbf/ft}^2}{(4.1 \times 10^4 \frac{\text{ft}}{\text{hr}})^2} \tag{9.76}$$

Substituting Eqs. (9.75) and (9.76) into (9.74) gives the following result for $V_{2,f}$:

$$V_{2,f} = \sqrt{\frac{g\ z}{\frac{1}{2} + 6.5}} = 0.378\ \sqrt{gz} \tag{9.77}$$

This value compares to $V_2 = \sqrt{2gz} = 1.41\sqrt{gz}$ [Eq. (9.72)] where V_2 is the velocity without friction loss, or

$$V_{2,f} = 0.27\ V_2 \tag{9.78}$$

9.18.C. Time to Uncover Core with Double-Ended Pipe Break

To calculate the time to uncover the core with a guillotine pipe break, we equate the following two expressions for the rate at which water is flowing out of the pool:

(1) Flow rate out of the broken pipe

$$= \rho S V_2 + \rho S V_{2,f}$$

$$= 1.27\ \rho S V_2 \quad \text{[from Eq. (9.78)]} \tag{9.79}$$

where S = pipe cross sectional area

(2) Since $-\frac{dz}{dt}$ = the rate of change of water level in the pool, the flow out of the pool is also

$$= -\rho A \frac{dz}{dt} \tag{9.80}$$

where A is the surface area of the pool.
Equating Eq. (9.79) and (9.80) for flow rate gives

$$\frac{dz}{dt} = \frac{-1.27S}{A} V_2$$

Substituting Eq. (9.72) for V_2 gives

$$\frac{dz}{dt} = -\frac{1.27S}{A}\sqrt{2gz}$$

Finally, the time, τ, for the water level to change from $(z_0 + z_1)$ to z_1 (i.e. the time to uncover the core), is

$$\tau = \int_{z_0+z_1}^{z_1} -\frac{A}{1.27S}\frac{dz}{\sqrt{2gz}} \qquad (9.81)$$

$$= \frac{2A}{\sqrt{2g}\,S}\left(\sqrt{z_0 + z_1} - \sqrt{z_1}\right)$$

Values used in the calculations reported in Section 9.18 are:

$g = 32.17$ ft/sec^2

$A = 32$ ft x 12 ft

$S = \frac{\pi}{4}\left(\frac{1}{2}\text{ ft}\right)^2$

$z_0 = 22.25$ ft

For pipe break at floor level of heat exchanger room, $z_1 = 1.92$ ft.

For pipe break at lowest point in pipe, $z_1 = 4.83$ ft. (See Fig. 9-14).

9.18.D Time to Uncover Core with Crack in Pool Wall

For a crack in the pool wall of width δ running the full height of the wall, the time necessary to uncover the core, assuming Bernoulli's equation with no frictional resistance, is

$$\tau = \frac{3A}{\delta\sqrt{2g}}\left(\frac{1}{\sqrt{z_1}} - \frac{1}{\sqrt{z_0 + z_1}}\right) \qquad (9.81)$$

where z_1 = distance between bottom of the pool and the bottom of the grid plate and z_0 = same as in Fig. 9-13.

REFERENCES FOR CHAPTER 9

1. Gambill, W.R., "Generalized Prediction of Burnout Heat Flux for Flowing, Subcooled, Wetting Liquids," Chemical Engineering Progress Symposium Series, Vol. 59, Houston, 1962.

2. Bergles, A. and Rohsenow, W., "The Determination of Forced-Convection Surface Boiling Heat Transfer," ASME Paper 63-HT-22 (1963).

3. Cox, J., "ORR Operations for Period April 1958 to April 1959," CR-59-39, Oak Ridge National Laboratory (April 1959).

4. Eckert, E.R.G. and Drake, R.M., "Heat and Mass Transfer." McGraw-Hill, New York, 1959.

5. Private Communication from Wallace R. Gambill, ORNL.

6. Bernath, L., "Theory of Local Boiling Burnout and its Application to Existing Data," Ch.E. Progress Symposium Series, Storrs, 1960.

7. Todeas, N., "Effect of Non-Uniform Axial Heat Flux Distribution on the Critical Heat Flux," Ph.D.. Dissertation, M.I.T., Sept. 1965.

8. DeBortoli, R.A., "Forced-Convection Heat Transfer Burnout Studies for Water in Rectangular Channels and Round Tubes at Pressures Above 500 psia," WAPD-188, Oct. 1958.

9. Gambrill, W.R., "Forced Convection Burnout," Nuclear Safety, Vol. 5, No. 2, Winter 1963-64.

10. Tong, L.S., "DNB Studies in an Open Lattice Core," WCAP-3736, Aug. 1964.

11. Perry, J.H. (ed), "Chemical Engineer's Handbook," McGraw-Hill, New York, 1950.

12. Esselman, W.H., et al, "Thermal and Hydraulic Experiments for Pressurized Water Reactors," Proceedings of the 2nd United Nations International Conference on the Peaceful Uses of Atomic Energy, Vol. 7 pg. 758, United Nations, Geneva, 1958.

13. Von Karman, T., NACA Technical Memo No. 611, 1931.

14. Gambill, W.R. and Bundy, R., "HFIR Studies of Turbulent Water Flow in Thin Rectangular Channels," ORNL-3079, June 1961.

15. Reynolds, J., "Local Boiling Pressure Drops," ANL-5178, March, 1954.

16. Barnett, P.G., "The Prediction of Burnout in Non-Uniformly Heated Rod Clusters from Burnout Data for Uniformly Heated Round Tubes," AEEW-R-362, November 1964.

17. "Non-Uniform Heat Generation Experimental Program," Quarterly Progress Report No. 5, July-September 1964, BAW-3238-5, Sept. 1964.

18. "Non-Uniform Heat Generation Experimental Program," Quarterly Progress Report No. 6, October-December 1964, BAW-3238-6, December 1964.

19. Sternberg, H.I., "Thermal Power Calibration and Correlation of UVAR by Foil Irradiation and Heat Balance," Master's Thesis, University of Virginia, June 1964.

20. Brunot, W.K., "An Analysis of Fuel Element Surface Temperature and Coolant Flow Rate in UVAR," Master's Thesis, University of Virginia, November, 1961.

21. Custer, G.A., "The Experimental Determination of the Thermal Neutron Flux in the University of Virginia Reactor Using an Aluminum Hydraulic Rabbit, Master's Thesis, University of Virginia, August 1960.

22. "1969 Status Report on the Omega West Reactor, with Revised Safety Analysis," Los Alamos Scientific Laboratory, LA-4192, July 1969.

23. DiNunno, J.J., et al. "Calculation of the Distance Factors for Power and Test Reactor Sites," TID-14844, 1962.

24. "University of Virginia Reactor Safety Analysis Report," University of Virginia, UVAR-18, Revised January 1979.

25. Dahlheimer, J.A., "Thermal-Hydraulic Safety Analysis of Pool Reactors", Master's Thesis, University of Virginia, 1967.

26. University of Michigan, "2DB-UM Appollo Version", Version #10, September 1986.

27. Freeman, D.L., "Neutronic Analysis for the UVAR HEU to LEU Conversion Project", Master's Thesis, University of Virginia, January 1990.

28. Smith R.S. and Woodruff W.L., "A Computer Code, NATCON, for the Analyses of Steady-State Thermal-Hydraulics and Safety Margins in Plate-Type Research Reactors Cooled by Natural Convection", ALN/RERTR/TM-12, December 1988.

29. "Technical Specifications for the University of Virginia", September 1982, Amended April 1988, and December 1988.

30. Telecopy from Argonne National Laboratory, "Properties of Fuel Meat Materials", August 19, 1988.

31. "Decay Heat Power in Light Water Reactors" American National Standard ANSI/ANS-5.1-1979, Reaffirmed July 1985, American Nuclear Society, La Grange 1979.

32. Meem, J. L., "Emergency Core Spray System Installation And Testing", Report to University of Virginia Reactor Safety Committee, September, 1971.

33. Nagler, A., Gilat, J., Hirshfeld, H., "Evaluation of LOCA in a Swimming-Pool Type Reactor Using the 3D-AIRLOCA Code," paper presented at the XII International Meeting on Reduced Enrichment for Research and Test Reactors, Berlin, Federal Republic of Germany, 10-13 September 1989.

Safety Analysis for the University of Virginia Reactor LEU Conversion

R.A. Rydin, D.W. Freeman, B. Hosticka and R.U. Mulder
Dept. of Nuclear Engineering and Engineering Physics
University of Virginia
Charlottesville, Virginia, USA

ABSTRACT

The University of Virginia is preparing to convert the 2MWT UVAR reactor from 18-curved plates/element high-enriched fuel to comparable flat plate low-enriched fuel. Depletion studies of low enriched cores suggest that the use of 22 plates/element in a 4-by-5 array will give a considerably longer core life and a generally higher thermal flux than direct replacement with 18 plates/element. The excess reactivity of this larger and more highly loaded core can be regulated by selectively changing portions of the reflector from graphite to water. Calculations of control rod worths, moderator and Doppler temperature coefficients, void coefficients, and kinetics parameters indicate that the LEU cores will have performance characteristics that are not very different from the HEU cores. Thermal hydraulic calculations indicate that these cores are acceptable with only small changes in safety system settings.

DESCRIPTION OF THE UVAR FACILITY

The UVAR is a 2 MWT swimming pool-type research reactor. It is made up of plate-type MTR fuel elements mounted on an 8-by-8 grid plate that is suspended from a movable bridge above a large open pool of water. The reactor can be moved to either end of the pool while the other pool half is drained for maintenance purposes. However, the core can only be operated at full power when it is mounted on the South end of the pool, directly above a coolant funnel that provides forced down-flow circulation. This position is shown in Figure 1, which also shows the location of the experimental beam ports.

The original UVAR design was done by J.L. Meem [1] et al., circa 1960, using analytical two-group theory. The Technical Specifications (TS) require maintenance of a minimum shut-down margin of 0.4% $\Delta k/k$ with the largest worth shim rod fully withdrawn, and a maximum excess reactivity of 5% $\Delta k/k$. Any core arrangement that will fit on the grid plate, and that meets this TS, can be used, providing that the control rods are experimentally recalibrated each time a new core arrangement, which was not previously tried, is assembled. The UVAR has been operated for more than twenty years using experimental techniques, essentially without benefit of computational modeling. During this time, both 12-flat-plate fuel elements and 18-curved-plate fuel elements have been used in separate cores, and arrangements having anywhere from 16 to 27 fuel elements have been operated. Some cores have been entirely water reflected, others graphite reflected, while most cores have had water on some sides and graphite on the others.

It is not really to our advantage to allow the UVAR core size to become as large as 27 elements, because the thermal flux available for experiments is correspondingly reduced. We believe that a more practical future strategy would be to try to operate with a core arrangement that is essentially fixed in a 4-by-5 array, with the shim rods placed close to the core center, as illustrated in Figure 2, to provide a high shutdown margin. We also believe that a planned fuel shuffling pattern should be used in place of our current ad hoc procedure of trying to obtain equal burnup for each element in inventory.

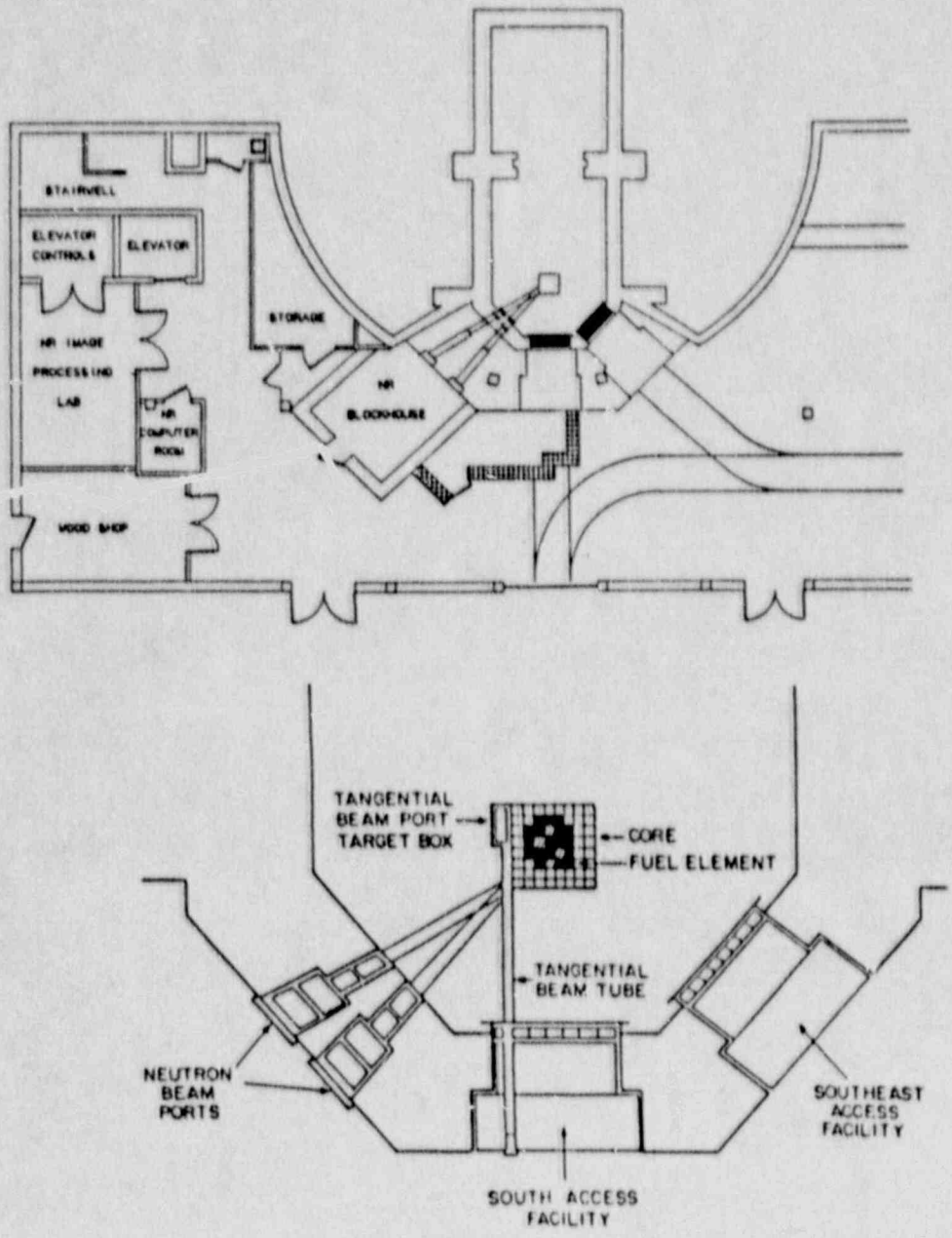

Figure 1. Sketch of UVAR Pool Showing 8-by-8 Grid Plate

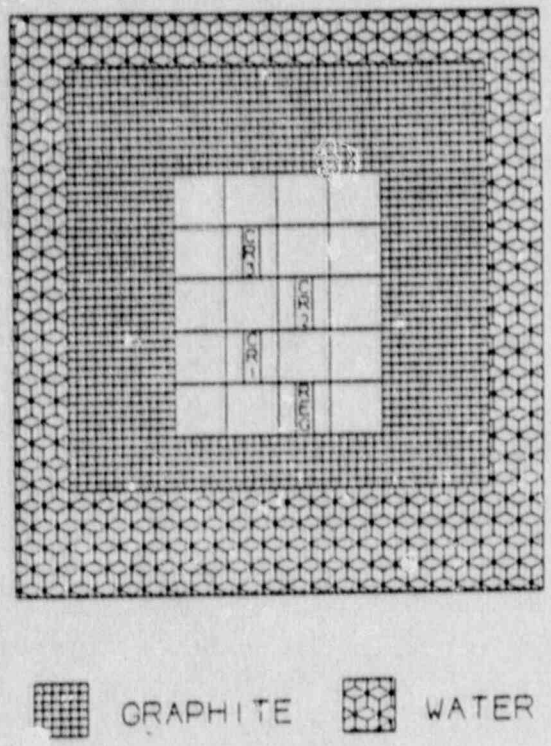

Figure 2. Ideal LEU UVAR Core Configuration

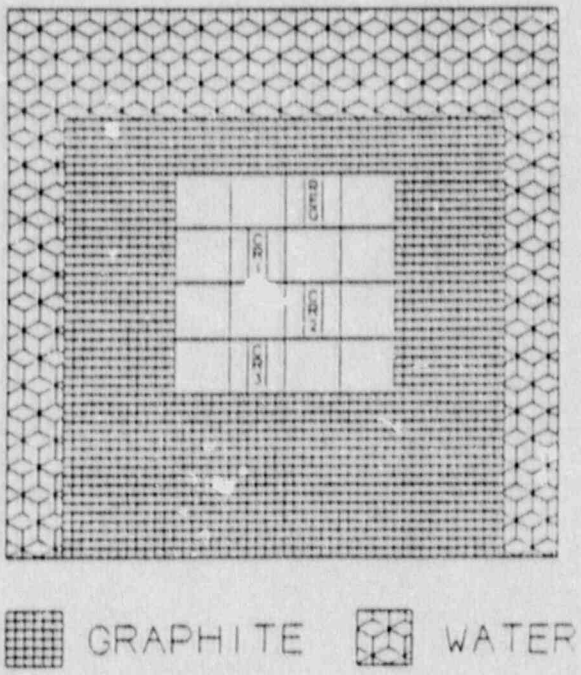

Figure 3. 1975 Texas A&M Core

BENCHMARK CALCULATIONS

The most recently measured UVAR-core configuration that met the conditions of being clean, unburned, and fully documented, was an initial 1975 loading of 18-plate Texas A&M fuel elements. This arrangement, shown in Figure 3, was a 4-by-4 element array, asymmetrically surrounded by graphite. Almost all other recent UVAR core arrangements have contained fuel elements having only an approximately known individual burnup history, making them unsuitable for benchmark purposes.

Available data for the Texas A&M core included measured individual control rod worth curves, an implied measured excess reactivity worth with all control rods withdrawn from the critical position, an approximate temperature defect worth obtained from single warm-up and cool-down swings, and an implied measured equilibrium xenon worth. Since the control rod worth curves are measured by repositioning any three control rods at equal depth to incrementally measure the fourth, some control rod interaction effects are built into the measurements.

Effective Control Rod Cross Sections

Control rods are strongly absorbing bodies having relatively small planar dimensions. They must be treated using transport theory, which must also take into account thermal spectrum hardening. We have developed effective diffusion theory cross sections in two groups, for both the boron steel shim rods and the stainless steel regulating rod, by applying the following procedure.

A transport theory model of a control rod surrounded by fuel material was made in slab geometry using the THERMOS thermalization code. Thermal group absorption fractions in both the fuel and absorber regions were obtained from this model. Fast group absorption fractions for the same regions were then obtained using the GAMTEC slowing down and thermalization code in cylindrical geometry; the GAMTEC thermal group result was cross checked against THERMOS. A cell model was then made using the 2D diffusion theory code EXTERMINATOR, and the fast group and thermal group absorption cross sections were iteratively varied until both the thermal and fast group absorption fractions matched those from THERMOS and GAMTEC. Finally, these effective cross sections were used with similar mesh spacings in the 2DBUM and 3DBUM diffusion theory codes for our reactor design studies.

Control Rod Worths

The procedure for obtaining effective control rod cross sections was applied separately to both HEU and LEU models. Within the uncertainties of the iterative process, the results were essentially the same for both. When these values were used in 2DBUM models of the 4-by-4 Texas A&M core (called HEU-18) the results shown in Table 1 were obtained.

Table 1. Control Rod Worths for the 4-by-4 Texas A&M Core and Replacements

Case	Rod 1* $	Rod 2* $	Rod 3* $	Rod 4* $
HEU-18 Expt.	4.75	5.00	3.06	0.57
HEU-18	4.71	4.96	2.86	0.73
LEU-18	4.61	4.86	2.79	0.83
LEU-22	4.69	4.91	2.90	0.84

*Experimental and Computational Uncertainties are ±5%

The integral rod worths for all three shim rods were predicted within the experimental accuracy of the measurements, while the regulating rod was predicted slightly high, probably because the boundary conditions on the cell model were not quite correct. Experimental uncertainties of ±5% are attributed to inaccuracies in period measurements and to uncertainties in the precise value of beta-effective, which was taken to be $\beta_{eff} = 0.008$.

Calculations were also made for LEU replacement cores having 18 plates/element (LEU-18) and 22 plates/element (LEU-22). The predicted control rod worths are also given in Table 1, where it is seen that they do not differ markedly from the HEU-18 results.

When the critical control rod positions for a core are entered into the experimentally measured integral control rod worth curves, the excess reactivity available for removing the rods entirely can be determined. The sum of these values for the Texas A&M core experiment is reported in Table 2. The value of k_{eff} that is obtained from the corresponding 2DBUM model of the same core, using axial B^2 values obtained from an ANL 3D model, is approximately 0 026 higher.

Three-dimensional calculations for this core were recently completed using 3DBUM. The rodded and unrodded k_{eff} values (Table 2) agree well with 2DBUM. The value of k_{eff} with the control rods placed at their critical positions is $k_{eff} = 1.026$, thus confirming that the difference between the measured and calculated k_{eff} values is real.

Table 2. Beginning-of-Life Unrodded k_{eff} for Texas A&M UVAR Core

CONDITION	k_{eff}
EXPERIMENTAL,* HEU-18	1.036 ± 0.004
2DB CALC, δ = 7.8 CM, B^2 = .0017 60-by-60 mesh	1.062
3DB CALC 60-by-60-by-21 mesh	1.062

* Implied From Control Rod Worth Curves

A series of 3DBUM calculations was performed where the control rods were moved together in a bank in order to simulate a composite integral control rod worth curve. The results are given in Figure 4, along with a corresponding experimental integral control rod worth curve constructed from the individually measured control rod worth curves. The data agree quite well, with the computed curve shifted only slightly towards the bottom of the core. The maximum uncertainty in the measured curves is therefore of the order of $\Delta\rho = .01$.

We conclude that the initial burnup status of the Texas A&M fuel elements was not known as accurately as we thought. The elements probably had somewhat more than the reported 0.84% average burnup during their many years of periodic operation at 100 KW. Indeed, the fuel elements used in the 1975 UVAR core may have had greater than average burnup. Furthermore, residual samarium could account for as much as $\Delta\rho = -0.005$ in this otherwise cold-clean configuration.

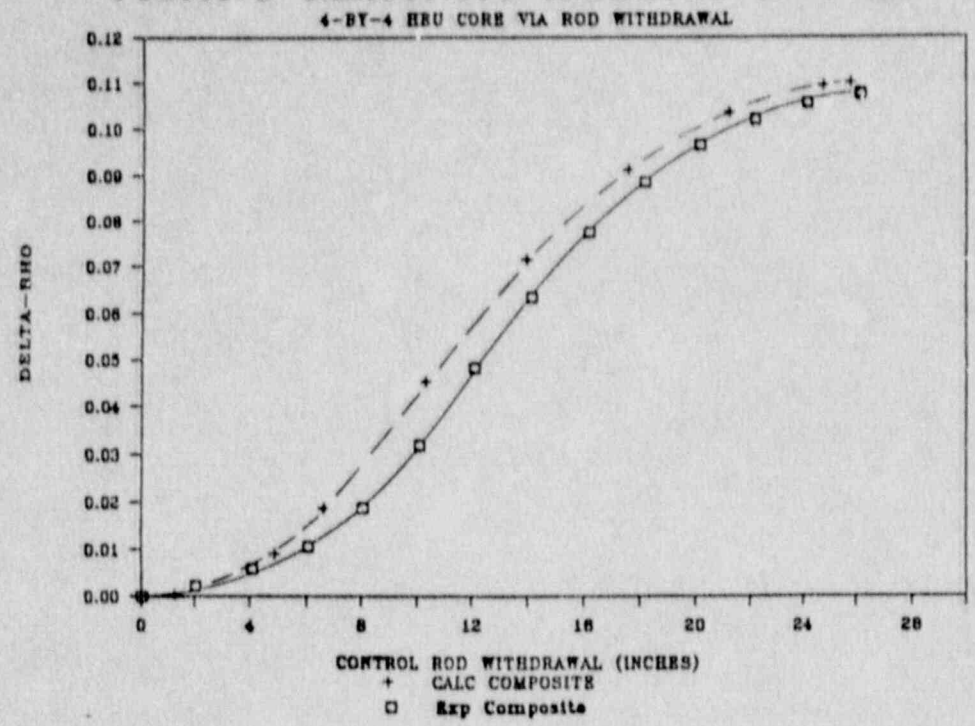

Figure 4. Composite Control Rod Worth Curves for the 1975 Texas A&M Core

Feedback Effects

Experimental values are also available for the Texas A&M core for the worth of equilibrium xenon and for the moderator temperature coefficient. The xenon worth was obtained from the differences in the critical control rod positions for the no-xenon case as implied from the measured integral control rod worth curves. The temperature coefficient was implied from a single heat-up experiment and a corresponding cool-down experiment whose worths differed by about 50%. The ΔT used for the experiment was one half the average core temperature rise; the effective ΔT is undoubtedly higher. Xenon buildup was also ignored. Hence, this measurement cannot be considered to provide anything more than an order of magnitude estimate.

The experimental Texas A&M core feedback results are given in Table 3, where they are compared with calculated results for both HEU and LEU models. The calculations of temperature coefficients were made from LEOPARD-LINX-2DBUM models of the full cores.

The experimentally derived xenon worth is about 0.004 lower than the calculated worth, which implies that samarium was already included in the initial criticality. The calculated temperature coefficients are lower than the measured value by more than a factor of two, but this is not considered bad agreement due to the inaccuracy of the measurements. The LEU cores have very slightly lower moderator coefficients than the HEU core, but they pick up a Doppler coefficient due to the increased ^{238}U loading.

Table 3. Feedback Effects for the 4-by-4 Texas A&M UVAR Cores and Replacements.

Case	Xenon-Samarium Worth $\Delta\rho$	Temperature* Defect $\Delta\rho$ ($\times 10^4$)	Moderator* Coefficient $\Delta\rho/\Delta T(^\circ C)$ ($\times 10^4$)	Doppler Coefficient $\Delta\rho/\Delta T(^\circ C)$ ($\times 10^5$)
HEU-18Expt	-1.9% (Xe)	-19.	-5.2	———
HEU-18	-2.3%	-7.6	-1.9	-0.09
LEU-18	-2.3%	-7.3	-1.8	-1.0
LEU-22	-2.4%	-6.8	-1.7	-1.2

*Experimental Measurements are ±50%

LEU DESIGN STUDIES

In order to make the design problem tractable, we picked three fixed arrays (4-by-4, 4-by-5 and 5-by-5) as the bases of comparison, and did core-life calculations with HEU-18 plate fuel and LEU-18 and LEU-22 plate replacement fuel. All LEU cores start out with a somewhat lower k_{eff} than the corresponding HEU cores because they have a harder neutron spectrum and a consequently greater leakage. The burnup curves for LEU are less steep than for HEU, and therefore the excess reactivity curves eventually cross as depletion increases. However, for the 4-by-4 core, the lower initial k_{eff} of LEU-18 fuel cannot be made up by the decreased burnup slope before the excess reactivity crosses zero, and therefore LEU-18 fuel will not last as long as HEU-18 fuel. On the other hand, LEU-22 fuel will have comparable performance to HEU-18 fuel.

For a 4-by-5 array, as seen in Figure 5, one finds that both the LEU-18 and HEU-18 fuel reach an asymptotic behavior, and these cores attain essentially equal burnup at the same point in life where the excess reactivity crosses zero. On the same basis, LEU-22 fuel lasts about 50% longer than LEU-18 fuel, even though the uranium loading is only 20% greater.

A similar behavior is seen for the 5-by-5 core models. Again, the HEU-18 and LEU-18 cores have essentially the same endpoint, while the LEU-22 core lasts about 50% longer. But the most interesting result is that the LEU-22 core in a 4-by-5 array lasts almost as long as an LEU-18 core in a 5-by-5 array. This means that an LEU-22 core can be kept in a 4-by-5 configuration, with attendant higher average thermal flux for experimental purposes, and still operate almost as long as our previous larger cores.

ANL[2] has independently calculated all of the 4-by-5 cases using a 3-dimensional model, and has verified that a 2-dimensional model gives similar results when the correct spatially-dependent axial B^2 values are used. Their results are shown in Figure 6. We find that our HEU results are in almost exact agreement with theirs, while our LEU results are offset low by about 1% in k_{eff}. Only minor differences exist between the UVA and ANL 4-by-5 LEU models. UVA included a small amount of ^{234}U and ^{236}U in the LEU fuel specification, whereas ANL used only ^{238}U. This change essentially accounts for the difference in results. The qualitative conclusions are still the same: LEU-22 fuel is a superior replacement, relative to LEU-18 fuel, for use in the UVAR.

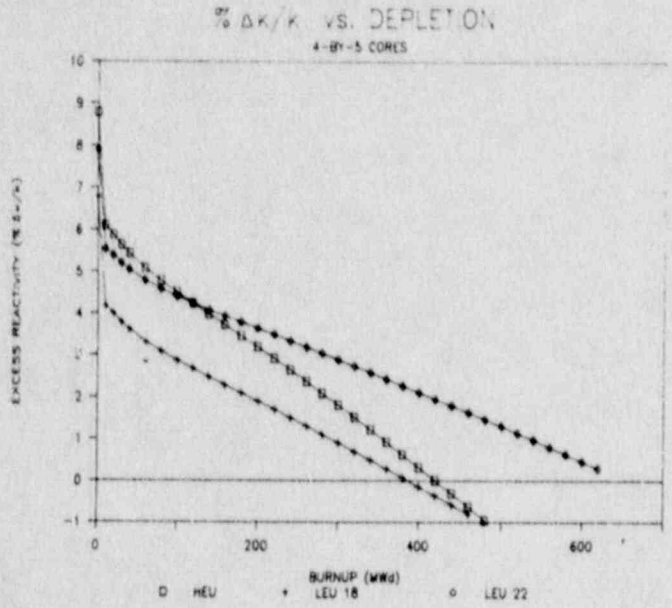

Figure 5. Unshuffled 4-by-5 Depletion of HEU and LEU Cores Using 2DBUM

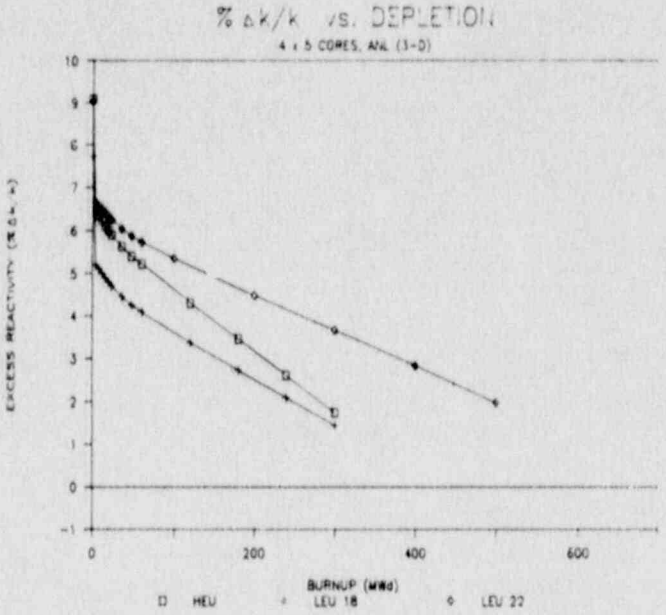

Figure 6. Unshuffled 4-by-5 Depletion of HEU and LEU Cores by ANL in 3D

Reflector Effects

The UVAR currently has a Technical Specification limit of 5% excess reactivity. Examination of Figure 5 reveals that the new 4-by-5 LEU cores will have between 7 and 10% excess reactivity. Therefore, some external action is needed to meet this specification.

We have done a series of calculations whereby various rows of reflector graphite have been replaced by pool water. This is accomplished in practice by inserting aluminum plugs in the grid plate. As shown in Table 4, selective use of water on one or more faces of the core provides an adequate means to cope with excess reactivity above TS limits. Fine tuning can be accomplished by replacing individual rows of graphite by water rather than replacing all graphite on a core face.

Table 4. UVAR Reflector Effects for 4-by-5 LEU Cores

WATER ON FACE	$\%\Delta\rho$
Bottom (B)	-1.2
Top (T)	-2.0
Left (L) or Right (R)	-2.3
TB	-3.4
TLB	-5.4
TLRB	-7.4

Temperature and Void Feedback

Temperature coefficients were calculated for 4-by-5 element cores using both HEU and LEU fuel. In all cases, the normal moderator temperature was taken to be 21°C, whereas the nominal fuel temperature was taken to be 33°C for HEU-18 and 30°C for LEU-22 fuel. Doppler coefficients were evaluated at 75, 100 and 200°C. Moderator coefficients were evaluated at 50 and 75°C.

The results are shown in Table 5. It should be noted that small variations of the temperature coefficients occur with temperature. The numbers quoted are estimated to have an uncertainty of about ± 10%. It is seen that the Doppler coefficients are comparable to those given in Table 3 for 4-by-4 cores, whereas the moderator coefficients are slightly lower.

Table 5. Temperature Coefficients for 4-by-5 Cores

Situation	Moderator $\Delta\rho/\Delta T(^{\circ}C)$	Doppler $\Delta\rho/\Delta T(^{\circ}C)$
LEU-22 Graphite	-1.4×10^{-4}	-1.1×10^{-5}
HEU-18 Graphite	-1.5×10^{-4}	-1.3×10^{-6}

Void feedback can be simulated by recalculating cross sections in LEOPARD using reduced water densities, and using these cross sections in 2DBUM. There is a limit to which the procedure can be applied due to limited data libraries, the range of validity of the LEOPARD treatment, and the applicability of diffusion theory. On the other hand, the order of magnitude of the effect is important to estimate.

A series of 2DBUM calculations were performed assuming both uniform voiding and relatively complete but local voiding near the hot spot in the core. Not surprisingly, the void coefficient changes with the percentage of core voiding due to neutron spectrum changes. Voiding will also take place locally near the hot spot, which tends to be in a position of high importance.

The results of the calculation are shown in Figure 7. For uniform voiding, HEU and LEU are comparable. On the other hand, for local voiding, HEU provides more feedback than LEU due to neutron spectrum effects. The void coefficients are also several times larger than for uniform voiding, showing the importance of the position where voiding is expected to take place.

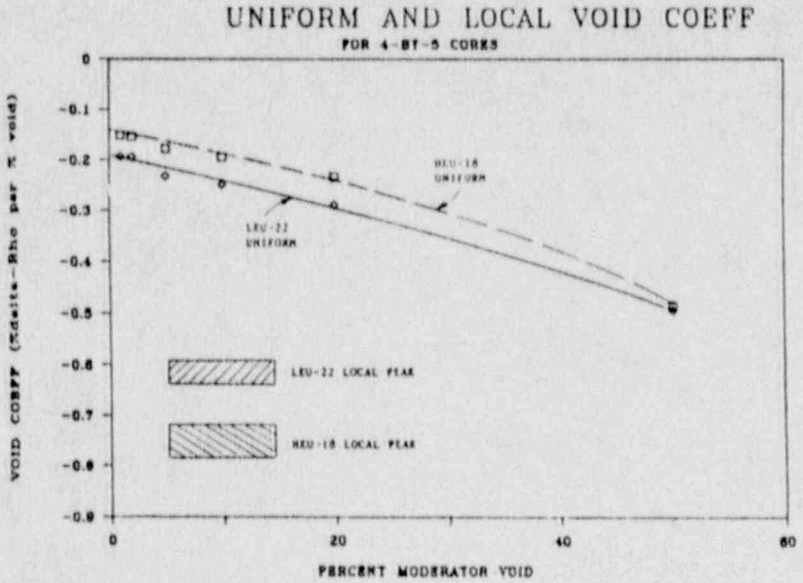

Figure 7. Uniform and Local Void Coefficients

Kinetics Parameters

Although a value of beta-effective of β_{eff} = .008 was in use for UVAR in 1975, soon afterwards it was changed to β_{eff} = .0075. A series of new calculations have now been completed to determine β_{eff} and the neutron lifetime, ℓ, for both LEU and HEU cores under various conditions. These calculations were made using the EXTERMINATOR code, with 4-group cross sections taken from both LEOPARD and EPRICELL.

The first step in the process was to compare the 4-group EXTERMINATOR models to the corresponding 2-group 2DBUM models. Calculated values of k_{eff} agree quite well when identical 60-by-60 mesh models are used.

Values for neutron lifetime are given in Table 6. In general, ℓ is about 15% lower for LEU cores than for HEU cores, due to greater neutron absorption in the core. In addition, ℓ is about 20% smaller for water reflectors than for graphite reflectors, due to increased neutron leakage. Changes of this order of magnitude will not lead to significantly different dynamic behavior for the new LEU cores as compared to the existing HEU UVAR cores.

Table 6. Neutron Lifetime for 4-by-5 UVAR Cores

Situation	ℓ(μsec)
LEU-22 GRAPHITE	67.0
LEU-22 GRAPHITE RODDED	66.5
HEU-18 GRAPHITE	78.8
LEU-22 WATER	53.0
HEU-18 WATER	64.4

4 GROUP, EXTERMINATOR

Beta effective calculations were made using recent delayed neutron data published by Brady et. al. [3]. For the present 4-group model, the delayed neutrons are essentially all born into the second group. However, in order to test the sensitivity of these results, some calculations were made with a fraction of the neutrons introduced into the fast group. The results are shown in Table 7.

Table 7. Beta Effective for 4-by-5 UVAR Cores

Situation	χ	β_{eff}
LEU-22 GRAPHITE	.2,.8,0,0	.00713
"	.1,.9,0,0	.00724
"	0,1,0,0	.00736
" RODDED	"	.00741
LEU-22 WATER	"	.00752
HEU-18 GRAPHITE	"	.00738

4 GROUP, EXTERMINATOR, β=.0065

β_{eff} was found to be relatively insensitive to reasonable variations in spectral assumptions, or to the fuel or reflector compositions. A value of β_{eff} = .0074, not much different from the value in current use, is suitable for all cases. Unfortunately, this value slightly worsens the agreement between measured and calculated control rod worths, mainly by over-estimating the worth of the regulating rod.

Beam Port Effects

An effort has also been made to simulate the reactivity effects of inserting a typical beamport next to the core. The actual beam port is a cylindrical tube 8 inches in diameter, entering at an angle, whose nosepiece contacts one core face roughly positioned in the middle of the face. Three cases were simulated: 1) a black region, representing an open beam tube; 2) a 6 inch thick tank of D_2O followed by water, representing a premoderated but closed beam port; and 3) 6 inches of D_2O followed by a black region, simulating a premoderated and open beamport. The beam tube was modeled by a rectangle, 6.78 inches by 7.23 inches, having an area essentially the same as the 8 inch pipe, but extending outward perpendicular to the core. The reactivity effects of these combinations are shown in Table 8.

Table 8. 3D Calculations of the Effect of Using an 8 inch Beamport

Situation	$\Delta\rho$
No beam port	0.0
6" D_2O, closed	+0.0005
6" D_2O, open	-0.0027
Open	up to -0.044

The simulation of an open beamport by a black region gives a considerable overestimate of the reactivity effect of an actual beamport. Nevertheless, the size of the reactivity loss could be significant, so that this method of operation would not be recommended. The effect of using 6 inches of D_2O in a tank to replace graphite is not large at all, and presents no problems. And the effect of opening the beamport behind this D_2O, while not insignificant, is also not a major problem, although some limits should be placed on the rate at which the tube is filled and emptied.

THERMAL HYDRAULIC ANALYSIS

The UVA thermal hydraulic analysis makes use of three basic computer code packages, PARET, THERHYD and NATCON. The PARET code from ANL was used to calculate an envelope of maximum achievable power transients, based upon pump coastdown and period trips, all accompanied by Scram. The net result of all of the PARET analyses is the fact that the control rod release and insertion times are the limiting factors for the UVAR, and that temperature feedback plays only a minor role. The responses for both HEU and LEU cores are quite similar. Transients not accompanied by Scram are argued to fall within the SPERT Experiment envelope.

The NATCON code from ANL was used to calculate the limits of core performance under natural convection conditions. The primary results are that adequate natural convection cooling exists for LEU-22 cores that are operated beneath our allowable TS limit of 200 KW. The use of additional fuel plates in our fuel elements increases the amount of natural convection cooling available.

The main tool for our thermal hydraulic analysis is the THERHYD code [4], developed at UVA in 1967. This code is used to calculate limiting-power versus system-flow envelopes for the UVAR, below which all PARET transients must lie. The code handles forced convection down-flow, using an axial power distribution fit and planar peaking factors from 2DBUM. The limiting condition is given using a burnout ratio of 1.49 (99% confidence that burnout will not occur) and taking into account channel and loading tolerances and bypass flow.

The peaking factors obtained from 2DBUM are shown in Table 9 for all of the cores that have been analyzed. Also shown is an older experimental measurement [5,6], scaled up to an 18-plate HEU fuel element. In general, the calculated peaking factors are a bit larger than the measured value, but lie within the experimental uncertainty.

Table 9. Planar Power Peaking Factors

CORE CONFIGURATION	CALCULATED	EXPERIMENTAL*
HEU-18 4-BY-4	1.59	1.45 ± 0.15
LEU-18 4-BY-4	1.64	
LEU-22 4-BY-4	1.69	
LEU-18 4-BY-5	1.73	
LEU-22 4-BY-5	1.78	

*Scaled From 12-Plate Measurement

When these data are employed in THERHYD, we obtain limiting-power versus system-flow curves, such as shown in Figure 8. In general, the inclusion of reasonable tolerances in fuel element manufacture causes the limiting envelope to approach the actual transient results from PARET. We conclude that reasonable control must be exercised on the process of making LEU fuel, especially for the LEU-22 assemblies.

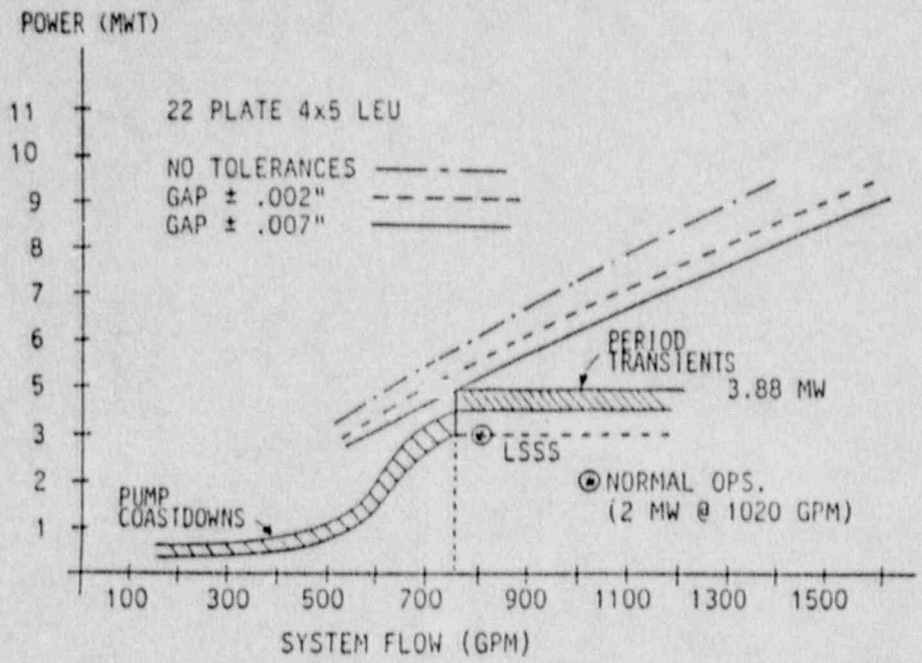

Figure 8. Limiting Power vs. Flow, 4-by-5 LEU-22 Plates/Element

The overall conclusion is that the LEU fuel is only slightly worse than HEU fuel from a thermal hydraulic standpoint. This result will require a small revision in the minimum safety system settings for the UVAP when it is converted. Otherwise, the small 4-by-4 core is more limiting than the larger 4-by-5 core (due to a higher average heat flux), and the 22-plate fuel element is more limiting than the 18-plate fuel element (due to manufacturing tolerances).

ANL have also suggested that we consider using an equilibrium-cycle shuffling pattern, based upon the adoption of a fixed 4-by-5 core array. This cycle appears to be very attractive for the UVAR, if LEU-22 fuel is indeed used to replace our present HEU-18 fuel. This option is under serious consideration, although we would like to retain the right to use bigger cores, if needed.

CONCLUSIONS

We conclude that the LEOPARD-LINX-2DBUM package of computer codes is in good working order at UVA and provides a reasonable basis of predicting the future performance of LEU replacement cores in the UVAR. A 3DBUM modeling capability is also now operational. It has been used to predict the effect of partially inserting control rods into the UVAR, thus confirming the previous 2D models and verifying the measured integral control rod worth curves. The 3D model is also useful for estimating the reactivity effects of proposed experimental facilities mounted near the core.

The best replacement option for the UVAR appears to be the use of 22-plate LEU fuel assemblies in a fixed 4-by-5 core array. We will seriously consider the adoption of the shuffle pattern recommended by ANL. On the other hand, it is to our advantage to retain the flexibility of loading UVAR cores to meet experimental needs.

None of the important feedback or kinetics parameters change greatly in going from HEU to LEU fuel. Furthermore, these parameters do not vary greatly with depletion, core size or reflector changes. We conclude that the dynamic performance of our new LEU core will be quite similar to that of our existing HEU cores.

Finally, all of the postulated LEU UVAR replacement cores meet the required thermal-hydraulic conditions for safe operation. However, we will have to make slight changes in current UVAR limiting safety system settings and pay close attention to the manufacturing tolerances placed on the new fuel.

REFERENCES

1. J.L. Meem, Two Group Reactor Theory, Appendix A, Gordon and Breach Science Publishers, New York, N.Y., 1964.

2. J.E. Matos, Private Communication from Argonne National Laboratory, August 1988.

3. M.C. Brady, R. Talmadge and W. Wilson, "Few-Group Analysis of Current Delayed Neutron Data", Transactions of the American Nuclear Society, 53, 1988.

4. J.A. Dahlheimer, "Thermal-Hydraulic Safety Analysis of Pool Reactors", M.S. Thesis, University of Virginia, 1967.

5. W.K. Brunot, "Ar Analysis of Fuel Element Surface Temperature and Coolant Flow Rate in the University of Virginia Reactor," M.S. Thesis, University of Virginia, 1961.

6. R.L.J. McGuinness, "Thermal-Hydraulic Safety Analysis of 18-Plate Reactor Fuel Elements", B.S. Thesis, University of Virginia, 1973.